Paneth cells: tales of a gutsy cell

Matthias Schewe

The studies described in this thesis were performed at the Department of Pathology, Erasmus MC Cancer Institute, Rotterdam, The Netherlands. The research described here was performed within the framework of the Erasmus Postgraduate School of Molecular Medicine.

Molecular Medicine
Postgraduate School

This research project was supported by the Dutch Cancer Society (KWF).

Cover design by Matteo Oliverio
Printing and binding by Ridderprint BV, Ridderkerk.

Paneth Cells: tales of a gutsy cell
Paneth-cellen: verhalen van een darmcel

Thesis

to obtain the degree of Doctor from the

Erasmus University Rotterdam

by command of the

Rector Magnificus

Prof.dr. R.C.M.E Engels

and in accordance with the decision of the Doctorate Board.

The public defense shall be held on

Wednesday 19 September 2018, at 15:30 hours

Matthias Schewe

born in Cagliari, Italy

Erasmus University Rotterdam

Doctoral committee

Supervisor: Prof.dr. R. Fodde

Other members: Prof.dr. C.P. Verrijzer

Prof.dr. J. Gribnau

Prof.dr. B.M.T. Burgering

This thesis is dedicated to my parents.

CONTENTS

CHAPTER 1

Introduction

Multitasking Paneth cells in the intestinal stem cell niche

Matthias Schewe and Riccardo Fodde

Dept. of Pathology, Erasmus MC Cancer Institute,
Erasmus University Medical Center, Rotterdam, The Netherlands

Advances in Stem Cells and their Niches # 2018 Elsevier Inc.
ISSN 2468-5097

ABSTRACT

The structure of the small intestine is designed to maximize its main function, namely the digestion of food into low molecular mass components and their subsequent absorption. The epithelial lining of the small intestine forms invaginations, called crypts of Lieberkühn, and finger-like structures protruding into the intestinal lumen, called villi. Notably, the small intestine is characterized by one of the highest turnover rate in our body, with the lower third of the crypt representing the main site where epithelial cells are generated *de novo* from resident stem cells. To date, five differentiated epithelial lineages have been characterized in the small intestine: enterocytes, Paneth, goblet, enteroendocrine, and tuft cells. These five lineages all arise from slender cells located in the crypt bottom called crypt base columnar cells (CBCs). CBCs are marked by expression of the seven-pass transmembrane receptor Leucine-rich repeat-containing G-protein coupled receptor 5 (*Lgr5*) and are thought to represent the main stem cell type of the small and large intestine. With the only exception of Paneth cells located at the crypt base in close physical contact with *Lgr5*$^{+}$ CBCs, the differentiated cell types migrate upwards towards the top of the villus where they undergo apoptosis and are shed into the gut lumen.

Paneth cells (PCs) are responsible for a plethora of functions both in intestinal homeostasis and in response to dietary changes and tissue insults. Apart from controlling the bacterial flora through secretion of antimicrobial compounds, Paneth cells play a causal role in the pathogenesis of inflammatory bowel disease. More recently, it was shown that they also exert an essential niche function in regulating intestinal stemness. Even 145 years after their discovery, research on Paneth cells is still revealing novel and fascinating aspects of their multi-tasking and context-dependent identity.

PANETH CELLS: FROM SCHWALBE AND PANETH TO THE DISCOVERY OF THEIR SECRETORY ROLE

Early studies anticipate Paneth cells' multi-tasking functional nature

Granulated cells in the fundus of the crypts of Lieberkühn were first described in 1872, along with the other cells of the intestinal epithelium, by Gustav A. Schwalbe, a German anatomist, histologist and anthropologist[1]. Nevertheless, they take their name from Joseph Paneth, an Austrian histologist and physiologist who first performed their detailed morphological analysis in 1888[2]. For many decades after their discovery however, the role of Paneth cells (PCs) remained obscure due to mainly observational studies limited by the available methods and mostly focused on the morphological features of PCs and their granular payload.

In 1899 W. Möller reported on the presence of Paneth cells in several animal species including mouse, guinea pig, hox, sheep, and horse[3]. Given the broad spectrum of species found to host Paneth cells and to feature acidophilic granules and mucus in the small intestinal epithelial lining, the question arose whether they represented independent zymogenic cells or were involved in mucus production[4]. Bizzozero claimed to have found cells with a dual Paneth/goblet cell fate, therefore raising the possibility of Paneth cells representing goblet cells precursors[4]. Few years later, Klein brought evidence supporting the independent zymogenic function of Paneth cells, distinct from goblet cells, based on staining analysis with mucus-specific dyes[5]. Mols and Cowdry studied the effects of different diets in murine Paneth cells and observed that their intracellular content changed depending on the specific diet fed[6,7], thus suggesting, already at these very early days, specific roles for this cell type in metabolism and nutrient sensing to be confirmed nearly a century later[8,9].

In 1937 Hertzog analyzed Paneth cells in man and reported on their reduced abundancy in the duodenum. Also PCs multiplicity and distribution did not appear to be influenced by sex or age and, of note, they occasionally appeared in colon, stomach and appendix in association with pathological conditions[10]. The latter observation led to additional studies on the alleged function of Paneth cells in disease[11-16]. The most accurate description came from studies by K. Lewin who described and counted the appearance and number of Paneth cells in the small and large intestine. Of note, Paneth cell multiplicity was shown to be affected upon inflammation depending on the specific type of pathology and the degree of the inflammatory damage. Decreased PC numbers were found in acute inflammation of the small intestine and in Crohn's disease. Interestingly, Paneth cells were also found to proliferate upon inflammation[16-18]. Contrary to what observed in the small intestine, an increased number of Paneth cell was found

in the colon in association with ulcerative colitis and other inflammatory diseases of the distal bowel. As of today, it is still unclear whether Paneth cell metaplasia (PCM), i.e. the appearance of Paneth cells in the large intestine, plays any functional role in the tissue response to inflammatory insults and in the increased colon cancer risk associated with inflammatory bowel disease (IBD). The role of Paneth cells in IBD will be discussed further in depth in a later section of this chapter.

Paneth cells have also been observed within intestinal tumors: several studies have reported on the presence of lysozyme-positive neoplastic cells in adenomas and carcinomas of the colon, often with proliferative features. The number of Paneth cells in colonic tumors was higher in proximal lesions when compared with distal neoplasias[19]. Notably, Paneth cells have been observed in colonic tumors from patients with but also without a history of inflammatory bowel diseases. As for the biogenesis of PCM in the colonic mucosa, early studies proposed that these Paneth-like cells arise through metaplastic changes brought about by the altered inflammatory and/or neoplastic milieu[19]. The term Paneth cell *metaplasia* (from the Greek *metaplasmos* = change in form) was therefore employed to indicate the conversion of a cell type into another. Metaplastic Paneth cells have been found in a broad spectrum of pathological conditions ranging from inflammatory bowel diseases to cancer[20,21].

The origin and fate of Paneth cells and their context-dependent proliferative state were investigated by Cheng and Leblond who found that PCs exists in a variety of maturation stages *in vivo* as a measure of the size of their granules (23% with granules smaller than 2µM and classified as 'young' PCs; 63% with granules between 2-3 µM; and 14% 'old' PCs with granules larger than 3 µM)[22]. These studies also showed that Paneth cells were post-mitotic in homeostatic conditions and persisted for long terms at the bottom of the crypt, unlike most intestinal epithelial cells that actively migrate upwards along the crypt-villus axis to be then exfoliated by apoptosis within 5-6 days.

Paneth cells: the secretory bodyguards of the crypt

The large acidophilic granules apically secreted into the crypt lumen that earmark Paneth cells have been the object of several electron microscopy studies. The secretory function of the Paneth cell is prominent throughout its different subcellular compartments featuring an extensive Golgi apparatus and very pronounced endoplasmic reticulum. However, the function of the secretory granules remained elusive until lysozyme was identified as one of their main components[23]. As lysozyme is a strong antibacterial agent, a role was proposed for Paneth cells in host defense mechanisms in response to bacterial flora.

Subsequently, two additional families of antimicrobial proteins, namely secretory phospholipases (e.g. *Pla2g2a*)[24], endowed with additional lipid modifying function, and

α-defensins (also known as cryptdins for their location at the bottom of the crypt)[25,26] were found to be expressed by murine Paneth cells and specifically localized in their secretory granules.

These studies sparked several additional efforts towards the elucidation of the mechanisms underlying Paneth cell secretion and the environmental stimuli that trigger it. To this aim, whole crypts were detached from the lamina propria and exposed to bacteria such as Salmonella typhimurium, Escherichia Coli, or Staphyloccocus Aureus. A potent induction of granule secretion and consequent antibacterial activity was observed upon stimulation of these *ex-vivo* isolated crypts with bacterial cells. More than 90% of the microorganisms to which the crypts were exposed were killed. Notably, most of the antimicrobial activity appeared to be elicited by cryptdins, as shown by the observed 70% reduction in bactericidal function of the granules upon exposure to antibodies directed against cryptdin and cryptdin-like enzymes. Exocytosis of Paneth cell granules was also observed upon exposure to bacterial surface products such as lypolysaccharide (LPS) in a dose-dependent manner[27]. Furthermore, granule secretion can be triggered by a broad range of stimuli including acetylcholinergic[28,29] and toll-like receptor agonists[30,31]. More recent studies suggest that secretion of the granules by Paneth cells is triggered by bacterial cells or antigens in an indirect way and requires interferon gamma, mainly secreted by leukocytes co-isolated with the crypts. To prove that stimulation of Paneth cell secretion is indirectly stimulated by bacterial antigens, crypts were cultured *ex-vivo* as self-renewing organoids or "mini-guts" (this technique is more accurately described further in this chapter) and the basal or luminal side of such structures exposed to LPS, flagellin, peptidoglycan (PGN), heat-inactivated E. Coli, and live bacterial cells[32]. No change in Paneth cell morphology or granule secretion was observed after 12 hours. Furthermore, no changes in intracellular or secreted lysozyme expression were observed. Paneth cell expression of bacterial receptors like Cd14 and Toll-like receptors 2,3,7,8, and 9 remained unchanged in the cultured organoids when compared to Paneth cells *in* vivo, the latter also indicating that these receptors are retained in *ex-vivo* cultured crypts. Consequently, several inflammatory molecules were tested for their capacity to induce discharge of Paneth cell granules. Among several molecules including interleukin 22 (IL22) and 6 (IL6), tumor necrosis factor (TNF), and interferon gamma (IFN-γ), only the latter proved to be a potent inducer of granule secretion by Paneth cells[32].

Additional *in vivo* experimental evidence for the role of IFN-γ as the main inflammatory molecule responsible for granule extrusion was provided by injecting wild-type and IFN-γ knock-out mice with anti-CD3 antibody to trigger T cell activation and interferon gamma expression. When wild-type mice were administered the CD3 antibody, Paneth cells degranulated as shown by decreased lysozyme content. Notably, no Paneth cell degranulation or any decrease in Paneth cell multiplicity was observed in

in CD3-treated IFN-γ knock-out mice[32].

Paneth cell granule secretion was also shown to be mediated by calcium fluxes. By tracking Ca^{2+} dynamics in *ex vivo* crypts during granules secretion, a biphasic increase in cytosolic Ca^{2+} was revealed with the first phase mainly arising from intracellular storage, whereas the second depends on extracellular calcium uptake[33]. The second rise in cytosolic Ca^{2+} can be reduced by selectively blocking the calcium activated potassium channel *IKCa1* (by means of clotrimazole (CLT) or charybdotoxin (ChTX)), and by measuring the levels of cryptdin secretion. The observed 50% reduction in secretion also corresponded to a similar reduction in antibacterial activity of crypts exposed to S. typhymurium[27,33,34].

The antimicrobial peptides (AMPs) secreted by Paneth cells have been proposed to encompass two main functions: i. protect the host from enteric pathogens; and ii. keep in balance and shape the composition of the microbiome[35]. These two deeply intertwined functions are of great relevance since the composition and number of Paneth cells might unfavorably alter the composition of microbiota, a condition known as dysbiosis, thus rendering the host more susceptible to a variety of infectious and non-infectious diseases[36-41].

The analysis and study of AMPs like defensins in the mouse is made more difficult by the complex genomic structure encompassing several gene paralogs within a single locus, and by the strain-dependent composition of AMPs among inbred mice[42-44].

As previously stated, Paneth cells are found in a wide range of species[3]. Likewise, AMPs have also been conserved throughout evolution[45]. One notable difference is represented by the presence of multiple defensins expressed by PCs in a broad spectrum of mammalian species, whereas their human counterparts only encode for two, i.e. defensin 5 and 6 (HD5, HD6)[46,47]. The function, activity and structure of defensins have been discussed in depth in several literature reviews[45,48-50].

The intestinal crypt stem cell niche

The discovery of the intestinal stem cell

The crypts of Lieberkühn were for long time suspected to harbor the elusive intestinal stem cells responsible to preserve homeostasis in one of the most dynamic and regenerative epithelial tissues. Indeed, seminal studies by Cheng and Leblond identified cycling cells located at the very bottom of the intestinal crypt, the so-called crypt base columnar cells or CBC's, and proposed them as the stem cells of the gut epithelium. Experimental evidence for the identity of CBCs as stem cells of the adult gut was provided by Nick Barker in the laboratory led by Hans Clevers, based on the identification of the transmembrane receptor *Lgr5* (Leucine-rich repeat-containing G-protein coupled receptor 5) as a specific marker of cycling CBCs. Lineage tracing experiments were

performed with a knock-in mouse model expressing both a green fluorescent protein (GFP) and a tamoxifen inducible C-recombinase under the control of the endogenous *Lgr5* gene promoter (*Lgr5*-eGFP-IRES-CreER^{t2})[51]. These mice, when bred with Rosa26-LacZ reporter animals and induced by tamoxifen, allow the excision of the roadblock (i.e. the stop sequences flanked by LoxP sites located upstream of the LacZ gene) and transcription of the reporter gene by Cre protein expression only in *Lgr5*$^{+}$ cells. In this way, LacZ expression, easily detectable by X-gal staining, will mark *Lgr5*$^{+}$ cells and their cellular progeny. Upon tamoxifen treatment, *Lgr5*-eGFP-IRES-CreER^{t2} mice gave rise to long ribbons of blue labelled cells starting from the bottom of the crypt to the villus tip. These blue ribbons persisted in the intestine of the mice for more than 300 days and encompassed all the intestinal cell lineages, thus showing that *Lgr5*$^{+}$ have long term self-renewal and multipotent differentiation capacity both in the small and large intestine.

Although stem cells have long been thought to divide infrequently, the intestinal epithelium almost entirely renews its cellular composition every 5 days suggestive of an actively proliferating stem or precursor cell. By using the above *Lgr5* knock-in mice, CBCs have been shown to divide approx. every 16 hours[52]. Another common view on stem cells is relative to their mitotic division modality, i.e. in symmetric vs. asymmetric fashion giving rise to two daughter cells with equal (two stem or two committed cells) or distinct (one stem cell and one committed progenitor) cell fates, respectively. By employing *Lgr5*-eGFP-IRES-CreER^{t2} mice bred with the Rosa26-confetti reporter, it was shown that *Lgr5*$^{+}$ stem cells divide symmetrically and that the follow a neutral drift dynamic[52].

Several studies suggested that stem cells in epithelial tissues come in two flavors: rapidly and slowly cycling[53]. *Lgr5*$^{+}$ cells divide every 16 hours and as such represent frequently cycling stem cells thought to underlie intestinal homeostasis under physiological conditions. A more quiescent or slowly cycling stem cell type located at position +4 from the crypt base was first identified by Chris Potten in 1974 based on its label-retaining properties[54]. Only several years later the first gene marker was identified to earmark the +4 label-retaining cells, namely the *Bmi1* (B cell-specific Moloney murine leukemia virus integration site 1) gene. By following a lineage tracing approach analogous to that employed for the *Lgr5*$^{+}$ CBCs, *Bmi1*$^{+}$ cells at the +4 position were shown to give rise to all the differentiated lineages of the small intestine[55]. Additional genes have also been proposed to specifically mark a subset of slowly dividing stem cells such as *mTert*, *Hopx*, and *Lrig1*[56-58]. Although lineage tracing provides valuable information on specific cell types and their progeny, it mainly relies on the specificity of the gene promoter under which the Cre recombinase is driven. *In situ* hybridization (ISH) analysis on single RNA molecules indicated that none of the aforementioned (+4) markers is uniquely expressed at a single position along the crypt-villus axis[59]. However, this is likely to be true for the vast majority of the genes/markers expressed by stem and

progenitor cells in the lower intestinal crypt. Most recently, the laboratory led by Eduard Battle identified a specific RNA binding protein called *Mex3a* that, in combination with *Lgr5*, marks a specific population of quiescent stem cells resident in the lower crypt also located at around position +3/+4[60]. Single cell RNAseq analysis of individual *Lgr5*$^{+}$ stem cells revealed the presence two populations differing by their cycling rates with *Mex3A* expression earmarking the slowly cycling *Lgr5*$^{+}$ subpopulation. Lineage tracing analysis using *Mex3A* knock-in mice bred with the Rosa26 reporter line conformed that *Mex3a*$^{+}$/*Lgr5*$^{+}$ cells represent *bona* fide infrequently dividing stem cells *in vivo*[60].

The presence of quiescent stem cells is of functional relevance as they have been proposed to underlie the regenerative response by compensating for the loss of rapid cycling *Lgr5*$^{+}$ CBCs upon tissue insults[61]. In the small intestine, tissue regeneration upon injury conditions has been shown to rely on the de-differentiation of terminally committed cells. Terminally differentiated cells have long been thought to be unable to rewire their cell fate and re-enter the cell cycle and acquire pluripotency. Recently however, distinct differentiated lineages of the small intestine, i.e. Paneth cells and *Alpi*$^{+}$ enterocytes, have been shown to act as stem/progenitor-like cells upon tissue injury[62,63]. The issue of plasticity as an intrinsic property of specific intestinal cell lineages raises several questions on the underlying pathways and molecular cues which are of relevance for our understanding of analogous mechanisms in pathological conditions such as tumor plasticity and resistance to therapy.

Paneth cells and crypt development

Both the small and large intestinal epithelium develop by tubulogenesis from the posterior endoderm following extensive folding[64,65]. The embryonic gut tube is lined by a simple epithelium that condenses to form a pseudostratified epithelium where all the cells are attached to the basement membrane. Around e14, the gut epithelium assumes a columnar form while it forms protruding structures called villi. Lineage specification is initiated at around e17 in proliferating cells confined in the intervillus region from where they subsequently invaginate to form intestinal crypts. Notably, whereas in the mouse crypt development occurs at early postnatal stages and is completed by the time of weaning, in man it occurs *in utero*[66].

Notwithstanding the absence of fully mature and granulated Paneth cells in the mouse intestinal epithelium during the first two postnatal weeks, expression of defensins 1 and 6 was found in scattered fashion throughout the newborn intestinal lining thus raising the possibility of an innate immune role for these peptides at early perinatal stages[66].

De novo crypt formation occurs through a process called 'crypt fission', a rate-limiting event in intestinal expansion and growth that consists in its essence of the division of

a crypt into two daughter crypts[67,68]. Crypt fission represents a form of epithelial tube branching through which the newly formed crypts of Lieberkühn divide and multiply thus extending and widening the intestinal tract during postnatal development. The lumen of the resulting two daughter crypts can be of equal or unequal length as the result of symmetric and asymmetric crypt fission, respectively. However, the cellular and molecular mechanisms underlying crypt fission are still poorly understood.

Recently, Inke Nathke and collaborators observed that the number and relative position of Paneth cells and *Lgr5*$^{+}$ CBCs at the bottom of the crypt are critical for the initiation of crypt fission[69]. Analysis of crypts undergoing fission revealed that the process can be divided into an early and a late phase[69]. During early fission, a change in cell patterning occurs with Paneth cells absent from the middle of the crypt bottom due to their migration to either side of the site of bifurcation/branching. Simultaneously to this side clustering of Paneth cells, *Lgr5*$^{+}$ CBCs form a distinct cluster in the middle of the crypt base thus marking the bifurcation site where, during the late fission phase, the epithelial lining is expanded upwards until the duplication of the two daughter crypts is completed.

The specific cell patterning observed during crypt fission reflects the intrinsic cell properties of *Lgr5*$^{+}$ CBCs and Paneth cells, the latter showing high stiffness and increased adhesion to the basement membrane. High β4 integrin expression allows Paneth cells to firmly anchor to the basement membrane when compared with other cell types.

In confirmation of previous studies showing that inhibition of ephrin (Eph) signaling causes misplacement of Paneth cells from the crypt base[70], inhibitory Eph protein fragments have been found to induce their mislocalization in *ex vivo* organoids though without altering the rate of crypt fission. However, altering PC localization skewed the balance between symmetric and asymmetric fission in favor of the latter, likely due to the formation of new branches further away from the crypts. Cell adhesion and integrin levels appear to play a central role in this process as shown by the observed 50% reduction in crypt fission in the presence of a β4 integrin antibody. It is therefore plausible to postulate that the enhanced adhesion, a feature of Paneth cells when compared to their neighboring cells, plays a key functional role in the early phase of crypt fission[69].

Paneth-specific signaling pathways: Wnt and Notch

Experimental evidence links *de novo* crypt formation to canonical Wnt signaling in view of the involvement of two of its downstream target genes (*EphB* and *cMyc*) in the migration and compartmentalization of Paneth and *Lgr5*$^{+}$ cells within the lower crypt. Cell migration within the crypt occurs in bidirectional fashion: whereas enteroendocrine cells, goblet cells, and enterocytes migrate upwards along the crypt-villus axis, Paneth cells descend in opposite direction toward the bottom of the crypts. In the mouse

prenatal intestine, the EphB2 and EphB3 receptors and their ligand Ephrin-B1 are expressed in complementary domains: both receptors and ligand are co-expressed in cells located at the periphery of the intervillus pockets, whereas expression of the EphB2 and 3 earmarks the cells present at the very bottom of the pockets[70]. In the adult small intestine, the expression pattern of the two ephrin receptors appears to be more complex with EphB3 being restricted to Paneth cells in the crypt bottom whereas *EphB2* expression earmarks the entire crypt bottom until position +4.

EphB3 receptor knock-out mice are characterized by misplaced Paneth cells throughout the crypt-villus axis, a phenotype not observed in *EphB2*$^{-/-}$ mice. Therefore, expression of the EphB3 receptor in Paneth cells appears necessary for their correct positioning at the bottom crypt[70]. Furthermore, the nuclear β-catenin accumulation characteristic of Paneth cells at the bottom of the crypt was lost in their misplaced equivalents in *EphB3*$^{-/-}$ mice thus indicating a non-cell autonomous and localization-dependent regulation of Wnt signaling in PCs[70]. As previously mentioned, Wnt signaling plays a pivotal role in the intestinal epithelium with both *Lgr5*$^{+}$ CBCs and Paneth cells are characterized by the accumulation of β-catenin in the nucleus where it binds with members of the family of Tcf transcription factors thus driving the expression of Wnt target genes[71].

Cytosolic levels of β-catenin are tightly controlled by a multi-protein complex encompassing the tumor suppressors Apc (Adenomatous polyposis coli) and Axin, the Ser/Thr kinases GSK3β (glycogen synthase kinase 3-beta) and CK1 (casein kinase 1), protein phosphatase 2A (PP2A), and the E3-ubiquitin ligase β-TrCP. In the absence of Wnt ligands, this "destruction complex" phosphorylates β-catenin promoting its ubiquitinilation and degradation by the proteasome[72]. Of note, canonical Wnt/β-catenin signaling has been shown to induce maturation of Paneth cells in the mouse small intestine: expression of the Paneth-specific gene program is lost in the intestine of *Tcf4*$^{-/-}$ embryos[73]. In particular, failure to express defensins and cryptdins caused Paneth cells maturation defects. Also, the frizzled (Fzd) family of receptors encompasses integral membrane proteins featuring seven transmembrane-spanning domains function in canonical Wnt signaling. Remarkably, *Fzd5* knock-out mice exhibit an identical phenotype to that of *EphB3*$^{-/-}$ animals with misplaced Paneth cells with no β-catenin nuclear accumulation, in confirmation of the positional cues provided by Wnt signals along the crypt-villus axis[70,73]. The Wnt-driven maturation of Paneth cells and their pronounced nuclear β-catenin accumulation is intriguing in view of the essential role played by canonical Wnt signaling in the regulation of stemness in the intestinal crypt. Hence, the same pathway controls the onset and maintenance of both multipotent and fully differentiated (and post-mitotic) lineages.

Studies aiming at the identification of the Wnt signals required for Paneth cell

maturation and maintenance have been performed by first establishing the expression patterns of Wnt ligands in the intestinal epithelium (i.e. Wnt3; uniquely expressed in PCs) and in the surrounding mesenchyme (Wnt2b, Wnt 4 and Wnt 5a). Notably, conditional ablation of Wnt3 throughout the intestinal epithelium (*Wnt3*$^{fl/fl}$/*Vil*^{CreERT2}) does not affect Paneth cells, indicative of functional redundancy between mesenchymal and epithelial Wnt ligands *in vivo*[74]. The latter was confirmed i. by the impaired growth of *ex vivo* cultured crypt organoids derived from the *Wnt3*$^{fl/fl}$/*Vil*^{CreERT2} mice upon removal of the floxed *Wnt3* allele, and ii. by the ability of exogenously added Wnt3 to rescue the growth impairment[74].

The orphan G protein-coupled receptor Lgr4 is expressed in small intestinal crypts above the PC zone (i.e. in the TA region), and in CBCs and in a subset of Paneth cells[75]. *Lgr4*$^{-/-}$ mice show reduced epithelial proliferation without any significant defect in the differentiation of absorptive, enteroendocrine and goblet cell lineages. However, absence of specific PC markers such as lysozyme and cryptdin 4 was also noticed in *Lgr4*$^{-/-}$ mice, likely indicative of a Paneth cell maturation defect. Accordingly, *ex vivo* cultured crypts from the *Lgr4* knock-out mice failed to form fully mature organoids and showed decreased expression levels of several stem cell-specific markers and Wnt targets such as *Axin2*, *Sox9*, and *Lgr5*. Accordingly, re-activation of Wnt signaling by addition of lithium chloride (LiCl) to the organoid culture medium partially rescued their growth impairment[75].

Among the Wnt targets observed to play a key role in Paneth cell onset, *Sox9* is expressed before the appearance of PCs in the embryonal gut and its expression overlaps with that of cryptdins in the intervillus pockets. Inducible genetic ablation of *Sox9* results in the disappearance of Paneth cells and a decrease of goblet cells[76,77]. As a consequence of the altered tissue morphology and absence of Paneth cells, the crypts of *Sox9*$^{fl/fl}$ mice present an enlarged proliferative compartment extended to the whole crypt bottom[76,77]. Constitutive *Sox9* expression as a consequence of loss of *Apc* function has also been shown to induce formation of ectopic Paneth cells in the mouse colon[78]. By employing a colon-specific promotor (*Cdx2*) to delete the *Apc* tumor suppressor gene, it was shown that adenoma formation is accompanied by the appearance of ectopic lysozyme-expressing Paneth-like cells. These metaplastic PCs were observed in regions outside of the crypt base, often at new crypt budding sites, coincident with high *Sox9* expression as the result of the induced *Apc* deletion. The latter is not surprising in view the role of *Sox9* as Wnt target but it is noteworthy that *Sox9* upregulation in the colon of these mice preceded the changes in β-catenin subcellular localization possibly due its easier detection, when compared to β-catenin stabilization, at early time points after *Apc* inactivation in the colon epithelium[78].

Alongside canonical Wnt, also Notch signaling plays an important role in Paneth

cell differentiation and maturation, mainly through one of its downstream targets genes, namely *Math1* encoding for a basic helix loop helix (bHLH) transcription factor. Studies performed on *Math1* knock-out mice revealed the ablation of all secretory lineages including Paneth and goblet cells, and enteroendocrine cells[79]. Thus, *Math1* is required for progenitor cells to commit towards a secretory fate. Notably, studies performed on mosaic *Math1* null crypts showed that commitment towards a secretory fate improves regeneration upon small bowel resection (SBR). *Math1*-deficient crypts showed decreased regenerative capacity after SBR when compared to proficient crypts, suggesting that secretory lineages may play a (niche) role in the response to tissue injury[80].

Constitutive expression of an active form of the Notch 1 receptor in the intestinal epithelium causes signs of malnourishment at postnatal day 1 (P1) and death at P3 as a consequence of the inhibition of all secretory lineages, a phenotype opposite to that observed in *Hes1* knock-out mice characterized by an excess of secretory cells at the expenses of enterocytes[81]. Hence, constitutive Notch 1 expression upregulates *Hes1* expression while downregulating *Math1*, a key gene in secretory lineage development.

Notch signaling inhibition has also been studied: mice treated with dibenzazepine (DBZ) showed an increment in Paneth cells numbers, with abnormal lysozyme staining, i.e. cytoplasmic and diffused rather than in the characteristic granular pattern, indicative of alterations in Paneth cells formation upon Notch signaling inhibition[82]. Upon further analysis, both the number and size of Paneth cell granules were shown to be decreased in addition to the expression of goblet-specific markers, suggesting the establishment of an intermediate phenotype in between the Paneth and goblet lineages upon Notch signaling inhibition. These findings highlight the importance of Notch signaling in terminal differentiation of Paneth cells[82]. Screens performed on *Math1*-proficient and -deficient mice led to the identification of the target genes of this transcription factor critical for the establishment of the secretory cell fate[83]. The *Gfi1* gene was found to be significantly downregulated upon *Math1* ablation. Likewise, *Gfi1* knock-out mice were deprived of mature Paneth cells together with a significant reduction of goblet cells and an increase in enteroendocrine cells. In these mice, secretory progenitors although already committed, are unable to differentiate into mature Paneth cells[83].

Another Paneth-specific gene known to affect Notch signaling in the crypt bottom encodes for the receptor of colony stimulation factor 1 (*Csf1r*), whose *Csf1* ligand is expressed by cells in close proximity to PCs. Csf1 receptor-deficient mice ($Csf1r^{-/-}$) are characterized by a marked reduction in fully mature Paneth cells[84,85]. Goblet cell multiplicity was also highly increased as a consequence of the *Csf1r* genetic ablation indicative of faulty cell fate determination in the common goblet and Paneth cell precursor. These results were also confirmed in *ex-vivo* cultured crypts, where $Csf1r^{-/-}$

organoids showed decreased clonogenicity and size, and reduced number of budding events. These experiments also suggested a role in Paneth cell maintenance for the Csf1 receptor: conditional *Csf1r* deletion by villin-Cre in organoids resulted in Paneth cells loss[86].

In view of the main secretory function of Paneth cells, it is not surprising that proteins involved in vesicle trafficking and secretion play significant roles in PC maturation. In particular, two classes of vesicle proteins have been investigated in gut epithelial homeostasis, namely Rab8A and αSNAP (soluble N-ethylmaleimide-sensitive factor-attachment protein alpha). The Rab family of small GTPases regulates both the sorting of transported molecules to the correct vesicles and vesicle delivery to target membranes. Of note, Rab8A has been linked to trafficking and secretion of Wnt ligands as it mediates anterograde transport of Gpr177 (wntless), a Wnt-specific transmembrane transporter.

Rab8a$^{-/-}$ mice lack fully mature Paneth cells and are instead characterized by immature cells with decreased numbers of granules[87]. Expression analysis of the intestinal epithelium of *Rab8a*$^{-/-}$ mice showed downregulation of several Wnt targets such as *Axin2* and *Ascl2* together with decreased nuclear β-catenin levels and reduced lysozyme and cryptdin 5 expression. When cultured *ex vivo*, crypts from *Rab8a*$^{-/-}$ mice showed less budding events and decreased clonogenicity. Accordingly, the negative effect brought about by *Rab8A* ablation can be rescued by adding Wnt3 in the organoid medium. The observed effect on cell maturation seems to be specific for Paneth cells and Wnt secretion, as goblet cell numbers, mucin trafficking, packaging and secretion were unaltered[87].

Trafficking and delivery to target membranes is followed by vesicle fusion that requires the SNARE complex, the post-fusion disassembling of which is regulated by the aforementioned factor αSNAP. A pronounced reduction in Paneth cell differentiation was reported in *ex vivo* cultured crypts derived from mice carrying a single amino acid substitution in the *αSNAP* gene leading to its decreased expression in the intestine[88]. These results point to a selective inhibition of terminal differentiation of Paneth cells due to the *αSNAP* gene defect and to a novel functional role for vesicle trafficking and fusion in the regulation of secretory cell fate.

Paneth cells constitute the main epithelial intestinal stem cell niche

The physical association of Paneth cells and *Lgr5*$^{+}$ CBCs at the bottom of the crypt is suggestive of an additional function for this multi-tasking secretory lineage, namely as niche cells capable of regulating the activity of stem cells in homeostasis and during regeneration upon tissue insults. Toshi Sato and collaborators in the Clevers' laboratory noticed that *Lgr5*$^{+}$ stem cells were extremely inefficient when employed to establish *ex vivo* organoids unless co-cultured with Paneth cells, which increased organoid

multiplicity by at least 20-fold[89]. Based on this seminal study, Paneth cells were proposed to represent the main epithelial niche for *Lgr5*$^+$ stem cells.

As discussed above, Wnt and Notch signaling play rate-limiting roles in regulating both stemness and in establishing secretory lineage fate; likewise, a tightly controlled balance between the two pathways is crucial to regulate intestinal homeostasis[90]. Specific Wnt and Notch factors encoded by Paneth cells, namely Wnt3, Dll1, and Dll4 (delta-like ligands 1 and 4), underlie their niche function[89]. The organoid assay (further discussed below) and the possibility of culturing these two cell types *ex vivo* has been instrumental for the identification of these and other key regulatory niche cues[91].

Due to their close physical association with *Lgr5*$^+$ cells, Paneth cells exert their niche function both through secreted short-range factors and by membrane-bound signaling ligands. Moreover, apart from their signalling modalities, Paneth cells provide additional support to *Lgr5*$^+$ stem cells in a contact-dependent manner[92]. Although these requirements are well-established for rapidly cycling *Lgr5*$^+$ CBCs, little is known about the niche requirements of other stem cell types, e.g. the more quiescent stem cells located at position +4.

Additional stem cell niche factors are thought to be secreted by the surrounding stroma. In particular myofibroblasts have been shown to secrete Wnt ligands[93]. Studies on Porcupine (*Porcn*), a gene encoding for an O-acetyltransferase essential for Wnt ligands secretion, showed that its genetic ablation in epithelial cells does not impair intestinal homeostasis and regeneration upon tissue insults. However, concomitant genetic *Porcn* ablation and administration of a specific porcupine inhibitor (C90) leading to impaired Wnt secretion in both the epithelial and stromal compartment, significantly reduced *Lgr5*$^+$ CBCs multiplicity in homeostasis and stalled proliferation and recovery after tissue injury[94]. These studies highlight the relative stromal vs. epithelial contribution in the secretion of Wnt and other ligands known to regulate intestinal stemness and must be taken into consideration when addressing the *in vivo* niche role of Paneth cells. Accordingly, *in vivo* depletion of Paneth cells, as observed in *Sox9* knock-out mice, does not results in any major differentiation defect among the different intestinal epithelial cell lineages[76]. Likewise, deletion of the *Atoh1*/*Math1* gene encoding for a transcription factor necessary for the commitment of secretory lineages, results in a loss of Paneth cells without affecting epithelial morphology and homeostasis[95]. Similar results were obtained by knocking out other genes (e.g. *Gfi1*[83], *Spdef*[96]). However, it is unclear whether the apparent absence of Paneth cells in these mouse models is limited to fully mature PCs or is extended to its immature progenitors which could still exert some of the relevant niche functions. Also, as reported below, Paneth cells are likely to play key roles (both as niche and stem-like cells) in the regeneration of the intestinal epithelium upon inflammation and other forms of tissue injury. As such, mouse models

depleted of Paneth cells should be challenged by inflammatory insults to fully evaluate the consequences of their partial or complete loss.

Paneth cells have mainly been studied in inbred C57BL/6J (B6) mice. This is of relevance as expression of PC-specific genes and pathways may differ among distinct inbred strains and as such differentially affect their secretory, niche, and other functions as illustrated by the case of the secretory phospholipase A2 (*Pla2g2a*). The *Pla2g2a* gene, specifically expressed in Paneth cells, represents a major genetic modifier of intestinal tumor multiplicity in the *Apc*^{Min} mouse model[97,98]. While the C57BL/6J strain carries a *null* secretory phospholipase A2 allele (*Pla2g2a*$^{-/-}$) due to a stop codon mutation, other inbred strains (e.g. FVB, AKR, BALB/C) are *Pla2g2a*-proficient (*Pla2g2a*$^{+/+}$). When bred into the *Apc*$^{Min/+}$ background, B6 animals show a strikingly high multiplicity of upper GI adenomas (approx. 90). In contrast, *Apc*$^{Min/+}$/*Pla2g2a*$^{+/+}$ mice are characterized by a pronounced reduction in intestinal tumor numbers. In a recent study, our laboratory has shown that the intracellular pool of phospholipase A2 downregulates Wnt signaling during homeostasis by modifying the subcellular localization of the yes associated protein 1 (Yap1) protein[99]. Upon inflammation, Pla2g2a is secreted into the lumen from where it activates a cascade of downstream signaling events culminating in the synthesis of prostaglandins and Wnt activation, thus supporting the regenerative response to the inflammatory insults[99].

Overall, it appears that Paneth cells exert their niche function throughout a complex and diverse network of secretory auto- and paracrine pathways and by their physical association with stem cells.

Paneth cells and nutrient sensing: a matter of metabolism?

As mentioned earlier in this chapter, already the first studies on Paneth cells observed a change in their content upon feeding mice with different diets[6,7] thus suggesting a functional connection with metabolism.

Although a set of defined factors including Notch and Wnt stimuli have been proposed to constitute the stem cell niche[89], very little is known about the metabolic requirements of *Lgr5*$^{+}$ CBCs and their niche. More recently, analysis of Paneth and *Lgr5*$^{+}$ cells revealed a striking metabolic dichotomy: while Paneth cells are earmarked by high glycolytic activity, *Lgr5*$^{+}$ CBCs rely on mitochondrial oxidative phosphorylation for their metabolic needs[8]. Notably, Paneth cells, characterized by a high glycolytic activity, secrete lactate which is taken up by the *Lgr5*$^{+}$ stem cells to fuel oxidative phosphorylation. As such, Paneth cells provide a metabolic niche to *Lgr5*$^{+}$ stem cells.

Other studies involving dietary modulation suggested that Paneth cells play a major role in sensing the organism's nutritional status. In particular, Yilmaz et al. showed that, upon longevity-promoting calorie restriction (CR), PCs elicit *Lgr5*$^{+}$ stem cell function by

downregulating mTORC1 (mechanistic target of rapamycin complex 1) signalling[9]. Of note, CR seems to primarily affect Paneth cells but not CBCs.

mTORC1 inhibition in Paneth cells leads to the activation of the ectoenzyme bone stromal antigen 1 (Bst1) which in turn triggers the secretion of cyclic ADP ribose (cADPR). During caloric restriction, this paracrine factor is secreted by PCs and favors stem cell self-renewal eventually resulting in an increase of *Lgr5*$^{+}$ CBCs' multiplicity. This effect could be mimicked *in vivo* by administration of rapamycin, the main mTORC1 pharmacological inhibitor. However, in a subsequent study, Igarashi and Guarente reported a more detailed analysis of the effects of CR with mTORC1 signalling being inhibited in PCs but upregulated in intestinal stem cells[100]. In this scenario, mTORC1 activation is mediated by SIRT1 in *Lgr5*$^{+}$ cells leading to an increase in protein synthesis and an increase in CBC multiplicity. Notably, in this study the *in vivo* administration of rapamycin was shown to abolish CBC expansion rather than mimicking calorie restriction effects[100]. Although a model was proposed where PC signalling could override any direct nutrient sensing in *Lgr5*$^{+}$ CBCs, further studies will be required to elucidate how drugs that modulate CR pathways may exert opposing effects on different cell types.

Culturing intestinal crypts ex vivo as organoids

Seminal work by the laboratories led by H. Clevers and C. Kuo's led to the establishment of novel 3D culture methods for the *ex vivo* culture of mouse intestinal crypts as organoids or "mini-guts", i.e. long-lived and self-renewing structures recapitulating the crypt-villus organization of the intestine and encompassing both *Lgr5*$^{+}$ and Paneth cells as the main units of the stem cell niche, in addition to other differentiated lineages[91,101]. Both methods successfully established long-term epithelial cultures from the small and large intestine by employing matrigel and collagen, respectively. Both studies identified R-spondin, the main ligand of the Lgr5 receptor and a potent canonical Wnt signaling amplifier, as the key growth factor for the successful organoid culture. Other important factors include the epithelial growth factor (EGF) and the Tgf- inhibitor Noggin. Organoid cultures are also partly dependent on the Wnt3A ligand, normally present in the basolateral membrane of Paneth cells[102]. Recently the combination of Wnt3A, R-spondin, and Noggin (WRN) has been found to be sufficient to grow *ex vivo* intestinal organoids from most companion and large animals[103].

The availability of an *ex vivo* culture system that, although in the absence of a mesenchymal/stromal niche support, recapitulates the complex *in vivo* structure of the intestine, stimulated and improved additional studies through the genetic and biochemical modifications of the whole crypt or its specific cell lineage components[8,99,104-106].

As organoids can also be established from patient-derived tumors, biobanks of human 3D cultures are currently being established from tumor material and matched healthy

tissues for several purposes including the preclinical assessment of (chemo) therapeutic approaches, and studies of stem cell tracing and plasticity within neoplastic lesions, tumor heterogeneity and metabolism. The establishment and *in* vitro maintenance of organoids from patient-derived colon cancers requires different and specific factors depending on the tumor subtype, also in reflection of the heterogeneity of the spectrum of malignancies affecting the large bowel[107].

As mentioned before, the main limitation of the currently available organoid culture methods is the lack of an intact stromal microenvironment. Also, since in its original formulation the protocol employs whole intestinal crypts as the biological substrate to establish organoids, this precludes functional studies of specific cell lineages within the stem cell niche, and in particular its two main components, namely the *Lgr5*$^{+}$ CBCs and Paneth cells.

In order to include and preserve the stromal and extracellular matrix (ECM) microenvironment where intestinal crypts normally reside, colonic stroma has been de- and re-cellularized with myofibroblasts, endothelial cells, and epithelial cells (whole organoids or sorted cells)[108]. This approach promises to provide additional insights into the normal gut physiology, not currently feasible with the canonical organoid culture protocol.

As for the second limitation, *Lgr5*$^{+}$ stem cells and PCs tend to physically interact when co-incubated to then give rise to organoids[89]. This key feature is the basis for the "organoid reconstitution assay" (ORA) further developed and implemented by us and others[99,100]. Sorting by FACS of CBCs and PCs allows their genetic and/or biochemical modification (or their isolation from genetically modified or treated mice) prior to their co-incubation and reconstitution into organoids, thus providing a handy functional study tool. A recent example of the usefulness of ORA, is represented by the demonstration of the striking metabolic dichotomy between Paneth cells (glycolytic) and *Lgr5*$^{+}$ stem cells (oxidative phosphorylation) and the functional relevance of these metabolic needs for the maintenance of homeostasis[8].

Paneth cells, dysbiosis, and inflammatory bowel disease

The intestinal microbiome hosts a diverse and abundant group of microorganisms known to be essential for gut homeostasis and development, as shown by studies on germ-free mice. Several environmental factors affect the composition of the microbiome such as diet[109,110], oxygen levels, and pH[111]. In the laboratory mouse, inbred strain-specific variations in the composition of the microbiome have been shown[44], analogous to the observed variations in PCs' multiplicity, distribution, and secretory function[36]. Dysbiosis i.e. the unfavorably altered composition of the microbiota is central to a broad spectrum of human pathologies, among other inflammatory bowel disease (IBD).

The term IBD is comprehensive of two main chronic and relapsing pathologies of the intestinal tract, namely ulcerative colitis (UC) and Crohn's disease (CD)[112]. Like many other pathological conditions such as diabetes, atherosclerosis, obesity, and cancer, IBD is nowadays thought to result from inappropriate inflammatory responses to dysbiosis in genetically susceptible individuals[36]. One of the main differences between UD and CD is the affected region of the gastrointestinal tract. Ulcerative colitis is characterized by chronic inflammation of the colon, initiating in the rectal region and subsequently spreading proximally, with tissue damage usually limited to the mucosa or submucosa featuring local crypt inflammation (*cryptitis*) and abscesses with neutrophilic exudate in the lumen. Crohn's disease instead affects both the large bowel and the distal part of the small intestinal tract, namely the ileum where Paneth cells are more abundant. At the microscopic level, CD's distinctive features include thickening of the submucosa, transmural inflammation, fissuring ulceration and granulomas[112].

As a consequence of the primary role played by Paneth cells in the secretion of antimicrobial peptides and in the control of the gut microbiota during homeostasis, their dysfunction (either due to genetic defects or to environmental 'stressors' such as infections, obesity, and graft versus host disease) has been shown to be causative in a broad spectrum of dysbiosis-associated pathologies, including IBD[36]. The complex multifactorial nature of IBD can be in fact reduced to the interaction of a quartet of host-derived and environmental factors: the genetic predisposition and susceptibility of the host, the intestinal microbiota, the immune system, and the above-mentioned environmental stressors[48].

Genetic susceptibility predisposes the individual to IBD and, likewise, family history does represent a risk factor as shown by genome wide association studies (GWAS). A multitude (>150) of IBD associated single nucleotide polymorphisms (SNPs) have been established as risk loci, 28 of which common to both Crohn's disease and ulcerative colitis. Of note, the very first genes to be identified are not only highly and specifically expressed in Paneth cells but also exert essential roles in PC's secretory function[113,114] including host-bacterial interaction and response (e.g. *NOD2*)[115,116], ER stress and unfolded protein response (*XBP1*)[117], and autophagy (*ATGL16L1*)[118,119].

Nod2 in IBD and Paneth cells

Although its physiological function in the intestine remains elusive, the *Nod2* gene, encoding for a a member of the nucleotide-binding oligomerization domain–leucine-rich repeat (NOD-LRR) family of proteins, is specifically expressed in Paneth cells and is most pronounced in the ileum of both healthy controls and IBD patients[120]. A role in bacterial sensing through innate and adaptive immunity was initially hypothesized and later confirmed by the laboratory of Richard Flavell[121]. Strikingly, Paneth cells from

Nod2-deficient mice were not able to sense specific microbial antigens such as muramyl dipepetide (MDP), a conserved bacterial peptidoglycan. Nevertheless, *Nod2*$^{-/-}$ mice did not display any overt symptoms of intestinal inflammation, and were not significantly susceptible to DSS-induced colitis. However, they were resistant to lipopolysaccharide (i.e. Toll-like receptor agonists) challenge with MDP priming, in confirmation of the role of *Nod2* in sensing and responding to bacterial antigens by activating the adaptive immune system either directly or by enhancing the production of α-defensins[121]. As such, Nod2 is essential to protect the host from intestinal bacterial infection. However, it still remains to be established whether the Paneth cell defect in MDP sensing is the only and even main mechanism through which *Nod2* mutations are related to CD development. Rather than representing the main initiating factor for the disease, *Nod2* gene defects might alter the physiological response to pathogenic bacteria and predispose the individual to CD.

Additional studies in germ-free mice revealed that lack of lysozyme expression also characterizes Paneth cells from *Nod2*$^{-/-}$ mice due to specific lysosomal degradation[122]. When antimicrobial peptides are synthetized in Paneth cells, they are sorted into specialized secretory granules called dense core vesicles (DCV). Accordingly, Nod2 is also recruited to AMP-containing DCVs that, in turn, is required for the DCV localization of the multiprotein kinase Lrkk2 and the GTPase Rab2a[122]. Defects in the Nod2-Lrkk2-Rab2a axis result in the lysosomal degradation of lysozyme[122].

ER stress and unfolded protein response in IBD and Paneth cells

As part of their secretory function, Paneth cells are characterized by a pronounced endoplasmic reticulum and Golgi apparatus, and by large secretory granules. As such, they act as protein factories responsible for the synthesis of many proteins with antimicrobial and essential for intestinal homeostasis. In secretory cells, nascent proteins enter the ER as unfolded polypeptide chains to complete folding and maturation. The folding capacity of the ER of secretory cells is targeted on the rate of nascent proteins entering the ER. Specific sensors monitor the ER lumen and signal to other cellular components. Whenever the rate of unfolded nascent proteins exceeds the folding capacity of the ER, a condition known as ER stress, the unfolded protein response (UPR) is triggered[123]. In this process, the molecular sensor and ER chaperone immunoglobulin binding protein B (BIP, HSPA5, or GRP78) plays a central role. During homeostatic conditions BIP is bound to the luminal side of three master regulators of the UPR response, namely transmembrane proteins inositol requiring 1 (IRE1), PKR-like ER kinase (PERK), and activating transcription factor 6 (ATF6). Upon ER stress activation, BIP dissociates from these sensors thus triggering their activation. The downstream pathways involve, among others, the Paneth-specific transcription factor X-box-binding protein-1 (XBP1) whose mRNA is converted upon ER

stress to an active form by the IRE-1 nuclease. This leads to the modulation of protein synthesis to adapt the ER folding capacity to the specific requirements of the cell. Whenever ER stress is not solved, apoptosis is triggered[123-124].

Paneth cells, as many secretory cells, are characterized by a basal ER stress level. Of note, the small intestine is the only tissue reported to date to express an isoform (IRE1β) of the proximal sensor IRE1[125]. Remarkably, in *Xbp1* knock-out mice ER stress was detected in the intestinal epithelium through GRP78 upregulation in association with an inflammatory phenotype reminiscent of human IBD with crypt abscesses, ulcerations, and leukocyte infiltration[117]. Furthermore, Paneth cell with normal granules were barely detectable together with a substantially decreased expression of cryptdins 1, 4 and 5. Also, Paneth cell apoptosis, most likely triggered by the failure of solving ER stress, was a feature of *Xbp1* genetic ablation. Last, *Xbp1* knock-out mice were more susceptible to infection by gram-positive bacteria and to DSS-induced colitis.

Autophagy in IBD and Paneth cells

The term autophagy refers to the natural process through which cellular components like organelles or large protein complexes which cannot be removed by the proteasome, are degraded and recycled in orderly and regulated fashion through the lysosome. Although the original function of autophagy is likely to have arisen as an adaptation to starvation or nutrient deprivation, it has evolved as a quality control process for organelles and proteins and to regulate energy homeostasis[126]. Moreover, it is also employed by the cell to degrade microorganisms (also referred to as xenophagy), as shown by the increased susceptibility to infections caused by intracellular pathogens upon mutation of autophagy genes[127]. Autophagy can also be selective when it triggers the degradation of specific damaged organelles, such as mitochondria or peroxisomes.

The formation of autophagic vesicles earmarks autophagy[128] and is dependent on the translocation of the mTOR substrate complex from the cytosol to the ER. Through recruitment of PI3 kinases to the ER, vesicle formation and elongation is started. The final stage of this process is mediated by a number of autophagy (Atg)-related proteins, namely, Atg12, Atg5 and Atg16, which form a complex with Atg8 and phospholipid phosphoethanolamine (PE), that catalyzes further elongation and maturation of the autophagic vesicles. Once mature, they are transported to lysosomes where they undergo degradation.

The autophagy machinery interfaces with cellular stress and response pathways, including those controlling immune responses and, in turn, inflammation. Large autophagic vesicles were observed to be prominent in Paneth cells after irradiation[129]. Several mice carrying hypomorhic variants of different *Atg* genes (i.e. *Atg16*, *Atg5*, and *Atg7*) were characterized by apparently mature Paneth cells though with secretory

granules decreased in size and numbers[119]. Defects in granules exocytosis leading to decreased AMP secretion into the lumen and differences in microbiome composition were also reported in these mice[119].

Several defects in autophagy, autophagy-related genes, and Paneth cell morphology have been observed in IBD patients[130]. As previously mentioned, single nucleotide polymorphisms in the *ATG* and related genes were found by GWAS to predispose to IBD[118,119,131]. More recently, a seminal study by Adolph et al. has functionally linked ER stress and autophagy in a specific cell type, the Paneth cell[132]. Here, mouse models were developed that were defective in the *Xbp1* gene in the small intestine. Upon induction of ER stress in the intestinal epithelium, autophagy was observed mostly at the bottom of the crypts where Paneth cells reside. To assess whether autophagy was induced to ameliorate ER stress, mice defective in both *Xbp1* and *Atg16L1* (or *Atg7*) in intestinal epithelium specific fashion[132]. These mice lacked UPR-induced autophagy resulting in constitutive ER stress in the absence of autophagy. Notably, the intestines of the double-mutant mice featured a strong inflammatory reaction with tissue damage reminiscent of Crohn's disease. In view of the potent autophagy induction in *Xbp1* defective mice at the bottom of the crypts, Paneth cells are likely to be the culprit of the CD-like phenotype of these mice. Indeed, Paneth-specific ablation of *Xbp1* and *Atg16L1* (or *Atg7*) recapitulated the phenotype of the above mice where the same genes were inhibited in the whole intestinal epithelium, thus providing additional experimental evidence for Paneth cells as the cellular site where ER stress and autophagy are functionally linked and as the origin of intestinal inflammation in IBD cases linked to ATG and ER stress loci[132]. As for the molecular mechanisms underlying the autophagy-driven amelioration of ER stress, upregulation of the NF-κB pathway was observed in the double-mutant mice. Accordingly, use of an NF-κB inhibitor led to a decrease in the overall number of cells undergoing apoptosis and a partial reversion of the inflammatory phenotype caused by the combined *Xbp1* and *Atg16L1* genetic deletion. Notably, NF-κB activation upon concomitant loss of *Xbp1* and *Atg16L1* function was not observed in germ-free mice again highlighting the relevance of the microbiome in these experimental settings and providing a suggestive functional connection between ER stress, autophagy and the microbiome in IBD[132].

The above findings open novel therapeutic scenarios for IBD patients, as illustrated by the use of NF-κB inhibitors to ameliorate and possibly resolve inflammation. Moreover, patients without single nucleotide polymorphisms in *Atg*-related genes, autophagy could be stimulated by treatment with rapamycin and mimicking caloric restriction[9]. Also, it is well-established that IBD patients carry an increased risk to colon cancer. From this perspective, the notion that Paneth cells are the site of origin of inflammation may also have implications for IBD-associated colon cancers in view of previous observations pointing at the capacity of PCs and their progenitors to de-differentiate and take active

part in the regenerative response to tissue damage[62]. Further studies will be required to elucidate whether Paneth cells might also represent the cell of origin of IBD-associated colorectal cancer.

The role of immunity and environmental factors

The immune system plays important roles in IBD in response to bacterial antigens, proteins and RNA. Innate or in-born immunity is a pre-requisite for the activation of the adaptive immunity which in turn seems to be causative for the tissue damage in IBD. Animal models of IBD, along with a more detailed understanding of the immune response in the digestive tract, have led to an unifying hypothesis relative to the role of the immune system in IBD. An inappropriate mucosal immune response to normal intestinal components leads to a local imbalance in cytokines resulting in a neutrophil and monocyte influx with subsequent secretion of oxygen radicals and enzymes, leading to tissue damage[133].

The incomplete penetrance of IBD animal models and the heterogeneity of the disease can be accounted for by additional environmental factors. Several epidemiological studies have shown increased IBD risk in migrants from countries at low to high risk countries[134]. Furthermore, since the 19th century the incidence of IBD has steadily increased in westernized countries[134]. Diet and vitamin D intake are supposedly additional modifying risk factors to IBD. Low dietary fiber intake is associated with increased IBD risk as fibers are metabolized by bacteria into short chain fatty acids that inhibit transcription of pro-inflammatory mediators[135,136]. Furthermore low zinc intake might impair autophagy and modulate immune functions[137,138]. Additional factors correlated with higher risk of developing IBD are lack of exercise and sleep although more experimental evidence is needed to link the latter functionally to IBD[139].

Paneth cells as IBD-specific disease markers

The broad range of processes coming together in IBD is indicative of the complexity and heterogeneity of the disease. In view of their striking multi-functionality ranging from the secretory and bactericidal function to innate gut immunity, Paneth cells seem to be endowed with the capacity to integrate cues from dietary nutrients and the microbiota, and translate them in to stem cell niche regulatory signals in homeostasis and tissue regeneration. Accordingly, changes in Paneth cells numbers and/or morphology or mutations in PC-specific genes underlie the etiology of at least a subset of IBD cases[130]. Stappenbeck and McGovern have proposed a classification of CD subtypes based on the detailed characterization of Paneth cell morphology (granules size and numbers) and IHC staining of AMPs like lysozyme (Lyz1) and defensins[130]. In this fashion Paneth cells can be studied retrospectively in archival resection specimens or from biopsies collected via endoscopy.

Paneth cells as stem cell niche in inflammation

The stem cell niche role of Paneth cells has been mostly studied in homeostasis and little is known on their function upon inflammation. Several reports suggest a decrease in mature Paneth cells' multiplicity in inflammation. One of the genes responsible for the incomplete maturation of Paneth cells in inflammation is protein kinase C iota or (*Prcki*). *Prcki* ablation in the intestinal epithelium did not affect Paneth cell number and granules. However, the PC-specific marker lysozyme was shown to co-localize with alcian blue positive cells characteristic of the goblet lineage. Hence, inflammation triggers Paneth cell de-differentiation to acquire an intermediate secretory precursor of both Paneth and goblet cells[140]. Expression analysis of PRCKI in IBD patients revealed an inverse correlation with disease progression[140].

The secretory phospholipase A2 group 2a (*Pla2g2a*) gene was shown to be able to modify and improve the Paneth cell niche function upon inflammation[99]. Contrary to the role of *Pla2g2a* in homeostasis where the protein downregulates Wnt signaling in Paneth cells, gene- and protein-based assays showed highly increased *Pla2g2a* expression and secretion upon inflammation leading to an increase in canonical Wnt in Paneth cells. When secreted, Pla2g2a, next to exerting its antibacterial function, binds to the M-type phospholipase A2 receptor 1 (Pla2R1). This interaction triggers an autocrine cascade of downstream events culminating in increased Wnt signaling and improved regenerative response to the inflammatory tissue damage[99]. These observations open new therapeutic options by stimulating Paneth cell functions in IBD to improve tissue regeneration[99].

CONCLUSIVE REMARKS

Multi-tasking Paneth cells in health and disease

The strikingly broad spectrum of functions covered by Paneth cells is reflected by the plethora of molecular and cellular mechanisms through which these secretory cells have been linked to several human pathological conditions related to dysbiosis, from obesity to graft versus host disease, inflammation, and cancer. The more recently elucidated niche role of Paneth cells in supporting and modulating intestinal stem cell function possibly represents the integration hub of their multiple tasks. By sensing environmetal factors like dietary changes and/or inflammatory stimuli, PCs seem to be capable of translating them into modifications of stem cell numbers, activity, and regenerative capacity. This is achieved either directly or indirectly by coordinated stress sensors such as UPR, ER stress, autophagy, and possibly many others. And yet, we are possibly only scratching the surface of the true functional identity of PCs. Many fascinating aspects remain unsolved: what is, if any, the functional role of Paneth cell metaplasia in colonic

inflammation and cancer? Can mature Paneth cells and their secretory precursors, next to their niche funtion, directly contribute to the regenerative response to tissue insults by de-differentiating and acquiring stem-like properties? Analogous to their regulatory role in response to caloric restrictions, can Paneth-like cells located in the colon alter their metabolic needs and niche functions upon Western-style nutrients known to increase colon cancer risk? Ongoing and future studies will contribute to the elucidation of these and other questions and possibly lead to PC-tailored therapeutic strategies for IBD and GI-tract cancer patients.

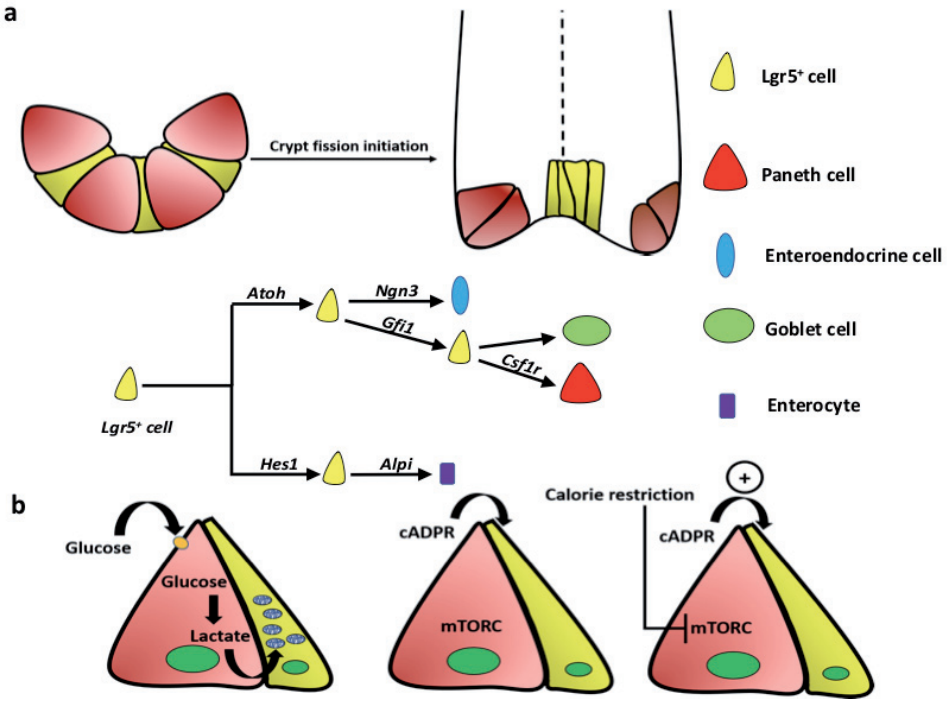

Figure 1. (A) At the bottom of the crypt of Lieberku€hn, Paneth cells (brown) and Lgr5+ stem cells (yellow) cluster away upon crypt fission initiation (Langlands et al., 2016). The increased stiffness of Paneth cells forms harder regions on the sides of the branching crypt, in contrast with the "softer" Lgr5+ stem cells positioned in the center. (B) Schematic diagram of the differentiation fates of the Lgr5+ stem cell and the genes that underlie the specific commitment steps. (C) Left: Paneth cells (brown) sustain the metabolism of Lgr5+ cells by using glucose as a substrate to secrete lactate that, during homeostasis, fuels oxidative phosphorylation in Lgr5+ stem cells. Center and right: mTORC1 inhibition in Paneth cells leads to the secretion of cyclic ADP ribose (cADPR). During caloric restriction, mTORC1 is inhibited in Paneth cells leading the enhanced cADPR secretion and increased Lgr5+ stem cell self-renewal and multiplicity

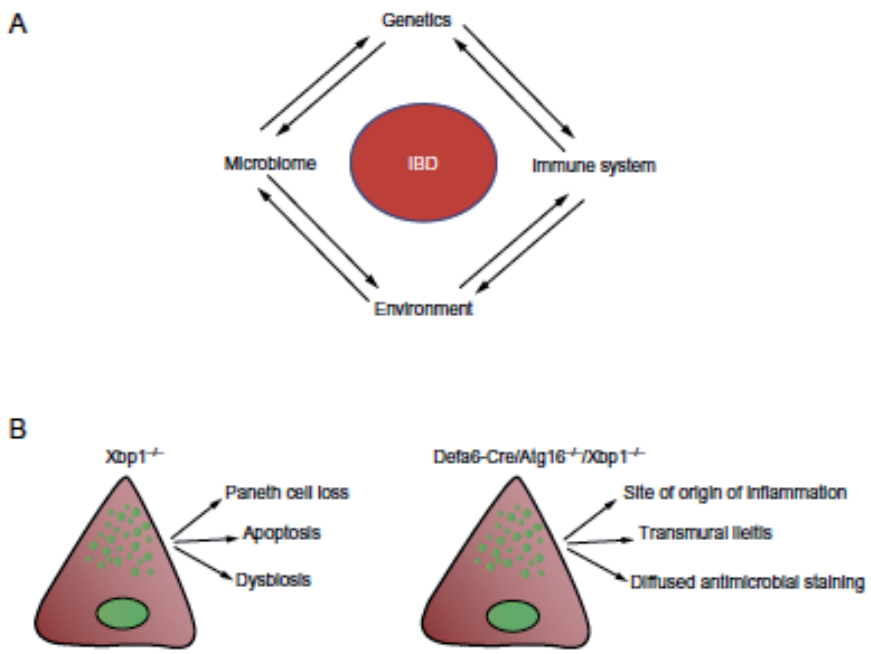

Figure 2. (A) Inflammatory bowel disease (IBD) is a complex multifactorial disease dominated by four major cross-interacting components, namely the genetic background of the host, the gut microbiome, the host's immune system, and the environment.
(B) Genetic depletion of the Xbp1 gene encoding for a key ER stress response proteincauses Paneth cell loss, increased apoptosis, and dysbiosis. Combined genetic loss of the Xbp1 and Atg16 genes in Paneth cells results in diffused lysozyme staining reminiscent of IBD and transmural ileitis, suggesting that PCs represent the site of origin of intestinal inflammation (Adolph et al., 2013).

REFERENCES

1 Schwalbe, G. Beitriage zur Kenntniss der Driisen in den Darmwandungen, in's Besondere der Brunner'schen Driisen. *Arch. f. mikr. Anat.* 8, 92-144 (I872).

2 J., P. Ueber die secernirenden Zellen des Dunndarm-Epithels. *Arch. f. mikr. Anat.* 31, 113-191 (1888).

3 Möller, W. Anatomische Beitrage zur Frage von der Sekretion und Resorption in der Darmschleimhaut. *Ztschr. f. wissensch. Zool.* 66, 69-135 (1899).

4 Bizzozero, G. Ueber die schlauchförmigen Druisen des Magendarmkanals und die Beziehungen ihres Epithels zu dem Oberflachenepithel der Schleimhaut. . 40, 325-375. (1892).

5 S, K. On the Nature of the Granule cells of Paneth in the intestinal glands of mammals. *Am. J. Anat.* 5, 315-330 (1906).

6 Georges, M. Recherches cytologiques et experimentales sur les cellules de Paneth (souris). *Arch. de biol.* 40, 111-150 (I930).

7 Cowdry, E. V. A Textbook of Histology. Functional Significance of Cells and Intercellular Substances. *Lea and Febiger* (1934).

8 Rodriguez-Colman, M. J. *et al.* Interplay between metabolic identities in the intestinal crypt supports stem cell function. *Nature* 543, 424-427, doi:10.1038/nature21673 (2017).

9 Yilmaz, O. H. *et al.* mTORC1 in the Paneth cell niche couples intestinal stem-cell function to calorie intake. *Nature* 486, 490-495, doi:nature11163 [pii] 10.1038/nature11163 (2012).

10 Hertzog, A. J. The Paneth Cell. *Am J Pathol* 13, 351-360 351 (1937).

11 Creamer, B. & Pink, I. J. Paneth-cell deficiency. *Lancet* 1, 304-306 (1967).

12 Creamer, B. Paneth-cell function. *Lancet* 1, 314-316 (1967).

13 Creamer, B. The turnover of the epithelium of the small intestine. *Br Med Bull* 23, 226-230 (1967).

14 Trier, J. S. The Paneth cells: an enigma. *Gastroenterology* 51, 560-562 (1966).

15 Trier, J. S. Structure of the mucosa of the small intestine as it relates to intestinal function. *Fed Proc* 26, 1391-1404 (1967).

16 Lewin, K. The Paneth cell in health and disease. *Ann R Coll Surg Engl* 44, 23-37 (1969).

17 Lewin, K. The Paneth cell in disease. *Gut* 10, 804-811 (1969).

18 Lewin, K. Histochemical observations on Paneth cells. *J Anat* 105, 171-176 (1969).

19 Lewin, K. Neoplastic Paneth cells. *J Clin Pathol* 21, 476-479 (1968).

20 Paterson, J. C. & Watson, S. H. Paneth cell metaplasia in ulcerative colitis. *Am J Pathol* 38, 243-249 (1961).

21 Symonds, D. A. Paneth cell metaplasia in diseases of the colon and rectum. *Arch Pathol* 97, 343-347 (1974).

22 Cheng, H. Origin, differentiation and renewal of the four main epithelial cell types in the mouse small intestine. IV. Paneth cells. *Am J Anat* 141, 521-535, doi:10.1002/aja.1001410406 (1974).

23 Deckx, R. J., Vantrappen, G. R. & Parein, M. M. Localization of lysozyme activity in a Paneth cell granule fraction. *Biochim Biophys Acta* 139, 204-207 (1967).

24 Senegas-Balas, F. *et al.* Immunohistochemical localization of intestinal phospholipase A2 in rat paneth cells. *Histochemistry* 81, 581-584 (1984).

25 Ouellette, A. J. & Cordell, B. Accumulation of abundant messenger ribonucleic acids during postnatal development of mouse small intestine. *Gastroenterology* 94, 114-121 (1988).

26 Ouellette, A. J., Miller, S. I., Henschen, A. H. & Selsted, M. E. Purification and primary structure of murine cryptdin-1, a Paneth cell defensin. *FEBS Lett* 304, 146-148 (1992).

27 Ayabe, T. *et al.* Secretion of microbicidal alpha-defensins by intestinal Paneth cells in response to bacteria. *Nat Immunol* 1, 113-118, doi:10.1038/77783 (2000).

28 Satoh, Y. Atropine inhibits the degranulation of Paneth cells in ex-germ-free mice. *Cell Tissue Res* 253, 397-402 (1988).

29 Qu, X. D., Lloyd, K. C., Walsh, J. H. & Lehrer, R. I. Secretion of type II phospholipase A2 and cryptdin by rat small intestinal Paneth cells. *Infect Immun* 64, 5161-5165 (1996).

30 Rumio, C. *et al.* Degranulation of paneth cells via toll-like receptor 9. *Am J Pathol* 165, 373-381, doi:10.1016/S0002-9440(10)63304-4 (2004).

31 Rumio, C. *et al.* Induction of Paneth cell degranulation by orally administered Toll-like receptor ligands. *J Cell Physiol* 227, 1107-1113, doi:10.1002/jcp.22830 (2012).

32 Farin, H. F. *et al.* Paneth cell extrusion and release of antimicrobial products is directly controlled by immune cell-derived IFN-gamma. *J Exp Med* 211, 1393-1405, doi:10.1084/jem.20130753 (2014).

33 Satoh, Y., Habara, Y., Ono, K. & Kanno, T. Carbamylcholine- and catecholamine-induced intracellular calcium dynamics of epithelial cells in mouse ileal crypts. *Gastroenterology* 108, 1345-1356 (1995).

34 Ayabe, T. *et al.* Modulation of mouse Paneth cell alpha-defensin secretion by mIKCa1, a Ca2+-activated, intermediate conductance potassium channel. *J Biol Chem* 277, 3793-3800, doi:10.1074/jbc.M107507200 (2002).

35 Vaishnava, S., Behrendt, C. L., Ismail, A. S., Eckmann, L. & Hooper, L. V. Paneth cells directly sense gut commensals and maintain homeostasis at the intestinal host-microbial interface. *Proc Natl Acad Sci U S A* 105, 20858-20863, doi:10.1073/pnas.0808723105 (2008).

36 Salzman, N. H. & Bevins, C. L. Dysbiosis--a consequence of Paneth cell dysfunction. *Semin Immunol* 25, 334-341, doi:10.1016/j.smim.2013.09.006 (2013).

37 Candela, M. *et al.* Human intestinal microbiota: cross-talk with the host and its potential role in colorectal cancer. *Crit Rev Microbiol* 37, 1-14, doi:10.3109/1040841X.2010.501760 (2011).

38 Turnbaugh, P. J. *et al.* An obesity-associated gut microbiome with increased capacity for energy harvest. *Nature* 444, 1027-1031, doi:10.1038/nature05414 (2006).

39 Dumas, M. E. *et al.* Metabolic profiling reveals a contribution of gut microbiota to fatty liver phenotype in insulin-resistant mice. *Proc Natl Acad Sci U S A* 103, 12511-12516, doi:10.1073/pnas.0601056103 (2006).

40 Koren, O. *et al.* Human oral, gut, and plaque microbiota in patients with atherosclerosis. *Proc Natl Acad Sci U S A* 108 Suppl 1, 4592-4598, doi:10.1073/pnas.1011383107 (2011).

41 Karlsson, F. H. *et al.* Symptomatic atherosclerosis is associated with an altered gut metagenome. *Nat Commun* 3, 1245, doi:10.1038/ncomms2266 (2012).

42 Amid, C. *et al.* Manual annotation and analysis of the defensin gene cluster in the C57BL/6J mouse reference genome. *BMC Genomics* 10, 606, doi:10.1186/1471-2164-10-606 (2009).

43 Shanahan, M. T., Tanabe, H. & Ouellette, A. J. Strain-specific polymorphisms in Paneth cell alpha-defensins of C57BL/6 mice and evidence of vestigial myeloid alpha-defensin pseudogenes. *Infect Immun* 79, 459-473, doi:10.1128/IAI.00996-10 (2011).

44 Gulati, A. S. *et al.* Mouse background strain profoundly influences Paneth cell function and intestinal microbial composition. *PloS one* 7, e32403, doi:10.1371/journal.pone.0032403 (2012).

45 Ouellette, A. J. Paneth cell alpha-defensins in enteric innate immunity. *Cell Mol Life Sci* 68, 2215-2229, doi:10.1007/s00018-011-0714-6 (2011).

46 Jones, D. E. & Bevins, C. L. Paneth cells of the human small intestine express an antimicrobial peptide gene. *J Biol Chem* 267, 23216-23225 (1992).

47 Jones, D. E. & Bevins, C. L. Defensin-6 mRNA in human Paneth cells: implications for antimicrobial peptides in host defense of the human bowel. *FEBS Lett* 315, 187-192 (1993).

48 Clevers, H. C. & Bevins, C. L. Paneth cells: maestros of the small intestinal crypts. *Annu Rev Physiol* 75, 289-311, doi:10.1146/annurev-physiol-030212-183744 (2013).

49 Bevins, C. L. Innate immune functions of alpha-defensins in the small intestine. *Dig Dis* 31, 299-304, doi:10.1159/000354681 (2013).

50 Lehrer, R. I. & Lu, W. alpha-Defensins in human innate immunity. *Immunol Rev* 245, 84-112, doi:10.1111/j.1600-065X.2011.01082.x (2012).

51 Barker, N. *et al.* Identification of stem cells in small intestine and colon by marker gene Lgr5. *Nature* 449, 1003-1007 (2007).

52 Snippert, H. J. *et al.* Intestinal crypt homeostasis results from neutral competition between symmetrically dividing Lgr5 stem cells. *Cell* 143, 134-144, doi:10.1016/j.cell.2010.09.016 (2010).

53 Fuchs, E. The tortoise and the hair: slow-cycling cells in the stem cell race. *Cell* 137, 811-819, doi:10.1016/j.cell.2009.05.002 (2009).

54 Potten, C. S., Kovacs, L. & Hamilton, E. Continuous labelling studies on mouse skin and intestine. *Cell Tissue Kinet* 7, 271-283 (1974).

55 Sangiorgi, E. & Capecchi, M. R. Bmi1 is expressed in vivo in intestinal stem cells. *Nat Genet* 40, 915-920, doi:10.1038/ng.165 (2008).

56 Carlone, D. L. & Breault, D. T. Slowly cycling versus rapidly cycling intestinal stem cells: distinct roles or redundancy. *Cell Cycle* 10, 723-724, doi:10.4161/cc.10.5.14867 (2011).

57 Powell, A. E. *et al.* The pan-ErbB negative regulator Lrig1 is an intestinal stem cell marker that functions as a tumor suppressor. *Cell* 149, 146-158, doi:10.1016/j.cell.2012.02.042 (2012).

58 Takeda, N. *et al.* Interconversion between intestinal stem cell populations in distinct niches. *Science (New York, N.Y* 334, 1420-1424, doi:10.1126/science.1213214 (2011).

59 Munoz, J. *et al.* The Lgr5 intestinal stem cell signature: robust expression of proposed quiescent '+4' cell markers. *EMBO J* 31, 3079-3091, doi:10.1038/emboj.2012.166 (2012).

60 Barriga, F. M. *et al.* Mex3a Marks a Slowly Dividing Subpopulation of Lgr5+ Intestinal Stem Cells. *Cell Stem Cell*, doi:10.1016/j.stem.2017.02.007 (2017).

61 Yan, K. S. *et al.* The intestinal stem cell markers Bmi1 and Lgr5 identify two functionally distinct populations. *Proc Natl Acad Sci U S A* 109, 466-471, doi:10.1073/pnas.1118857109 (2012).

62 Roth, S. *et al.* Paneth cells in intestinal homeostasis and tissue injury. *PloS one* 7, e38965, doi:10.1371/journal.pone.0038965 PONE-D-12-10735 [pii] (2012).

63 Tetteh, P. W. *et al.* Replacement of Lost Lgr5-Positive Stem Cells through Plasticity of Their Enterocyte-Lineage Daughters. *Cell Stem Cell* 18, 203-213, doi:10.1016/j.stem.2016.01.001 (2016).

64 Noah, T. K., Donahue, B. & Shroyer, N. F. Intestinal development and differentiation. *Exp Cell Res* 317, 2702-2710, doi:10.1016/j.yexcr.2011.09.006 (2011).

65 Zorn, A. M. & Wells, J. M. Vertebrate endoderm development and organ formation. *Annu Rev Cell Dev Biol* 25, 221-251, doi:10.1146/annurev.cellbio.042308.113344 (2009).

66 Darmoul, D., Brown, D., Selsted, M. E. & Ouellette, A. J. Cryptdin gene expression in developing mouse small intestine. *Am J Physiol* 272, G197-206 (1997).

67 Clarke, R. M. The effect of growth and of fasting on the number of villi and crypts in the small intestine of the albino rat. *J Anat* 112, 27-33 (1972).

68 St Clair, W. H. & Osborne, J. W. Crypt fission and crypt number in the small and large bowel of postnatal rats. *Cell Tissue Kinet* 18, 255-262 (1985).

69 Langlands, A. J. *et al.* Paneth Cell-Rich Regions Separated by a Cluster of Lgr5+ Cells Initiate Crypt Fission in the Intestinal Stem Cell Niche. *PLoS Biol* 14, e1002491, doi:10.1371/journal.pbio.1002491 (2016).

70 Batlle, E. *et al.* Beta-catenin and TCF mediate cell positioning in the intestinal epithelium by controlling the expression of EphB/ephrinB. *Cell* 111, 251-263 (2002).

71 van de Wetering, M. *et al.* The beta-catenin/TCF-4 complex imposes a crypt progenitor phenotype on colorectal cancer cells. *Cell* 111, 241-250 (2002).

72 Stamos, J. L. & Weis, W. I. The beta-catenin destruction complex. *Cold Spring Harbor perspectives in biology* 5, a007898 (2013).

73 van Es, J. H. *et al.* Wnt signalling induces maturation of Paneth cells in intestinal crypts. *Nature cell biology* 7, 381-386 (2005).

74 Farin, H. F., Van Es, J. H. & Clevers, H. Redundant sources of Wnt regulate intestinal stem cells and promote formation of Paneth cells. *Gastroenterology* 143, 1518-1529 e1517, doi:10.1053/j.gastro.2012.08.031 (2012).

75 Mustata, R. C. *et al.* Lgr4 is required for Paneth cell differentiation and maintenance of intestinal stem cells ex vivo. *EMBO Rep* 12, 558-564, doi:10.1038/embor.2011.52 (2011).

76 Mori-Akiyama, Y. *et al.* SOX9 is required for the differentiation of paneth cells in the intestinal epithelium. *Gastroenterology* 133, 539-546, doi:10.1053/j.gastro.2007.05.020 (2007).

77 Bastide, P. *et al.* Sox9 regulates cell proliferation and is required for Paneth cell differentiation in the intestinal epithelium. *J Cell Biol* 178, 635-648, doi:10.1083/jcb.200704152 (2007).

78 Feng, Y. *et al.* Sox9 induction, ectopic Paneth cells, and mitotic spindle axis defects in mouse colon adenomatous epithelium arising from conditional biallelic Apc inactivation. *Am J Pathol* 183, 493-503, doi:10.1016/j.ajpath.2013.04.013 (2013).

79 Yang, Q., Bermingham, N. A., Finegold, M. J. & Zoghbi, H. Y. Requirement of Math1 for secretory cell lineage commitment in the mouse intestine. *Science (New York, N.Y* 294, 2155-2158, doi:10.1126/science.1065718 (2001).

80 Shroyer, N. F. *et al.* Intestine-specific ablation of mouse atonal homolog 1 (Math1) reveals a role in cellular homeostasis. *Gastroenterology* 132, 2478-2488, doi:10.1053/j.gastro.2007.03.047 (2007).

81 Fre, S. *et al.* Notch signals control the fate of immature progenitor cells in the intestine. *Nature* 435, 964-968, doi:10.1038/nature03589 (2005).

82 VanDussen, K. L. *et al.* Notch signaling modulates proliferation and differentiation of intestinal crypt base columnar stem cells. *Development* 139, 488-497, doi:10.1242/dev.070763 (2012).

83 Shroyer, N. F., Wallis, D., Venken, K. J., Bellen, H. J. & Zoghbi, H. Y. Gfi1 functions downstream of Math1 to control intestinal secretory cell subtype allocation and differentiation. *Genes Dev* 19, 2412-2417, doi:10.1101/gad.1353905 (2005).

84 Huynh, D. *et al.* Colony stimulating factor-1 dependence of paneth cell development in the mouse small intestine. *Gastroenterology* 137, 136-144, 144 e131-133, doi:10.1053/j.gastro.2009.03.004 (2009).

85 Huynh, D. *et al.* CSF-1 receptor-dependent colon development, homeostasis and inflammatory stress response. *PloS one* 8, e56951, doi:10.1371/journal.pone.0056951 (2013).

86 Akcora, D. *et al.* The CSF-1 receptor fashions the intestinal stem cell niche. *Stem Cell Res* 10, 203-212, doi:10.1016/j.scr.2012.12.001 (2013).

87 Das, S. *et al.* Rab8a vesicles regulate Wnt ligand delivery and Paneth cell maturation at the intestinal stem cell niche. *Development* 142, 2147-2162, doi:10.1242/dev.121046 (2015).

88 Lechuga, S., Naydenov, N. G., Feygin, A., Jimenez, A. J. & Ivanov, A. I. A vesicle trafficking protein alphaSNAP regulates Paneth cell differentiation in vivo. *Biochem Biophys Res Commun* 486, 951-957, doi:10.1016/j.bbrc.2017.03.135 (2017).

89 Sato, T. *et al.* Paneth cells constitute the niche for Lgr5 stem cells in intestinal crypts. *Nature* 469, 415-418 (2011).

90 Tian, H. *et al.* Opposing activities of Notch and Wnt signaling regulate intestinal stem cells and gut homeostasis. *Cell Rep* 11, 33-42, doi:10.1016/j.celrep.2015.03.007 (2015).

91 Sato, T. *et al.* Single Lgr5 stem cells build crypt-villus structures in vitro without a mesenchymal niche. *Nature* 459, 262-265 (2009).

92 Gracz, A. D. *et al.* A high-throughput platform for stem cell niche co-cultures and downstream gene expression analysis. *Nature cell biology* 17, 340-349, doi:10.1038/ncb3104 (2015).

93 Vermeulen, L. *et al.* Wnt activity defines colon cancer stem cells and is regulated by the microenvironment. *Nat Cell Biol* 12, 468-476, doi:10.1038/ncb2048 (2010).

94 Kabiri, Z. *et al.* Stroma provides an intestinal stem cell niche in the absence of epithelial Wnts. *Development* 141, 2206-2215, doi:10.1242/dev.104976 (2014).

95 Durand, A. *et al.* Functional intestinal stem cells after Paneth cell ablation induced by the loss of transcription factor Math1 (Atoh1). *Proc Natl Acad Sci U S A* 109, 8965-8970, doi:10.1073/pnas.1201652109 (2012).

96 Gregorieff, A. *et al.* The ets-domain transcription factor Spdef promotes maturation of goblet and paneth cells in the intestinal epithelium. *Gastroenterology* 137, 1333-1345 e1331-1333, doi:10.1053/j.gastro.2009.06.044 (2009).

97 Dietrich, W. F. *et al.* Genetic identification of Mom-1, a major modifier locus affecting Min-induced intestinal neoplasia in the mouse. *Cell* 75, 631-639 (1993).

98 MacPhee, M. *et al.* The secretory phospholipase A2 gene is a candidate for the Mom1 locus, a major modifier of ApcMin-induced intestinal neoplasia. *Cell* 81, 957-966 (1995).

99 Schewe, M. *et al.* Secreted Phospholipases A2 Are Intestinal Stem Cell Niche Factors with Distinct Roles in Homeostasis, Inflammation, and Cancer. *Cell Stem Cell* 19, 38-51 (2016).

100 Igarashi, M. & Guarente, L. mTORC1 and SIRT1 Cooperate to Foster Expansion of Gut Adult Stem Cells during Calorie Restriction. *Cell* 166, 436-450, doi:S0092-8674(16)30595-5 [pii] 10.1016/j.cell.2016.05.044 (2016).

101 Ootani, A. *et al.* Sustained in vitro intestinal epithelial culture within a Wnt-dependent stem cell niche. *Nat Med* 15, 701-706, doi:10.1038/nm.1951 (2009).

102 Farin, H. F. *et al.* Visualization of a short-range Wnt gradient in the intestinal stem-cell niche. *Nature* 530, 340-343, doi:10.1038/nature16937 (2016).

103 Powell, R. H. & Behnke, M. S. WRN conditioned media is sufficient for in vitro propagation of intestinal organoids from large farm and small companion animals. *Biol Open*, doi:10.1242/bio.021717 (2017).

104 Koo, B. K. *et al.* Controlled gene expression in primary Lgr5 organoid cultures. *Nat Methods* 9, 81-83, doi:10.1038/nmeth.1802 (2011).

105 Andersson-Rolf, A. *et al.* Simultaneous paralogue knockout using a CRISPR-concatemer in mouse small intestinal organoids. *Dev Biol* 420, 271-277, doi:10.1016/j.ydbio.2016.10.016 (2016).

106 Andersson-Rolf, A. *et al.* One-step generation of conditional and reversible gene knockouts. *Nat Methods* 14, 287-289, doi:10.1038/nmeth.4156 (2017).

107 Fujii, M. *et al.* A Colorectal Tumor Organoid Library Demonstrates Progressive Loss of Niche Factor Requirements during Tumorigenesis. *Cell Stem Cell* 18, 827-838, doi:10.1016/j.stem.2016.04.003 (2016).

108 Chen, H. J. *et al.* A recellularized human colon model identifies cancer driver genes. *Nat Biotechnol* 34, 845-851, doi:10.1038/nbt.3586 (2016).

109 Claesson, M. J. *et al.* Gut microbiota composition correlates with diet and health in the elderly. *Nature* 488, 178-184 (2012).

110 Wu, G. D. *et al.* Linking long-term dietary patterns with gut microbial enterotypes. *Science (New York, N.Y* 334, 105-108 (2011).

111 Bevins, C. L. & Salzman, N. H. The potter's wheel: the host's role in sculpting its microbiota. *Cell Mol Life Sci* 68, 3675-3685 (2011).

112 Kaser, A., Zeissig, S. & Blumberg, R. S. Inflammatory bowel disease. *Annu Rev Immunol* 28, 573-621, doi:10.1146/annurev-immunol-030409-101225 (2010).

113 Cho, J. H. The genetics and immunopathogenesis of inflammatory bowel disease. *Nature reviews* 8, 458-466 (2008).

114 VanDussen, K. L. *et al.* Genetic variants synthesize to produce paneth cell phenotypes that define subtypes of Crohn's disease. *Gastroenterology* 146, 200-209, doi:10.1053/j.gastro.2013.09.048 (2014).

115 Hugot, J. P. *et al.* Association of NOD2 leucine-rich repeat variants with susceptibility to Crohn's disease. *Nature* 411, 599-603 (2001).

116 Ogura, Y. *et al.* A frameshift mutation in NOD2 associated with susceptibility to Crohn's disease. *Nature* 411, 603-606 (2001).

117 Kaser, A. *et al.* XBP1 links ER stress to intestinal inflammation and confers genetic risk for human inflammatory bowel disease. *Cell* 134, 743-756, doi:10.1016/j.cell.2008.07.021 (2008).

118 Cadwell, K. *et al.* A key role for autophagy and the autophagy gene Atg16l1 in mouse and human intestinal Paneth cells. *Nature* 456, 259-263, doi:10.1038/nature07416 (2008).

119 Cadwell, K., Patel, K. K., Komatsu, M., Virgin, H. W. t. & Stappenbeck, T. S. A common role for Atg16L1, Atg5 and Atg7 in small intestinal Paneth cells and Crohn disease. *Autophagy* 5, 250-252 (2009).

120 Ogura, Y. *et al.* Expression of NOD2 in Paneth cells: a possible link to Crohn's ileitis. *Gut* 52, 1591-1597 (2003).

121 Kobayashi, K. S. *et al.* Nod2-dependent regulation of innate and adaptive immunity in the intestinal tract. *Science* 307, 731-734, doi:10.1126/science.1104911 (2005).

122 Zhang, Q. *et al.* Commensal bacteria direct selective cargo sorting to promote symbiosis. *Nat Immunol* 16, 918-926, doi:10.1038/ni.3233 (2015).

123 Ron, D. & Walter, P. Signal integration in the endoplasmic reticulum unfolded protein response. *Nat Rev Mol Cell Biol* 8, 519-529, doi:10.1038/nrm2199 (2007).

124 Schroder, M. & Kaufman, R. J. The mammalian unfolded protein response. *Annu Rev Biochem* 74, 739-789, doi:10.1146/annurev.biochem.73.011303.074134 (2005).

125 Walter, P. & Ron, D. The unfolded protein response: from stress pathway to homeostatic regulation. *Science (New York, N.Y* 334, 1081-1086, doi:10.1126/science.1209038 (2011).

126 He, C. & Klionsky, D. J. Regulation mechanisms and signaling pathways of autophagy. *Annu Rev Genet* 43, 67-93, doi:10.1146/annurev-genet-102808-114910 (2009).

127 Glick, D., Barth, S. & Macleod, K. F. Autophagy: cellular and molecular mechanisms. *J Pathol* 221, 3-12, doi:10.1002/path.2697 (2010).

128 Mizushima, N., Yoshimori, T. & Ohsumi, Y. The role of Atg proteins in autophagosome formation. *Annu Rev Cell Dev Biol* 27, 107-132, doi:10.1146/annurev-cellbio-092910-154005 (2011).

129 Gorbunov, N. V. & Kiang, J. G. Up-regulation of autophagy in small intestine Paneth cells in response to total-body gamma-irradiation. *J Pathol* 219, 242-252, doi:10.1002/path.2591 (2009).

130 Stappenbeck, T. S. & McGovern, D. P. Paneth Cell Alterations in the Development and Phenotype of Crohn's Disease. *Gastroenterology* 152, 322-326, doi:10.1053/j.gastro.2016.10.003 (2017).

131 Liu, T. C. *et al.* LRRK2 but not ATG16L1 is associated with Paneth cell defect in Japanese Crohn's disease patients. *JCI Insight* 2, e91917, doi:10.1172/jci.insight.91917 (2017).

132 Adolph, T. E. *et al.* Paneth cells as a site of origin for intestinal inflammation. *Nature* 503, 272-276, doi:10.1038/nature12599 (2013).

133 Brown, S. J. & Mayer, L. The immune response in inflammatory bowel disease. *Am J Gastroenterol* 102, 2058-2069, doi:AJG1343 [pii] 10.1111/j.1572-0241.2007.01343.x (2007).

134 Segal, A. W. Making sense of the cause of Crohn's - a new look at an old disease. *F1000Res* 5, 2510, doi:10.12688/f1000research.9699.2 (2016).

135 Ananthakrishnan, A. N. *et al.* A prospective study of long-term intake of dietary fiber and risk of Crohn's disease and ulcerative colitis. *Gastroenterology* 145, 970-977, doi:S0016-5085(13)01140-2 [pii] 10.1053/j.gastro.2013.07.050 (2013).

136 Ananthakrishnan, A. N. *et al.* Long-term intake of dietary fat and risk of ulcerative colitis and Crohn's disease. *Gut* 63, 776-784, doi:gutjnl-2013-305304 [pii] 10.1136/gutjnl-2013-305304 (2014).

137 Ananthakrishnan, A. N. *et al.* Zinc intake and risk of Crohn's disease and ulcerative colitis: a prospective cohort study. *Int J Epidemiol* 44, 1995-2005, doi:dyv301 [pii] 10.1093/ije/dyv301 (2015).

138 Liuzzi, J. P., Guo, L., Yoo, C. & Stewart, T. S. Zinc and autophagy. *Biometals* 27, 1087-1096, doi:10.1007/s10534-014-9773-0 (2014).

139 Blumberg, R. S. Environment and Genes: What Is the Interaction? *Dig Dis* 34, 20-26, doi:10.1159/000442920 (2016).

140 Nakanishi, Y. *et al.* Control of Paneth Cell Fate, Intestinal Inflammation, and Tumorigenesis by PKClambda/iota. *Cell Rep* 16, 3297-3310, doi:10.1016/j.celrep.2016.08.054 (2016).

CHAPTER 2

The Organoid Reconstitution Assay (ORA) for the Functional Analysis of Intestinal Stem and Niche Cells

J. Vis. Exp. (129), e56329, doi:10.3791/56329 (2017).

jove Journal of Visualized Experiments www.jove.com

Video Article

The Organoid Reconstitution Assay (ORA) for the Functional Analysis of Intestinal Stem and Niche Cells

Matthias Schewe[1], Andrea Sacchetti[1], Mark Schmitt[1], Riccardo Fodde[1]

[1]Department of Pathology, Erasmus MC Cancer Institute, Erasmus University Medical Center

Correspondence to: Matthias Schewe at matthias.schewe@helsinki.fi

URL: https://www.jove.com/video/56329
DOI: doi:10.3791/56329

Keywords: Bioengineering, Issue 129, mini-gut organoids, *Lgr5*$^+$ stem cells, Paneth cells, intestinal stem cell niche, organoid reconstitution assay, intestinal co-culture

Date Published: 11/20/2017

Citation: Schewe, M., Sacchetti, A., Schmitt, M., Fodde, R. The Organoid Reconstitution Assay (ORA) for the Functional Analysis of Intestinal Stem and Niche Cells. *J. Vis. Exp.* (129), e56329, doi:10.3791/56329 (2017).

Abstract

The intestinal epithelium is characterized by an extremely rapid turnover rate. In mammals, the entire epithelial lining is renewed within 4 - 5 days. Adult intestinal stem cells reside at the bottom of the crypts of Lieberkühn, are earmarked by expression of the *Lgr5* gene, and preserve homeostasis through their characteristic high proliferative rate[1]. Throughout the small intestine, *Lgr5*$^+$ stem cells are intermingled with specialized secretory cells called Paneth cells. Paneth cells secrete antibacterial compounds (*i.e.*, lysozyme and cryptdins/defensins) and exert a controlling role on the intestinal flora. More recently, a novel function has been discovered for Paneth cells, namely their capacity to provide niche support to *Lgr5*$^+$ stem cells through several key ligands as Wnt3, EGF, and Dll1[2].

When isolated *ex vivo* and cultured in the presence of specific growth factors and extracellular matrix components, whole intestinal crypts give rise to long-lived and self-renewing 3D structures called organoids that highly resemble the crypt-villus epithelial architecture of the adult small intestine[3]. Organoid cultures, when established from whole crypts, allow the study of self-renewal and differentiation of the intestinal stem cell niche, though without addressing the contribution of its individual components, namely the *Lgr5*$^+$ and Paneth cells.

Here, we describe a novel approach to the organoid assay that takes advantage of the ability of Paneth and *Lgr5*$^+$ cells to associate and form organoids when co-cultured. This approach, here referred to as "organoid reconstitution assay" (ORA), allows the genetic and biochemical modification of Paneth or *Lgr5*$^+$ stem cells, followed by reconstitution into organoids. As such, it allows the functional analysis of the two main components of the intestinal stem cell niche.

Video Link

The video component of this article can be found at https://www.jove.com/video/56329/

Introduction

The intestinal epithelium is the most rapidly self-renewing tissue in the mammalian body and, as such, has been the object of a plethora of studies aimed at the identification and functional characterization of the adult stem cells residing at the bottom of the crypt of Lieberkühn, earmarked by expression of the *Lgr5* gene and dependent on canonical Wnt signals[1]. Notably, *Lgr5*$^+$ stem cells are flanked and supported by specialized niche cells, *i.e.* Paneth cells, which also depend on Wnt signaling for their maturation[2]. Together, these two cell types underlie self-renewal of the intestinal epithelial lining and preserve the daily homeostatic equilibrium: *Lgr5*$^+$ stem cells rapidly divide and give rise to progenitor and more specialized intestinal epithelial cells; Paneth cells provide essential niche factors (*e.g.*, Dll1, Wnt3, EGF) to *Lgr5*$^+$ stem cells[2]. The capacity of intestinal crypts when plated *ex vivo* to form organized and self-renewing structures called organoids, or "mini-guts", has been exploited as an experimental tool to provide insight into processes such as self-renewal and differentiation in normal and pathological conditions including cancer[4]. Organoid cultures have been established from several tissues, including the intestine, pancreas, liver, and kidney, from both mouse and human samples[4]. The extraction method and the growth factors employed to develop these organoid cultures are tissue-specific and designed to drive multi-lineage differentiation and mimic as closely as possible the original stem cell niche *in vivo*. Organoids may have potential applications including the treatment of genetic diseases, the assessment of therapeutic efficacy in cancer, the analysis of drug toxicity, or the study of organogenesis *in vitro*[5].

Overall, the main limitation of organoid cultures when established from tissue samples is a lack of cell-specificity. For example, intestinal organoids established from whole intestinal crypts do not allow the analysis of individual cellular components encompassed within the tissue source (*e.g.*, whole crypts contain *Lgr5*$^+$, Paneth, and progenitor cells).

Here, we describe a novel method, referred to as ORA, that combines the advantages of intestinal organoid cultures with the functional analysis of its most fundamental components, namely stem (*Lgr5*$^+$) and niche (Paneth) cells. This is achieved through the unique ability of Paneth and *Lgr5*$^+$ cells to physically associate with each other when co-incubated and give rise to organoids[2,6,10]. We took advantage of this feature and pre-treated the two cell types individually before allowing them to reconstitute organoids. When doing so, each cell component can be exposed to

any given drug, growth factor, biochemical inhibitor, genetic modification, or chemical treatment prior to reconstitution and organoid formation. Therefore, using the ORA assay will allow the determination of whether a specific drug treatment or genetic modification has a specific effect on the stem cells or their niche counterpart.

Protocol

All procedures were done according to local animal welfare laws and guidelines.

1. Preparation of Instruments, Culture Media, and Dishes

1. Autoclave 1 set of intestinal scissors, normal scissors, and forceps in a sterile container.
2. Place a 96-well (flat bottom) dish in an incubator at 37 °C.
3. Prepare 10 mL of complete culture medium with the reagents listed in table of materials.
4. Incubate the complete medium at 37 °C in a water bath.
5. Thaw reconstituted basement membrane by placing it in an ice bucket. The reconstituted basement membrane will become liquid at 4 °C .
6. Fill 4 Petri dishes with cold phosphate-buffered saline or abbreviated PBS (4 °C).

2. Isolation of Small Intestinal Crypts

1. Sacrifice by CO_2 inhalation a *Lgr5*-eGFP-IRES-CreER^{t2} mouse on a C57BL6/J background. Dissect the peritoneum longitudinally with a pair of scissors.
2. Hold the stomach with the forceps and cut it transversally in half.
3. Using the intestinal scissors from now on, pull out the intestine and place it in a Petri dish containing PBS.
   NOTE: Intestinal scissors have a sharp and a blunt tip. The blunt tip of these scissors is meant to not damage the crypt-villus architecture while opening the intestine.
4. Start by placing the blunt tip into the stomach and gently push it through the pylorus. Proceed by cutting with the scissors and pulling with the forceps.
5. Once the whole small intestine is opened longitudinally, wash it in cold PBS by holding it with the forceps and gently rinse it in the PBS solution with U-shaped movements.
6. Once all the stool remnants are cleared, proceed to flatten the intestine on a cutting board, luminal side up. The luminal side is easily recognizable by the absence of blood vessels and by its pale appearance when compared with the outer part.
7. With a glass slide, gently remove the villi by scraping the flattened intestine. Perform this step twice along the whole length of the tissue.
8. Cut the small intestine with a sterile surgical blade into 2 - 5 mm pieces.
9. Place the small intestinal fragments in a 50 mL tube containing 10 mL of ice cold PBS.
10. Clean the tissue fragments, removing any remaining impurities by pipetting them up and down in the PBS. Discard supernatant and repeat this step until the PBS is completely clear.
11. Add 15 mL cold PBS, to bring the total final volume of PBS to 25 mL. Add 2 mM ethylenediaminetetraacetic acid (EDTA) and incubate for 45 min on a roller at 4 °C.
12. Discard the PBS/EDTA.
13. Add 10 mL of PBS and detach the crypts by harshly pipetting the tissue fragments up and down (at least three times). Collect the supernatant.
14. Repeat step 2.13 four times. Add culture medium to reach a final volume of 50 mL.
15. Pellet the cells by centrifugation (300 x g for 5 min).
16. Resuspend the pellet in 10 mL of culture medium and pellet the crypts by centrifugation (80 x g for 3 min).

3. Single Cell Preparation

1. Discard the supernatant of the pelleted crypts and resuspend them in 1 mL trypsin like-enzymes together with 50 µL DNAse (50 µg/mL).
2. Incubate the cells in a water bath at 32 °C for 2 min.
3. Add 10 mL of culture medium. Dissociate the crypts into single cells by harshly pipetting up and down at least 5 times.
4. Filter the solution through a 40 µm strainer (to eliminate clumps and other impurities) and pellet the single cells at 300 x g for 5 min.

4. Flow Cytometry and Plating

1. Prepare 50 mL of 1x Hank's buffered salt solution or HBSS/2% fetal cow serum (FCS) solution and resuspend the pellet in 1 mL for every 10^6 cells
2. Add to the cell suspension BV421 Lin$^-$ (CD31, CD45, TER119) at a concentration of 1:100, and CD24-APC and CD117-PE both at a concentration of 1:250 antibodies for 30 min.
3. Sort *Lgr5*$^+$ stem cells and Paneth cells into separate low bind tubes. For details on sorting protocols for *Lgr5*$^+$ and Paneth cells, please see Roth *et al.*[7] and Schewe *et al.*[6]
   1. Centrifuge the sorted cells at 300 x g for 5 min. Resuspend the cells in 100 µL medium with the components described as in 1.3 (see the **Table of Materials**).
4. Treat (*e.g.*, by chemical or genetic modification) the Paneth cells (n = 2000) or the *Lgr5*$^+$ stem cells (n = 2000).
   1. To treat cells, use 5 µL of liposome-mediated transfection reagent in a total volume of 100 µL culture medium and small interfering RNA (siRNA) at a concentration of 100 nM. Incubate for 30 min at 37 °C for siRNA or for the time necessary for the chosen modification.

5. Wash the cells twice in 500 µL culture medium.
6. Centrifuge at 300 x g for 5 min and resuspend the cells in 10 µL culture medium.
7. Pool the two cellular components (Paneth or *Lgr5*$^{+}$ cells) in a 20 µl total volume and centrifuge at 300 x g for 5 min at RT.
8. Co-incubate the Paneth and *Lgr5*$^{+}$ cells for 10 min at RT.
9. Remove 10 µL of the supernatant and leave a meniscus of liquid to be sure to not aspirate the cell pellet.
10. Add 30 µL of reconstituted basement membrane to the cells for a total volume of 40 µL, resuspend the cells and plate in a pre-warmed 96 well plate. After 10 min, add 200 µL of complete medium (see the **Table of Materials**). Change medium every 48 h.
11. Count organoid multiplicity at day 5.

Representative Results

The organoid reconstitution assay allows the separate functional analysis of the essential niche and stem cell components of the intestinal epithelium, here demonstrated by small interfering RNA (siRNA) of the *Apc* gene.

To achieve this aim, we first utilized fluorescent activated cell sorting (FACS) to separate 8000 *Lgr5*$^{+}$ cells and 6000 Paneth cells from inbred C57BL6/J mice. In **Figure 1a**, a flowchart of the ORA assay is depicted. Organoid reconstitution capacity was assessed by incubating *Lgr5*$^{+}$ cells with siRNA oligonucleotides directed against the mRNA of *Apc* or encompassing a scrambled sequence (SCR) as a control. After treatment, the same siRNA-treated *Lgr5*$^{+}$ cells were either directly plated in organoid medium/reconstituted basement membrane, or incubated with an equal number of untreated Paneth cells and subsequently plated out. As a control, untreated *Lgr5*$^{+}$ cells were plated alone (*i.e.*, without Paneth cells) to determine the number of organoids derived from untreated *Lgr5*$^{+}$ cells. Furthermore, as an additional control, Paneth cells alone were plated to check for the background of organoid formation derived from the contamination of Paneth-Lgr5 cell doublets sorted in the Paneth cell gate. As expected, siRNA mediated knockdown of the murine *Apc* gene in *Lgr5*$^{+}$ stem cells (and the resulting activation of the canonical Wnt/β-catenin signaling pathway) positively affected organoid multiplicity when compared to untreated counterparts or the scrambled control (**Figure 1B**). The constitutive Wnt activation also rescued the requirement for Paneth cells, as previously reported[1]. Furthermore, these organoids appeared as hollow spheres (spheroids), a well described phenotype for *Apc*-mutant or Wnt-stimulated organoids (**Figure 1C**, panel 1), when compared with the morphology of those obtained from Paneth-Lgr5 cell doublets (**Figure 1C**, panel 2)[8,9]. Collectively, these results demonstrate that reconstituting Paneth cells and *Lgr5*$^{+}$ cells can give insight on cell-specific mechanisms within these two cell types; morphological analysis of the organoids by microscopy can be valuable in this respect since the morphology of the organoids reflects their cell composition (*e.g.*, spheroids are constituted by *Lgr5*$^{+}$ cells only). Another important parameter to be taken into account is the complexity of the organoid (*e.g.*, the number of crypt budding events).

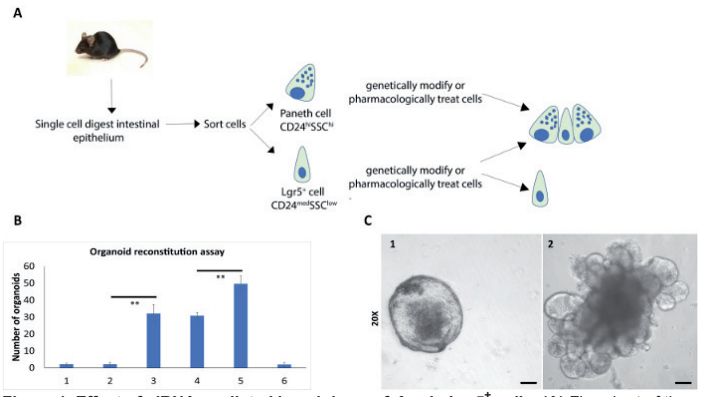

Figure 1. Effect of siRNA mediated knockdown of *Apc* in Lgr5^{+} cells. (A) Flowchart of the experimental procedure. *Lgr5*^{EGFP} reporter mice (*Lgr5*$^{EGFP\text{-}IRES\text{-}creERT2}$)[1] were employed as a source of *Lgr5*$^{+}$ sorted stem cells. Paneth cells were sorted as indicated and previously described[6,7]. **(B)** Organoid multiplicity observed upon reconstitution of *Lgr5*$^{+}$ stem cells and Paneth cells. When indicated cells were pretreated with siRNA oligonucleotides directed against the *Apc* (siRNA *Apc*) or scrambled (SCR) control sequence. The asterisks indicate statistically significant differences (n = 3, *p <0.05 **p <0.001). Error bars refer to SD. (1) *Lgr5*$^{+}$ cells, (2) *Lgr5*$^{+}$ cells SCR, (3) *Lgr5*$^{+}$ cells siRNA *Apc*, (4) *Lgr5*$^{+}$ cells + Paneth cells, (5) *Lgr5*$^{+}$ cells siRNA *Apc* + Paneth cells, (6) Paneth cells. **(C)** Representative images of organoids derived from (1) *Lgr5*$^{+}$ cells siRNA *Apc*, (2) *Lgr5*$^{+}$-Paneth cells. Scale bar = 10 µm. Please click here to view a larger version of this figure.

Discussion

The ORA allows the refined functional analysis of the two essential components of the intestinal stem cell niche, namely *Lgr5*$^{+}$ and Paneth cells. This approach has been previously employed by us and others with slight modifications[6,10,11]. Here, we present the ORA procedure as a reproducible and standardized laboratory protocol. Also, we report on the effects of *Apc* downregulation in *Lgr5*$^{+}$ stem cells, as an example of the possibility of implementing genetic (or biochemical[6]) modifications to the sorted cellular components. Collectively, the data show that siRNA mediated knockdown of *Apc* enhances the stem cell function of *Lgr5*$^{+}$ cells, as indicated by the increased organoid multiplicity (**Figure 1B**).

Several advantages of using intestinal 3D organoid cultures have already been listed in reviews[4], including the striking resemblance of their organization with that of the crypt-villus architecture *in vivo*, especially when compared to the architecture from standard 2D culture methods with

immortalized cell lines. However, one of the major limitations of this method is that in most cases, organoid cultures are established from whole intestinal crypts, a process which does not allow the functional analysis of its individual components and, in particular, of the stem and niche cells, here represented by *Lgr5*$^{+}$ and Paneth cells, respectively.

The ORA overcomes these limitations. Stem and niche cells can be separately sorted from the animal and reconstituted to generate organoids. As such, this approach allows the functional analysis of these two cellular components by either employing mouse models carrying specific genetic modifications or exposed to specific stress factors (*e.g.*, DSS and/or specific diets); or by directly modifying the sorted cells genetically (siRNA, CRISPR-Cas9) or biochemically, before reconstituting them to generate organoids. The multiplicity, morphology, self-renewal capacity, and extent of differentiation (and eventually the extent of metaplastic changes) of the resulting organoids can be employed as functional read-outs. In the case of genetic manipulation, such as siRNA, when a morphological effect is not evident, cells should be analyzed one hour after transfection to validate the knockdown of the mRNA of interest. Paneth and *Lgr5*$^{+}$ can also be sorted from mice genetically engineered with different mutations to study whether different mutations in stem and niche cells lead to altered interactions between these two cell types and a different organoid formation efficiency and/or morphology.

Critical steps within the protocol are the removal of the villi (step 2.7) and the resuspension of the cells in HBSS/2%FCS (step 4.1). Removal of the villi is critical to enrich Paneth and *Lgr5*$^{+}$ cells located in the lower third of the crypts and to improve the efficiency of sorting. Although FACS protocols commonly suggest sorting cells in PBS/FCS, the use of HBSS instead of PBS increased and kept cell viability stable throughout the sorting time. Other important steps are steps 4.7 and 4.8, where physical association of Paneth and *Lgr5*$^{+}$ *cells* allows these lineages to form doublets that will eventually give rise to organoids.

Disclosures

The authors have no competing financial interest or other conflicts of interest

Acknowledgements

This study was made possible by funding from the Dutch Cancer Society (KWF; EMCR 2012-5473) and the World Cancer Research Funds International (WCRF; project no. 2014-1181)

References

1. Barker, N. *et al.* Identification of stem cells in small intestine and colon by marker gene Lgr5. *Nature.* **449**, 1003-1007 (2007).
2. Sato, T. *et al.* Paneth cells constitute the niche for Lgr5 stem cells in intestinal crypts. *Nature.* **469**, 415-418 (2011).
3. Sato, T. *et al.* Single Lgr5 stem cells build crypt-villus structures in vitro without a mesenchymal niche. *Nature.* **459**, 262-265 (2009).
4. Clevers, H. Modeling Development and Disease with Organoids. *Cell.* **165**, 1586-1597 (2016).
5. Cantrell, M. A., & Kuo, C. J. Organoid modeling for cancer precision medicine. *Genome Med.* **7**, 32 (2015).
6. Schewe, M. *et al.* Secreted Phospholipases A2 Are Intestinal Stem Cell Niche Factors with Distinct Roles in Homeostasis, Inflammation, and Cancer. *Cell Stem Cell.* **19**, 38-51 (2016).
7. Roth, S. *et al.* Paneth cells in intestinal homeostasis and tissue injury. *PLoS One.* **7**, e38965, PONE-D-12-10735 [pii] (2012).
8. Rodriguez-Colman, M. J. *et al.* Interplay between metabolic identities in the intestinal crypt supports stem cell function. *Nature.* **543**, 424-427 (2017).
9. Dow, L. E. *et al.* Apc Restoration Promotes Cellular Differentiation and Reestablishes Crypt Homeostasis in Colorectal Cancer. *Cell.* **161**, 1539-1552 (2015).
10. Yilmaz, O. H. *et al.* mTORC1 in the Paneth cell niche couples intestinal stem-cell function to calorie intake. *Nature.* **486**, 490-495 [pii] (2012).
11. Igarashi, M., & Guarente, L. mTORC1 and SIRT1 Cooperate to Foster Expansion of Gut Adult Stem Cells during Calorie Restriction. *Cell.* **166**, 436-450 [pii] (2016).

CHAPTER 3

Secreted phospholipases A2 are stem cell niche factors with distinct roles in homeostasis, inflammation and cancer

Cell Stem Cell, 19(1):38-51 (2016).

Article

Cell Stem Cell

Secreted Phospholipases A2 Are Intestinal Stem Cell Niche Factors with Distinct Roles in Homeostasis, Inflammation, and Cancer

Graphical Abstract

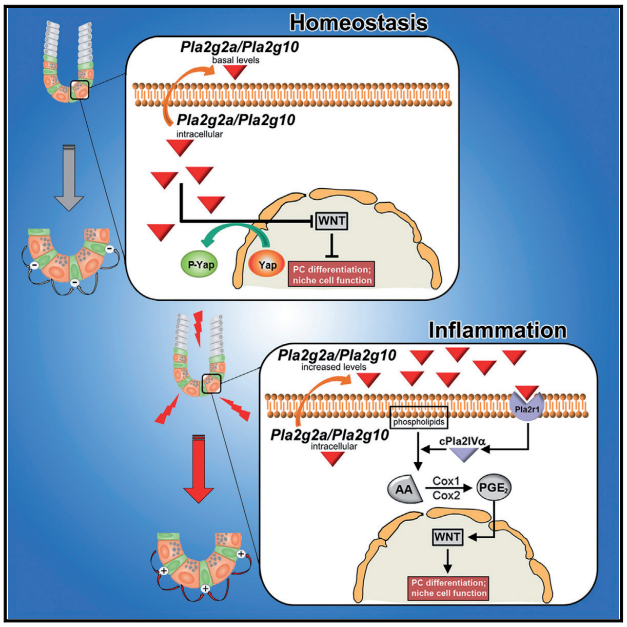

Highlights

- Intracellular group IIA and X phospholipases A2 restrict Wnt signaling through Yap1
- During inflammation, the same phospholipases are secreted and promote Wnt signaling
- Group X phospholipase A2 is expressed in Paneth-like cells in the colon
- Genetic ablation of both group IIA and X predisposes mice to colon cancer

Authors

Matthias Schewe, Patrick F. Franken, Andrea Sacchetti, ..., Robert T. Cormier, Gérard Lambeau, Riccardo Fodde

Correspondence

r.fodde@erasmusmc.nl

In Brief

Pla2g2a, encoding group IIA secreted phospholipase A2, is an important genetic modifier of intestinal tumorigenesis. Schewe et al. report group IIA/X secreted phospholipases A2 are intestinal stem cell niche factors with cell-intrinsic and secreted functions in Wnt signaling and prostaglandin synthesis that modulate intestinal homeostasis, inflammation, and cancer susceptibility.

Schewe et al., 2016, Cell Stem Cell *19*, 38–51
July 7, 2016
http://dx.doi.org/10.1016/j.stem.2016.05.023

CellPress

Secreted Phospholipases A2 Are Intestinal Stem Cell Niche Factors with Distinct Roles in Homeostasis, Inflammation, and Cancer

Matthias Schewe,[1] Patrick F. Franken,[1] Andrea Sacchetti,[1] Mark Schmitt,[1] Rosalie Joosten,[1] René Böttcher,[2] Martin E. van Royen,[1,3] Louise Jeammet,[4] Christine Payré,[4] Patricia M. Scott,[5] Nancy R. Webb,[6] Michael Gelb,[7] Robert T. Cormier,[5] Gérard Lambeau,[4] and Riccardo Fodde[1,*]

[1]Department of Pathology
[2]Department of Urology
[3]Erasmus Optical Imaging Centre
Erasmus MC Cancer Institute, Rotterdam 3000CA, The Netherlands
[4]Institute of Molecular and Cellular Pharmacology, Centre National de la Recherche Scientifique and University of Nice Sophia Antipolis, Valbonne 06560, France
[5]Department of Biomedical Sciences, University of Minnesota Medical School Duluth, Duluth, MN 55812-3031, USA
[6]Department of Pharmacology and Nutritional Sciences, University of Kentucky, Lexington, KY 40506-9983, USA
[7]Department of Chemistry, University of Washington, Seattle, WA 98195-1700, USA
*Correspondence: r.fodde@erasmusmc.nl
http://dx.doi.org/10.1016/j.stem.2016.05.023

SUMMARY

The intestinal stem cell niche provides cues that actively maintain gut homeostasis. Dysregulation of these cues may compromise intestinal regeneration upon tissue insult and/or promote tumor growth. Here, we identify secreted phospholipases A2 (sPLA2s) as stem cell niche factors with context-dependent functions in the digestive tract. We show that group IIA sPLA2, a known genetic modifier of mouse intestinal tumorigenesis, is expressed by Paneth cells in the small intestine, while group X sPLA2 is expressed by Paneth/goblet-like cells in the colon. During homeostasis, group IIA/X sPLA2s inhibit Wnt signaling through intracellular activation of Yap1. However, upon inflammation they are secreted into the intestinal lumen, where they promote prostaglandin synthesis and Wnt signaling. Genetic ablation of both sPLA2s improves recovery from inflammation but increases colon cancer susceptibility due to release of their homeostatic Wnt-inhibitory role. This "trade-off" effect suggests sPLA2s have important functions as genetic modifiers of inflammation and colon cancer.

INTRODUCTION

In 1993, by taking advantage of an inbred mouse model predisposed to multiple intestinal neoplasia (*Min*), Dove and collaborators identified the *Mom-1* (modifier of Min) locus as a major modifier of intestinal tumor multiplicity driven by mutations in the *Apc* (adenomatous polyposis coli) tumor suppressor gene (Dietrich et al., 1993). Subsequently, *Pla2g2a*, encoding the secreted type IIA phospholipase A2 (sPLA2-IIA), was identified as the main responsible gene within the *Mom-1* locus (MacPhee et al., 1995). sPLA2-IIA and other sPLA2 members produce biologically active lipid mediators such as lysophosphatidic acid (LPA) and arachidonic acid (AA), the latter a substrate for prostaglandin E2 (PGE_2) biosynthesis (Lambeau and Gelb, 2008). Notably, *Mom-1*-susceptible strains (e.g., C57BL/6J) carry a single nucleotide insertion in the *Pla2g2a* gene, resulting in a *null* allele, whereas *Mom-1*-resistant strains (e.g., FVB/N, BALB/c, CBA) are *Pla2g2a* proficient (MacPhee et al., 1995). More definitive evidence for the identity of the *Pla2g2a* gene as *Mom-1* came from a transgenic mouse overexpressing *Pla2g2a* in the C57BL/6J inbred genetic background that, in the presence of the Apc^{Min} mutation, causes a significant reduction in tumor multiplicity, though without fully recapitulating the decrease in tumor multiplicity observed in resistant *Mom-1* strains (Cormier et al., 1997, 2000).

Somatic inactivation of the human *APC* gene is a rate-limiting and initiating event in the vast majority of sporadic colon cancer cases (Fodde et al., 2001). Based on the above mouse studies, *PLA2G2A*, i.e., the human ortholog of *Mom-1*/*Pla2g2a*, was thought to represent a modifier of bowel cancer risk in the general population. However, studies failed to find either somatic or germline *PLA2G2A* alterations in sporadic colon tumors or hereditary colon cancer patients, respectively (Riggins et al., 1995; Spirio et al., 1996). This may be due to the specific expression of the *PLA2G2A*/*Pla2g2a* gene in Paneth cells, a secretory lineage almost exclusively found in the small intestine and only to a lesser extent in the distal colon (Cormier et al., 2000; Mounier et al., 2008). Accordingly, *Apc* mutant mice mainly develop multiple upper GI (gastrointestinal) adenomas with very infrequent colonic lesions. Therefore, other members of the sPLA2 multigene family may act as colon cancer genetic modifiers in man.

The Paneth-cell-specific expression pattern of *Pla2g2a* is of interest in view of the "niche" role played by these secretory cells in supporting $Lgr5^{+}$ intestinal stem cells (ISCs) in the intestinal crypt (Sato et al., 2011). Moreover, both Paneth cells and their

secretory precursors were shown to represent infrequently dividing stem-like cells capable of re-entering the cell cycle upon tissue insults, thus contributing to the regenerative response (Buczacki et al., 2013; Roth et al., 2012). Therefore, we hypothesized that sPLA2s may represent ISC niche factors with specific functional roles in homeostasis, inflammation, and cancer.

RESULTS

Pla2g2a Expression Modulates ISC Function and Paneth Cell Differentiation

To test the hypothesis that *Pla2g2a* is an important stem cell niche factor, we employed the "mini-gut" assay (Sato et al., 2011) as a readout of stem cell function in small intestinal crypts from *Mom-1*-sensitive ($Mom1^S$ or $Pla2g2a^{-/-}$; C57BL/6J and 129/SW) or *Mom*-1-resistant ($Mom1^R$ or $Pla2g2a^{+/+}$; FVB/N, BALB/c, CBA) inbred mouse lines (MacPhee et al., 1995). The multiplicity of organoids derived from $Mom1^S$ strains is significantly higher when compared with $Mom1^R$ mice (Figure 1A). However, these inbred strains differ at several loci other than *Pla2g2a*, and thus differences in organoid formation cannot be attributed directly to the *Mom-1* locus. Therefore, we employed a transgenic mouse model in which expression of the *Pla2g2a* gene is restored in the C57BL/6J background (Tg-*Pla2g2a*) (Cormier et al., 1997) at slightly higher levels (~1.5- to 2-fold at the protein level) compared to *Pla2g2a*-proficient inbred strains such as FVB/N (Figure S1, available online). There was a significant decrease in organoid formation in both male and female transgenic mice compared with $Pla2g2a^{-/-}$ (C57BL/6J) littermates (Figure 1B), confirming that expression of the *Pla2g2a* gene negatively affects the ability of isolated crypts to form intestinal organoids. The overall organoid morphology did not differ among strains (data not shown).

The *Pla2g2a* gene is mainly, yet not exclusively, expressed in the small intestine and in particular by Paneth cells (Figure S1A). As *Pla2g2a* inhibits organoid growth, we investigated the histopathology of the digestive tract of Tg-*Pla2g2a* mice. Notably, immunohistochemical (IHC) analysis revealed an almost complete absence of lysozyme-positive Paneth cells in the transgenic mice (Figure 1C). In addition, the proliferating ($Ki67^+$) compartment, normally limited to the transient amplifying (TA) progenitors in control C57BL/6J mice, was extended to the lower crypt of Tg-*Pla2g2a* mice, where post-mitotic Paneth cells are usually located (Figure 1D). However, granulated Paneth-like cells were present in the crypt bottom of transgenic animals (Figure S2A). qRT-PCR (Figure 1E) and IHC (Figure S2B) analysis of additional lineage-specific markers confirmed the absence of mature Paneth cells in the Tg-*Pla2g2a* model. Furthermore, IHC (Figures S3A and S3B) and fluorescence-activated cell sorting (FACS) (Figures S3C and S3D) analyses of lineage-specific markers confirmed the accumulation of the $Lgr5^+/ChgA^+$ (chromogranin A) secretory (Paneth and goblet cells) precursor lineage (Buczacki et al., 2013) in transgenic animals. Notably, the overall FACS pattern obtained from C57BL/6J and Tg-*Pla2g2a* mice did not differ with the CD24/SSC marker combination (data not shown). Thus, the results point to a reduction in fully mature Paneth cells rather than the complete ablation of this lineage in the transgenic mice, possibly due to a maturation defect. Overall, *Pla2g2a* may modulate ISC function by inhibiting Paneth cell differentiation and full maturation.

Intracellular Pla2g2a Inhibits Wnt Signaling by Increasing Yap1 Phosphorylation

The above experiments were carried out under homeostatic conditions, i.e., in mice kept under normal conditions and fed ad libitum. As *Pla2g2a* encodes the sPLA2-IIA protein whose expression and secretion are highly enhanced during inflammation but are thought to be kept at a basal level during homeostasis, we investigated whether the observed inhibitory effects on intestinal organoid growth are exerted by the intracellular pool or by the basal secreted fraction of sPLA2-IIA. The organoid assay was repeated on crypts from FVB ($Pla2g2a^{+/+}$), C57BL/6J ($Pla2g2a^{-/-}$), and Tg-*Pla2g2a* mice in the presence of the soluble (non-membrane-bound) sPLA2-IIA receptor Pla2r1 to scavenge any secreted Pla2g2a protein (Rouault et al., 2007). The lack of effect on organoid multiplicity (Figure S3E) indicated that the inhibitory effect exerted by Pla2g2a is likely due to its intracellular (non-secreted) fraction.

The canonical Wnt signaling plays a role in both ISC maintenance and in Paneth cell maturation (van Es et al., 2005a). As such, it may underlie the organoid formation and Paneth cell maturation defects observed in *Pla2g2a*-expressing transgenic mice. Therefore, we analyzed the effects of *PLA2G2A* expression on Wnt signaling in human colon cancer cell lines with constitutive pathway activity due to mutations in the *APC* or β-catenin genes. Transient expression of *PLA2G2A* caused significant downregulation of Wnt signaling activity in all three lines (Figure 2A).

To elucidate the mechanisms underlying Pla2g2a-driven inhibition of Wnt signaling, we analyzed previously published intestinal expression profiling studies comparing Tg-*Pla2g2a* mice to C57BL/6J controls (Fijneman et al., 2008, 2009) and found upregulation of *Yap1* (yes-associated protein 1) in intestinal cells from Tg-*Pla2g2a* mice (2.63-fold; p value 0.0072). Although Yap1 has oncogenic and growth-stimulating capacities, it also has unexpected growth-suppressive functions; while nuclear Yap1 promotes growth, its phosphorylation by Hippo kinases prevents nuclear translocation and restricts Wnt signaling (Azzolin et al., 2014; Barry et al., 2013; Camargo et al., 2007). We FACS purified Paneth cells from *Lgr5–EGFP–ires–CreERT2* reporter mice (Barker et al., 2007) on Tg-*Pla2g2a* and C57BL/6J backgrounds, as previously described (Roth et al., 2012). Yap1 was specifically upregulated in Paneth cells from Tg-*Pla2g2a* mice (Figure 2B), reflecting the Paneth-specific *Pla2g2a* expression pattern in those animals (Figure S1B). In contrast, *Pla2g2a* expression levels did not differ between $Lgr5^+$ stem cells from control and transgenic animals. Moreover, *Yap1* was expressed at higher levels in Paneth cells from FVB/N ($Pla2g2a^{+/+}$) mice (Figure 2B). This was confirmed by IHC and IF analysis: whereas in wild-type (C57BL/6J) crypts only the slender $Lgr5^+$ stem cells stain positive for Yap1, clear Yap1 cytoplasmic staining was observed in the (immature) Paneth cells from Tg-*Pla2g2a* mice (Figures 2C and S4C). FACS analysis of wild-type (C57BL/6J) and Tg-*Pla2g2a* mice confirmed increased YAP1 phosphorylation in Paneth cells from the transgenic animals (Figures S4A and S4B), consistent with decreased organoid formation in these mice.

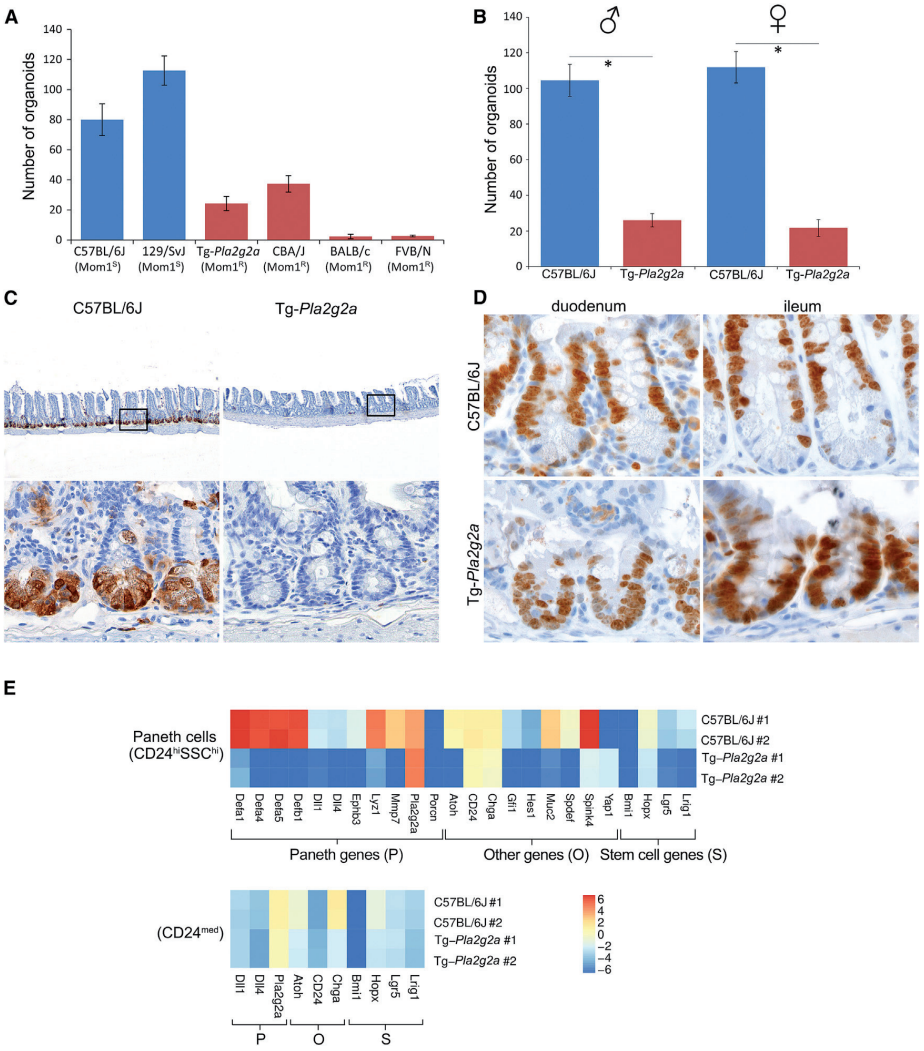

Figure 1. *Pla2g2a* Expression Modulates ISC Function and Paneth Cell Differentiation

(A) Organoid assays performed with crypts from indicated *Mom-1*-sensitive or *Mom-1*-resistant strains. Differences are statistically significant ($p < 0.001$) except for Tg*Pla2g2a* versus CBA/J and FVB/N versus BALB/c.

(B) Organoid assays performed on C57BL/6J (*Pla2g2a*$^{-/-}$) and Tg-*Pla2g2a* male and female mice (n = 5, *$p < 0.001$).

(C) Lysozyme IHC analysis of duodenal sections of C57BL/6J (*Pla2g2a*$^{-/-}$) and Tg-*Pla2g2a* mice.

(D) Ki67 IHC analysis of small intestinal crypts (duodenum and ileum) from *Pla2g2a*$^{-/-}$ (C57BL/6J) and Tg-*Pla2g2a* mice.

(E) Heatmap representation qRT-PCR expression analysis of Paneth- and stem-cell-specific genes from FACS-purified CD24/SSC lineages.

We then confirmed the central role of Paneth cells and of Yap1 downstream of Pla2g2a in the regulation of the ISC niche during homeostasis. Organoid formation was assessed by sorting and co-incubating *Lgr5*$^{+}$ stem cells from control (C57BL/6J; *Pla2g2a*$^{-/-}$) mice with Paneth cells from Tg-*Pla2g2a* mice, and vice versa (Figure 3A). A substantial decrease in organoid numbers was observed only when *Pla2g2a*-expressing Paneth cells from transgenic mice were mixed with control *Lgr5*$^{+}$ stem cells (Figure 3B), demonstrating that inhibitory effects of *Pla2g2a* expression on organoid formation are largely mediated by the immature Paneth cells. Live cell time-lapse imaging of the re-association of sorted single *Lgr5*$^{+}$ stem cells (EGFP^{+}; green) and single Paneth cells from wild-type C57BL/6J mice confirmed that physical contact between the stem cells and Paneth cells

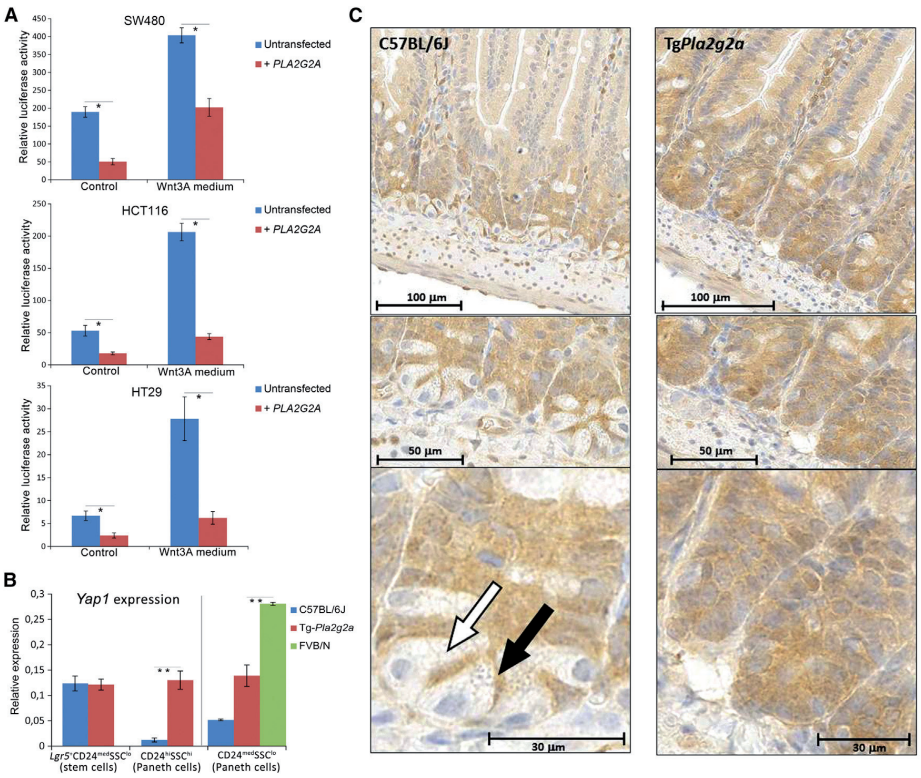

Figure 2. *Pla2g2a* Expression Modulates Wnt Signaling through Yap1 Phosphorylation

(A) TOP-Flash luciferase reporter analysis of Wnt signaling activity in the colon cancer cell lines SW480, HCT116, and HT29 upon transient transfection with a *PLA2G2A* expression vector in the presence/absence of Wnt3a conditioned medium (n = 3, *p < 0.05).

(B) *Yap1* qRT-PCR analysis in Paneth cells ($CD24^{hi}SSC^{hi}$), secretory precursors ($CD24^{med}SSC^{lo}$), and stem cells (*Lgr5*$^{+}CD24^{med}SSC^{lo}$) sorted by FACS from C57BL/6J (*Pla2g2a*$^{-/-}$) and Tg-*Pla2g2a* mice in the *Lgr5*$^{EGFP\text{-}IRES\text{-}creERT2}$ (*Lgr5*$^{+}$) background (left). $CD24^{hi}SSC^{hi}$ Paneth cells were also sorted from *Pla2g2a*$^{+/+}$ (FVB/N) mice and compared with the corresponding subpopulations sorted from *Pla2g2a*$^{-/-}$ (C57BL/6J) and Tg-*Pla2g2a* mice (right) (n = 3, **p < 0.001).

(C) Phospho-Yap1 IHC analysis of small intestinal crypts from C57BL/6J (*Pla2g2a*$^{-/-}$; left panel) and Tg-*Pla2g2a* mice (right panel). The black and white arrows indicate an *Lgr5*$^{+}$ stem cell (positive for Yap1) and a Paneth cell (negative for Yap1), respectively.

is required for organoid formation (Sato et al., 2011). Multiple cell clusters formed and occasionally fused to form larger structures (Movie S1). However, when Paneth cells from Tg-*Pla2g2a* mice were employed, their interactions with the $EGFP^{+}$ *Lgr5*$^{+}$ stem cells were significantly decreased, as was the corresponding number of organoids (Movie S2).

The relationship between *Pla2g2a* and *Yap1* was further confirmed by small interfering RNA (siRNA)-mediated knockdown in Paneth cells purified from C57BL6/J, Tg-*Pla2g2a*, and *Pla2g2a*-proficient FVB/N animals. *Yap1* is expressed at higher levels in the FVB/N Paneth cells compared with Paneth cells from Tg-*Pla2g2a* mice (Figure 2B) and, as expected, with those from the *Pla2g2a*-deficient strain C57BL/6J. Accordingly, siRNA-driven knockdown of *Pla2g2a* or *Yap1* in Paneth cells from Tg-*Pla2g2a* and FVB/N mice effectively rescued the inhibitory effects of *Plag2g2a* on organoid formation (Figure 3C). Similarly, siRNA-driven *YAP1* knockdown in human colon cancer cells fully rescued the Wnt-inhibitory effects of transient *PLA2G2A* expression (Figure 3D). Overall, these data indicate that intracellular *Pla2g2a* expression inhibits Wnt signaling in Paneth cells, through increased Yap1 expression and phosphorylation, to negatively regulate the ability of ISCs to form organoids. Consistently, transgenic *Pla2g2a* expression in the C57BL/6J inbred genetic background blocks Paneth cell maturation, leading to the accumulation of secretory precursors (see Graphical Abstract).

Secreted Pla2g2a Enhances ISC Function upon Inflammation

Pla2g2a expression and secretion is increased upon inflammation (Lambeau and Gelb, 2008), and its concentration is expected to increase in the intestinal lumen. To mimic and assess the effects of secreted Pla2g2a on the ISC niche, the organoid assays were repeated from C57BL/6J mice with recombinant

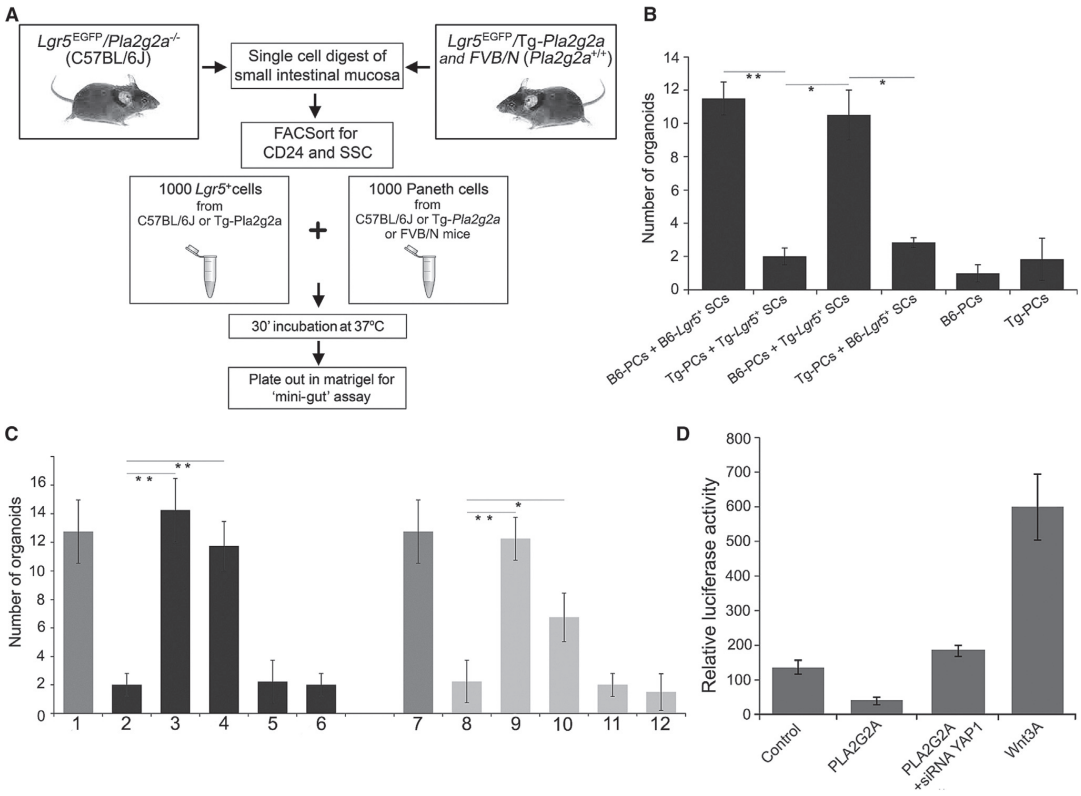

Figure 3. Reconstitution Organoid Assays Highlight the Role of *Pla2g2a* in Inhibiting Wnt Signaling through Yap1

(A) Flowchart of the reconstitution organoid assay. Single-cell suspensions were obtained from small intestinal crypts isolated from C57BL/6J (*Pla2g2a*$^{-/-}$) and Tg-*Pla2g2a* mice previously bred with *Lgr5*-EGFP reporter animals (*Lgr5*$^{EGFP\text{-}IRES\text{-}creERT2}$). Purified *Lgr5*$^{+}$ stem cells (*Lgr5*$^{+}$CD24^{med}SSC^{lo}) and Paneth cells (CD24^{hi}SSC^{hi}) were mixed and plated in matrigel for organoid growth.

(B) Results of the reconstitution organoid assay with Paneth cells (PCs) and *Lgr5*$^{+}$ stem cells (SCs) from C57BL/6J (B6) and Tg-*Pla2g2a* (Tg) mice previously bred with *Lgr5*-EGFP reporter animals (*Lgr5*$^{EGFP\text{-}IRES\text{-}creERT2}$) (n = 3, *p < 0.05; **p < 0.001).

(C) Organoid formation following reconstitution of *Lgr5*$^{+}$stem cells (SCs) and Paneth cells (PCs) sorted from *Pla2g2a*$^{-/-}$ (B6), Tg-*Pla2g2a* (Tg), and FVB/N (FVB) mice. When indicated, PCs were pretreated with siRNA oligonucleotides directed against *Pla2g2a*, *Yap1*, or a "scrambled" (SCR) control sequence (n = 3, *p < 0.05; **p < 0.001). (1) B6-PCs + B6-SCs, (2) Tg-PCs + Tg-SCs, (3) Tg-PCs [siRNA-*Pla2g2a*] + B6-SCs, (4) Tg-PCs [siRNA-*Yap1*] + B6-SCs, (5) Tg-PCs [siRNA-SCR] + B6-SCs, (6) Tg-PCs, (7) B6-PCs + B6-SCs, (8) FVB-PCs + B6-SCs, (9) FVB-PCs [siRNA-*Pla2g2a*] + B6-SCs, (10) FVB-PCs [siRNA-*Yap1*] + B6-SCs, (11) FVB-PCs [siRNA-SCR] + B6-SCs, and (12) FVB-PCs.

(D) TOP-Flash reporter analysis of Wnt signaling activity in the colon cancer cell line SW480 upon transient transfection with a *PLA2G2A* expression vector in the presence/absence of siRNA-driven *YAP1* downregulation (n = 3, *p < 0.05).

Pla2g2a protein added to the culture medium. A >2-fold increase ($p < 0.001$) was observed in organoid formation upon addition of recombinant sPLA2-IIA even at low concentrations (i.e., in the nM range; Figure 4A). Repeating the experiment in the presence of soluble Pla2r1 receptor, which sequesters the recombinant sPLA2-IIA protein with high affinity (Rouault et al., 2007), completely prevented these stimulatory effects (Figure 4A).

We then utilized an in vivo model of inflammation to confirm increased Pla2g2a secretion exerts a positive effect on ISC function. Inflammation was induced in C57BL/6J (*Pla2g2a*$^{-/-}$), FVB/N (*Pla2g2a*$^{+/+}$), and Tg-*Pla2g2a* mice by adding 3% dextran sodium sulfate (DSS) to their drinking water for a week. This results in loose stools, fecal bleeding, infiltration of the mucosa with granulocytes, and significant body weight loss (Wirtz et al., 2007). The DSS treatment causes an inflammatory response throughout the entire GI tract (pan-gastroenteritis) (Yazbeck et al., 2011) and is therefore suited to study the role of Pla2g2a secretion in the small intestine. Notably, the overall disease activity index (DAI) (Cooper et al., 1993) following DSS treatment, here employed as a general indicator of the detrimental effects of inflammation, was moderately improved in Tg-*Pla2g2a* compared to C57BL/6J mice (DAI = 5.2 and 8.1, respectively; Table S1). The subtle nature of this effect was confirmed by the observation that histologic parameters (i.e., CD3- and

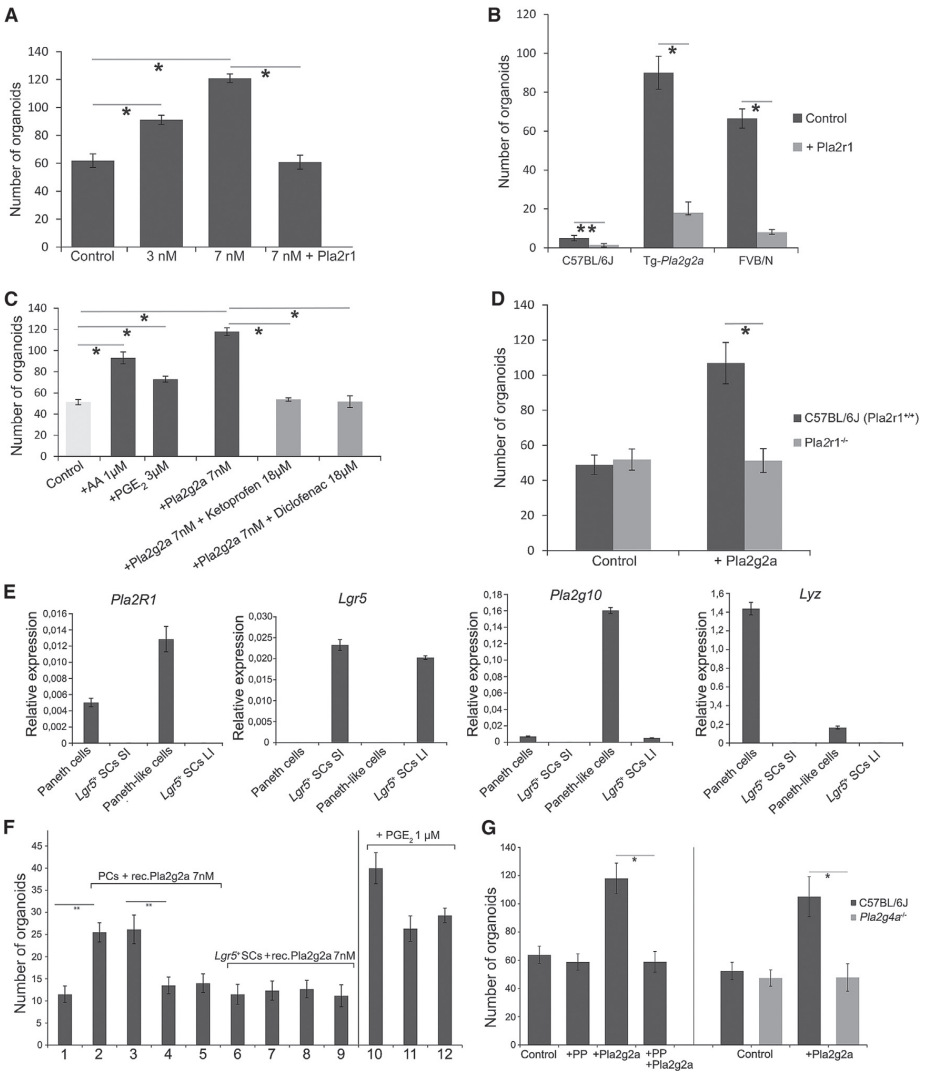

Figure 4. Secreted Pla2g2a Enhances ISC Function through PGE_2 Synthesis and Wnt Signaling upon Inflammation

(A) C57BL/6J organoid formation in the absence/presence of recombinant Pla2g2a and soluble Pla2r1 receptor (n = 5, *p < 0.001).

(B) Quantified organoid formation following DSS treatment of C57BL/6J (*Pla2g2a*$^{-/-}$), Tg-*Pla2g2a*, and FVB/N (*Pla2g2a*$^{+/+}$) mice, in the absence/presence of soluble Pla2r1 (n = 3, *p < 0.001; **p < 0.05).

(C) Results of organoid assays performed on *Pla2g2a*$^{-/-}$ (C57BL/6J) mice in the presence of agonists (AA, PGE_2) and antagonists (NSAIDs; ketoprofen and diclofenac), the latter in the presence of recombinant Pla2g2a (n = 5, *p < 0.001).

(D) Results of organoid assays from C57BL/6J versus *Pla2r1*$^{-/-}$ mice in the absence/presence of recombinant Pla2g2a (n = 5, *p < 0.001).

(E) qRT-PCR expression analysis of *Pla2r1* in sorted *Lgr5*$^{+}$, Paneth, and p16 (Paneth-like) cells of the small (SI) and large (LI) intestine. Control qRT-PCR analyses were performed to validate the quality and identity of the sorted stem (*Lgr5*), Paneth (*Lyz*), and p16 (*Pla2g10*) cells.

(F) Left panel (2–9): organoid numbers following reconstitution of Paneth cells (PCs) (2–5) or *Lgr5*$^{+}$ stem cells (SCs) (6–9) sorted from the small intestine of *Lgr5*-reporter C57BL/6J (B6) mice pretreated with recombinant Pla2g2a. When indicated, sorted cells were also treated with siRNA oligonucleotides specific for *Pla2r1* and *Cox2*, or scrambled sequences (SCR) (n = 3, *p < 0.05; **p < 0.001). (1) B6-PCs + B6-SCs (negative control; no rec. Pla2g2a), (2) B6-PCs + B6-SCs, (3) B6-PCs [siRNA-SCR] + B6-SCs, (4) B6-PCs [siRNA-*Pla2R1*] + B6-SCs, (5) B6-PCs [siRNA-*Cox2*] + B6-SCs, (6) B6-PCs + B6-SCs, (7) B6-PCs + B6-SCs [siRNA-SCR], (8) B6-PCs + B6-SCs [siRNA-*Pla2R1*], and (9) B6-PCs + B6-SCs [siRNA-*Cox2*]. Right panel (10–12): organoid numbers upon reconstitution of B6-PCs with B6-SCs in

(legend continued on next page)

MUC1-positive cells, presence of infiltrating cells and ulcers, and destruction of tissue architecture) did not differ between the two genotypes (data not shown). We also confirmed a substantial increase in Pla2g2a secretion following DSS-induced inflammation by ELISA on stool samples from Tg-*Pla2g2a* and C57BL/6J mice (Figure S5A, left).

Consistently, a striking increase in organoid multiplicity was observed upon DSS-induced inflammation from the *Pla2g2a*-proficient strains (Tg-*Pla2g2a* and FVB/N mice) when compared to *Pla2g2a*-deficient C57BL/6J mice (Figure 4B). Notably, both Tg-*Pla2g2a* and FVB/N were characterized by a low organoid-forming capacity under homeostatic conditions (Figures 1A and 1B). The soluble Pla2r1 scavenger inhibited this increase, confirming that Pla2g2a secretion underlies this measure of enhanced ISC function (Figure 4B). This conclusion was confirmed by treating organoids with the pro-inflammatory cytokine interferon-gamma (IFN-γ) to trigger Paneth cell degranulation and release of Pla2g2a into the culture medium (Farin et al., 2014), which significantly increased organoid multiplicity from Tg-*Pla2g2a*, but not C57BL/6J, mice.

sPLA2-IIA proteins play important roles in prostaglandin synthesis. sPLA2 proteins hydrolyze phospholipids to produce AA that is converted by cyclooxygenases (Cox1 and Cox2) into prostaglandin E2 (PGE_2) (Lambeau and Gelb, 2008). Accordingly, a >100-fold increase in PGE_2 synthesis was observed in intestinal organoids from C57BL/6J (*Pla2g2a*$^{-/-}$) upon addition of recombinant Pla2g2a to the culture medium (Figure S5C).

To test whether the observed positive effect exerted by secreted Pla2g2a on ISC function is due to increased PGE_2 production, we repeated the organoid assays in the presence of prostaglandin biosynthesis agonists (AA, PGE_2) and antagonists (NSAIDs; ketoprofen and diclofenac). Both AA and PGE_2 had positive effects on organoid multiplicity similar to recombinant Pla2g2a, whereas either NSAID inhibited the Pla2g2a-dependent increase in number of organoids obtained from C57BL/6J animals (Figure 4C). Additionally, changes in organoid morphology into enterospheres, spherical structures primarily composed of stem cells and that lack budding and branching structures (Stelzner et al., 2012), were noted upon addition of Pla2g2a, AA, and PGE_2, and in organoids obtained by DSS-treated mice (Figure S5D). Conversion of organoids to enterospheres is regulated by Wnt signaling (Mustata et al., 2013). Consistent with these results and previous reports of synergism between PGE_2 and the canonical Wnt pathway in hematopoietic stem cells (Goessling et al., 2009) and colon carcinoma cells (Castellone et al., 2005; Shao et al., 2005), PGE_2 enhanced Wnt activity in SW480 and HCT116 colon cancer cell lines (Figure S5E).

To elucidate how exogenous Pla2g2a triggers PGE_2 biosynthesis, we tested the organoid-forming capacity of Pla2g2a receptor type 1 (*Pla2r1*) knockout mice in the presence/absence of recombinant Pla2g2a. While no change in organoid number was seen between wild-type (C57BL/6J) and *Pla2r1*$^{-/-}$ mice in the absence of exogenous Pla2g2a, the latter did not respond to recombinant Pla2g2a (Figure 4D). Hence, *Pla2r1* mediates the positive effects of exogenous Pla2g2a on ISC function. We then determined that within the intestine, *Pla2r1* expression was exclusively detected in Paneth cells (Figure 4E). To functionally validate this observation, we performed organoid reconstitution assays with Paneth cells pretreated with siRNA oligonucleotides against *Pla2r1*. Knockdown of *Pla2r1* in Paneth cells, though not in *Lgr5*$^{+}$ stem cells, abolished the positive effect of recombinant Pla2g2a on organoid multiplicity (Figure 4F, left).

The cytosolic phospholipase A2 group IVα (Pla2g4a or cPLA2α) is activated by Pla2r1 to catalyze AA biosynthesis (Lambeau and Gelb, 2008). The specific cPLA2α inhibitor pyrrophenone suppressed the increase in organoid multiplicity observed by adding exogenous Pla2g2a (Figure 4G, left); also, organoids grown from *Pla2g4a* knockout mice (Bonventre et al., 1997) were insensitive to the stimulatory effects of exogenous Pla2g2a (Figure 4G, right). Additional reconstitution assays with sorted Paneth cells treated with PGE_2 (Figure 4F, right) and anti-Cox2 siRNA oligonucleotides (Figure 4F, left) confirmed that prostaglandin biosynthesis plays a central role in mediating effects of secreted Pla2g2a on ISC function. In sum, these results show that secreted Pla2g2a positively regulates ISC proliferation through the Pla2r1 receptor, which activates Pla2g4a/cPLA2α. This triggers the release of AA, which is then converted by Cox1/2 into PGE_2 to synergistically activate the canonical Wnt pathway.

Pla2g10 Is Expressed by the Paneth-like Secretory Cell Lineage in the Mouse Colon

Similarly to Paneth cells in supporting *Lgr5*$^{+}$ ISCs in the small intestine, we hypothesized that a secretory cell lineage with similar niche functions may be present in the colon and could physically associate with *Lgr5*$^{+}$ CBCs to promote organoid formation. A *c-Kit*$^{+}$ subpopulation of secretory epithelial cells from the colon was recently shown to promote organoid formation from *Lgr5*$^{+}$ ISCs (Rothenberg et al., 2012). We performed FACS analysis of the colonic epithelium from *Lgr5*-EGFP reporter mice with CD24 and c-Kit markers and defined four distinct sorting gates (p11, CD24^{med}/cKit^{lo}; p15, CD24^{med}/cKit^{med}; p16, CD24^{hi}/cKit^{hi}; p18, CD24^{med}/cKit^{hi}) (Figure 5A). Within these gates, *Lgr5*$^{+}$ cells were present either as single cells (mostly in p11) or in physical association (as doublets or triplets) with potential niche cells.

Reconstitution organoid assays were then performed by incubating colonic *Lgr5*$^{+}$ stem cells (p11; *Lgr5*$^{+}$/CD24^{med}/cKit^{lo}) with the same number of (GFP^{-}) single cells from each of the p15, p16, and p18 subpopulations. *Lgr5*$^{+}$ doublets and triplets were excluded by sorting, as previously described (Roth et al., 2012). The p16 subpopulation (c-Kit^{+}/CD24^{hi}) unequivocally promotes organoid formation compared with all other subpopulations, each of which gave rise to no or very few organoids (Figure 5B). Confocal microscopy confirmed that only the p16 subpopulation contained doublets and triplets of smaller *Lgr5*$^{+}$ stem cells and larger *Lgr5*-negative cells (these clusters were subsequently excluded during sorting; Figures 5C and S6). Sorted p16 cells expressed a mixed signature of

the presence of 1 μM PGE_2 for 30 min. (10) Both B6-SCs and B6-PCs pretreated with PGE_2, (11) only PCs pretreated with PGE_2, and (12) only PCs pretreated with PGE_2.

(G) Organoid assays from C57BL/6J (*Pla2g2a*$^{-/-}$) mice in the presence/absence of pyrrophenone (PP) and recombinant Pla2g2a (left panel), and from C57BL/6J versus *Pla2g4a*$^{-/-}$ in the absence/presence of recombinant Pla2g2a (right panel) (n = 5, *p < 0.001).

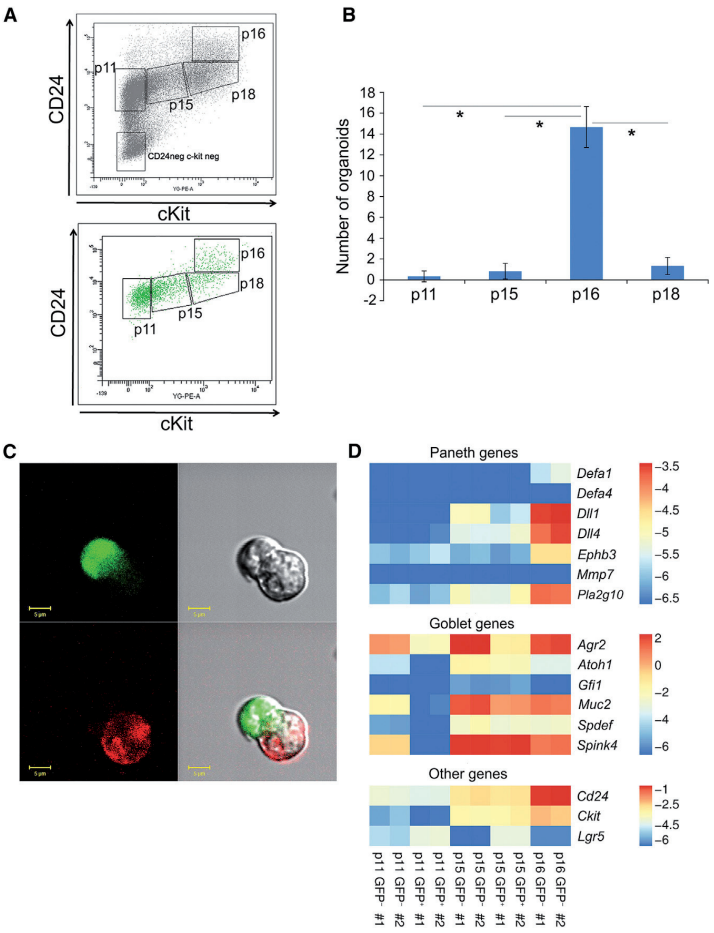

Figure 5. *Pla2g10* Is Expressed by the Paneth-like Secretory Cell Lineage in the Mouse Colon

(A) CD24/cKit/SSC FACS sorting strategy employed for colonic epithelial cells from *Lgr5*-EGFP reporter animals (*Lgr5*$^{EGFP\text{-}IRES\text{-}creERT2}$). Upper panel, whole colon; lower panel, GFP$^+$ (*Lgr5*$^+$) fraction. Sorting gates were defined as follows: p11 (CD24^{med}/cKit^{lo}), p15 (CD24^{med}/cKit^{med}), p16 (CD24^{hi}/cKit^{hi}), and p18 (CD24^{med}/cKit^{hi}).

(B) Organoid formation assay upon reconstitution of 1,000 cells from the p15/16/18 gates (after depletion of GFP-positive doublets by side scatter) with 1,000 Lgr5$^+$ stem cells (p11) (n = 3, *p < 0.001).

(C) Confocal microscopy images of doublets constituted by smaller *Lgr5*$^+$ (GFP$^+$) stem cells and larger Lgr5-negative and c-Kit$^+$ (red) cells found in p16.

(D) Heatmap representation of the results of the qRT-PCR expression analysis of sorted p16, p15, and p11 cells for Paneth- and goblet-specific genes.

Paneth- (*Mmp7*, *Dll1*, *Dll4*, *Ephb3*) and goblet-cell-specific genes (*Muc2*, *Spdef*, *Spink4*) (Figure 5D). Notably, another member of the sPLA2 family, namely *Pla2g10* encoding the mouse group X secreted phospholipase A2 (sPLA2-X or mGX-sPLA$_2$), was expressed at a significantly higher level in p16 than in the other populations (Figure 5D). Accordingly, previous reports indicated that sPLA2-X is expressed in the colon (Mounier et al., 2008).

Pla2g10 Has Opposing Roles in Regulating Wnt Signaling and ISC Function in the Colon during Homeostasis and Inflammation

We then assessed whether *Pla2g10* controls stem cell function in the colon. We performed organoid assays from colonic crypts derived from *Pla2g10*$^{-/-}$ knockout mice in the C57BL/6J background (therefore null for *Pla2g2a* and *Pla2g10*) (Shridas et al., 2010) and *Pla2g10*$^{+/+}$ controls. Genetic ablation of *Pla2g10* significantly increased the number of colon organoids (Figure 6A). We then assessed whether the negative effect of *Pla2g10* expression on colonic stem cell proliferation resulted from Wnt signaling inhibition, similarly to *Pla2g2a* in the small intestine. Transient *PLA2G10* expression inhibited TOPflash Wnt reporter activity in colon cancer lines with constitutive Wnt activation (Figure 6B). Consistently, stable *PLA2G10* expression in colon cancer cells significantly reduced CSC multiplicity as shown by ''megacolony'' formation (Yeung et al., 2010) (Figure S7B).

Plag2g10 expression in p16 cells mediates these inhibitory effects. Pre-treating p16 cells (c-Kit$^+$/CD24^{hi}) with *Pla2g10* siRNA before reconstituting them with *Lgr5*$^+$ stem cells (p11; CD24^{med}/cKit^{lo}) from the colonic epithelium of *Lgr5*-EGFP reporter mice effectively increased colon organoid formation (Figure 6C), confirming the results obtained with the *Pla2g10*-deficient mice. Similar to the small intestine, siRNA-mediated *Yap1* downregulation rescued the capacity of p16 cells from C57BL/6J mice to form colon organoids when reconstituted with *Lgr5*$^+$ stem cells (Figure 6C) and suppressed the inhibitory effect of *PLA2G10* expression on Wnt in human colon cancer cells (Figure 6D). Hence, under homeostatic conditions *Pla2g10* negatively regulates Wnt signaling and stem cell proliferation in the colon via Yap1, analogous to *Pla2g2a* in the small intestine.

The parallels between *Pla2g2a* and *Pla2g10* in regulating stem cell function extend beyond homeostasis. Addition of recombinant sPLA2-X protein in organoid reconstitution assays to mimic the effects of its secretion significantly enhanced organoid formation (Figure 7A); this effect was negated by addition of soluble Pla2r1. The catalytic mGX sPLA2 mutant H48Q also enhanced organoid multiplicity (Figure 7A), indicating that the effects of sPLA2-X are mediated primarily via Pla2r1, which binds

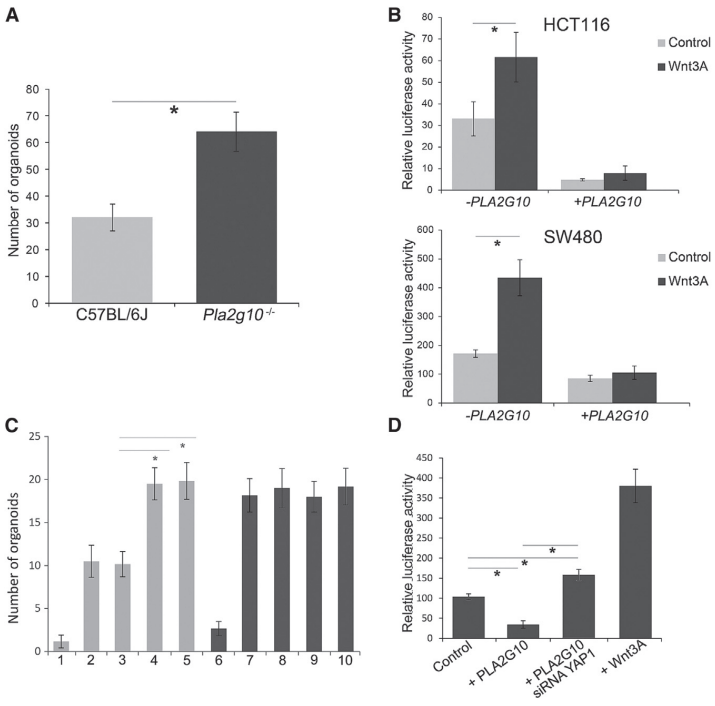

Figure 6. *Pla2g10*, Analogous to *Pla2g2a* in the Small Intestine, Has Opposing Roles in Regulating Wnt and ISC Function in the Colon during Homeostasis and Inflammation

(A) Colon organoid assay of C57BL/6J (*Pla2g2a*$^{-/-}$/*Pla2g10*$^{+/+}$) and *Pla2g10*-knockout (*Pla2g2a*$^{-/-}$/*Pla2g10*$^{-/-}$) mice (n = 3, *p < 0.001).

(B) TOP-Flash reporter assay of Wnt activity in colon cancer cell lines SW480 and HCT116 upon transient transfection with a *PLA2G10* expression plasmid (n = 3, *p < 0.001).

(C) Organoid formation following reconstitution of colonic *Lgr5*$^{+}$ stem cells (SCs) with *Pla2g10*-proficient (B6) and *Pla2g10*- deficient (*Pla2g10*KO) Paneth-like cells (p16). When indicated, p16 cells were pretreated with siRNAs against *Pla2g10*, *Yap1*, or a "scrambled" (SCR) control sequence (n = 3, *p < 0.05; **p < 0.001). (1) B6-p16, (2) B6-p16 + B6-SCs, (3) B6-p16 [siRNA-SCR] + B6-SCs, (4) B6-p16 [siRNA-*Pla2g10*] + B6-SCs, (5) B6-p16 [siRNA-*Yap1*] + B6-SCs, (6) *Pla2g10*KO-p16, (7) *Pla2g10*KO-p16 + B6-SCs, (8) *Pla2g10*KO-p16 [siRNA-SCR] + B6-SCs, (9) *Pla2g10*KO-p16 [siRNA-*Pla2g10*] + B6-SCs, and (10) *Pla2g10*KO-p16 [siRNA-*Yap1*] + B6-SCs.

(D) TOP-Flash Wnt reporter assay in the colon cancer cell line SW480 upon transient transfection with a *PLA2G10*-expression plasmid and siRNA-driven YAP1 downregulation (n = 3, *p < 0.05).

sPLA2-X with high affinity in the mouse colon (Rouault et al., 2007). As observed for Pla2g2a, PGE_2-driven Wnt stimulation contributes to this stimulatory effect, supported by the significant increase in prostaglandin level in the culture medium of colonic organoids from C57BL/6J mice upon addition of recombinant sPLA2-X (Figure S5C). As expected, this increase was entirely suppressed by the addition of NSAIDs (ketoprofen and diclofenac, inhibitors of cyclooxygenase activity) to the culture medium together with the recombinant Pla2g2a (Figure S5C). Accordingly, the positive effects on organoid formation upon addition of recombinant Pla2g10 were inhibited by an antibody directed against mouse Pla2r1 (Rouault et al., 2007), the two NSAIDs, and the cPLA2α inhibitor pyrrophenone (Lambeau and Gelb, 2008), thus confirming that the pathway through which the secreted Pla2g10 stimulates PGE_2 synthesis is analogous to that observed for secreted Pla2g2a (Figure 7B). As it was observed for Paneth cells in the small intestine, *Pla2r1* expression was exclusively found in p16 and not in *Lgr5*$^{+}$ stem cells of the colon (Figure 4E). Moreover, knockdown of *Pla2r1* in the same p16 cells, though not in *Lgr5*$^{+}$ cells, abolishes the positive effect brought about by the recombinant Pla2g10 on organoid multiplicity in reconstitution assays (Figure S7A). Additional reconstitution assays performed with sorted p16 cells treated with PGE_2 and with siRNAs directed against Cox2 confirmed the central role of the prostaglandin biosynthesis pathway in underlining the positive effect of secreted Pla2g10 on colonic stem cell function (Figure S7A). In vivo validation for these observations was provided by the significantly increased organoid formation capacity upon DSS treatment of *Pla2g10* knockout mice when compared with C57BL/6J (*Pla2g10*$^{+/+}$) (Figure 7D). Accordingly, Pla2g10 is secreted upon inflammation, as shown by TR-FIAs analysis of stool samples from DSS-treated C57BL/6J mice (Eerola et al., 2006) (Figure S5A, right).

Overall, these results confirm that the previously shown opposite roles of *Pla2g2a* as intracellular and secreted stem cell niche factor in Paneth cells of the small intestine are conserved by the *Pla2g10* gene in p16 (Paneth-like) secretory cells of the colon.

Pla2g2a and Pla2g10 Are Genetic Modifiers of IBD and Colon Cancer: The "Trade-Off" Effect

In view of the C57BL/6J (*Pla2g2a*$^{-/-}$) inbred background of the *Pla2g10*$^{-/-}$ mice, a more thorough genetic analysis was needed to address the distinct roles of the two phospholipases as modifiers of intestinal bowel inflammation and colon cancer. To this aim, we first administered 3% DSS in the drinking water for a week to mice of all four Pla2 genotypes (*Pla2g2a*$^{-/-}$/*Pla2g10*$^{+/+}$ [C57BL/6J], Tg-*Pla2g2a*/*Pla2g10*$^{+/+}$ [Tg-*Pla2g2a*], Tg-*Pla2g2a*/*Pla2g10*$^{-/-}$, and *Pla2g2a*$^{-/-}$/*Pla2g10*$^{-/-}$). The DAI (Table S1) (Cooper et al., 1993) and in particular the loss of weight (Figure 7C) show that genetic ablation of *Pla2g10* resulted in an improved response to the DSS-induced colitis both in the presence or absence of a functional *Pla2g2a* allele. As also observed in the small intestine, immune-histopathologic parameters in the colon (number of colonic ulcers, presence of inflammatory cells) did not show any major difference among the four genotypes (data not shown).

Supporting these data, the organoid formation capacity upon DSS treatment of *Pla2g2a*$^{-/-}$/*Pla2g10*$^{-/-}$ mice was significantly

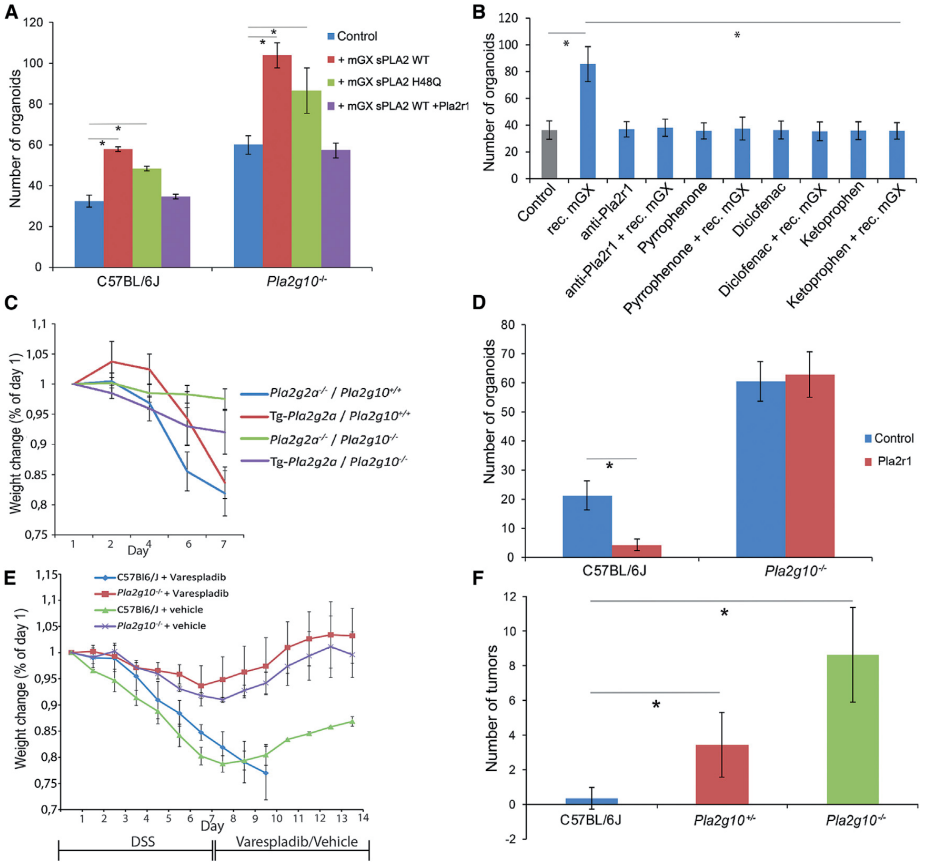

Figure 7. *Pla2g2a* and *Pla2g10* Are Genetic Modifiers of IBD and Colon Cancer

(A) Results of colon organoid assay of C57BL/6J ($Pla2g2a^{-/-}/Pla2g10^{+/+}$) and *Pla2g10*-knockout ($Pla2g2a^{-/-}/Pla2g10^{-/-}$) mice in the presence/absence of recombinant mGX sPLA2 (both wild-type and the H48Q catalytic mutant proteins were employed), and of the recombinant (soluble) Pla2r1 receptor (n = 3, *p < 0.001; **p < 0.05).

(B) Results of colon organoid assays performed on C57BL/6J mice in the presence of recombinant mGX sPLA2 alone or in combination with an antibody directed against the mouse Pla2r1 receptor (Rouault et al., 2007), pyrrophenone, a specific cPLA2α inhibitor (Lambeau and Gelb, 2008), and NSAIDs (ketoprofen and diclofenac) (n = 3, *p < 0.001).

(C) Quantification of the response to DSS-induced inflammation in mice of the four *Pla2g2a*/*Pl2g10* genotypes as measured by percentage of weight loss (compared with starting weight). See also Table S1 for more details.

(D) Results of colon organoid assay of C57BL/6J ($Pla2g2a^{-/-}/Pla2g10^{+/+}$) and *Pla2g10*-knockout ($Pla2g2a^{-/-}/Pla2g10^{-/-}$) mice upon DSS-driven inflammation in the presence/absence of the soluble Pla2r1 receptor (n = 3, *p < 0.001).

(E) Quantification of the response to DSS-induced inflammation and varespladib administration (from day 8 onward) in mice of the four *Pla2g2a*/*Pl2g10* genotypes as measured by percentage of weight loss (compared with starting weight). Varespladib treatment of C57BL/6J animals prevented their recovery, and the mice had to be euthanized at day 10. See also Table S2 for more details.

(F) Incidence of colonic tumors in $Pla2g2a^{-/-}/Pla2g10^{+/+}$ (C57BL/6J), $Pla2g2a^{-/-}/Pla2g10^{-/+}$, and $Pla2g2a^{-/-}/Pla2g10^{-/-}$ mice upon AOM-DSS treatment (n = 10, *p < 0.001).

increased when compared with C57BL/6J ($Pla2g2a^{-/-}/Pla2g10^{+/+}$) mice (Figure 7D). In the same set of experiments, addition of the recombinant Pla2r1 soluble receptor to the culture medium reduced organoid multiplicity from C57BL/6J mice, whereas it had, as expected, no effect on organoids from $Pla2g2a^{-/-}/Pla2g10^{-/-}$ mice (Figure 7D). This indicates that the increase in organoid numbers observed in double knockout (DKO) mice upon inflammation cannot be replicated in DSS-treated $Pla2g2a^{-/-}/Pla2g10^{+/+}$ animals by scavenging the secreted group X PLA2 with the soluble Pla2r1 receptor.

To further investigate the role of the secreted phospholipases in response to inflammation, we repeated the DSS treatment of $Pla2g2a^{-/-}/Pla2g10^{-/-}$ and C57BL/6J ($Pla2g2a^{-/-}/Pla2g10^{+/+}$) mice as described above, followed by administration of

varespladib, a non-permeable inhibitor of group IIA, V, and X sPLA2 (Smart et al., 2006). As shown in Figure 7E and Table S2, loss of body weight and the overall DAI scores were significantly improved in DKO mice when compared with the C57BL/6J controls independently of varespladib or vector administration. However, while vehicle-treated C57BL/6J animals started recovering body weight from day 8 onward, treatment with varespladib prevented their recovery and led to severe deterioration (i.e., increased loss of weight, diarrhea, gross fecal bleeding, and lethargic state) of these mice, which had to be euthanized at day 10 (Figure 7E). Hence, group X sPLA2 inhibition in the absence of sPLA2-IIA prevents recovery from acute inflammation, whereas null mutations at both *Pla2g2a* and *Pla2g10* genes improve the overall response to the inflammatory insult, analogous to the effect of Pla2r1 on organoid multiplicity after DSS treatment.

As presented above, several reports failed to demonstrate that the human *PLA2G2A* gene represents a major modifier of colon cancer in man (Riggins et al., 1995; Spirio et al., 1996). In view of these reports, we asked whether the combined genetic ablation of both *Pla2g2a* and *Pla2g10* confers susceptibility to colon cancer. To this aim, we applied the well-established AOM-DSS protocol to elicit colon tumors in $Pla2g2a^{-/-}/Pla2g10^{+/-}$ and $Pla2g2a^{-/-}/Pla2g10^{-/-}$ mice when compared with C57BL/6J ($Pla2g2a^{-/-}/Pla2g10^{+/+}$) controls (Neufert et al., 2007; Tanaka et al., 2003). Notably, the C57BL/6J strain has been reported to be resistant to this protocol (Suzuki et al., 2006). Upon a single AOM injection followed by 1 week with 3% DSS in the drinking water, $Pla2g2a^{-/-}/Pla2g10^{+/-}$ and $Pla2g2a^{-/-}/Pla2g10^{-/-}$ animals developed a significantly increased number of colonic tumors when compared with $Pla2g2a^{-/-}/Pla2g10^{+/+}$ littermates (Figure 7F). Histological and IHC analysis of the colonic tumors obtained in $Pla2g10^{-/-}$ mice revealed carcinoma in situ features with β-catenin nuclear translocation (data not shown), as also shown in other AOM-DSS rodent models of colon carcinogenesis. However, no histopathological differences were observed between tumors found in $Pla2g10^{-/-}$ and those arising in $Pla2g10^{+/-}$ and $Pla2g10^{+/+}$ mice (data not shown). Hence, the combined deficiency of *Pla2g2a* and *Pla2g10* increases susceptibility to colon cancer in the context of DSS-induced colitis.

Hence, it appears that while complete genetic depletion of both *Pla2g2a* and *Pla2g10* protects against the detrimental effects of the DSS-induced intestinal inflammation, the trade-off for this protective effect is the pronouncedly increased predisposition to multifocal colon cancers.

DISCUSSION

Collectively, the data presented in our study show that the *Pla2g2a* and *Pla2g10* genes, encoding for the group IIA and group X sPLA2s, play regulatory roles as stem cell niche factors in both the small intestine (in Paneth cells) and in the large bowel (in secretory Paneth-like cells of the colon). Notably, their stem cell regulatory functions are context dependent: both inhibit Wnt signaling from within the intracellular compartment during homeostasis, thus controlling maturation and the stem-cell-supporting function of these secretory lineages. Upon inflammation, however, they are secreted into the intestinal lumen and stimulate Wnt in autocrine fashion through PGE_2 biosynthesis, thus contributing to the regenerative response (Zhang et al., 2015) (see Graphical Abstract). It should be noted that although Wnt has been the major object of our investigations, it is likely that other signaling pathways play important roles downstream of the A2 phospholipases. For example, the observed cell-cell defect (see Movie S1) is likely to result from the decreased expression of the Notch ligands *Dll1* and *Dll4* in Paneth cells from Tg-*Pla2g2a* mice (Figure 1E) as it has been shown that $Lgr5^+$ CBCs require Notch signals, which are governed by direct cell-cell contacts (Fre et al., 2005; van Es et al., 2005b).

Based on the above, the human *PLA2G2A* and *PLA2G10* genes and other members of the here-identified pathways are likely to represent important genetic modifiers of inflammatory bowel disease (IBD) and colon cancer in man. In a recently published GWAS association study of IBD (Liu et al., 2015), 38 risk loci were identified, including three genes, namely *PTGS2* (*COX2*), *PLA2G4A*, and *PLA2R1*, which are integral members of the prostaglandin biosynthesis pathway through which sPLA2s positively affect ISC function during inflammation. In the context of inflammation, group IIA and X sPLA2 are secreted into the intestinal lumen, where they promote PGE_2 synthesis through interaction with the Pla2r1 receptor, activation of cPLA2α (Pla2g4a), and AA synthesis from membrane phospholipids. AA represents the main substrate of Cox2 for production of PGE_2. As previously shown and here confirmed, prostaglandin exerts stimulatory effects on Wnt signaling (Castellone et al., 2005; Goessling et al., 2009; Shao et al., 2005). Accordingly, inhibition of the prostaglandin-degrading enzyme 15-PGDH (15-hydroxyprostaglandin dehydrogenase) increases regenerative capacity in a broad spectrum of tissues, including bone marrow and the colon (Zhang et al., 2015).

Based on the model arising from the above data, expression of the group IIA and X secreted phospholipases is expected to improve the overall response to inflammation, whereas *null* or hypomorphic alleles at these genes are predicted to increase susceptibility to the detrimental effects of IBD. This was in part confirmed in the Tg*Pla2g2a* mice compared to the *Pla2g2a*-deficient C57BL/6J inbred strain. In the presence of a functional *Pla2g10* gene, Pla2g2a secretion upon DSS-treatment improves stem cell function and the overall response to the deleterious effects of inflammation (Table S1). Surprisingly, the most improved response to DSS-induced inflammation was observed in $Pla2g2a^{-/-}/Pla2g10^{-/-}$mice, i.e., in the absence of the secreted group IIA and X phospholipases (Figure 7C; Table S1).

Two distinct results obtained here may point to a likely explanation for this apparently contradictory observation. First, addition of the Pla2r1 soluble receptor to the culture medium negatively affected organoid multiplicity from DSS-treated C57BL/6J mice (Figure 7D). This shows that the high organoid multiplicity observed in DKO mice upon inflammation cannot be replicated by scavenging the secreted Pla2g10 in DSS-treated C57BL/6J ($Pla2g2a^{-/-}/Pla2g10^{+/+}$) mice. This ex vivo result was then confirmed in vivo by administrating varespladib, a non-permeable inhibitor of both Pla2g2a and Pla2g10 (Smart et al., 2006), to C57BL/6J mice after DSS administration. Whereas vehicle-treated C57BL/6J animals started recovering only a few days after DSS treatment, varespladib administration prevented recovery and severely compromised the overall

health status of these animals (Figure 7E; Table S2). Hence, scavenging of group X sPLA2 (in the absence of sPLA2-IIA) fails to reproduce the improved response to the inflammatory insult observed in DKO mice. This suggests that the underlying cause of the protective effect to the detrimental effects of DSS observed in DKO mice may reside in the functional role that both phospholipases play in the ISC niche during homeostasis when they exert a regulatory function on niche cells by inhibiting Wnt. Genetic ablation of *Pla2g10* and *Pla2g2a* relieves this intracellular inhibitory effect, thus enhancing Wnt and positively affecting ISC function and tissue regeneration. Accordingly, the expression of known Wnt targets in sorted p16 (Paneth-like) and total colon cells from mice of all four genotypes was assayed. As shown in Figure S7C, during homeostasis specific Wnt targets (i.e., *Axin2*, *Jun*, *Klf4*, *Efnb2*, *Sox9*) are upregulated in Paneth-like cells of the colon in a gradient from *Pla2g10*/*Pla2g2a*-proficient mice to the DKO animals. This effect was not seen when whole crypts were analyzed (Figure S7C). The observed increase in Wnt activity upon genetic ablation of both genes is also reflected by the highest organoid formation efficiency obtained from the colon of DKO mice both in homeostasis (Figure 6A) and upon inflammation (Figure 7D). These data support the upregulation of Wnt signaling in niche cells of the colon upon *Pla2g10* and *Pla2g2a* genetic ablation and provide a plausible explanation for their improved response to acute inflammation.

Among the Wnt targets found to be upregulated in colonic Paneth-like cells of DKO mice, *Sox9* is noteworthy as it encodes for an established transcription factor in Paneth cell differentiation (Bastide et al., 2007; Mori-Akiyama et al., 2007). Moreover, *Sox9* expression was also associated with the appearance of ectopic Paneth cells in the colon upon inducible *Apc* loss and constitutive Wnt activation (Feng et al., 2013). Hence, *SOX9* upregulation is likely to underlie Paneth cell metaplasia in IBD patients with improved response to the inflammatory insult (Paterson and Watson, 1961). Increased Wnt signaling in colonic p16 cells triggers *Sox9* upregulation and the consequent maturation toward the Paneth cell lineage. Metaplastic Paneth cells provide additional niche support and thereby improve the regenerative response to inflammation.

Whereas the observed Wnt activation, elicited by the genetic ablation of both *Pla2g2a* and *Pla2g10*, can explain the improved regenerative response to the detrimental effects of inflammation, it is also likely to enhance susceptibility to colon cancer. Indeed, $Pla2g2a^{-/-}/Pla2g10^{-/-}$ mice revealed a striking multifocal colon cancer phenotype upon AOM/DSS treatment. To assess whether the increased colon cancer susceptibility of the DKO mice was dependent on inflammation, we bred them with $Apc^{1638N/+}$, a model characterized by a mild upper GI tumor phenotype but no colon tumors (Fodde et al., 1994). Notwithstanding the limited number of animals here analyzed ($Apc^{1638N/+}/Pla2g2a^{-/-}/Pla2g10^{-/+}$, n = 5, 28 weeks old; $Apc^{1638N/+}/Pla2g2a^{-/-}/Pla2g10^{-/-}$, n = 3, 22 weeks old; $Apc^{1638N/+}/Pla2g2a^{-/-}/Pla2g10^{+/+}$, n = 3, 28 weeks old), hetero- and homozygous *Pla2g10* mutant mice were shown to develop a significantly increased multiplicity of aberrant crypt foci (average per mouse was 1.8 and 4.0, respectively, versus 0.7 in controls) and tumors (average per mouse was 1.6 and 3.7, respectively, versus 0 in controls) in the colon. Hence, the predisposition to colon cancer conferred by *Pla2g10* seems to be independent of inflammation.

Overall, although hypomorphic alleles at the *PLA2G2A* and *PLA2G10* genes and at other loci encoding for members of the same biochemical pathways may protect the individual from the detrimental effects of inflammation of the bowel, the trade-off of this initial beneficial effect may lie in an increased susceptibility to colon cancer. In the near future, it would be of interest to establish whether Paneth cell metaplasia in IBD patients is associated with improved response to inflammation in combination with increased cancer risk. In conclusion, the observed ''yin-yang'' mode of action of two sPLA2s in intestinal homeostasis and inflammation can have profound consequences for an individual's response and susceptibility to inflammation and to both sporadic (i.e., non-inflammatory) and IBD-related colon cancer. Finally, in view of the abundance of sPLA2s in several mammalian tissues, it will be of interest to assess whether their newly identified role as key ISC niche factors in health and disease holds true for a broader spectrum of organs.

EXPERIMENTAL PROCEDURES

Organoid Assays

To form organoids ex vivo, two distinct sources of cells were employed, namely whole crypts and single-cell suspensions from small intestine or colon. Whole crypt cultures were performed as previously described (Sato et al., 2009).

All organoid assays were performed in several biological replicates (i.e., with independent animals of the same genotype and/or experimental conditions) defined by ''n,'' whereas three technical replicates were implemented for each biological replicate. Organoids were counted at day 5 in most of the experiments unless stated otherwise.

AOM/DSS-Induced Colon Carcinogenesis

To induce colon cancer in the context of inflammation, a modification of the well-established AOM/DSS protocol was employed (Neufert et al., 2007). In short, mice were administered a single azoxymethane (AOM) injection (intraperitoneal; 10 mg/kg), followed by 1 week with the inflammatory agent DSS (MP Biomedicals) in the drinking water (2.5%). Mice were then euthanized 16 weeks after AOM injection or at the first appearance of signs of discomfort. All procedures were performed in agreement with local animal welfare laws and guidelines.

DAI Scores and Varespladib Treatment

To establish DAI scores upon DSS-induced inflammation, we employed the method originally described by Cooper et al. (1993), with minor modifications. Mice were administered 3% DSS in the drinking water for a week, during which they were monitored for a number of parameters including stool consistency, blood loss, appearance, and percent weight loss. For the treatment with varespladib, mice were first administered 3% DSS for 1 week, followed by varespladib treatment at day 8 in the drinking water (60 μM). The vehicle in which the varespladib is dissolved is 5% DMSO, 5% ETOH, and 30% PEG 300 in water.

sPLA2 Quantification

Time-resolved fluoroimmunoassays (TR-FIAs) for Pla2g2a were performed as described previously with minor modifications (Eerola et al., 2006).

More comprehensive Experimental Procedures can be found in the Supplemental Experimental Procedures.

SUPPLEMENTAL INFORMATION

Supplemental Information includes Supplemental Experimental Procedures, seven figures, two tables, and two movies and can be found with this article online at http://dx.doi.org/10.1016/j.stem.2016.05.023.

AUTHOR CONTRIBUTIONS

Experimental contributions were as follows: organoid assays (M. Schewe and P.F.F.); qRT-PCR analysis (M. Schewe and R.B.); siRNA and TOP-Flash assays (M. Schewe); colon cancer cell line culture and transfections (M. Schewe); immunohistochemistry (P.F.F.); FACS analysis and sorting (A.S.); western blot analysis (M. Schmitt); mouse colony management, AOM/DSS treatments, and phenotypic analysis (M. Schewe and R.J.); transgenic mice (R.T.C., P.M.S., M.G., C.P., G.L., and N.R.W.); recombinant proteins (C.P., M.G., and G.L.); ELISA assays (L.J. and C.P.); and live imaging of organoid formation (M.E.vR. and M. Schewe). The project was conceived by R.F. and M. Schewe with substantial contributions from R.T.C. and G.L. The manuscript was written by R.F. with substantial contributions from M. Schewe, G.L., and R.T.C. All authors contributed to the final version of the manuscript.

ACKNOWLEDGMENTS

The authors are grateful to Mr. Frank van der Panne for his help with the artwork, and to Dr. Len Augenlicht, Dr. Hans Clevers, and Dr. Pekka Katajisto for critical reading of the manuscript. This study was made possible by funding from the Dutch Cancer Society (KWF; EMCR 2012-5473) and from the Netherlands Institute of Regenerative Medicine (NIRM; http://www.regeneratieve-geneeskunde.nl/) to R.F., and from CNRS and the Fondation ARC pour la Recherche sur le Cancer to G.L.

Received: August 31, 2015
Revised: February 10, 2016
Accepted: May 19, 2016
Published: June 9, 2016

REFERENCES

Azzolin, L., Panciera, T., Soligo, S., Enzo, E., Bicciato, S., Dupont, S., Bresolin, S., Frasson, C., Basso, G., Guzzardo, V., et al. (2014). YAP/TAZ incorporation in the β-catenin destruction complex orchestrates the Wnt response. Cell *158*, 157–170.

Barker, N., van Es, J.H., Kuipers, J., Kujala, P., van den Born, M., Cozijnsen, M., Haegebarth, A., Korving, J., Begthel, H., Peters, P.J., and Clevers, H. (2007). Identification of stem cells in small intestine and colon by marker gene Lgr5. Nature *449*, 1003–1007.

Barry, E.R., Morikawa, T., Butler, B.L., Shrestha, K., de la Rosa, R., Yan, K.S., Fuchs, C.S., Magness, S.T., Smits, R., Ogino, S., et al. (2013). Restriction of intestinal stem cell expansion and the regenerative response by YAP. Nature *493*, 106–110.

Bastide, P., Darido, C., Pannequin, J., Kist, R., Robine, S., Marty-Double, C., Bibeau, F., Scherer, G., Joubert, D., Hollande, F., et al. (2007). Sox9 regulates cell proliferation and is required for Paneth cell differentiation in the intestinal epithelium. J. Cell Biol. *178*, 635–648.

Bonventre, J.V., Huang, Z., Taheri, M.R., O'Leary, E., Li, E., Moskowitz, M.A., and Sapirstein, A. (1997). Reduced fertility and postischaemic brain injury in mice deficient in cytosolic phospholipase A2. Nature *390*, 622–625.

Buczacki, S.J., Zecchini, H.I., Nicholson, A.M., Russell, R., Vermeulen, L., Kemp, R., and Winton, D.J. (2013). Intestinal label-retaining cells are secretory precursors expressing Lgr5. Nature *495*, 65–69.

Camargo, F.D., Gokhale, S., Johnnidis, J.B., Fu, D., Bell, G.W., Jaenisch, R., and Brummelkamp, T.R. (2007). YAP1 increases organ size and expands undifferentiated progenitor cells. Curr. Biol. *17*, 2054–2060.

Castellone, M.D., Teramoto, H., Williams, B.O., Druey, K.M., and Gutkind, J.S. (2005). Prostaglandin E2 promotes colon cancer cell growth through a Gs-axin-beta-catenin signaling axis. Science *310*, 1504–1510.

Cooper, H.S., Murthy, S.N., Shah, R.S., and Sedergran, D.J. (1993). Clinicopathologic study of dextran sulfate sodium experimental murine colitis. Lab. Invest. *69*, 238–249.

Cormier, R.T., Hong, K.H., Halberg, R.B., Hawkins, T.L., Richardson, P., Mulherkar, R., Dove, W.F., and Lander, E.S. (1997). Secretory phospholipase Pla2g2a confers resistance to intestinal tumorigenesis. Nat. Genet. *17*, 88–91.

Cormier, R.T., Bilger, A., Lillich, A.J., Halberg, R.B., Hong, K.H., Gould, K.A., Borenstein, N., Lander, E.S., and Dove, W.F. (2000). The Mom1AKR intestinal tumor resistance region consists of Pla2g2a and a locus distal to D4Mit64. Oncogene *19*, 3182–3192.

Dietrich, W.F., Lander, E.S., Smith, J.S., Moser, A.R., Gould, K.A., Luongo, C., Borenstein, N., and Dove, W. (1993). Genetic identification of Mom-1, a major modifier locus affecting Min-induced intestinal neoplasia in the mouse. Cell *75*, 631–639.

Eerola, L.I., Surrel, F., Nevalainen, T.J., Gelb, M.H., Lambeau, G., and Laine, V.J. (2006). Analysis of expression of secreted phospholipases A2 in mouse tissues at protein and mRNA levels. Biochim. Biophys. Acta *1761*, 745–756.

Farin, H.F., Karthaus, W.R., Kujala, P., Rakhshandehroo, M., Schwank, G., Vries, R.G., Kalkhoven, E., Nieuwenhuis, E.E., and Clevers, H. (2014). Paneth cell extrusion and release of antimicrobial products is directly controlled by immune cell-derived IFN-γ. J. Exp. Med. *211*, 1393–1405.

Feng, Y., Sentani, K., Wiese, A., Sands, E., Green, M., Bommer, G.T., Cho, K.R., and Fearon, E.R. (2013). Sox9 induction, ectopic Paneth cells, and mitotic spindle axis defects in mouse colon adenomatous epithelium arising from conditional biallelic Apc inactivation. Am. J. Pathol. *183*, 493–503.

Fijneman, R.J., Peham, J.R., van de Wiel, M.A., Meijer, G.A., Matise, I., Velcich, A., and Cormier, R.T. (2008). Expression of Pla2g2a prevents carcinogenesis in Muc2-deficient mice. Cancer Sci. *99*, 2113–2119.

Fijneman, R.J., Bade, L.K., Peham, J.R., van de Wiel, M.A., van Hinsbergh, V.W., Meijer, G.A., O'Sullivan, M.G., and Cormier, R.T. (2009). Pla2g2a attenuates colon tumorigenesis in azoxymethane-treated C57BL/6 mice; expression studies reveal Pla2g2a target genes and pathways. Cell. Oncol. *31*, 345–356.

Fodde, R., Edelmann, W., Yang, K., van Leeuwen, C., Carlson, C., Renault, B., Breukel, C., Alt, E., Lipkin, M., Khan, P.M., et al. (1994). A targeted chain-termination mutation in the mouse Apc gene results in multiple intestinal tumors. Proc. Natl. Acad. Sci. USA *91*, 8969–8973.

Fodde, R., Smits, R., and Clevers, H. (2001). APC, signal transduction and genetic instability in colorectal cancer. Nat. Rev. Cancer *1*, 55–67.

Fre, S., Huyghe, M., Mourikis, P., Robine, S., Louvard, D., and Artavanis-Tsakonas, S. (2005). Notch signals control the fate of immature progenitor cells in the intestine. Nature *435*, 964–968.

Goessling, W., North, T.E., Loewer, S., Lord, A.M., Lee, S., Stoick-Cooper, C.L., Weidinger, G., Puder, M., Daley, G.Q., Moon, R.T., and Zon, L.I. (2009). Genetic interaction of PGE2 and Wnt signaling regulates developmental specification of stem cells and regeneration. Cell *136*, 1136–1147.

Lambeau, G., and Gelb, M.H. (2008). Biochemistry and physiology of mammalian secreted phospholipases A2. Annu. Rev. Biochem. *77*, 495–520.

Liu, J.Z., van Sommeren, S., Huang, H., Ng, S.C., Alberts, R., Takahashi, A., Ripke, S., Lee, J.C., Jostins, L., Shah, T., et al.; International Multiple Sclerosis Genetics Consortium; International IBD Genetics Consortium (2015). Association analyses identify 38 susceptibility loci for inflammatory bowel disease and highlight shared genetic risk across populations. Nat. Genet. *47*, 979–986.

MacPhee, M., Chepenik, K.P., Liddell, R.A., Nelson, K.K., Siracusa, L.D., and Buchberg, A.M. (1995). The secretory phospholipase A2 gene is a candidate for the Mom1 locus, a major modifier of ApcMin-induced intestinal neoplasia. Cell *81*, 957–966.

Mori-Akiyama, Y., van den Born, M., van Es, J.H., Hamilton, S.R., Adams, H.P., Zhang, J., Clevers, H., and de Crombrugghe, B. (2007). SOX9 is required for the differentiation of paneth cells in the intestinal epithelium. Gastroenterology *133*, 539–546.

Mounier, C.M., Wendum, D., Greenspan, E., Fléjou, J.F., Rosenberg, D.W., and Lambeau, G. (2008). Distinct expression pattern of the full set of secreted phospholipases A2 in human colorectal adenocarcinomas: sPLA2-III as a biomarker candidate. Br. J. Cancer *98*, 587–595.

Mustata, R.C., Vasile, G., Fernandez-Vallone, V., Strollo, S., Lefort, A., Libert, F., Monteyne, D., Pérez-Morga, D., Vassart, G., and Garcia, M.I. (2013). Identification of Lgr5-independent spheroid-generating progenitors of the mouse fetal intestinal epithelium. Cell Rep. *5*, 421–432.

Neufert, C., Becker, C., and Neurath, M.F. (2007). An inducible mouse model of colon carcinogenesis for the analysis of sporadic and inflammation-driven tumor progression. Nat. Protoc. *2*, 1998–2004.

Paterson, J.C., and Watson, S.H. (1961). Paneth cell metaplasia in ulcerative colitis. Am. J. Pathol. *38*, 243–249.

Riggins, G.J., Markowitz, S., Wilson, J.K., Vogelstein, B., and Kinzler, K.W. (1995). Absence of secretory phospholipase A2 gene alterations in human colorectal cancer. Cancer Res. *55*, 5184–5186.

Roth, S., Franken, P., Sacchetti, A., Kremer, A., Anderson, K., Sansom, O., and Fodde, R. (2012). Paneth cells in intestinal homeostasis and tissue injury. PLoS ONE *7*, e38965.

Rothenberg, M.E., Nusse, Y., Kalisky, T., Lee, J.J., Dalerba, P., Scheeren, F., Lobo, N., Kulkarni, S., Sim, S., Qian, D., et al. (2012). Identification of a cKit(+) colonic crypt base secretory cell that supports Lgr5(+) stem cells in mice. Gastroenterology *142*, 1195–1205.e6.

Rouault, M., Le Calvez, C., Boilard, E., Surrel, F., Singer, A., Ghomashchi, F., Bezzine, S., Scarzello, S., Bollinger, J., Gelb, M.H., and Lambeau, G. (2007). Recombinant production and properties of binding of the full set of mouse secreted phospholipases A2 to the mouse M-type receptor. Biochemistry *46*, 1647–1662.

Sato, T., Vries, R.G., Snippert, H.J., van de Wetering, M., Barker, N., Stange, D.E., van Es, J.H., Abo, A., Kujala, P., Peters, P.J., and Clevers, H. (2009). Single Lgr5 stem cells build crypt-villus structures in vitro without a mesenchymal niche. Nature *459*, 262–265.

Sato, T., van Es, J.H., Snippert, H.J., Stange, D.E., Vries, R.G., van den Born, M., Barker, N., Shroyer, N.F., van de Wetering, M., and Clevers, H. (2011). Paneth cells constitute the niche for Lgr5 stem cells in intestinal crypts. Nature *469*, 415–418.

Shao, J., Jung, C., Liu, C., and Sheng, H. (2005). Prostaglandin E2 Stimulates the beta-catenin/T cell factor-dependent transcription in colon cancer. J. Biol. Chem. *280*, 26565–26572.

Shridas, P., Bailey, W.M., Boyanovsky, B.B., Oslund, R.C., Gelb, M.H., and Webb, N.R. (2010). Group X secretory phospholipase A2 regulates the expression of steroidogenic acute regulatory protein (StAR) in mouse adrenal glands. J. Biol. Chem. *285*, 20031–20039.

Smart, B.P., Oslund, R.C., Walsh, L.A., and Gelb, M.H. (2006). The first potent inhibitor of mammalian group X secreted phospholipase A2: elucidation of sites for enhanced binding. J. Med. Chem. *49*, 2858–2860.

Spirio, L.N., Kutchera, W., Winstead, M.V., Pearson, B., Kaplan, C., Robertson, M., Lawrence, E., Burt, R.W., Tischfield, J.A., Leppert, M.F., et al. (1996). Three secretory phospholipase A(2) genes that map to human chromosome 1P35-36 are not mutated in individuals with attenuated adenomatous polyposis coli. Cancer Res. *56*, 955–958.

Stelzner, M., Helmrath, M., Dunn, J.C., Henning, S.J., Houchen, C.W., Kuo, C., Lynch, J., Li, L., Magness, S.T., Martin, M.G., et al.; NIH Intestinal Stem Cell Consortium (2012). A nomenclature for intestinal in vitro cultures. Am. J. Physiol. Gastrointest. Liver Physiol. *302*, G1359–G1363.

Suzuki, R., Kohno, H., Sugie, S., Nakagama, H., and Tanaka, T. (2006). Strain differences in the susceptibility to azoxymethane and dextran sodium sulfate-induced colon carcinogenesis in mice. Carcinogenesis *27*, 162–169.

Tanaka, T., Kohno, H., Suzuki, R., Yamada, Y., Sugie, S., and Mori, H. (2003). A novel inflammation-related mouse colon carcinogenesis model induced by azoxymethane and dextran sodium sulfate. Cancer Sci. *94*, 965–973.

van Es, J.H., Jay, P., Gregorieff, A., van Gijn, M.E., Jonkheer, S., Hatzis, P., Thiele, A., van den Born, M., Begthel, H., Brabletz, T., et al. (2005a). Wnt signalling induces maturation of Paneth cells in intestinal crypts. Nat. Cell Biol. *7*, 381–386.

van Es, J.H., van Gijn, M.E., Riccio, O., van den Born, M., Vooijs, M., Begthel, H., Cozijnsen, M., Robine, S., Winton, D.J., Radtke, F., and Clevers, H. (2005b). Notch/gamma-secretase inhibition turns proliferative cells in intestinal crypts and adenomas into goblet cells. Nature *435*, 959–963.

Wirtz, S., Neufert, C., Weigmann, B., and Neurath, M.F. (2007). Chemically induced mouse models of intestinal inflammation. Nat. Protoc. *2*, 541–546.

Yazbeck, R., Howarth, G.S., Butler, R.N., Geier, M.S., and Abbott, C.A. (2011). Biochemical and histological changes in the small intestine of mice with dextran sulfate sodium colitis. J. Cell. Physiol. *226*, 3219–3224.

Yeung, T.M., Gandhi, S.C., Wilding, J.L., Muschel, R., and Bodmer, W.F. (2010). Cancer stem cells from colorectal cancer-derived cell lines. Proc. Natl. Acad. Sci. USA *107*, 3722–3727.

Zhang, Y., Desai, A., Yang, S.Y., Bae, K.B., Antczak, M.I., Fink, S.P., Tiwari, S., Willis, J.E., Williams, N.S., Dawson, D.M., et al. (2015). Tissue regeneration. Inhibition of the prostaglandin-degrading enzyme 15-PGDH potentiates tissue regeneration. Science *348*, aaa2340.

CHAPTER 4

Interplay between metabolic identities in the intestinal crypt supports stem cell function

Nature. 543, 424-427 (2017).

LETTER

doi:10.1038/nature21673

Interplay between metabolic identities in the intestinal crypt supports stem cell function

Maria J. Rodríguez-Colman[1], Matthias Schewe[2], Maaike Meerlo[1], Edwin Stigter[1], Johan Gerrits[3], Mia Pras-Raves[3], Andrea Sacchetti[2], Marten Hornsveld[1], Koen C. Oost[1], Hugo J. Snippert[1], Nanda Verhoeven-Duif[3], Riccardo Fodde[2] & Boudewijn M.T. Burgering[1]

The small intestinal epithelium self-renews every four or five days. Intestinal stem cells (Lgr5$^+$ crypt base columnar cells (CBCs)) sustain this renewal and reside between terminally differentiated Paneth cells at the bottom of the intestinal crypt[1]. Whereas the signalling requirements for maintaining stem cell function and crypt homeostasis have been well studied, little is known about how metabolism contributes to epithelial homeostasis. Here we show that freshly isolated Lgr5$^+$ CBCs and Paneth cells from the mouse small intestine display different metabolic programs. Compared to Paneth cells, Lgr5$^+$ CBCs display high mitochondrial activity. Inhibition of mitochondrial activity in Lgr5$^+$ CBCs or inhibition of glycolysis in Paneth cells strongly affects stem cell function, as indicated by impaired organoid formation. In addition, Paneth cells support stem cell function by providing lactate to sustain the enhanced mitochondrial oxidative phosphorylation in the Lgr5$^+$ CBCs. Mechanistically, we show that oxidative phosphorylation stimulates p38 MAPK activation by mitochondrial reactive oxygen species signalling, thereby establishing the mature crypt phenotype. Together, our results reveal a critical role for the metabolic identity of Lgr5$^+$ CBCs and Paneth cells in supporting optimal stem cell function, and we identify mitochondria and reactive oxygen species signalling as a driving force of cellular differentiation.

In the small intestine, crypts of Lieberkühn encircle each intestinal villus. At the base of these crypts the Lgr5$^+$ crypt base columnar stem cells reside and generate transit amplifying progenitors, which migrate upwards and differentiate into enterocytes, tuft, goblet or enteroendocrine cells[1]. Paneth cells support stem cell function of Lgr5$^+$ CBCs by supplying essential factors (WNT, Delta-like 1 and epidermal growth factor). Cell metabolism has been implicated in stem cell maintenance and differentiation in some adult stem cell populations[2–5]. Recently, calorie restriction has been shown to increase Lgr5$^+$ CBCs and Paneth cell numbers[6], but otherwise the role of metabolism in the intestinal crypt homeostasis remains unknown. We analysed the metabolome of Lgr5$^+$ CBCs, Paneth cells and the remaining population of cells (CD24$^-$Lgr5$^-$) isolated from the small intestine of Lgr5–GFP mice. Principal component analysis (PCA) of liquid chromatography–tandem mass spectrometry (LC-MS/MS)-based metabolomics shows clear clustering of the metabolic profiles based on cell identity (Fig. 1a, Extended Data Fig. 1a). The pyruvate/lactate ratio, a measure of the relative contribution to cellular bioenergetics of mitochondrial respiration versus glycolysis, differed between populations, indicating increased mitochondrial activity in Lgr5$^+$ CBCs (Fig. 1b). Small intestinal organoids recapitulate *in vitro* many aspects of the intestine, including crypt structure and the interaction between Paneth cells and stem cells (reviewed in refs 7, 8). Live imaging of mitochondria and mitochondrial membrane potential (MMP), indicates increased mitochondrial activity in Lgr5$^+$ CBCs when compared to the adjacent Paneth cells (Fig. 1c, d, Extended Data Fig. 1b, c). Additionally, organoids enriched with Lgr5$^+$ CBCs[9] showed a 20% increase in respiration, supporting the notion that Lgr5$^+$ CBCs display increased mitochondrial activity (Extended Data Fig. 1d, e). Mitochondrial-derived reactive oxygen species (ROS) can contribute to cellular redox stress. Therefore, we analysed the level of mitochondrial superoxide and cytosolic ROS in organoids. Although mitochondrial superoxide is higher in Lgr5$^+$ CBCs compared to Paneth cells, cytoplasmic ROS levels do not differ between Paneth cells and CBCs (Extended Data Fig. 1f, g), indicating that higher mitochondrial activity does not necessarily result in increased redox stress in Lgr5$^+$ CBCs.

In standard medium (ENR; containing epidermal growth factor, noggin, and R-spondin 1) organoids grow as mini-guts with defined crypt domains. However, the addition of Wnt3a-conditioned medium (WENR) results in spherical organoids that lack differentiated cell types and homogeneously proliferate[10] (Fig. 2a, b). This differs from mini-gut organoids where proliferation is restricted to Lgr5$^+$ CBCs and transit amplifying cells (Fig. 2b, Extended Data Fig. 2a). Stem cell markers *Lgr5* and *Olfm4* are downregulated in spherical organoids (Fig. 2a, Extended

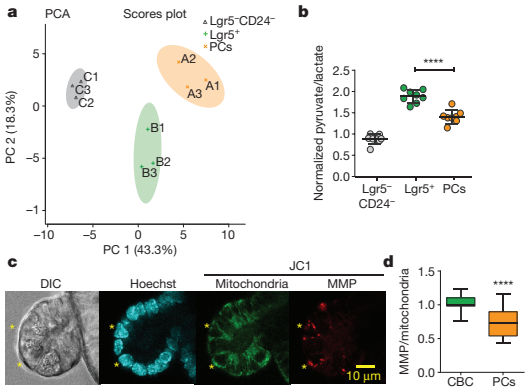

Figure 1 | Metabolic compartmentalization in the crypt. a, Lgr5$^+$ CBCs, Paneth cells (PCs) and Lgr5$^-$CD24$^-$ cells populations were obtained by FACS followed by LC-MS/MS metabolomics and PCA ($n = 3$; cells sorted from two mice were pooled for each independent measurement) **b**, Pyruvate/lactate ratio. **c**, JC-1 staining of mitochondria (green) and mitochondria with high MMP (red) in an organoid crypt. *Indicates CBCs located between Paneth cells. DIC, differential interference contrast. **d**, Quantification of JC-1 in CBCs (20) and Paneth cells (10) from 3 different organoids (one representative experiment of 3 independent ones). Graphs show mean and s.d. Two-tailed *t*-test (**b**) and Mann–Whitney test (**d**), $****P < 0.0001$.

[1]Molecular Cancer Research, Center Molecular Medicine, University Medical Center Utrecht, Heidelberglaan 100, 3584CG Utrecht, The Netherlands. [2]Department of Pathology, Erasmus MC Cancer Institute, Erasmus University Medical Center, Rotterdam, The Netherlands. [3]Department of Genetics and Center for Molecular Medicine, Lundlaan 6, 3584 EA Utrecht, The Netherlands.

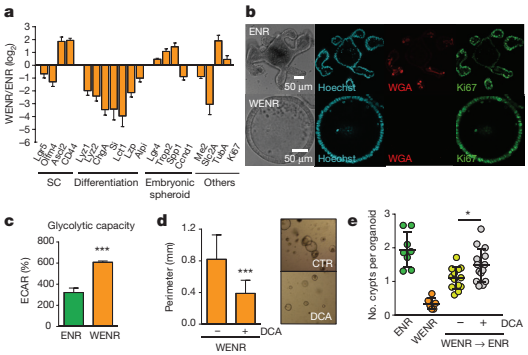

Figure 2 | Characterization of WENR organoids. a, Gene expression in WENR organoids was determined by quantitative PCR and represented as ratio relative to ENR organoids. Plotted values statistically differ from ENR condition ($n = 5$; two-tailed t-test $P < 0.05$). **b**, Representative images of immunostained mini-gut (ENR) and spherical organoids (WENR). Paneth cells and proliferative cells were detected with WGA and Ki67 antibody, respectively ($n = 3$). **c**, Glycolytic capacity was determined by glycolysis stress test (Seahorse). **d**, WENR organoids were treated with DCA and the perimeter was measured with ImageJ. **e**, Crypt formation by inhibition of glycolysis was analysed by differentiation assay adding DCA. Results show one representative experiment of $n = 5$ (**e**) and $n = 3$ (**c**, **d**). Mean and s.d. are plotted. Two-tailed t-test, $*P < 0.05$, $***P < 0.001$.

Data Fig. 2b), whereas the expression of embryonic stem cell markers (*Trop2* and *Spp1*) is increased (Fig. 2a). Remarkably, spherical WENR organoids resemble embryonic small intestine organoids, as both grow as homogenous proliferative spheres that lack differentiated cells and share a similar gene expression signature, which is distinct from adult Lgr5$^+$ CBCs[11]. Embryonic organoids can differentiate spontaneously (intestinalization) and become mini-gut organoids[11,12]. WENR organoids can reproduce this process; by removal of Wnt3a from the medium after splitting, Paneth cells and Lgr5$^+$ CBCs emerge in budding structures and crypt formation is restored[10,13,14] (Extended Data Fig. 2b, c). Thus, switching spherical organoids from WENR to ENR medium establishes a model to study differentiation preceding crypt formation.

Spherical WENR organoids display enhanced glycolytic metabolism when compared to mini-guts (Fig. 2c, Extended Data Fig. 2d, e). Accordingly, spherical organoids showed a decreased pyruvate/lactate ratio (Extended Data Fig. 2f). Inhibition of pyruvate dehydrogenase kinase 1 by dichloroacetate (DCA), and hence inhibition of glycolysis[15,16] (Extended Data Fig. 2g), resulted in reduced proliferation (Fig. 2d, Extended Data Fig. 2h). Inhibition of proliferation probably precedes the onset of differentiation. Indeed, glycolytic perturbation by addition of DCA or 2-deoxy-D-glucose enhanced the number of crypts per organoid and the expression of the Paneth cell markers *Lyz1* and *Lyz2* (Fig. 2e, Extended Data Fig. 2i–k). ATP production relies on mitochondrial oxidative phosphorylation (OXPHOS) when glycolysis is perturbed, therefore we analysed OXPHOS contribution to differentiation. Galactose, through the Leloir pathway, activates OXPHOS[17,18]. Substitution of glucose with galactose enhanced crypt formation (Extended Data Fig. 2l), suggesting that mitochondrial activation drives differentiation. In addition, mitochondrial copy number increased during differentiation (Extended Data Fig. 3a). Phenotypically, crypt formation in organoids is initiated through an increase in cell density, forming a bud-like structure, and mitochondrial activity appears increased within the initiating crypt (Fig. 3a, Extended Data Fig. 3b). Inhibition of mitochondrial OXPHOS by blocking the electron transport chain complex I or IV or ATP synthase reduced crypt formation (Extended Data Fig. 3c, d). Notably, Wnt3a enhanced the effect of blocking the electron transport chain (Extended Data Fig. 3e). Together, these results indicate that mitochondrial electron transport chain activity is required for crypt formation initiation. Increased OXPHOS activity may lead to ROS generation with consequent alteration of the cellular redox state. Glutathione is the main cellular anti-oxidant and its oxidized/reduced state in mitochondria can be analysed by the genetically encoded sensor mtGrx1–roGFP[19] (mitochondrial encoded glutaredoxin1 fused to reduction–oxidation sensitive GFP) in organoids (Extended Data Fig. 3f). Spherical organoids display throughout a homogeneous redox ratio, but following initiation of differentiation, redox state in budding areas is altered (Fig. 3b, Extended Data Fig. 3g). Thus, increased mitochondrial activity results in mitochondrial redox changes and consequent ROS signalling that may initiate differentiation and crypt formation. Indeed, exogenous antioxidants, mitoTEMPO, and to a lesser extent EUK-134, inhibited crypt formation and Paneth cell marker expression (Extended Data Fig. 3h, i). Furthermore, low concentrations of paraquat, to mimic mitochondrial ROS signalling, enhanced expression of Paneth cell markers, but did not result in a significant increase of the numbers of crypts (Extended Data Fig. 3j, k), suggesting that other functions of mitochondria (that is, ATP, metabolic intermediates) also contribute to crypt formation.

p38 MAP kinases respond to cellular redox changes[20,21]. In organoids, mitochondrial-derived ROS signals activate p38 and its activity also increases during differentiation (Extended Data Fig. 4a, b, Supplementary Fig. 1). To measure p38 activation at the cellular level, we employed the genetically encoded sensor p38KTRClover[22]. We validated p38KTRClover in organoids (Extended Data Fig. 4c) and confirmed that mitochondrial ROS activates p38 (Fig. 4a). Notably, during differentiation, p38 activity increased at budding sites and was active in in emerging Lyz-positive cells (Paneth cells) and CBCs (Fig. 4b, c). p38 activity is sustained during crypt maturation and in mature crypts, where it becomes less active towards the villi domain (Fig. 4c). Further, immunohistochemistry of mouse intestine corroborates these results and also shows increased phospho-p38 at the base of the intestinal crypt and in Paneth cells and CBCs (Fig. 4d,

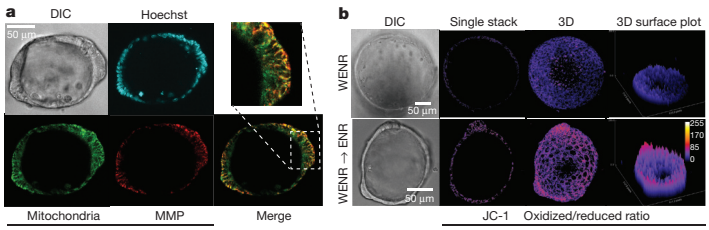

Figure 3 | Mitochondrial OXPHOS and ROS signalling drive differentiation and crypt formation. a, Representative confocal image of mitochondria and high MMP mitochondria of JC-1-stained organoids in transition to differentiation. **b**, Representative images of mitochondrial redox state analysed in mtGrx1–roGFP organoids. Images represent oxidized/reduced roGFP. One representative experiment of $n = 3$ are shown.

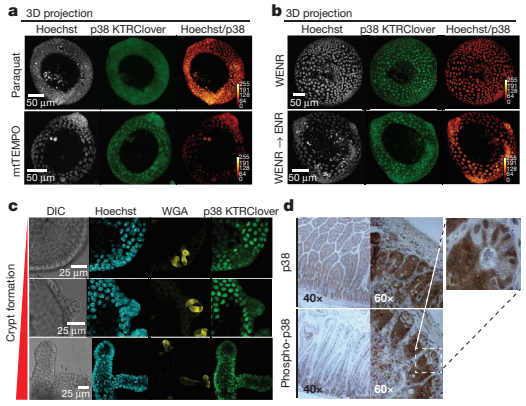

Figure 4 | p38 activity drives differentiation and crypt formation. **a**, **b**, Representative images of p38 activity as determined by confocal microscopy of p38KTRClover organoids by calculating the Hoechst/p38KTRClover ratio ($n = 5$). **c**, Detailed visualization of p38 activity at different stages of crypt formation on p38KTRClover organoids ($n = 5$). **d**, immunohistochemistry of p38 and pp38 on mouse intestinal sections.

Extended Data Fig. 4d). Inhibition of p38 activity reduced differentiation and crypt formation (Extended Data Fig. 4e, f) and thereby phenocopied mitochondrial ROS scavenging. Together, our results show that mitochondrial OXPHOS activity drives differentiation and crypt formation by a mechanism that involves p38 activation through mitochondrial ROS signalling.

Lastly, we addressed the role of metabolism in the maintenance of stem cell function. We therefore employed the organoid reconstitution assay, in which isolated Lgr5$^+$ CBCs were combined with Paneth cells to produce self-renewing organoids. This assay serves as a proxy for stem and niche cell function[6,10,23,24]. To test the relevance of metabolic compartmentalization between Lgr5$^+$ CBCs and Paneth cells, we treated either cell population with metabolic inhibitors that showed expected efficacy and did not affect cell viability (Extended Data 5a, b). Notably, Paneth cells pre-treated with inhibitors of glycolysis or glucose and lactate transporters were inefficient in supporting organoid formation upon reconstitution with Lgr5$^+$ CBCs, whereas upon treatment with OXPHOS inhibitors, Paneth cells retained their niche-supporting function (Fig. 5b). Conversely, treatment of Lgr5$^+$ CBCs with OXPHOS inhibitors clearly reduced organoid reconstitution, whereas the other inhibitors showed a mild effect (Fig. 5a). These results show that the glycolytic phenotype in Paneth cells and increased OXPHOS in Lgr5$^+$ CBCs are required in supporting both niche and stem cell function.

Lactate is the end product of glycolysis and can be back converted into pyruvate and fuel OXPHOS. We hypothesized that lactate produced by Paneth cells could provide the respiratory substrate to sustain OXPHOS in Lgr5$^+$ CBCs. Wnt ligands can substitute for Paneth cells in supporting *ex vivo* Lgr5$^+$ CBCs to form organoids[6,10,23]. We therefore repeated reconstitution assays, replacing Paneth cell function with Wnt3a and either glucose or lactate. Indeed, lactate strongly enhanced the ability of Lgr5$^+$ CBCs to establish organoids (Fig. 5c). Thus, besides Wnt3a, glycolysis towards lactate in Paneth cells establishes the stem cell niche. Next, we analysed the effects of replacing lactate by pyruvate, inhibition of pyruvate transport into mitochondria, and inhibition of ROS and p38 signalling. Our results indicate that in Lgr5$^+$ CBCs, lactate is converted into pyruvate to fuel mitochondrial OXPHOS, leading to ROS signalling and activation of p38 and differentiation (Fig. 5d, e, Extended Data Fig. 5c–g). Together, our results reveal the existence of metabolic compartmentalization in the intestinal crypt in which Paneth cells support Lgr5$^+$ CBC oxidative metabolism, constituting a metabolic niche that provides optimal stem cell function (Fig. 5f).

Several studies have indicated a role for metabolism in stem cell function, but a clear understanding has been lacking[2–5]. Here, we report that a metabolic transition towards mitochondrial OXPHOS is required to drive differentiation in an organoid model representing the development of the intestinal crypt *in vivo*. Importantly, this metabolic transition towards OXPHOS and consequent p38 activation is maintained in adult Lgr5$^+$ CBCs and ultimately regulates stem cell function by self-renewal and differentiation capacity. In agreement with our results, deregulation of mitochondrial COX1 in *Drosophila*

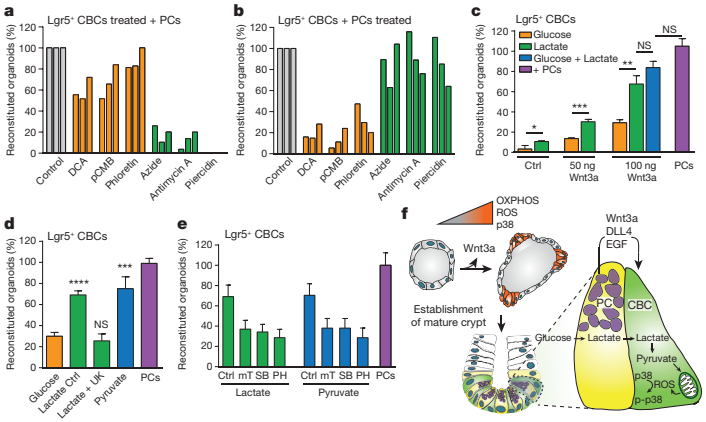

Figure 5 | Metabolic regulation of Lgr5$^+$ CBC stem cell function. **a**, **b**, OXPHOS in Lgr5$^+$ CBCs (**a**) and glycolysis in Paneth cells (**b**) are required for stem cell function. Organoid reconstitution efficiency was determined in Lgr5$^+$ CBCs or Paneth cells were treated with glycolysis (orange) or OXPHOS inhibitors (green) before combining and plating on matrigel ($n = 3$). **c**, Single Lgr5$^+$ CBCs were plated in ENR medium supplemented as indicated and organoid reconstitution efficiency was determined ($n = 6$). **d**, **e**, Organoid reconstitution efficiency was assessed by plating single Lgr5$^+$ CBCs in medium supplemented with 100 ng Wnt3a and the indicated compounds ($n = 6$). Ctrl, control; mT, mitoTEMPO; PH, PH-797804; SB, SB203580; UK, UK-5099. Average and s.d. are shown. Two-tailed *t*-test, $*P < 0.05$, $**P < 0.01$, $***P < 0.001$, NS, not significant. **f**, Schematic representation of the main findings in this work. p-p38, phospho-p38.

melanogaster leads to loss of CBCs and decreased number of crypts[25]. Also, conditional p38α-knockout mice show altered epithelial homeostasis in colon and small intestine[26]. Studies on ROS and stem cell fate have focused mostly on ROS as a causal mechanism for DNA damage rather than on its role in signalling (discussed in ref. 27). However, mitochondrial-derived ROS does not inevitably result in increased DNA damage[28,29], and our results indicate that increased OXPHOS in Lgr5$^+$ CBCs generates ROS signalling rather than stress. Interestingly, gene expression profiling suggests that there is similarity between normal Lgr5$^+$ CBCs and colon cancer stem cells[25], and this could also be true of their metabolism. Indeed, increased mitochondrial metabolism in cancer stem cells has been previously reported[30]. Thus, whereas the bulk of cancer cells adopt a 'Warburg metabolism', the minor population of cancer stem cells may rely on OXPHOS. Therefore, targeting mitochondria may provide therapeutic benefit in eradicating cancer stem cells, as opposed to other strategies that target the bulk of a tumour.

Online Content Methods, along with any additional Extended Data display items and Source Data, are available in the online version of the paper; references unique to these sections appear only in the online paper.

Received 9 May 2016; accepted 30 January 2017.
Published online 8 March 2017.

1. Barker, N. *et al.* Identification of stem cells in small intestine and colon by marker gene *Lgr5*. *Nature* **449,** 1003–1007 (2007).
2. Zhang, J. *et al.* UCP2 regulates energy metabolism and differentiation potential of human pluripotent stem cells. *EMBO J.* **30,** 4860–4873 (2011).
3. Owusu-Ansah, E. & Banerjee, U. Reactive oxygen species prime *Drosophila* haematopoietic progenitors for differentiation. *Nature* **461,** 537–541 (2009).
4. Tormos, K. V. *et al.* Mitochondrial complex III ROS regulate adipocyte differentiation. *Cell Metab.* **14,** 537–544 (2011).
5. Hamanaka, R. B. *et al.* Mitochondrial reactive oxygen species promote epidermal differentiation and hair follicle development. *Sci. Signal.* **6,** ra8 (2013).
6. Yilmaz, Ö. H. *et al.* mTORC1 in the Paneth cell niche couples intestinal stem-cell function to calorie intake. *Nature* **486,** 490–495 (2012).
7. Yin, X. *et al.* Engineering stem cell organoids. *Cell Stem Cell* **18,** 25–38 (2016).
8. Barker, N. Adult intestinal stem cells: critical drivers of epithelial homeostasis and regeneration. *Nat. Rev. Mol. Cell Biol.* **15,** 19–33 (2014).
9. Yin, X. *et al.* Niche-independent high-purity cultures of Lgr5$^+$ intestinal stem cells and their progeny. *Nat. Methods* **11,** 106–112 (2014).
10. Sato, T. *et al.* Paneth cells constitute the niche for Lgr5 stem cells in intestinal crypts. *Nature* **469,** 415–418 (2011).
11. Mustata, R. C. *et al.* Identification of Lgr5-independent spheroid-generating progenitors of the mouse fetal intestinal epithelium. *Cell Reports* **5,** 421–432 (2013).
12. Fordham, R. P. *et al.* Transplantation of expanded fetal intestinal progenitors contributes to colon regeneration after injury. *Cell Stem Cell* **13,** 734–744 (2013).
13. Sato, T. & Clevers, H. Growing self-organizing mini-guts from a single intestinal stem cell: mechanism and applications. *Science* **340,** 1190–1194 (2013).
14. Sato, T. *et al.* Long-term expansion of epithelial organoids from human colon, adenoma, adenocarcinoma, and Barrett's epithelium. *Gastroenterology* **141,** 1762–1772 (2011).
15. Kankotia, S. & Stacpoole, P. W. Dichloroacetate and cancer: new home for an orphan drug? *Biochim. Biophys. Acta* **1846,** 617–629 (2014).
16. Michelakis, E. D., Webster, L. & Mackey, J. R. Dichloroacetate (DCA) as a potential metabolic-targeting therapy for cancer. *Br. J. Cancer* **99,** 989–994 (2008).
17. Zhdanov, A. V., Waters, A. H., Golubeva, A. V., Dmitriev, R. I. & Papkovsky, D. B. Availability of the key metabolic substrates dictates the respiratory response of cancer cells to the mitochondrial uncoupling. *Biochim. Biophys. Acta* **1837,** 51–62 (2014).
18. Aguer, C. *et al.* Galactose enhances oxidative metabolism and reveals mitochondrial dysfunction in human primary muscle cells. *PLoS One* **6,** e28536 (2011).
19. Gutscher, M. *et al.* Real-time imaging of the intracellular glutathione redox potential. *Nat. Methods* **5,** 553–559 (2008).
20. Tormos, A. M., Taléns-Visconti, R., Nebreda, A. R. & Sastre, J. p38 MAPK: a dual role in hepatocyte proliferation through reactive oxygen species. *Free Radic. Res.* **47,** 905–916 (2013).
21. Wagner, E. F. & Nebreda, A. R. Signal integration by JNK and p38 MAPK pathways in cancer development. *Nat. Rev. Cancer* **9,** 537–549 (2009).
22. Regot, S., Hughey, J. J., Bajar, B. T., Carrasco, S. & Covert, M. W. High-sensitivity measurements of multiple kinase activities in live single cells. *Cell* **157,** 1724–1734 (2014).
23. Sato, T. *et al.* Single Lgr5 stem cells build crypt-villus structures *in vitro* without a mesenchymal niche. *Nature* **459,** 262–265 (2009).
24. Schewe, M. *et al.* Secreted phospholipases A2 are intestinal stem cell niche factors with distinct roles in homeostasis, inflammation, and cancer. *Cell Stem Cell* **19,** 38–51 (2016).
25. Merlos-Suárez, A. *et al.* The intestinal stem cell signature identifies colorectal cancer stem cells and predicts disease relapse. *Cell Stem Cell* **8,** 511–524 (2011).
26. Otsuka, M. *et al.* Distinct effects of p38α deletion in myeloid lineage and gut epithelia in mouse models of inflammatory bowel disease. *Gastroenterology* **138,** 1255–1265 (2010).
27. Liang, R. & Ghaffari, S. Stem cells, redox signaling, and stem cell aging. *Antioxid. Redox Signal.* **20,** 1902–1916 (2014).
28. Hoffmann, S., Spitkovsky, D., Radicella, J. P., Epe, B. & Wiesner, R. J. Reactive oxygen species derived from the mitochondrial respiratory chain are not responsible for the basal levels of oxidative base modifications observed in nuclear DNA of Mammalian cells. *Free Radic. Biol. Med.* **36,** 765–773 (2004).
29. Cleaver, J. E. *et al.* Mitochondrial reactive oxygen species are scavenged by Cockayne syndrome B protein in human fibroblasts without nuclear DNA damage. *Proc. Natl Acad. Sci. USA* **111,** 13487–13492 (2014).
30. Song, I. S. *et al.* FOXM1-induced PRX3 regulates stemness and survival of colon cancer cells via maintenance of mitochondrial function. *Gastroenterology* **149,** 1006–1016 (2015).

Supplementary Information is available in the online version of the paper.

Acknowledgements This work was financially supported by CGC.nl (M.J.R.-C., H.J.S.), Utrecht Life Sciences (M.M.), Dutch Cancer Society ((KWF), EMCR 2012-5473 (M.S.), and UU 2013-6070 (K.C.O.)) and from the Netherlands Institute of Regenerative Medicine (R.F.). We thank H. Bos, T. Dansen and S. van Mil for helpful discussions and proofreading; F. de Sauvage (Genentech) for providing DTR–LGR5–GFP mice; T. Dick (DKFZ) for mtGrx1–roGFP and I. Verlaan (UMC Utrecht) for R-spondin/Wnt3a-conditioned medium.

Author Contributions M.J.R.-C. and B.M.T.B. conceived the project, designed and performed experiments and wrote the manuscript; M.S. designed and performed organoid reconstitution experiments; M.M. performed experiments; E.S. and J.G. performed metabolic measurements. M.P.-R. and N.V.-D. performed metabolic data analysis. A.S. performed FACS of intestinal cells. M.H. performed p38 IHC. K.C.O. and H.J.S. provided organoid cultures, and H.J.S. co-wrote the manuscript. R.F. designed experiments and co-wrote the manuscript.

Author Information Reprints and permissions information is available at www.nature.com/reprints. The authors declare no competing financial interests. Readers are welcome to comment on the online version of the paper. Publisher's note: Springer Nature remains neutral with regard to jurisdictional claims in published maps and institutional affiliations. Correspondence and requests for materials should be addressed to B.M.B. (b.m.t.burgering@umcutrecht.nl).

Reviewer Information *Nature* thanks T. Sato, A. Schulze and the other anonymous reviewer(s) for their contribution to the peer review of this work.

METHODS

Data reporting. No statistical methods were used to predetermine sample size. The experiments were not randomized and the investigators were not blinded to allocation during experiments and outcome assessment.

Organoid culture. Small intestinal organoids were derived from isolated crypts collected from the entire length of the small intestine of wild-type, LGR5–GFP or DTR–LGR5–GFP mice as described ref. in 14. The basic culture medium (ENR) contained advanced DMEM/F12 supplemented with penicillin/streptomycin, 10 mM HEPES, 1× Glutamax, 1× B27 (all from Life Technologies) and 1 mM N-acetylcysteine (Sigma) that was supplemented with murine recombinant epidermal growth factor (Peprotech), R-spondin1-CM (5% v/v) and noggin-CM (10% v/v). WENR medium was prepared with ENR medium supplemented with R-spondin1-CM (20% v/v) and 50% Wnt3a-CM (conditioned medium) (v/v). A mycoplasma-free status was confirmed routinely.

Lentiviral infection. mtGrx1–roGFP in pLPCX redox sensor was cloned into a lentiviral vector under the control of *Hef1* promoter and with puromycin resistance cassette. pLentiPGK Puro DEST p38KTRClover was purchased in Addgene. p38KTRClover[30] facilitates tracking of p38 activity by live imaging of nuclear (inactive) and cytoplasmic (active) localization of the GFP sensor. mtGrx1–roGFP in pLPCX was a gift of T. Dick (Cancer Research Center, Heidelberg, Germany). The genetically encoded sensor mtGrx1–roGFP allows for ratiometric quantification in mitochondria of oxidized/reduced glutathione by excitation with 405 and 488 nm, respectively, and emission in the green channel[26]. Both genetic encoded sensors were introduced in organoids by lentiviral infection according to ref. 31.

Differentiation assay. Organoids were grown in WENR medium until crypts were no longer visible (approximately 7 days per one passage). WENR spherical organoids were split up and plated in either WENR or ENR medium. Galactose and glucose media were prepared using advanced F12 glucose free medium and supplemented with either galactose or glucose to a final concentration of 15 mM and used as regular F12 to prepare ENR medium. Compounds were added along with the medium directly after plating, with the exception of EUK134, mitoTEMPO, paraquat and antimycinA, which were added 14–16 h after plating. EUK134 mimics catalase and superoxide dismutase activity and, in this way, scavenges ROS in the cytosol, and mitoTEMPO is a scavenger of mitochondrial superoxide[32]. DCA concentration was 15 mM. Pictures were taken after 48 or 72 h after treatment. All compounds were purchased from Sigma. The number of organoids and crypts were blindly counted with the cell counter (ImageJ plugin) and crypt formation was scored as the number of crypts divided by the number of organoids per picture. For each condition, a minimum of six pictures with approximately 6–10 organoids per picture were counted (see Extended Data Fig. 2j for an example). Statistical analyses were performed using Graphpad Prism 6. For crypt formation assays, an independent experiment (*n*) refers to independent splitting, plating and treatment of organoids performed on different days.

DNA and RNA extraction and qPCR. Organoids were washed once with cold PBS and collected in RLT buffer. RNA was extracted with the RNeasy kit (Qiagen), with on-column DNase treatment (Qiagen), according to the manufacturer's instructions. RNA was reverse-transcribed with oligodT primers and the CBCript cDNA synthesis kit (Biorad). For DNA extraction, organoids were washed once with cold PBS and DNA was extracted with the QIAamp DNA Micro Kit (Qiagen). DNA was used as a template to amplify nuclear and mitochondria-encoded genes. In both cases, qPCR was performed with FastStart SYBR Green Master mix (Roche). Relative gene expression was calculated using the C_t method by normalization to HNRNPA1 and CycA. Statistics were done with Graphpad Prism 6. Primer sequences: *Glut1* forward (5′-GCAGTTCGGCTATAACACT-3′), *Glut1* reverse (5′-GGTGGTTCCATGTTTGATTG-3′); *Hk1* forward (5′-AAGGATGACCAAGTCAAAAAGATTG-3′), *Hk1* reverse (5′-CGGGAGAGGCCATTCTTCATC-3′); *Mct1* forward (5′-GATGGACCTCATTGGACCCC-3′), *Mct1* reverse (5′-GAGGCGGCCTAAAAGTGGT-3′); *Hnrnpa1* forward (5′-TGACAGCTATAACAACGGAG-3′), *Hnrnpa1* reverse (5′-AAAGTTTCCTCCCTTCATCG-3′); *Pbgd* forward (5′-CCTCGACTCTGCTTCGTCTG-3′), *Pbgd* reverse (5′-CACAGACCACAAATCCATGA-3′); *Tuba1a* forward (5′-AGGATTATGAGGAGGTTGGT-3′), *Tuba1a* forward (5′-ATAAACACTCCCTGTGGAAGC-3′); *Ppia* forward (5′-ACTGAATGGCTGGATGGCAA-3′), *Ppia* reverse (5′-CAAAACGCTCCATGGCTTCC-3′); *Lyz1* forward (5′-CGTTGTGAGTTGGCCAGAA-3′); *Lyz1* reverse (5′-GCTAAACACACCCAGTCAGC-3′); *Lyz2* forward 2 (5′-TGAACGTTGTGAGTTTGCCA-3′), *Lyz2* reverse (5′-TGAGCTAAACACACCCAGTCG-3′); *Ki67* forward (5′-CCTTTGCTGTCCCCGAAGA-3′), *Ki67* reverse (5′-GGCTTCTCATCTGTTGCTTCCT-3′); *Slc2a* forward (GLUT2) (5′-ATCGCTCCAACCACACTCAG-3′), *Slc2a* reverse (5′-GCTGAGGCCAGCAATCTGAC-3′); *Olfm4* forward (5′-TGAAGGAGATGCAAAAACTGG-3′), *Olfm4* reverse (5′-CTCCAGCTTCTCTACCAAGAGG-3′); *Me2* forward (5′-AGGCGTCCGGGGAGAG-3′), *Me2* reverse (5′-ATGAGTGGCTTGCCCTTCTC-3′); *Alpi* forward (5′-AACTCACCTCATGGGCCTCTT-3′), *Alpi* reverse (5′-GGGTTTCGGTTGGCATCATA-3′); *Lct* forward (5′-CGTCTGCTTCCTATCAGGTTGAA-3′), *Lct* reverse (5′-GTGGGAAAATGTGTCCCAGATACT-3′); *Lgr5* forward (5′-GTTCAAGATGAGCGGGACCT-3′), *Lgr5* reverse (5′-ATAGGTGCTCACAGGGCTTG-3′); *Pkm* forward (5′-ATGCAGCACCTGATAGCTCG-3′), *Pkm* reverse (5′-AGGTCTGTGGAGTGACTGGA-3′). Sequences of primers for *Ascl2*, *Cd44*, *Chga*, Si, LZP, *Lgr4*, *Trop2*, *Spp1* and CCND1 were obtained from ref. 11.

Protein lysates and western blot. Organoids were washed once with cold PBS and collected in cell recovery solution (Corning) according to the manufacturer's instructions. Total proteins were collected by direct lysis of organoids in Laemli sample buffer. Proteins were run in SDS–PAGE and transferred to Polyscreen PVDF transfer membranes (PerkinElmer). Antibodies used in this work: anti-GAPDH (Millipore), P38 antibody (Biolabs 9212); phospho-p38 (Cell Signaling CS9215); GAPDH (Millipore MAB374); Ki67 (Abcam ab15580); lysozyme (DAKO A0099), phospho-p38 MAPK (Thr180/Tyr182) (9211S, Cell Signaling), phospho-p38 MAPK (Thr180/Tyr182) (4511S, Cell Signaling).

Immunostaining, live imaging in organoids and immunohistochemistry. Organoids were plated in 4-well round Cellview plates. Samples were fixed with 4% paraformaldehyde (PFA) for 45 minutes at 4 °C. After fixation organoids were washed with cold PBS and permeabilized with PBS buffer containing 10% DMSO, 2% Triton and 10 g l^{-1} BSA. Antibody incubation was performed in the same buffer; anti-Ki67 (Abcam), rabbit anti-lysozyme (Dako). Fluorescence was detected using anti-rabbit Alexa Fluor 488 antibody. Paneth cells were also stained with wheat germ agglutinin (WGA) and DNA was stained with Hoechst (both Molecular Probes). Images were captured using a SP8 confocal microscope (Leica Microsystems). For live imaging, organoids were stained with the following probes; JC-1 (T3168), MitoTracker Deep Red FM (M22426), Tetramethylrhodamine (TMRM, T668), CellRox (C10448), MitoSOX (M36008). JC-1 dye accumulates in mitochondria; it exists as a monomer at low concentrations and yields green fluorescence. The dye forms J-aggregates at high mitochonrial membrane potential and the emission shifts to red. The ratio of green to red fluorescence is dependent only on the membrane. All probes were applied following manufacturer recommendations and were purchased from Thermo Fisher. Imaging of mtGrx1–roGFP (Fig. 3b, Extended Data Fig. 3g) was performed in 3 independent experiments and 17 organoids were analysed. Data analysis was performed according to ref. 33. Imaging of p38KTRClover (Fig. 4) was performed in 4 independent experiments and 24 organoids were analysed. Additionally, p38KTRClover organoids were treated with 1 mM mitoTEMPO overnight or 7.5 mM parquat for 90 min (Fig. 4a) and then imaged. Experiments were performed twice with 2 technical replicates in each and 30 organoids were analysed. The ratios Hoechst/Clover was considered as a measurement of p38 activity and is represented in Real Glow scale (ImageJ). ImageJ was used for all imaging analysis. For immunohistochemistry, fresh mouse intestine of one mouse was fixed in 4% formaldehyde for 24 h followed by dehydration in 70% ethanol and embedding in paraffin. Rehydrated slides were blocked for endogenous peroxidase activity in phosphate buffer (pH 5.8) containing 1.5% hydrogen peroxide. For antigen retrieval, samples were cooked for 20 min in 10 mM citrate buffer (pH 6) in a microwave. Primary and secondary horseradish-peroxidase-conjugated antibodies were incubated overnight or 1 h at 4 °C, respectively. Staining of slides was performed using diaminobenzidine and haematoxylin. For imaging, independent experiments (*n*) refer to the number of independent stainings performed and imaged on different days.

Metabolomics. Cells were sorted by FACS from intestinal crypts of mice[6]. To reach the minimal amount for analysis, cells sorted from two mice were pooled for each independent measurement, so 6 mice were used for $n = 3$. LC/MS was performed on the 3 independent samples and each sample was measured 3 times. Direct infusion mass spectrometry (DI-MS) metabolomics was performed on the 3 independent samples with 3 technical replicates measured 3 times each leading to a total of 9 measurements per group. Cells were sorted by FACS and collected directly in ice-cold methanol. After homogenization, the extracts were diluted in water and internal standards in methanol for DI-MS. Direct infusion was performed using chip-based infusion (400 nozzles, nominal internal Ø 5 μm) on the TriVersa NanoMate (Advion). High resolution mass spectrometry (140,000) was performed using a Q-ExactivePlus (Thermo Scientific GmbH) using a scan range of m/z 70 to 600 in positive and negative modes. Besides mass calibration of the instrument, internal lock masses were used for high mass accuracy. Cells were collected in biological triplicates. Cell extracts were diluted (1:1 v/v) using 70 μl stable isotopes solution in methanol (NSK-A-amino acids and NSK-B-free carnitine and acylcarnitine reference standards (Cambridge Isotope Laboratories). After dilution with 60 μl 0.3% formic acid, samples were filtered using a preconditioned (with methanol) 96-well filter plate (Acro prep, 0.2 μm GHP, NTRL, 1 ml well; Pall Corporation). The sample filtrate was collected using cleaned

96-well plate (Advion). A volume of 13 μl was infused into the DI-HRMS system in triplicate (technical replicates). RAW data files were converted to mzXML format using MSConvert[34]. The data were processed using an in-house-developed untargeted metabolomics pipeline written in the R programming language (http://www.r-project.org). First, the mzXML files were converted to readable format by the XCMS package[35]. For every sample, peak finding was performed and peaks with the same *m/z* (within 0.5 × full width at half maximum) were grouped over different samples. Peak groups that were not present in three out of three technical replicates in at least one biological sample were discarded. The intensities of the technical replicates were averaged. Peak groups were identified using all entries in the HMDB, including their most likely adducts (Na^+, K^+, $NH4^+$ in positive mode and Cl^- and formate in negative mode) and isotopes, using an accuracy of 3 p.p.m. or better. For LC-MS/MS analysis, 200 μl of the methanol extract was evaporated to dryness after the addition of internal standards. The residue was dissolved in 100 μl 10% acetonitrile in ultrapure water of which 5 μl was injected for analysis. Analysis was conducted with a Thermo Scientific Acella UHPLC system and an Acquity BEH C-8 column (1 × 150 mm, 1.7 μm). The column outlet was coupled to a Thermo Scientific Orbitrap XL equipped with an electrospray ion source operated in either negative or positive mode. The system was operated at a flow rate of 150 μl min^{-1} and 40 °C. The mobile phases consisted of 6.5 mM ammonium carbonate pH 8 (solvent A), and 6.5 mM ammonium carbonate in methanol (solvent B) in negative mode. For positive mode analysis the solvents were 0.1% formic acid in ultrapure water and 0.1% formic acid in methanol, respectively. A 10-min linear gradient of 0–100% B was started 3 min after the injection of the sample. The system was kept at 100% B for the next 4 min, after which the system returned to its starting situation. Total runtime was 22 min. All acquired MS-data was searched against available databases. Statistics and analysis was performed on replicates (LC-MS/MS) and on replicates and technical replicates (DI-MS). PCA analyses were performed with http://www.metaboanalyst.ca (ref. 36).

Bioenergetics. Seahorse Bioscience XFe24 Analyzer was used to measure extracellular acidification rates (ECAR) in mpH (milli pH) per min and oxygen consumption rates (OCR) in pmol O_2 per min. Organoids were seeded in 3 μl matrigel per well in XF24 cell culture microplates (Seahorse Bioscience). 1 h before the measurements, culture medium was replaced and the plate was incubated for 60 min at 37 °C. For the mitochondrial stress test, culture medium was replaced by Seahorse XF Base medium (Seahorse Bioscience), supplemented with 20 mM glucose (Sigma-Aldrich), 2 mM L-glutamine (Sigma-Aldrich), 5 mM pyruvate (Sigma-Aldrich) and 0.56 μl NaOH (1 M). During the test, 5 μM oligomycin, 2 μM FCCP and 1 μM of Rotenone and Antimycin A (all Sigma-Aldrich) were injected to each well after 18, 45 and 63 min, respectively. For the glycolysis stress test, culture medium was replaced by Seahorse XF Base medium, supplemented with 2 mM L-glutamine and 0.52 μl ml^{-1} NaOH (1 M). During the test 10 mM glucose, 5 μM oligomycin and 100 mM 2-deoxyglucose (Sigma-Aldrich) were injected to each well after 18, 36 and 65 min, respectively. After injections, measurements of 2 min were performed in triplicate, preceded by 4 min of mixture time. The first measurements after oligomycin injections were preceded by 5 min mixture time, followed by 8 min waiting time for the mitochondrial stress test and 5 min mixture time followed by 10 min waiting time for the glycolysis stress test.

Reconstitution assays. Reconstitution of *Lgr5*-EGFP^{hi} stem cells (purity >99%) with Paneth cells (CD24^{hi}SSC^{hi}; purity >98%) was performed by pelleting sorted cells at 300*g* for 5 min in Eppendorf LoBind Tubes, and by co-incubating them for 15 min at room temperature as previously described[14]. *Lgr5*-EGFP^{hi} stem cells were co-incubated with Paneth cells in equal numbers as previously described[24]. Incubation with 20 mM DCA, 100 μM pCMB, 50 μM Floretin, 50 μM Azide, 200 μM Antimycin A (all purchased in Sigma) was performed for 2 h on ice. Cells were then pelleted at 300*g* for 5 min and washed twice with ENR medium and pelleted again at 300*g*. Cells were then co-incubated for 15 min and plated as previously described. Organoids grown from single *Lgr5*-EGFP^{hi} stem cells with lactate or glucose were performed in ENR medium (base medium SILAC Advanced DMEM/F12 supplemented with arginine and lysine) supplemented with 17.5 mM glucose, Na-pyruvate or lactate where indicated. Recombinant Wnt3a (R&D systems) was used where indicated at 50 μg ml^{-1} and 100 μg ml^{-1} to promote organoid formation from single *Lgr5*-EGFP^{hi} stem cells. Where indicated cells were treated with 0.5 mM mitoTEMPO, 5 μM EUK5099, 2 μM php7879 or 5 μM SB202190. Organoid number was counted at day 5 and after counting 5 mM glucose was added to all non-glucose conditions to allow crypt formation. Pictures of organoids for crypt counting were taken at day 12. A total of 35 organoids were counted per condition. Each independent experiment refers to mice intestinal crypt isolation, FACS sorting and treatments performed on different days.

Animal experiments. Experiments involving live mice (generation of organoids) were performed in compliance with local and national ethical regulations and codes (DEC, Dier Experimenteel Commissie).

Data availability. Source Data are provided for all figures with the online version of the paper, excluding mass-spectrometry metabolomics data, which is available from the corresponding author upon reasonable request.

31. Van Lidth de Jeude, J. F., Vermeulen, J. L., Montenegro-Miranda, P. S., Van den Brink, G. R. & Heijmans, J. A protocol for lentiviral transduction and downstream analysis of intestinal organoids. *J. Vis. Exp.* http://dx.doi.org/10.3791/52531 (2015).
32. Baker, K. *et al.* Synthetic combined superoxide dismutase/catalase mimetics are protective as a delayed treatment in a rat stroke model: a key role for reactive oxygen species in ischemic brain injury. *J. Pharmacol. Exp. Ther.* **284,** 215–221 (1998).
33. Morgan, B., Sobotta, M. C. & Dick, T. P. Measuring E_{GSH} and H_2O_2 with roGFP2-based redox probes. *Free Radic. Biol. Med.* **51,** 1943–1951 (2011).
34. Chambers, M. C., Song, K. H. & Schneider, D. S. *Listeria monocytogenes* infection causes metabolic shifts in *Drosophila melanogaster*. *PLoS One* **7,** e50679 (2012).
35. Smith, C. A., Want, E. J., O'Maille, G., Abagyan, R. & Siuzdak, G. XCMS: processing mass spectrometry data for metabolite profiling using nonlinear peak alignment, matching, and identification. *Anal. Chem.* **78,** 779–787 (2006).
36. Xia, J., Sinelnikov, I. V., Han, B. & Wishart, D. S. MetaboAnalyst 3.0—making metabolomics more meaningful. *Nucleic Acids Res.* **43,** W251–W257 (2015).

a

ANOVA	p.value	FDR	Post-hoc tests
2-Oxobutanoate	1.96E-07	1.41E-05	Lgr5^{+}- Neg.; Paneth - Neg.
Indole-3-acetaldehyde	2.39E-05	0.00086	Neg. - Lgr5^{+}; Paneth - Neg.; Paneth - Lgr5^{+}
2-Aminoadipate	0.000159	0.00326	Neg. - Lgr5^{+}; Neg. - Paneth
(iso)Leucine	0.000223	0.00326	Neg. - Lgr5^{+}; Neg. - Paneth; Lgr5^{+} - Paneth
Glucosamine	0.000271	0.00326	Neg. - Lgr5^{+}; Neg. - Paneth; Lgr5^{+} - Paneth
Hypoxanthine	0.000283	0.00326	Neg. - Lgr5^{+}; Neg. - Paneth; Lgr5^{+}- Paneth
Palmitoylcarnitine	0.000317	0.00326	Paneth - Neg.; Paneth - Lgr5^{+}
4-Methylene-L-glutamate	0.000552	0.00497	Neg. - Paneth; Lgr5^{+} - Paneth
Tryptophan	0.000886	0.00709	Neg. - Paneth; Lgr 5^{+}- Paneth
2,6 dimethylheptanoyl carnitine	0.001003	0.00722	Lgr5^{+}- Neg.; Paneth - Neg.; Lgr5$^{\pm}$ Paneth

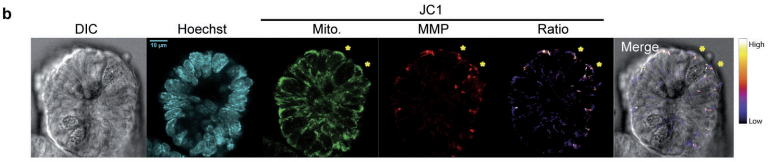

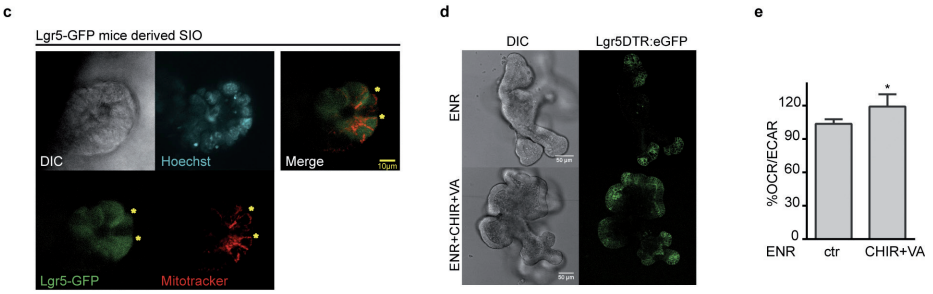

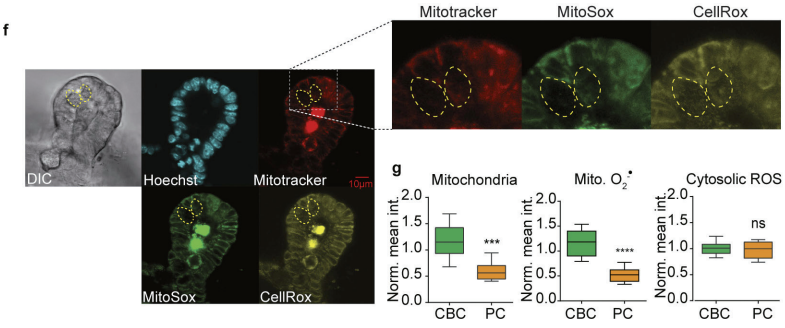

Extended Data Figure 1 | Metabolic compartmentalization and mitochondria and redox state in the crypt. a, Top 10 most different metabolites between Lgr5^{+} CBCs, Paneth cells (PCs) and all other differentiated cell types ('Neg.'). *P* value and false discovery rate (FDR) refer to the significance, and post hoc tests indicate the groups being compared. Results were obtained by analysis with http://metaboanalyst.ca. **b**, Live confocal microscopy of organoid crypts. All mitochondria (green) and high MMP (red) was determined by JC-1 staining. MMP/mitochondria ratio is represented in fire intensity scale (ImageJ). **c**, Live imaging of Lgr5–GFP-derived organoid stained with Mitotracker Deep-Red confirmed increased mitochondria in Lgr5^{+} CBCs. In both cases Hoechst was used to stain nuclei. Asterisks indicate stem cells in between Paneth cells ($n = 1$). **d**, Representative images of DTR–Lgr5–eGFP organoids grown in ENR medium or ENR medium supplemented with CHIR99021 (3 μM) and valproic acid (2 mM) during 72 h. **e**, Mitochondrial respiration/glycolysis (basal) was measured during mitochondrial stress test using Seahorse technology. Organoids were grown in ENR medium and after 24 h CHIR99021 and valproic acid were added to half of the plate during 72 h before running the assay. Graph represents mean and s.d. of 6 independent Seahorse experiments. Two-tailed *t*-test, $^{*}P < 0.05$. **f**, ROS in the crypt was stained with CellRox (cytosolic ROS), MitoSOX (mitochondrial superoxide) and Mitotracker (mitochondria). Dashed yellow regions indicate Paneth cells. **g**, Quantification of ROS in CBCs (16) and Paneth cells (6) from 3 organoids. One representative experiment of 2 independent ones. Graphs show mean and s.d. Two tailed *t*-test, $^{****}P < 0.0001$, NS, not significant.

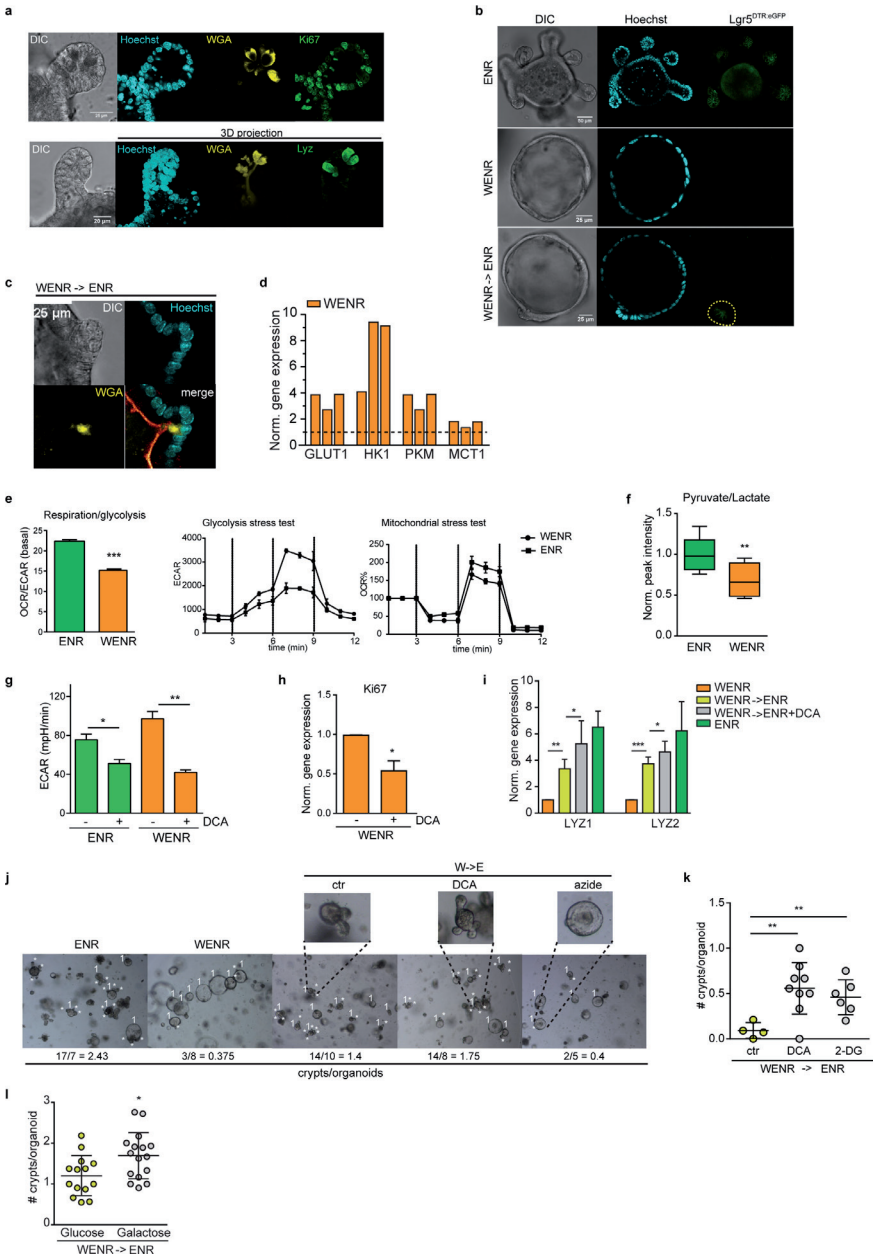

Extended Data Figure 2 | See next page for caption.

Extended Data Figure 2 | WENR organoids represent a homogeneous population of glycolytic dividing cells that retain pluripotency. **a**, Confocal images of organoid crypts. PC and nuclei were detected using WGA or Lyz antibody, and Hoechst, respectively. *z*-stacks are represented as 3D projections. **b**, Confocal live imaging of DTR–Lgr5–eGFP-derived mouse organoids. $Lgr5^{+}$ cells are visualized in green. Dashed yellow region indicates a bud structure that constitutes a starting crypt. **c**, Confocal microscopy of immunostaining of an emerging crypt. Phalloidin was used to stain F-actin (in red) ($n = 3$ (**a**–**c**)). **d**, Gene expression of glycolytic genes in WENR organoids normalized by the expression in ENR organoids (dashed line) ($n = 3$). **e**, Bioenergetics was determined by Seahorse technology. Results show one representative experiment of 3 independent ones. **f**, Pyruvate/lactate ratio was analysed by DIMS metabolomics. Boxes and error bars correspond to mean and s.d. of 3 technical replicates of 3 biological samples. **g**, DCA inhibition of glycolysis in ENR or WENR grown organoids was determined by Seahorse technology 1 representative experiment of $n = 3$. **h**, Proliferation was measured by Ki67 gene expression by qPCR. **i**, Gene expression of PC markers ($n = 5$ independent experiments). **j**, Representative images of a differentiation assay and the effect of DCA and azide; spherical organoids (grown in WENR) forming crypts (WENR→ENR) and cryptic organoids (grown in ENR medium). **k**, Effect of glycolysis inhibition on crypt formation was analysed by differentiation assay using DCA or 2-deoxyglucose (one representative experiment, $n = 2$). **l**, Increased crypt formation by activation of mitochondria (**h**) was analysed by differentiation assay replacing glucose by galactose in ENR medium. Two-tailed *t*-test, $^{***}P < 0.001$; $^{**}P < 0.01$; $^{*}P < 0.05$.

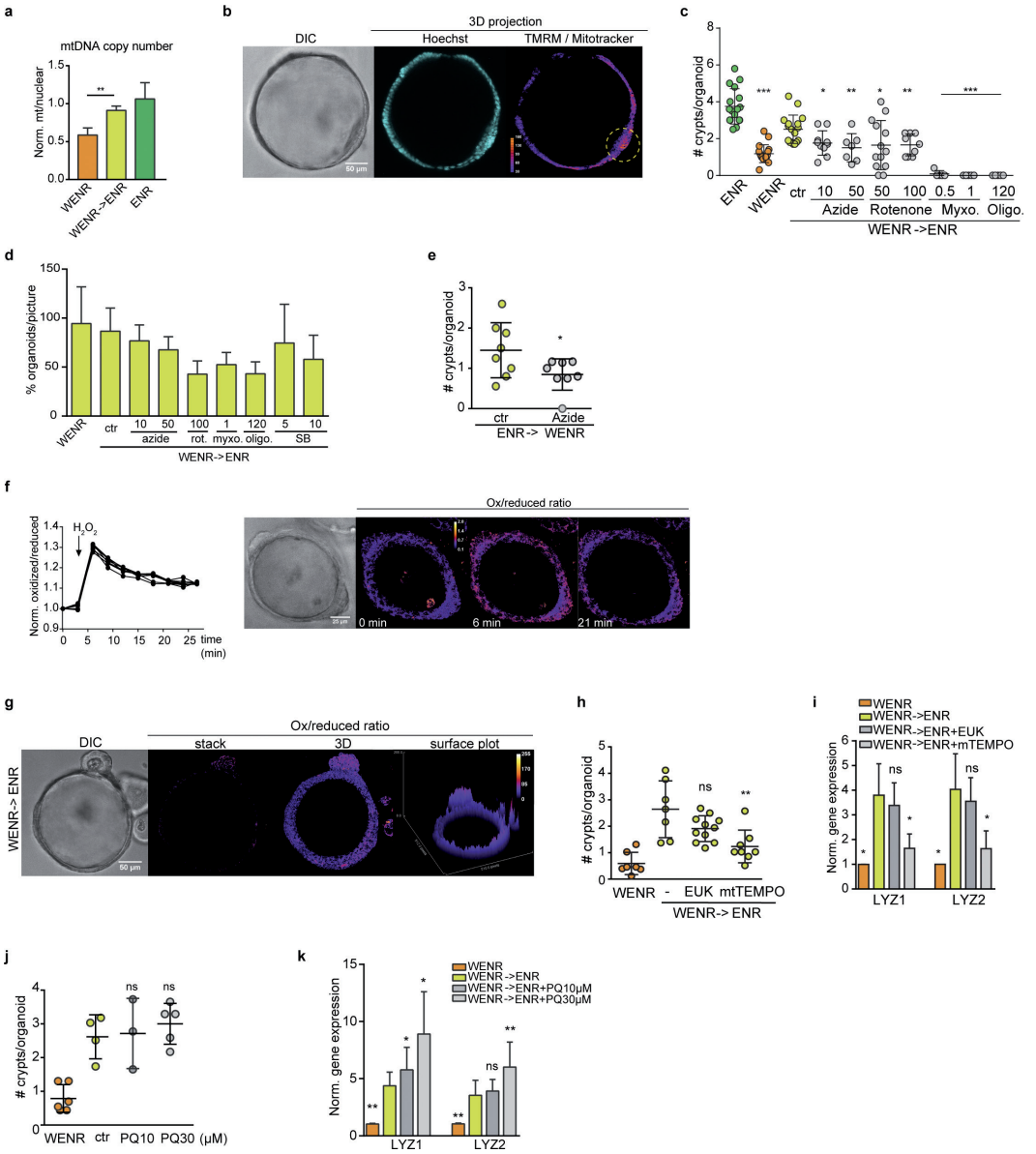

Extended Data Figure 3 | See next page for caption.

Extended Data Figure 3 | Mitochondrial OXPHOS and ROS signalling drive differentiation and crypt formation. a, Mitochondrial DNA copy number was quantified by qPCR on total DNA. Plot represents one representative experiment ($n = 2$). **b**, Mitochondrial membrane potential and total mitochondria were analysed with the combination of Mitotracker Deep Red (mitochondria) and TMRM (mitochondrial membrane potential). Staining is represented as a ratio using fire intensity scale (ImageJ). Dashed yellow region indicates a bud structure that constitutes a starting crypt. **c**, Decreased crypt formation by inhibition of mitochondria was analysed by differentiation assay adding OXPHOS inhibitors: azide, myxothiazol (myxo.), rotenone and oligomycin (oligo.) (concentrations in μM). **d**, Toxicity of OXPHOS inhibitors was measured by counting the number of organoids growing in the depicted conditions. Values are plotted as percentages of the WENR condition (mean). **e**, Mitochondrial inhibition enhances inhibition of crypt formation occurring when plating ENR organoids in WENR medium. Azide (50 μM) was added to the medium, pictures were taken after 48 h and the number of crypts per organoid was counted using ImageJ. Average and s.d. are shown. Representative of one experiment ($n = 2$). **f**, The sensitivity to redox changes of the mtGrx1–roGFP in organoids was analysed by live imaging, applying 500 μM hydrogen peroxide and following the redox response in time. Images represent the ratio of oxidized/reduced sensor. **g**, Mitochondria redox state of a forming crypt was assessed by live imaging of mtGrx1–roGFP. **h**, **i**, Effect of ROS scavengers on crypt formation was analysed by differentiation assay (**h**) and Paneth cell markers gene expression (**i**) in the presence of EUK134 (5 μM) and mitoTEMPO (0.5 mM). **j**, **k**, The effect of triggering mitochondrial ROS on crypt formation was performed by differentiation assays applying paraquat and counting the number of crypts per organoids (**j**) and by the expression of Paneth cell markers by qPCR (**k**). One representative experiment of $n = 3$ (**c**, **d**) or $n = 5$ (**h**, **j**). Mean and s.d. are shown. Two tailed *t*-test; asterisks or NS indicate comparison to WENR→ENR control, * $P < 0.05$, ** $P < 0.01$.

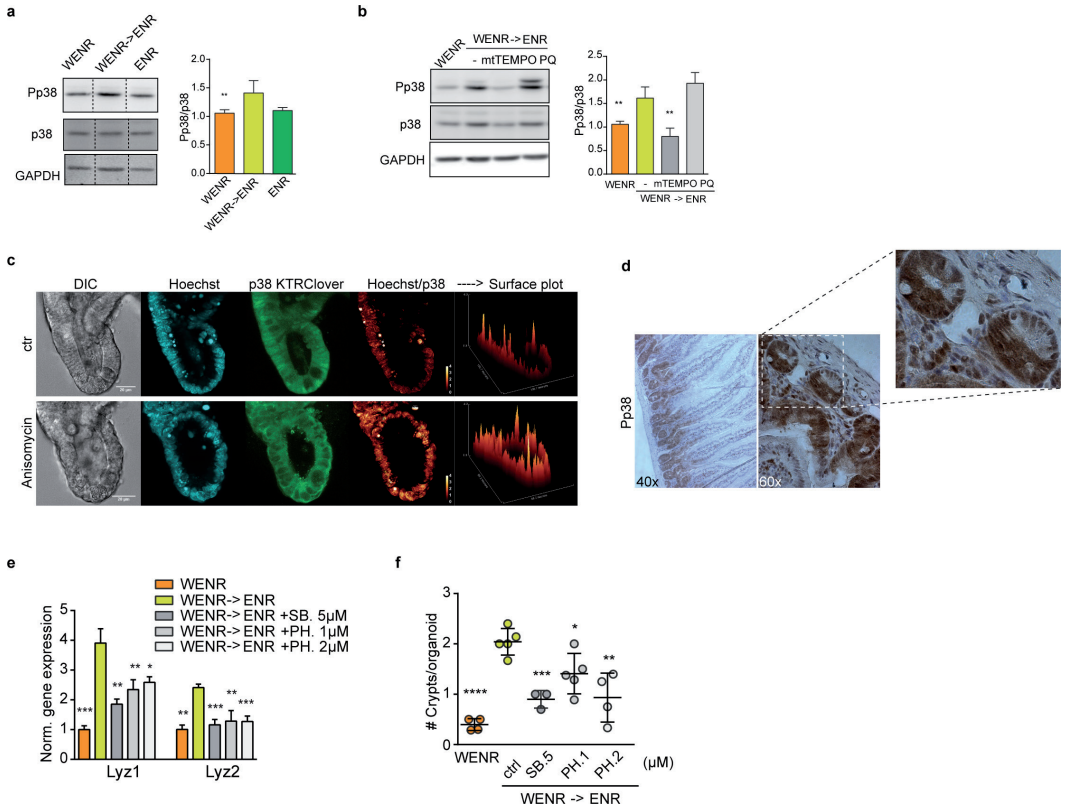

Extended Data Figure 4 | p38 activity drives differentiation and crypt formation in a mitochondrial ROS signalling dependent manner. **a**, **b**, P38 activation was analysed by western blot and quantified. For gel source data see Supplementary Fig. 1. Organoids were treated with mitoTEMPO (0.5 mM overnight) or paraquat (7.5 mM, 1.5 h) ($n = 3$) (**b**). **c**, p38KTRClover organoids were challenged with anisomycin (75 µg ml^{-1}) in order to analyse p38 activity. Images were obtained during 45 min after the addition of the compound. *z*-stacks of p38KTRClover or Hoechst/p38KTRClover ratio are represented as 3D projections and surface plot of 3D projections. Ratios are represented in either fire or real glow scale (ImageJ). **d**, Immunohistochemistry of p38 on mouse intestinal sections. **e**, **f**, Decreased differentiation and crypt formation upon p38 inhibition was analysed by differentiation assays (one representative experiment of $n = 5$) (**e**) and gene expression of *Lyz1* and *Lyz2* (**f**) in the presence of p38 inhibitors SB203580 and PH-797804. Mean and s.d. are shown ($n = 5$). Asterisks indicate comparison to WENR→ENR control; two-tailed paired *t*-test, $^{*}P < 0.05$, $^{**}P < 0.01$, $^{***}P < 0.001$ and $^{****}P < 0.0001$.

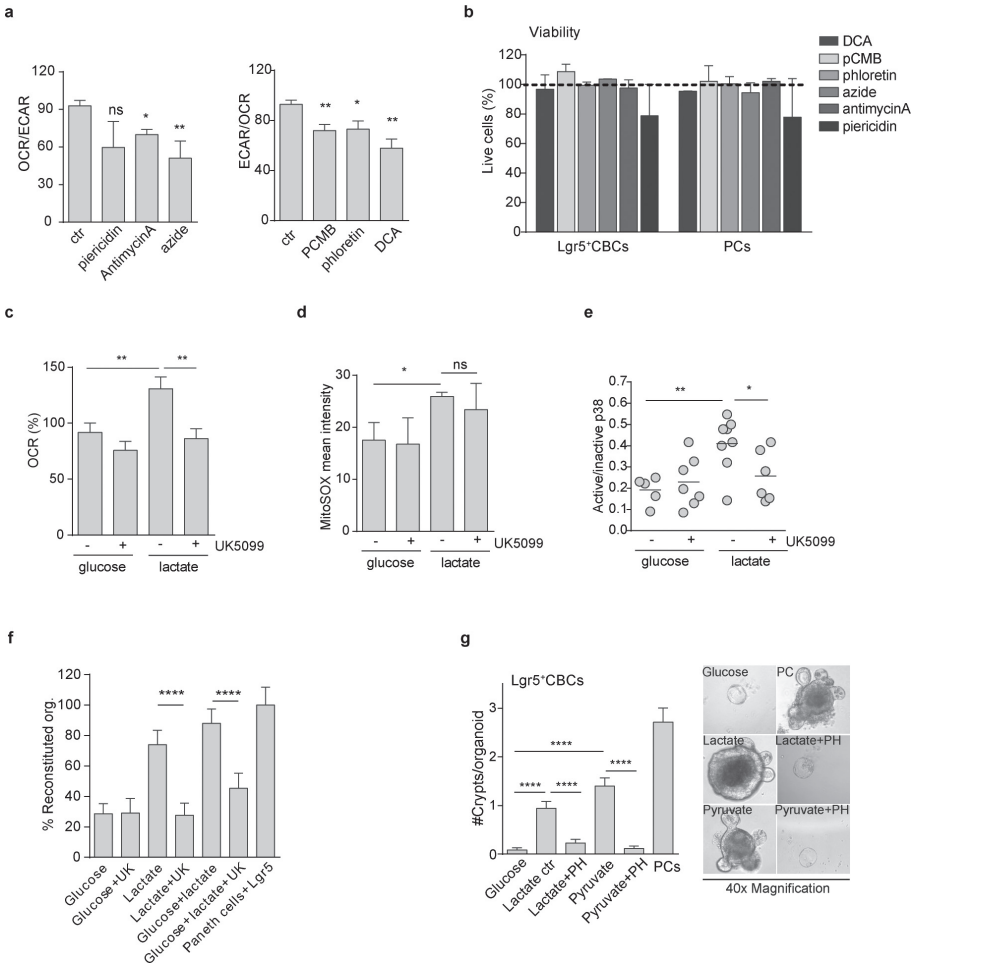

Extended Data Figure 5 | Mitochondrial activity, mitochondria ROS signalling and p38 activity regulate stem cell function of Lgr5$^+$ CBCs. **a**, The effects of the indicated compounds on respiration and glycolysis were tested after 3 h of the treatments using mitochondrial stress test (Seahorse technology). Bars and error bars represent the mean of the basal ratios and s.e.m. of 4 independent experiments with 4 technical replicates each. **b**, Cell viability after mitochondria and glycolysis inhibition treatments on CBCs and Paneth cells. Primary intestinal Lgr5$^+$ CBCs and Paneth cells were treated with the indicated compounds for 2 h and then washed and stained with PI before FACS. PI negative and positive cells were counted as alive and dead, respectively. Values are plotted as percentages of the untreated cells (100%) indicated as a dashed line. Mean and s.d. of 2 independent experiments with 2 technical replicates each are represented in the graph. **c**, Effect of lactate and inhibition of pyruvate mitochondrial transport on mitochondrial respiration. Maximal respiration was measured by performing mitochondrial stress test after two hours of incubation with glucose or lactate with or without UK5099. Mean and s.d. are shown of 3 independent experiments with 4 technical replicates in each. **d**, Effect of lactate and inhibition of pyruvate mitochondrial transport on mitochondrial superoxide production. Mitochondrial superoxide was measured by FACS analysis of single cells stained with MitoSOX after 2 h of incubation with the indicated compounds. The graph represents the mean and s.d. of 4 independent experiments. **e**, P38 activity was monitored in p38KTRClover organoids growing for three days in the indicated conditions. P38 activity is measured by the ratio of cells with active (cytosolic localization)/inactive (nuclear localization) of the signal. The graph shows the counting of one representative experiment of 3 independent ones and each dot represents one organoid. **f**, The effect of inhibition of pyruvate transport to mitochondria on stem cell function was measured as number of reconstituted organoids from primary Lgr5$^+$ CBCs in the depicted conditions. The graph represent the mean and s.d. of 3 independent experiments. Two-tailed *t*-test, $^*P < 0.05$, $^{**}P < 0.01$, $^{***}P < 0.001$. **g**, Number of crypts per reconstituted organoid and representative images of the referred conditions. The plot represents mean and s.e.m. of 35 organoids of one representative experiment of $n = 6$. Mann–Whitney test, $^{****}P < 0.0001$. In **a**, **c**–**e**, organoids were grown on ENR, CHIR99021 and valproic acid to enrich them with stem cells and the experiments were performed on single cells after trypsinization. In **b**, **f**, **g**, experiments were performed in mouse intestinal crypt FACS-sorted cells.

96-well plate (Advion). A volume of 13 μl was infused into the DI-HRMS system in triplicate (technical replicates). RAW data files were converted to mzXML format using MSConvert[34]. The data were processed using an in-house-developed untargeted metabolomics pipeline written in the R programming language (http://www.r-project.org). First, the mzXML files were converted to readable format by the XCMS package[35]. For every sample, peak finding was performed and peaks with the same *m/z* (within 0.5 × full width at half maximum) were grouped over different samples. Peak groups that were not present in three out of three technical replicates in at least one biological sample were discarded. The intensities of the technical replicates were averaged. Peak groups were identified using all entries in the HMDB, including their most likely adducts (Na^+, K^+, $NH4^+$ in positive mode and Cl^- and formate in negative mode) and isotopes, using an accuracy of 3 p.p.m. or better. For LC-MS/MS analysis, 200 μl of the methanol extract was evaporated to dryness after the addition of internal standards. The residue was dissolved in 100 μl 10% acetonitrile in ultrapure water of which 5 μl was injected for analysis. Analysis was conducted with a Thermo Scientific Acella UHPLC system and an Acquity BEH C-8 column (1 × 150 mm, 1.7 μm). The column outlet was coupled to a Thermo Scientific Orbitrap XL equipped with an electrospray ion source operated in either negative or positive mode. The system was operated at a flow rate of 150 μl min^{-1} and 40 °C. The mobile phases consisted of 6.5 mM ammonium carbonate pH 8 (solvent A), and 6.5 mM ammonium carbonate in methanol (solvent B) in negative mode. For positive mode analysis the solvents were 0.1% formic acid in ultrapure water and 0.1% formic acid in methanol, respectively. A 10-min linear gradient of 0–100% B was started 3 min after the injection of the sample. The system was kept at 100% B for the next 4 min, after which the system returned to its starting situation. Total runtime was 22 min. All acquired MS-data was searched against available databases. Statistics and analysis was performed on replicates (LC-MS/MS) and on replicates and technical replicates (DI-MS). PCA analyses were performed with http://www.metaboanalyst.ca (ref. 36).

Bioenergetics. Seahorse Bioscience XFe24 Analyzer was used to measure extracellular acidification rates (ECAR) in mpH (milli pH) per min and oxygen consumption rates (OCR) in pmol O_2 per min. Organoids were seeded in 3 μl matrigel per well in XF24 cell culture microplates (Seahorse Bioscience). 1 h before the measurements, culture medium was replaced and the plate was incubated for 60 min at 37 °C. For the mitochondrial stress test, culture medium was replaced by Seahorse XF Base medium (Seahorse Bioscience), supplemented with 20 mM glucose (Sigma-Aldrich), 2 mM L-glutamine (Sigma-Aldrich), 5 mM pyruvate (Sigma-Aldrich) and 0.56 μl NaOH (1 M). During the test, 5 μM oligomycin, 2 μM FCCP and 1 μM of Rotenone and Antimycin A (all Sigma-Aldrich) were injected to each well after 18, 45 and 63 min, respectively. For the glycolysis stress test, culture medium was replaced by Seahorse XF Base medium, supplemented with 2 mM L-glutamine and 0.52 μl ml^{-1} NaOH (1 M). During the test 10 mM glucose, 5 μM oligomycin and 100 mM 2-deoxyglucose (Sigma-Aldrich) were injected to each well after 18, 36 and 65 min, respectively. After injections, measurements of 2 min were performed in triplicate, preceded by 4 min of mixture time. The first measurements after oligomycin injections were preceded by 5 min mixture time, followed by 8 min waiting time for the mitochondrial stress test and 5 min mixture time followed by 10 min waiting time for the glycolysis stress test.

Reconstitution assays. Reconstitution of *Lgr5*-EGFP^{hi} stem cells (purity >99%) with Paneth cells (CD24^{hi}SSC^{hi}; purity >98%) was performed by pelleting sorted cells at 300*g* for 5 min in Eppendorf LoBind Tubes, and by co-incubating them for 15 min at room temperature as previously described[14]. *Lgr5*-EGFP^{hi} stem cells were co-incubated with Paneth cells in equal numbers as previously described[24]. Incubation with 20 mM DCA, 100 μM pCMB, 50 μM Floretin, 50 μM Azide, 200 μM Antimycin A (all purchased in Sigma) was performed for 2 h on ice. Cells were then pelleted at 300*g* for 5 min and washed twice with ENR medium and pelleted again at 300*g*. Cells were then co-incubated for 15 min and plated as previously described. Organoids grown from single *Lgr5*-EGFP^{hi} stem cells with lactate or glucose were performed in ENR medium (base medium SILAC Advanced DMEM/F12 supplemented with arginine and lysine) supplemented with 17.5 mM glucose, Na-pyruvate or lactate where indicated. Recombinant Wnt3a (R&D systems) was used where indicated at 50 μg ml^{-1} and 100 μg ml^{-1} to promote organoid formation from single *Lgr5*-EGFP^{hi} stem cells. Where indicated cells were treated with 0.5 mM mitoTEMPO, 5 μM EUK5099, 2 μM php7879 or 5 μM SB202190. Organoid number was counted at day 5 and after counting 5 mM glucose was added to all non-glucose conditions to allow crypt formation. Pictures of organoids for crypt counting were taken at day 12. A total of 35 organoids were counted per condition. Each independent experiment refers to mice intestinal crypt isolation, FACS sorting and treatments performed on different days.

Animal experiments. Experiments involving live mice (generation of organoids) were performed in compliance with local and national ethical regulations and codes (DEC, Dier Experimenteel Commissie).

Data availability. Source Data are provided for all figures with the online version of the paper, excluding mass-spectrometry metabolomics data, which is available from the corresponding author upon reasonable request.

31. Van Lidth de Jeude, J. F., Vermeulen, J. L., Montenegro-Miranda, P. S., Van den Brink, G. R. & Heijmans, J. A protocol for lentiviral transduction and downstream analysis of intestinal organoids. *J. Vis. Exp.* http://dx.doi.org/10.3791/52531 (2015).
32. Baker, K. *et al.* Synthetic combined superoxide dismutase/catalase mimetics are protective as a delayed treatment in a rat stroke model: a key role for reactive oxygen species in ischemic brain injury. *J. Pharmacol. Exp. Ther.* **284,** 215–221 (1998).
33. Morgan, B., Sobotta, M. C. & Dick, T. P. Measuring E_{GSH} and H_2O_2 with roGFP2-based redox probes. *Free Radic. Biol. Med.* **51,** 1943–1951 (2011).
34. Chambers, M. C., Song, K. H. & Schneider, D. S. *Listeria monocytogenes* infection causes metabolic shifts in *Drosophila melanogaster*. *PLoS One* **7,** e50679 (2012).
35. Smith, C. A., Want, E. J., O'Maille, G., Abagyan, R. & Siuzdak, G. XCMS: processing mass spectrometry data for metabolite profiling using nonlinear peak alignment, matching, and identification. *Anal. Chem.* **78,** 779–787 (2006).
36. Xia, J., Sinelnikov, I. V., Han, B. & Wishart, D. S. MetaboAnalyst 3.0—making metabolomics more meaningful. *Nucleic Acids Res.* **43,** W251–W257 (2015).

a

ANOVA	p.value	FDR	Post-hoc tests
2-Oxobutanoate	1.96E-07	1.41E-05	Lgr5^{+}- Neg.; Paneth - Neg.
Indole-3-acetaldehyde	2.39E-05	0.00086	Neg. - Lgr5^{+}; Paneth - Neg.; Paneth - Lgr5^{+}
2-Aminoadipate	0.000159	0.00326	Neg. - Lgr5^{+}; Neg. - Paneth
(iso)Leucine	0.000223	0.00326	Neg. - Lgr5^{+}; Neg. - Paneth; Lgr5^{+} - Paneth
Glucosamine	0.000271	0.00326	Neg. - Lgr5^{+}; Neg. - Paneth; Lgr5^{+} - Paneth
Hypoxanthine	0.000283	0.00326	Neg. - Lgr5^{+}; Neg. - Paneth; Lgr5^{+}- Paneth
Palmitoylcarnitine	0.000317	0.00326	Paneth - Neg.; Paneth - Lgr5^{+}
4-Methylene-L-glutamate	0.000552	0.00497	Neg. - Paneth; Lgr5^{+} - Paneth
Tryptophan	0.000886	0.00709	Neg. - Paneth; Lgr 5^{+}- Paneth
2,6 dimethylheptanoyl carnitine	0.001003	0.00722	Lgr5^{+}- Neg.; Paneth - Neg.; Lgr5$^{\pm}$ Paneth

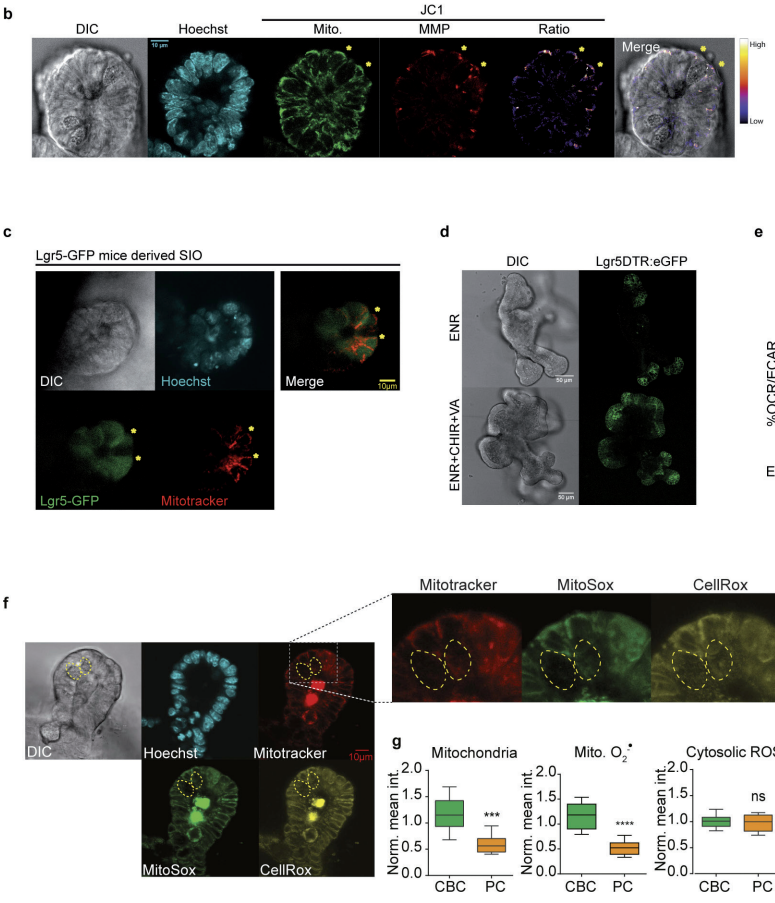

Extended Data Figure 1 | Metabolic compartmentalization and mitochondria and redox state in the crypt. a, Top 10 most different metabolites between Lgr5^{+} CBCs, Paneth cells (PCs) and all other differentiated cell types ('Neg.'). *P* value and false discovery rate (FDR) refer to the significance, and post hoc tests indicate the groups being compared. Results were obtained by analysis with http://metaboanalyst.ca. **b**, Live confocal microscopy of organoid crypts. All mitochondria (green) and high MMP (red) was determined by JC-1 staining. MMP/mitochondria ratio is represented in fire intensity scale (ImageJ). **c**, Live imaging of Lgr5–GFP-derived organoid stained with Mitotracker Deep-Red confirmed increased mitochondria in Lgr5^{+} CBCs. In both cases Hoechst was used to stain nuclei. Asterisks indicate stem cells in between Paneth cells ($n = 1$). **d**, Representative images of DTR–Lgr5–eGFP organoids grown in ENR medium or ENR medium supplemented with CHIR99021 (3 μM) and valproic acid (2 mM) during 72 h. **e**, Mitochondrial respiration/glycolysis (basal) was measured during mitochondrial stress test using Seahorse technology. Organoids were grown in ENR medium and after 24 h CHIR99021 and valproic acid were added to half of the plate during 72 h before running the assay. Graph represents mean and s.d. of 6 independent Seahorse experiments. Two-tailed *t*-test, $^{*}P < 0.05$. **f**, ROS in the crypt was stained with CellRox (cytosolic ROS), MitoSOX (mitochondrial superoxide) and Mitotracker (mitochondria). Dashed yellow regions indicate Paneth cells. **g**, Quantification of ROS in CBCs (16) and Paneth cells (6) from 3 organoids. One representative experiment of 2 independent ones. Graphs show mean and s.d. Two tailed *t*-test, $^{****}P < 0.0001$, NS, not significant.

CHAPTER 5

Paneth cells respond to inflammation and contribute to tissue regeneration by acquiring stem-like features through activation of the SCF/c-Kit signaling axis

Manuscript accepted in Cell reports.

Paneth cells respond to inflammation and contribute to tissue regeneration by acquiring stem-like features through activation of the SCF/c-Kit signaling axis

Mark Schmitt[1‡], Matthias Schewe[1‡], Andrea Sacchetti[1], Danny Feijtel[1], Wesley van de Geer[2], Miriam Teeuwssen[1], Hein F. Sleddens[1], Rosalie Joosten[1], Martin E. van Royen[3], Harmen J.G. van de Werken[2], Johan van Es[4], Hans Clevers[4], Riccardo Fodde[1]*

[1]Department of Pathology, [2]Cancer Computational Biology Center and Department of Urology, and [3]Erasmus Optical Imaging Center, Erasmus MC Cancer Institute, Erasmus University Medical Center, Rotterdam, The Netherlands. [4]Hubrecht Institute, University Medical Center Utrecht and Princess Maxima Center, Utrecht, The Netherlands.

[‡]These authors have equally contributed to this study.

*Contact Information:

prof. dr. Riccardo Fodde, PhD

Department of Pathology, Erasmus MC Cancer Center,

Erasmus University Medical Center,

PO Box 2040, 3000 CA Rotterdam, The Netherlands.

E-mail r.fodde@erasmusmc.nl

Summary

IBD syndromes such as Crohn's disease and ulcerative colitis result from the persistent inflammation of specific intestinal segments. Although many studies have reported on the regenerative response of intestinal progenitors and stem cells to tissue injury, very little is known on the response of differentiated lineages to more clinically relevant inflammatory cues. Here, we show that acute inflammation of the mouse small intestine is followed by a rapid and dramatic loss of *Lgr5*$^{+}$ stem cells. Instead, Paneth cells re-enter the cell cycle, lose their characteristic secretory expression signature, and acquire stem cell properties. As such they contribute to the tissue regenerative response to inflammation. Stem Cell Factor secretion upon inflammation triggers signaling through the c-Kit receptor and a cascade of downstream events culminating in GSK3β inhibition and Wnt activation in Paneth cells. Hence, the plasticity of the intestinal epithelium in response to inflammation goes well beyond stem and progenitor cells and extends to the fully differentiated and post-mitotic Paneth cells.

Introduction

Adult stem cells have long been postulated to be intrinsically of slow-cycling nature, mainly based on the necessity to preserve the integrity of their genome by preventing mutations occurring during DNA replication (Fuchs, 2009). In the hematopoietic field in particular, there is a general consensus on the inverse correlation between cycling frequency and long-term stem cell activity (Orford and Scadden, 2008). However, tissues characterized by a high cellular turnover (e.g. intestine, skin) seem to represent notable exceptions to these rules-of-thumb as highly proliferative stem cells, e.g. the *Lgr5*$^{+}$ crypt base columnar (CBC) cells in the intestinal crypt of Lieberkühn (Barker et al., 2007), have remarkable long-term self-renewal capacity. In these cases, a dichotomy of cycling and more quiescent stem cell lineages is thought to coexist within the niche: while actively cycling stem cells underlie daily homeostasis, their more quiescent equivalents are thought to play key roles in the response to tissue damage upon which they re-enter the cell cycle thus contributing to the regeneration process (Fuchs, 2009).

In the intestinal epithelium, *Lgr5*$^{+}$ stem cells are positioned at the very crypt bottom (pos. +1), usually flanked on both sides by secretory Paneth cells in the small intestine, and by analogous Paneth-like cells in the colon (Rothenberg et al., 2012; Sasaki et al., 2016; Sato et al., 2011; Schewe et al., 2016). Of note, apart from their canonical antimicrobial function exerted through the secretion of bactericidal compounds into the lumen (Clevers and Bevins, 2013), Paneth cells were also shown to play an essential niche role in supporting *Lgr5*$^{+}$ CBCs both through cell-cell contacts and by secreting specific factors such as EGF, Wnt3a, and Dll4 (Sato et al., 2011).

As for the less proliferative intestinal stem cell types, to date several candidates have been identified and partially characterized (Roth and Fodde, 2011). Among others, cells located at position +4 from the base of the crypt and earmarked by *Bmi1* expression were shown to self-renew and give rise to all the differentiated cell lineages of the small intestine epithelium (Sangiorgi and Capecchi, 2008). Notably, the +4 position of these *Bmi1*$^{+}$ stem cells is reminiscent of the BrdU-retaining cells originally identified by Potten and colleagues (Potten, 1998). However, the marker genes identified to date as proxies of these quiescent cell types are often not unique to a specific stem cell lineage but rather co-expressed at lower levels in other cells (Clevers, 2016; Grun et al., 2016; Li et al., 2014; Munoz et al., 2012).

Previously, we employed an *in vivo* label-retaining method as a marker-free approach for the isolation of infrequently dividing cells and identified Paneth cells and their precursors as the least cycling and longest-lasting intestinal cell lineage. Notably, we showed that upon tissue injury, these secretory cells and their immature precursors are capable of losing expression of some Paneth-specific genes (Roth et al., 2012). More recently, Buczacki et al. showed that label-retaining cells located at around position +3/+4 represent precursors committed to the Paneth and entero-

endocrine lineages but also potentially capable of giving rise to all intestinal cell types (Buczacki et al., 2013). These findings suggest that committed progenitors, and possibly even fully-differentiated and post-mitotic intestinal lineages as postulated in the present study, may serve as an alternative source of stem cells contributing to the regenerative response to tissue damage. Accordingly, irradiation-induced injury is usually accompanied by loss of CBCs and by the de-differentiation of secretory progenitor cells earmarked by *Dll1* expression (usually located at position +5 or higher) into stem-like cells (van Es et al., 2012). In addition to secretory lineages, enterocyte progenitors expressing the intestinal alkaline phosphate (*Alpi*) gene have also been shown to regain stem cell potential upon *Lgr5*$^{+}$ CBCs ablation (Tetteh et al., 2016).

The role played by precursors of secretory lineages and in particular by Paneth cells (PCs) in the regenerative response to intestinal tissue damage is of interest especially in the context of inflammatory bowel disease (IBD), a cumulative name for syndromes such as Crohn's disease (CD) and ulcerative colitis (UC) featuring chronic inflammation of either both the small and large intestine (CD) or only the colon (UC) (Clevers and Bevins, 2013; Schewe and Fodde, 2018). In particular, Crohn's disease has been shown to be a disorder of the Paneth cell and vice versa PCs are regarded as the site of origin of intestinal inflammation in CD, as defects in its unfolded protein response function are likely to trigger the inflammatory reaction (Adolph et al., 2013).

In this study we elucidated the role played by Paneth cells, a terminally differentiated and post-mitotic secretory lineage, in the regenerative response to inflammation and its capacity to de-differentiate and acquire stem cells characteristics to contribute to intestinal regeneration. Of note, expression of stem cell factor (SCF), i.e. the ligand of the c-Kit receptor specifically expressed in PCs, is enhanced in IBD patients and the DSS (dextran sodium sulfate) model. Indeed, the mechanisms underlying Paneth cell de-differentiation and stemness acquisition rely on the activation of PI3K/Akt and Wnt downstream the SCF/c-Kit signaling axis.

Results

Intestinal expression of the c-Kit ligand SCF is enhanced in IBD patients and in mouse models of pan-gastroenteritis.

It has been previously reported that expression of stem cell factor (SCF) is increased in IBD patients (Andersson et al., 2017; Comar et al., 2012). This observation is of potential interest as the *SCF* gene, also known as *KITLG*, encodes the ligand of the tyrosine-kinase receptor c-KIT known to regulate survival, maintenance and self-renewal of stem cells (Lennartsson and Ronnstrand, 2012). Of note, both secretory Paneth cells (PCs) in the small intestinal epithelium and Paneth-like cells (PLCs) in the colon express the c-KIT receptor (Rothenberg et al., 2012). In contrast, the *Lgr5*$^{+}$ CBCs do not express c-KIT (Clevers, 2016; Grun et al., 2016; Li et al., 2014; Munoz et al., 2012). In view of the known niche role played by Paneth cells in supporting *Lgr5*$^{+}$ stem cells (Sato et al., 2011) and of their own capacity to respond to tissue damage by re-entering the cell cycle and acquiring stem-like cell properties (Buczacki et al., 2013; Roth et al., 2012; Schewe et al., 2016), we set to study the functional significance of SCF activation upon inflammatory insults by first validating the upregulation of SCF expression in IBD patients (i.e. Crohn's disease (CD) and Ulcerative Colitis (UC)) and in the DSS mouse model of acute intestinal inflammation of the entire GI tract (*pan gastroenteritis*)(Elsheikh et al., 2012).

SCF IHC analysis of a small cohort of IBD patients (n= 9, of which 5 UC and 4 CD, together with normal tissues from two colorectal cancer patients as controls) revealed increased expression in the epithelial lining, the mucosa and submucosa of the inflamed small intestinal and colon tissues from CD and UC patients, respectively (**Figure 1A** and **S1A**). As expected, Paneth cell metaplasia was also frequently observed in the colon of the analyzed IBD patients (3 out of 5 UC patients; **Figure S1B**). Next, we analyzed SCF expression in the DSS mouse model. DSS was administered orally (3% in drinking water) for a week in order to cause acute inflammation. At day 7 of DSS treatment, intestinal tissues were harvested and analyzed for SCF expression by RNA *in situ* hybridization which confirmed increased SCF expression in the small intestinal epithelium as well as the mucosa and submucosa of the treated mice (**Figure 1B** and **S1C**). RNA probes against PPIB (peptidyl-prolyl cis-trans isomerase B), here employed as positive controls, showed no differences between control and DSS-treated mice (**Figure S1C**).

In order to assess whether increased SCF/c-Kit signaling plays a critical role during intestinal inflammation, we inhibited the pathway by administrating the specific c-Kit inhibitor ISCK03 in the drinking water together with DSS. ISCK03 alone had no effect on the overall health of the animals as shown by their unchanged body weight (**Figure 1C**), disease activity index (DAI; **Figure 1D** and **S1D**), and infiltrating CD3^{+} T-lymphocytes multiplicity (**Figure S1E-F**) when compared to control mice. However, mice treated with ISCK03 in combination with DSS suffered more severely compared to

mice treated with DSS alone, as shown by increased weight loss and DAI scores (**Figure 1C-D** and **S1D**) and number of infiltrating $CD3^+$ T-lymphocytes (**Figure S1E**).

Overall, these results confirm that expression of the c-Kit ligand SCF is enhanced upon intestinal inflammation and that activation of the SCF/c-Kit signaling axis is critical in the physiological response to the inflammatory insult. In view of the multifunctional nature of Paneth cells and of their expression of the c-Kit receptor, we set to analyze the functional consequences of the activation of the SCF/c-Kit signaling axis on the intestinal stem cell niche.

Inflammation-driven SCF expression enhances intestinal stem cell function.

In order to study the effects of inflammation and enhanced SCF expression on the intestinal stem cell niche, we employed *ex vivo* 'mini-gut' organoid formation as readout of stemness (Sato et al., 2009; Schewe et al., 2016). To this aim we administered 3% DSS in the drinking water to C57BL/6J mice for one week and collected small intestinal crypts to assess their ability to form organoids at day 3 after withdrawal of DSS, i.e. at the peak of the regenerative response. As shown in **Figure 1E**, DSS treatment resulted in a significant increment in organoids multiplicity (~2 fold). Moreover, organoids from DSS-treated mice were of increased size and of more complex morphology (increased no. of budding events) when compared to the organoids from control animals (**Figure 1E**).

To assess the role of increased SCF expression on the observed positive effect of DSS-driven inflammation on intestinal stem cell function, we harvested crypts from DSS-treated and control mice and supplemented the culture medium with a soluble c-Kit receptor, able to bind and sequester SCF thus preventing its interaction with its membrane-bound receptor (Dahlen et al., 2001). In parallel, c-Kit activity was also repressed by using the receptor tyrosine kinase inhibitor masitinib (Dubreuil et al., 2009). Whereas both the c-Kit receptor and masitinib had no significant effect on organoids derived from control animals, they substantially abrogated the increased organoid multiplicity observed in DSS-treated mice (**Figure 1F**).

Next, we tested whether SCF alone was sufficient to improve organoid formation. As depicted in **Figure 1G**, the presence of SCF in the culture medium increased the overall number of intestinal organoids as well as the complexity of their morphology to a very similar degree of that observed in organoids of from DSS-treated animals (~2 fold).

Hence, enhanced SCF expression upon inflammation appears to play a critical role in the tissue's regenerative response by improving intestinal stem cell function.

$Lgr5^+$ stem cells are depleted upon inflammation.

The observed positive effect of SCF on intestinal stem cell function in the regenerative response to inflammation raises the question on whether this is mediated by an increase in the self-renewal

and overall multiplicity of *Lgr5*$^{+}$ stem cells. To this aim, we administered 3% DSS to *Lgr5*^{EGFP} (*Lgr5–EGFP–ires–CreERT2*)(Barker et al., 2007) reporter mice for seven days followed by a three day recovery phase, to then determine *Lgr5*$^{+}$ and PC multiplicity by FACS. Notably, *Lgr5*$^{+}$ cells multiplicity was severely decreased in DSS-treated animals (~3 fold; **Figure 2A-B** and **S2A-B**), indicative of a severe loss of intestinal stem cells upon acute inflammation. No significant change in PCs multiplicity was observed upon DSS treatment compared to control mice (**Figure 2B** and **S2A**).

We then compared the lineage tracing ability of *Lgr5*$^{+}$ stem cells between control and DSS-treated mice. To this aim, we treated *Lgr5*-EGFP-IRES-CreERT2/R26-LSL-RFP mice with Tamoxifen to trigger recombination and lineage tracing from *Lgr5*$^{+}$ CBCs. These animals were administered 3% DSS for one week to then be analyzed at day 3 after withdrawal of DSS. In line with the FACS data, confocal microscopy revealed a severe loss of *Lgr5*$^{+}$ CBCs and a severe reduction of *Lgr5*-derived lineage tracing in the small intestine of DSS treated mice (**Figure 2C-D** and **S2B**). Of note, the residual tracing events extend throughout the length of the crypt villus axis, suggesting that the *Lgr5*$^{+}$ stem cells that escape the DSS treatment fully retain their self-renewal and differentiation capacity.

To rule out that the DSS-driven inflammation suppresses *Lgr5* gene expression without affecting intestinal CBCs, we performed IHC analysis on intestinal tissues from DSS-treated mice with an antibody directed against the Olfm4 protein whose expression overlaps with that of *Lgr5* (van der Flier et al., 2009a). As shown in **Figure 2E-F** and **S2C**, a significant reduction in Olfm4^{+} cells is evident in intestinal crypts from DSS-treated animals, especially at the crypt base where they normally are intermingled with PCs.

Altogether, these results demonstrate that acute inflammation causes a severe loss of intestinal stem cells that are consequently no longer capable of contributing to the regenerative response to the tissue damage.

Paneth cells underlie enhanced intestinal stem cell function upon inflammation.

The loss of *Lgr5*$^{+}$ stem cells upon acute inflammation is in sharp contrast with the positive effect exerted by DSS on intestinal stem cell function as shown by organoid assays. To assess whether any *de novo* proliferating cell type is detectable in the intestinal crypt upon inflammation, we performed Ki67 staining on small intestinal tissues from DSS-treated and control mice. In the latter, Ki67 expression is restricted to the slender CBCs (*Lgr5*$^{+}$) cells at the bottom of the crypt and to the transient amplifying compartment, whereas the post-mitotic PCs are negative (**Figure 3A**, left panel). In DSS-treated mice however, apart from the absence of cells morphologically similar to CBCs, the granulated PCs are Ki67-positive (**Figure 3A**, right panel). We confirmed the Paneth cell identity of these proliferating cells by confocal microscopy: lysozyme/Ki67 double positive cells are present in the intestinal crypts of DSS-treated mice (**Figure S3A**). Quantification of the number of crypts

encompassing proliferative PCs (Ki67$^+$; >30%) highlights the relatively high frequency of reacquisition of proliferative capacity by Paneth cells upon tissue damage (**Figure 3B**). Notably, Ki67$^+$ PCs could also be detected in the inflamed ileal tissues of CD patients (**Figure S3B**; 2 out of 4).

In view of these and previous results (Roth et al., 2012), we addressed the functional role played by these secretory cells in the regenerative response of the intestinal stem cell niche to the inflammatory insult. To this aim, the organoid reconstitution assay (ORA) was employed (Schewe et al., 2016; Schewe et al., 2017). Here, *Lgr5*$^+$ and PCs are sorted by FACS from control and DSS-treated *Lgr5*^{EGFP} mice to then be reconstituted in different combinations to form intestinal organoids (**Figure 3C-D**). As expected, reconstitution of *Lgr5*$^+$ with PCs both from control mice led to the formation of organoids, whereas neither *Lgr5*$^+$ nor Paneth cells alone were able to form organoids. Reconstitution of *Lgr5*$^+$ and PCs from DSS-treated mice resulted in a significant increase in organoid numbers, similar to the effect of DSS on organoid formation from whole intestinal crypts. Reconstitution of *Lgr5*$^+$ cells from DSS-treated mice with PCs from controls did not differ in organoids numbers from the control (both cell types from untreated mice), suggesting that stem cell function of the residual *Lgr5*$^+$ cells, as also observed *in vivo* (**Figure 2C**), is unaffected. Last, Paneth cells from DSS-treated mice reconstituted with control *Lgr5*$^+$ stem cells resulted in a significant increase in organoid multiplicity when compared to the reconstitution of control *Lgr5*$^+$ and PCs. This indicates that the enhanced stem cell function elicited by inflammation is mediated by Paneth cells, possibly through their previously reported niche role in support of *Lgr5*$^+$ stem cells (Sato et al., 2011). However, the observed proliferative response of PCs to inflammation suggests alternative scenarios where the post-mitotic secretory cells directly contribute to tissue regeneration by de-differentiation and acquisition of stem cell features. Indeed, Paneth cells from DSS-treated mice were able to form organoids autonomously (i.e. in the absence of *Lgr5*$^+$ cells) (**Figure 3C-D**).

Next, we took advantage of the ORA by exposing Paneth (and *Lgr5*$^+$) cells sorted from control mice to recombinant SCF, prior to their reconstitution in different combinations (**Figure 3E**). As expected, untreated *Lgr5*$^+$ or PCs gave rise to very low numbers of organoids when plated alone. The latter was also true for *Lgr5*$^+$ cells pretreated with SCF. However, SCF treatment of PCs resulted in a striking increase in organoid multiplicity (approx. 10-fold). Accordingly, reconstitution of SCF-treated *Lgr5*$^+$ cells with untreated PCs did not affect the number of organoids when compared to the controls. Instead, SCF-treated Paneth cells gave rise to the highest organoid multiplicity when reconstituted with untreated *Lgr5*$^+$ cells (**Figure 3E**).

To provide definitive evidence of the Paneth cell origin of these organoids, we repeated the DSS treatments and organoid experiments using *Lys*^{CreERT2}/*R26*$^{LSL-YFP}$ mice and YFP$^+$ PCs isolated during the regenerative phase. The resulting organoids were entirely composed of YFP$^+$ cells, confirming that, upon inflammation, Paneth cells acquire stem cell features and give rise to mini-gut structures *ex*

vivo (**Figure 3F**, left panel). Also in the case of SCF treatment we repeated the experiment with PCs from tamoxifen-treated *Lys*^{CreERT2}/*R26*$^{LSL-YFP}$ mice, and confirmed that the organoids are entirely composed of YFP^{+} cells (**Figure 3F**, right panel).

To demonstrate that Paneth cells can also act *in vivo* as stem cells in response to inflammation, we administered DSS to *Lys*^{CreERT2}/*R26*$^{LSL-YFP}$ mice and analyzed their small intestine for lineage tracing events at several time points after withdrawal of DSS. In tamoxifen-treated control mice, YFP fluorescence was entirely restricted to PCs located at the crypt base (**Figure 4A,C**). However, FACS analysis of tamoxifen-treated *Lys*^{CreERT2}/*R26*$^{LSL-YFP}$ mice revealed that only a small proportion (~12%) of PCs express YFP after 3 consecutive injections of Tamoxifen (2 mg/20g bodyweight/day) (**Figure S4A** upper panel and **S4B**). Nonetheless, virtually all (97%) of the YFP+ cells were confirmed to be PCs by FACS (**Figure S4B** lower panel, and **S4C**). No YFP signal was detected prior to tamoxifen administration (**Figure S4C**). In DSS- (and tamoxifen-) treated animals, the YFP signal was still restricted to Paneth cells at the crypt base one day after DSS removal (**Figure S4D**). However, already at this time point a proportion of the YFP^{+} cells started to show nuclear Ki67, indicative of cell cycle re-activation in PCs (**Figure 4B**). Three days after DSS removal, short ribbons of YFP^{+} cells were observed within the intestinal crypts. Seven days after removal of DSS, YFP stained approximately 50-70% of the crypt-villus axis and reached the tip of the villi at day 10 (**Figure 4A**). These *in vivo* results demonstrate that, upon DSS-driven acute inflammation, Paneth cells acquire stem cell features and repopulate the intestinal epithelium thus contributing to the tissue regenerative response.

To assess the pluripotency of the Paneth-derived stem cells, we carried out IF analysis with lineage-specific markers of the YFP^{+} ribbons from DSS-treated *Lys*^{CreERT2}/*R26*$^{LSL-YFP}$ mice at day 7 of the recovery phase. As shown in **Figure 4D**, YFP^{+} cells located at the bottom of the crypt co-expressed Olfm4 indicating that new CBCs are generated from lysozyme-expressing PCs. As for the YFP^{+} cells located above the crypt base and along the villus axis, expression of entero-endocrine (ChrA^{+}/YFP^{+}), goblet (Muc2^{+}/YFP^{+}), and Tuft (Dclk1^{+}/YFP^{+}) lineage-specific markers was detected (**Figure 4E**). Hence, the Paneth-derived stem cells give rise to ribbons which recapitulate both the crypt-villus architecture and heterogeneous cell lineage composition of the intestinal epithelium.

Taken together, our results show that upon acute inflammation Paneth cells de-differentiate into proliferating stem-like cells able to form 3D organoids *ex vivo*, and to repopulate *in vivo* the epithelial lining giving rise to stem cells as well as all the differentiated lineages of the adult intestinal epithelium. Activation of the SCF/c-Kit signaling pathway plays a central role in acquisition of stem-like features by Paneth cells upon inflammation.

Activation of the SCF/c-Kit signaling axis and of the downstream PI3K/Akt and Wnt pathways elicit stemness in Paneth cells upon inflammation.

SCF/c-Kit signaling has been shown to activate several downstream signaling pathways (Lennartsson and Ronnstrand, 2012). In order to assess which of these pathways may play a role in the observed de-differentiation and acquisition of stem-like features in Paneth cells upon inflammation and the consequent SCF/c-Kit signaling activation, we treated whole small intestinal crypts with SCF in combination with several inhibitors of known downstream pathways such as MAPK, mTor, PI3K/Akt and Jak/Stat signaling, and tested their capacity to form organoids (**Figure S5A**). As shown before, SCF treatment alone significantly increased organoid multiplicity when compared to untreated crypts. MAPK signaling inhibition completely repressed organoid growth both in the presence or absence of SCF thus indicating an essential role for this pathway in organoid growth independently of the activation of the SCF/c-Kit signaling axis. In contrast, the mTOR inhibitor rapamycin did not affect organoid multiplicity with or without SCF. Inhibition of Jak1 instead increased organoid numbers to the same extent both in the absence and presence of SCF. Out of the 4 main downstream pathways tested, only the inhibition of PI3K/Akt signaling completely and specifically abrogated the positive effects exerted by SCF on organoid growth (**Figure S5A**).

To establish whether SCF activates PI3K/Akt signaling in Paneth cells, whole intestinal crypts from *Lgr5*^{EGFP} mice were treated with SCF and analyzed by IF with antibodies directed against pan- and phosphorylated Akt. Although Akt was expressed in all cell types of the intestinal crypt (**Figure S5B**), Akt phosphorylation was exclusively observed in Paneth cells upon SCF stimulation (**Figure 5A** and **S5C**). Western blot analysis of Paneth cells sorted by FACS and incubated with SCF confirmed the increased pAkt levels in the secretory cells. In contrast, analysis of the c-Kit negative *Lgr5*$^{+}$ stem cells did not reveal any change (**Figure 5B-C**).

To assess the relevance of the role played by PI3K/Akt signaling in the response to inflammation, PCs were sorted from DSS-treated mice and cultured to generate organoids in the presence of specific PI3K- (BKM120(Wen et al., 2012)) and Akt- (AKTVIII(Barnett et al., 2005)) inhibitors. In confirmation of the above result with whole intestinal crypts, both PI3K as well as Akt inhibition significantly reduced the number of organoids obtained from Paneth cells alone (**Figure 5D-E**). Likewise, in reconstitution assays, inhibition of PI3K or Akt in PCs significantly repressed organoid growth when *Lgr5*$^{+}$ and Paneth cells from DSS-treated mice were employed though not from untreated mice (**Figure 5D**).

In order to evaluate the global effects of acute inflammation on Paneth cells, we performed RNA expression analysis by NGS (RNAseq) on sorted cells from control and DSS-treated mice. In agreement with the *in vivo* data, the RNAseq results revealed the upregulation of genes related to cell proliferation and the cell cycle, and the downregulation of PC-specific markers such as lysozymes and defensins (**Figure 5F**). Of note, a group of genes known to earmark infrequently dividing and quiescent stem cells (i.e. *Tert*, *Ascl2*, *EphB2*, *Dclk1*, and *Lrig1*; **Figure S5D**) were upregulated in PCs

from DSS-treated mice, whereas the expression of other stem cell markers such as *Lgr5*, *Bmi1*, and *Hopx* appeared to be reduced (**Figure S5D**).

Last, pathway analysis performed on the differentially expressed genes pointed at the activation of the canonical Wnt signaling pathway, as shown by the upregulation of several Wnt target genes of (**Figure 5F**). This is likely to be related with the observed role played by PI3K/Akt signaling downstream of SCF/cKit: it has been shown that PI3K/Akt activation can increase Wnt signaling activity through GSK3β inhibitory phosphorylation at Ser-9(Doble and Woodgett, 2003). IF analysis of whole-mount intestinal crypts revealed that, as for Akt, GSK3β is expressed in all epithelial cells (**Figure S6A**). In these control crypts, *Lgr5*$^{+}$ stem cells as well as the proliferative TA compartment express high levels of phosphorylated GSK3β as a result of Wnt signaling activation in these lineages (**Figure 6A**). In contrast, PCs appear negative for pGSK3β, notwithstanding their characteristic nuclear β-catenin localization(van Es et al., 2005). However, upon SCF treatment an increase of GSK3β phosphorylation in Paneth cells becomes evident (**Figure 6A-B**). Western blot analysis of sorted *Lgr5*$^{+}$ and Paneth cells confirmed the increased GSK3β phosphorylation in PCs, though not in CBCs upon DSS treatment (**Figure 6C-D**).

GSK3β inhibitory phosphorylation in SCF-treated Paneth cells is expected to inhibit β-catenin proteolytic degradation leading to its cytoplasmic accumulation and translocation into the nucleus where it acts as a co-transcriptional factor to activate expression of Wnt target genes. To validate the ability of SCF to increase Wnt signaling even in already Wnt-active cells, the TOP/FOP Wnt reporter gene assay was implemented in the colon cancer cell line CaCo2. Supplementation of the culture medium with recombinant SCF significantly enhanced Wnt signaling in this *APC*-mutant cell line (**Figure 6E**). In order to validate that SCF can activate Wnt signaling also in PCs, qRT-PCR analysis of specific Wnt target genes was performed on sorted Paneth cells treated with SCF. In line with the results of the reporter gene assay and in confirmation of the RNAseq data from DSS-treated mice, upregulation of *Axin2*, *Jun*, and *Ccdn1* (cyclin D1) was found in SCF-treated PCs (**Figure 6F**).

To confirm that inflammation enhances Wnt signaling in Paneth cells *in vivo*, we analyzed by IHC their intracellular β-catenin distribution. As expected, nuclear β-catenin was observed in PCs from control animals with hardly any cytoplasmic staining. In contrast, PCs from DSS-treated mice showed a clear increase in cytoplasmic β-catenin, indicative of its increased stability and, consequentially, of enhanced Wnt signaling (**Figure 6G**).

Since Paneth cell differentiation is known to be driven by Wnt (van Es et al., 2005), the functional consequences of its further activation downstream of the SCF/c-Kit signaling axis in a cell type already earmarked by nuclear β-catenin in the context of the regenerative response to inflammation are yet unclear. In order to elucidate this aspect, we employed CHIR99021 (Chiron), a potent and selective GSK3β inhibitor leading to robust Wnt signaling activation, in organoid assays. As shown in

Figure 6H-I, upon Chiron supplementation in the culture medium PCs from control animals gave rise to high organoid numbers. As expected, Chiron treatment had a similar effect on *Lgr5*$^{+}$ CBCs. Of note, although a majority of *enterospheres*, i.e. spherical structures primarily composed of stem cells and lacking budding and branching structures (Stelzner et al., 2012), was observed during the early phase of the culture, upon Chiron withdrawal differentiation occurred and 'normal' organoid morphologies were observed both from PCs and *Lgr5*$^{+}$ cells (**Figure 6I**). Indeed, conversion between enterospheres and organoids has been shown to be regulated by Wnt signaling (Fordham et al., 2013; Mustata et al., 2013).

Finally, in order to demonstrate the *in vivo* relevance of the activation of the SCF/c-Kit signaling axis in Paneth cells during the regenerative response to inflammation, we administered the specific c-Kit inhibitor ISCK03(Na et al., 2007) to DSS-treated mice. As previously shown (**Figure 1C-D**), mice treated with both DSS and ISCK03 suffered from increased loss of body weight and an overall decrease in DAI scores when compared to animals treated with DSS alone. To assess whether this deleterious effect parallels the lack of Wnt "super-activation" downstream of the SCF/cKit signaling axis, β-catenin IHC analysis was again performed in small intestinal tissues from mice treated with DSS alone or in the presence of the ISCK03 inhibitor. As shown in **Figure 7A**, DSS treatment alone causes enhanced β-catenin accumulation in the cytoplasm and nucleus of PCs, indicative of increased Wnt signaling activation. This effect is almost entirely abrogated in mice treated simultaneously with both DSS and ISCK03. Furthermore, ISCK03 significantly reduced the number of Ki67^{+} PCs in DSS-treated mice (**Figure 7B-C** and **S7A**). Accordingly, combined DSS/ISCK03 treatment of Lyz-Cre/YFP mice strongly compromised the ability of Paneth cells to lineage trace upon inflammation (**Figure 7D-E**).

Taken together, these results show that inhibition of the SCF/c-Kit signaling axis prevents downstream Wnt signaling activation in Paneth cells thus compromising their capacity to acquire stem-like feature and to contribute to the regenerative response of the intestinal epithelium to the inflammatory insult.

Discussion

Inflammatory bowel disease (IBD) is regarded as an emerging global ailment in view of its steadily rising incidence during the last decades (M'Koma, 2013). Apart from its profound negative effects on the patient's quality of life, IBD is associated with an increased risk of developing intestinal cancer (Itzkowitz and Yio, 2004; Jia et al., 2008; Rosen and Jordan, 2009). From this perspective, the elucidation of the cellular and molecular mechanisms underlying the regenerative response of the intestinal stem cell niche to inflammatory tissue damage is of fundamental and translational relevance. Due to the complexity of the tissue response to injury and in view of the fact that IBD syndromes as ulcerative colitis and Crohn's disease affect different segments of the digestive tract, we have here chosen to model IBD in the mouse through DSS administration in the drinking water (Elsheikh et al., 2012). The mucosal injury caused by DSS results in acute inflammation of the entire GI tract (*pan gastroenteritis*) through recruitment and activation of inflammatory cells, followed by a rapid tissue regeneration phase (Vowinkel et al., 2004) thus providing a useful preclinical *in vivo* inflammation model for both UC and CD.

Enhanced secretion of the stem cell factor (SCF) has been reported in the plasma of IBD patients (Andersson et al., 2017; Comar et al., 2012) and here confirmed both in the intestinal epithelium and underlying stroma of UC and CD patients and in the DSS mouse model. This is of interest in view of the specific expression of the SCF transmembrane receptor c-Kit in Paneth cells and their equivalent in the colon (Rothenberg et al., 2012). Increased SCF expression was also observed in intestinal epithelial cells in response to Cholera Toxin or Salmonella thypimurium infection (Klimpel et al., 1995; Klimpel et al., 1996). SCF/c-Kit signaling is a major regulator of proliferation and differentiation in the hematopoietic system (Broudy, 1997). Mast cells and dendritic cells express high *c-Kit* levels even when fully differentiated, yet retaining the capacity to re-enter the cell cycle in response to extracellular SCF stimulation (Metcalfe et al., 1997; Ray et al., 2010). Besides, the functional analysis of the response of Paneth cells to SCF as shown here is of broader interest as indicated by the role played by SCF expression from differentiated tumor cells in the maintenance of c-Kit expressing colon cancer stem cells (Fatrai et al., 2015).

We here show that severe loss of *Lgr5*$^{+}$ CBCs characterizes the primary response to DSS-driven inflammation. Targeted ablation of *Lgr5*$^{+}$ stem cells in the mouse intestinal epithelium showed that these cells are in fact dispensable and that their role is taken over by their quiescent counterparts (Tian et al., 2011; van der Flier et al., 2009b). Depletion of *Lgr5*$^{+}$ stem cells has also previously been reported in the colon of DSS-treated mice where they reappear at day 5 of the recovery phase to then reach normal levels one day after (Davidson et al., 2012). Similarly, loss of *Lgr5*$^{+}$ CBCs has been observed upon high-dose γ-irradiation (Yan et al., 2012). In both cases the depletion is temporary and the CBC pool at the base of the crypt is rapidly restored.

More persistant CBCs loss upon tissue injury is compensated by the regenerative response of alternative stem cell pools including the infrequently cycling *Bmi1*$^{+}$ stem cells at position +4 (Sangiorgi and Capecchi, 2008; Yan et al., 2012), secretory (*Dll1*$^{+}$)(van Es et al., 2012) and enterocyte (*Alpi*$^{+}$)(Tetteh et al., 2016) progenitors, in addition to LRCs expressing Paneth cell markers (Buczacki et al., 2013; Roth et al., 2012), capable of reacquiring proliferative and self-renewal cell capacity upon tissue injury or targeted CBCs ablation. As such, the intestinal epithelium shows remarkable plasticity with several stem and progenitors cell types contributing to the restoration of tissue integrity and the re-establishment of the actively cycling *Lgr5*$^{+}$ CBCs (Yousefi et al., 2017). However, the ablation and tissue injury protocols employed in these studies are not directly relevant for IBD and the tissue damage caused by inflammation. Also, it is not clear whether the plasticity of the intestinal epithelium, apart from the above stem and progenitor cells, also extends to more committed and even post-mitotic lineages. Here, we show that, following the initial loss of *Lgr5*$^{+}$ CBCs, the response to acute inflammation features fully differentiated Paneth cells capable of re-entering the cell cycle, lose their secretory features, and acquire self-renewal and pluripotency thus contributing to the repair and regeneration of the damaged intestinal tissue.

As mentioned above, the specific expression of the c-Kit receptor in Paneth cells and in their counterparts in the colon (Rothenberg et al., 2012; Schewe et al., 2016), and the increased secretion of its natural ligand SCF upon inflammation both in IBD patients and in the DSS mouse model are of functional relevance for cell cycle re-entry, dedifferentiation, and acquisition of stem cell properties by these mature and normally post-mitotic secretory cells. Stimulation of the SCF/c-Kit signaling axis results in a cascade of downstream events from PI3/Akt pathway activation to GSK3β inhibitory phosphorylation. Of note, PI3K/Akt activation upon SCF/c-kit signaling induction has been shown to promote cell proliferation, growth, and survival in several models including colon cancer cell lines (Jeon et al., 2009; Vajravelu et al., 2015; Yasuda et al., 2007). Among the many pleiotropic effects of GSK3β inhibition, Wnt/β-catenin signaling activation is likely to play a central role in conferring proliferative and stem-like features to Paneth cells as here observed. However, it is well-established that Wnt signaling also underlies Paneth cell differentiation (van Es et al., 2005) and is retained in the mature secretory cells as indicated by their characteristic nuclear β-catenin staining. Distinct Wnt signaling dosages are associated with different downstream target genes and stem cell differentiation outcomes, as previously shown by our laboratory (Gaspar and Fodde, 2004; Kielman et al., 2002). Moreover, ectopic activation of canonical Wnt signaling was shown to be essential for the quiescence exit of *mTert*$^{+}$ stem cells as well as for *Dll1*$^{+}$ progenitors to regain stemness (Montgomery et al., 2011; van Es et al., 2012). Indeed, *ex vivo* enhancement of Wnt signaling in Paneth cells by GSK3β inhibition results in *de novo* organoid formation thus highlighting the central

role of the 'super-activation' of this pathway downstream the SCF/c-Kit axis in the de-differentiation and cell cycle re-entry of secretory cells during tissue regeneration.

Of note, the regenerative capacity of Paneth cells is maintained *ex vivo,* as shown by their capacity to form small intestinal organoids when isolated from DSS-treated mice (or upon SCF-stimulation) in the absence of *Lgr5*$^{+}$ CBCs. Thus, Paneth cells represent an additional pool of reserve stem cells capable of contributing to tissue regeneration upon injury. However, in view of their role in supporting *Lgr5*$^{+}$ CBCs (Sato et al., 2011), it is also plausible that inflammatory cues may enhance their niche function next to the expansion of the stem cell pool. Although *ex vivo* reconstitution of Paneth cells from DSS-treated animals with *Lgr5*$^{+}$ CBCs from control mice resulted in a markedly increase in organoid multiplicity, analysis of their expression profiles did not reveal a significantly increase in the expression of niche signals (e.g. EGF, TGF, Wnt3 or Dll4; data not shown) usually provided by Paneth cells to maintain stemness of CBCs (Sato et al., 2011). Nevertheless, inflammation is likely to exert context-dependent effects in the small and large intestine. Indeed, SCF was found among the proteins previously shown to be present at significantly different abundances between UC and CD (Andersson et al., 2017). Paneth cell metaplasia, i.e. the appearance of Paneth cells in the colon where they normally do not belong (Paterson and Watson, 1961), is frequently observed among UC patients and may result from differentiation of the *c-Kit*$^{+}$ cells to provide further niche support to stem cells in response to inflammation. On the other end, metaplastic Paneth cells have also been observed in colon adenomas and carcinomas (Lewin, 1968; Wada et al., 1992) and as such proposed to represent important precursors of IBD-associated colon cancer (Wada, 2009; Wada et al., 2005). Hence, the regenerative response to inflammatory tissue damage may differ between small intestine and colon and reflect the distinct predisposition to bowel cancer among IBD patients. Lineage tracing of the *c-Kit*$^{+}$ Paneth-like cells of the colon upon DSS administration will likely clarify this aspect.

The presence of multiple and distinct pools of low-cycling stem cells in the intestinal epithelium raises the issue of their individual roles and relative contributions to tissue regeneration upon inflammation. Two studies showed that Paneth cells depletion does not have major consequences and as such may be dispensable in intestinal tissue homeostasis/regeneration (Durand et al., 2012; Garabedian et al., 1997). However, it is unclear whether the ablation of Paneth cells in these mouse models is limited to fully mature cells as their secretory precursors may compensate for the loss of niche and stem cell functions. Also, these depletion models have not been challenged by inflammation. In support of their essential role, other studies demonstrated that Paneth cells are critical to provide niche support and maintain the *Lgr5*$^{+}$ stem cell population during crypt regeneration (Geiser et al., 2012; Parry et al., 2013; Sato et al., 2011). Given these rather controversial observations, future studies should focus on the role of Paneth cells in ensuring intestinal tissue integrity particularly in the context of inflammation. Notably, inhibition of SCF/c-Kit

signaling resulted in an increased weight loss and disease activity index upon inflammation likely to result at least partially from the prevention of Paneth cells to take part in intestinal tissue repair. However, as c-Kit is expressed in other cell types regulating inflammatory responses such as mast, dendritic, and interstitial cells of Cajal (Miettinen and Lasota, 2005), further studies are required to reveal the specific role of c-Kit inhibition of Paneth cells in the response to inflammation.

In conclusion, we show that activation of the SCF/c-Kit signaling axis upon inflammation induces cell cycle re-entry, dedifferentiation, and acquisition of stem cell properties in Paneth cells by enhancing Wnt through PI3K/Akt activation and GSK3β inhibition. As such, beside their role as regulators of the intestinal microflora and as niche cells for actively cycling CBCs, Paneth cells serve as a pool of quiescent stem cells that can be reactivated upon tissue insults and contribute to tissue regeneration. The diversity and complexity of their functional roles in IBD, dysbiosis, and cancer make of Paneth(-like) cells in the small bowel and in the colon a central node for intestinal homeostasis and diseases.

Acknowledgements

This study was made possible by funding from the Dutch Cancer Society (KWF; EMCR 2012-5473), the Netherlands Institute of Regenerative Medicine (NIRM; www.nirm.nl), and the World Cancer Research Funds (WCRF no. 2014/1181).

Author Contributions

MSch: study concept and design; data acquisition, analysis and interpretation; ms revision. MSchm: study concept and design; data acquisition, analysis and interpretation; ms revision. AS/DF/WvdG/MT/HS/MvR/JvE/HC: data acquisition, analysis and interpretation; RF: study concept and design; data analysis and interpretation; ms writing and revision, obtained funding; study supervision.

Declaration of interest

The authors of this study do not have any conflict of interest to disclose.

Experimental procedures

Animals

All mice employed in this study were aged between 8-12 weeks of age, fed *ad libitum*, and maintained at the Erasmus MC animal facility (EDC) and the IPMC animal facility under conventional SPF conditions. Inbred C57BL/6J mice were from Charles River Laboratories. All procedures were performed in agreement with local animal welfare laws and guidelines.

The generation and characterization of the $Lys^{CreERT2}/R26^{LSL\text{-}YFP}$ model will be described elsewhere (JH van Es, in preparation). In short: the $pLys^{CreERT2}$ mouse model was generated through homologous recombination in IB10 embryonic stem cells (129/Ola). The CreERT2 gene was knocked onto the ATG start codon of the of the lysozyme (*Lys*) gene. Both flanking arms were generated by high-fidelity PCR reactions from male 129/Ola-derived BAC DNA and subsequently cloned into PL451. The targeting construct (100 µg) was linearized and transfected into male 129/Ola-derived IB10 embryonic stem cells by electroporation (800V, 3F). Recombinant ES cell clones expressing the neomycin gene were selected in medium supplemented with G418 (250 µg/ml). Recombinant embryonic stem cell clones were screened by Southern blotting. The frequency of homologous recombination was 4%. Two positive clones were selected and injected into C57BL/6 derived blastocysts using standard procedures. Both injected clones gave germline transmission. The neomycin selection cassette was flanked by Frt recombination sites and excised *in vivo* by crossing the mice with the general FLP deleter strain (Jackson Lab.). $Lys^{CreERT2}$ mice were then crossed with $R26^{LSL\text{-}YFP}$ mice (R26R-YFP, #006148, Jackson Lab).

To activate C-recombinase, $Lgr5^{EGFP\text{-}IRES\text{-}creERT2}/R26^{LSL\text{-}RFP}$ mice were intraperitoneally (i.p) injected once with 1mg/20g bodyweight of Tamoxifen (#T5648, Sigma); the $Lys^{CreERT2}/R26^{LSL\text{-}YFP}$ were i.p. injected three times on consecutive days with 1 mg/20 g body weight. Tamoxifen was dissolved in 100% Ethanol (stock concentration 200mg/ml). For i.p. injection the Tamoxifen stock solution was diluted 1:10 in sunflower oil (#S5007, Sigma). As controls, mice were injected with 10% Ethanol in sunflower oil.

Disease Activity Index (DAI) scores upon DSS-induced inflammation were obtained according to (Cooper et al., 1993) with minor modifications. Mice were administered 3% dextran sulfate sodium salt (colitis-grade; #0216011050, MP Biomedicals) through the drinking water for seven days during which the animals were monitored for a specific set of parameters including stool consistency, blood loss, appearance, and % weight loss. DAI scores were as follows: stool consistency = normal (0), loose (1), diarrhea (2); blood loss = no loss (0),

gross bleeding (1); appearance = normal (0), hunched (1), starey coat (2), lethargic (3); % weight loss = none (0), 0-10 (2), 10-20 (2), >20 (3).

ISCK03 (#15781, Cayman Chemical) was administered via drinking water to the mice at a concentration of 0.1 mg/ml. For lineage tracing experiments, IF, IHC, or RNA *in situ* hybridization (ISH) analysis, mice were sacrificed at indicated time points post DSS treatment.

Immunohistochemistry (IHC) analysis

Mouse tissues were fixed overnight in 4% PFA and embedded in paraffin. Human tissues (normal and IBD) were already available as paraffin blocks from the department of Pathology at the Erasmus MC. Four µm sections were mounted on slides. IHC was performed using antibodies against SCF (1:500; #600-401-EE1, Rockland), OLFM4 (1:200; #39141, CST), Mki67 (1:200; #NB500-170, Novus biologicals) β-catenin (1:500; #610154, BD Biosciences) and CD3 (1:400; #ab5690 Abcam). Briefly, paraffin embedded sections were dewaxed with Xylene and hydrated in 100% and 70% ethanol. Antigen retrieval was performed using pressure cooker pretreatment in a Tris-EDTA buffer (pH 9.0). Slides were then incubated at 25°C in 3% hydrogen peroxidase for 15' to block endogenous peroxidase activity. Tissue sections were washed and blocked with 5% BSA in PBS-Tween for 1 hour to then be incubated with the primary antibody overnight at 4 °C. Slides were washed twice with PBS-Tween and incubated with Rabbit EnVision+ System-HRP (#K4011, Dako) or Mouse EnVision+ System-HRP (#K4007, Dako) for 30 min. Sections were counterstained with Mayer's Hematoxylin and dehydration was performed by incubation in 70% and 100% ethanol followed by Xylene, before slides were mounted using Pertex (#00811, Histolab). The quantification of $Ki67^+$ Paneth cells refers to the amount of crypts containing at least one Ki67+ Paneth cell was detected.

The quantification of $Olfm4^+$ cells is based on the average number of Olfm4-positive cells per crypt throughout the length of the small intestine. The quantification of $CD3^+$ cells is based on the average number of $CD3^+$ -positive cells infiltrating the intestinal epithelium per villus. For each quantification, at least 50 crypts or villi per mouse, and at least 3 experimental mice were employed.

Immunfluoresence (IF) and lineage tracing analysis

Paraffin embedded tissues were prepared as described for IHC up to the peroxidase blocking step. For cryo-sections, tissue samples were first dissected and washed with PBS, to then be fixed for 2 hours at 25°C with 4%

buffered formaldehyde solution (Klinipath). Tissues were cryo-protected in 30% sucrose (Sigma) overnight at 4°C, embedded in OCT (KP cryocompound, #1620-C, Klinipath), frozen on dry ice, and sectioned at −20°C. Tissues were cut in 4-8 µm thick sections. When applicable, sections were incubated in blocking buffer (5% milk powder in PBS-T) for 30 min. at 25°C, and stained with primary antibodies directed against the following proteins: Mki67 (1:100; #NB500-170, Novus biologicals), lysozyme (C19) (1:100; sc-27958, Santa Cruz), lysozyme EC 3.2.1.17 (1:1000; #A0099, Dako), OLFM4 (1:100; #39141, CST), Muc2 (H-300) (1:500; #sc-15334, Santa Cruz), chromogranin A (1:200; #NB120-15160, Novus Biologicals), and DCAMKL1 (1:200; #ab31704, Abcam) in blocking buffer overnight at 4°C. After washing in PBS-T, slides were incubated for 2 hours with the following secondary antibodies: Goat anti-Rabbit IgG (H+L) secondary Antibody, Alexa Fluor® 568 conjugate, (1:250; # A-11011, Life Technologies), Donkey anti-Rabbit IgG (H+L) secondary Antibody, Alexa Fluor® 568 conjugate (1:250; # A-21202, Life technologies) or Donkey anti-Goat secondary Antibody, Alexa Fluor® 633 conjugate (1:250; #A-21082, Life technologies). Tissues were counterstained with Alexa Fluor® 568 Phalloidin (1:100; #A12380, Invitrogen) or Alexa Fluor® 633 Phalloidin (1:100; #A22284, Invitrogen), and DAPI (#D8417, Sigma) for 30 min. at 25°C and washed in PBS-T. Tissues were mounted in VECTASHIELD HardSet Antifade Mounting Medium (#H-1400, Vector Labs) and imaged with a Zeiss LSM700 confocal microscope. Images were processed with ImageJ (U.S. National Institutes of Health, Bethesda, MD, USA).

Lineage tracing frequency of $Lys^{CreERT2}/R26^{LSL\text{-}YFP}$ was quantified by dividing the number of intestinal crypt/villus axes containing YFP^+ ribbons by YFP^+ crypts.

RNA *in-situ* hybridization (ISH)

Paraffin embedded tissues were prepared as described for IHC. SCF ISH analysis was performed by using the RNAscope kit (ACDbio) according to the manufacturer's instructions. Four µm formalin-fixed, paraffin-embedded tissue sections were pretreated with heat and protease before hybridization with a target probe to SCF mRNA (RNAscope® 2.5 VS Probe- Mm-Kitl (#423409, ACDbio)). An HRP-based signal amplification system was then applied followed by colorimetric development with DAB. Positive staining was identified as brown, punctate dots. Specificity of the SCF-RNA probes were tested by using PPIB (Cyclophilin B) and DapB gene (accession # EF191515) as positive and negative controls, respectively.

Organoid assays

To establish organoid cultures *ex vivo*, two distinct sources of cells were employed namely either whole crypts or single cell suspensions both from freshly resected mouse intestinal tissues. Whole crypts were extracted from the small intestine by incubating the minced tissues with 2 mM EDTA for 30 min. at 4°C. Crypts were then pelleted and passed through a 70 µm strainer. Whole crypt cultures were performed as previously described in standard ENR medium (Sato et al., 2009) supplemented, when indicated, with SCF (150ng/ml; #250-03, Peprotech), soluble c-kit receptor (500ng/ml; #1356-SR-050, R&D Systems), masitinib (200nM; #S1064, Selleckchem), rapamycin (10 nM; #13346, Cayman Chemicals), U0126 (1 µM; #70970-1; Cayman Chemicals), LY294002 (5 µM; #70920, Cayman Chemicals),and ruxolitinib (0.5 µM; #11609-1, Cayman Chemicals).

As for organoid reconstitution assays (ORA), isolated crypts were first digested to single cells after incubation with TrypLE (Life Technologies) and 2000 U/ml-1 Dnase (Sigma) for 10 min. at 37°C. Dissociated cells were passed through a 40 µm strainer, stained with an APC-conjugated CD24 antibody (clone M1/69 BioLegend), and, to exclude non-epithelial cells, with the following Ab's for 30 min. at 4°C: BV421-conjugated TER119 (#TER-119, Biolegend), CD31 (#390, Biolegend), CD45 (#30-F11, Biolegend). For Paneth cell analysis, an additional staining with a PE-conjugated CD117 antibody (#2B8, Biolegend) was also performed. Cells were then sorted by FACS (BD FACSAriaIII; BD Bioscience). Single viable epithelial cells were gated by CD24 and side scatter (SSC), and by negative selection against the above BV421-conjugated Ab's and with DAPI to discriminate live from dead cells. Detailed FACS gating strategy for the small intestine was performed as previously described (Roth et al., 2012). Reconstitution of *Lgr5*-EGFP^{hi} stem cells (purity >99%) with Paneth cells (CD24hiSSChi; purity >98%) was performed by pelleting sorted cells at 300 g. for 5 minutes in Eppendorf LoBind Tubes, and by co-incubating them for 15 min. at 25°C as previously described (Sato et al., 2011). In order to implement the reconstitution assay upon activation of sorted cells with SCF, Paneth or *Lgr5*-EGFP^{hi} cells were first incubated with 150 ng/ml of recombinant murine SCF for 30 min. at 37°C in DMEM F12 before reconstitution. In order to inactivate GSK3β, sorted Paneth and *Lgr5*$^{+}$ cells were incubated with standard reconstitution medium + 5 µM Chiron (CHIR99021, #4423, Tocris) for 4 days followed by incubation in standard ENR medium. In order to inhibit PI3K and AKT, sorted Paneth cells were incubated with specific chemical inhibitors NVP-BKM120 for PI3K (1 µM; #11587, Cayman Chemical) and AKT inhibitor VIII for AKT (4µM; #14870, Cayman Chemicals) for 30 min., centrifuged at 300g for 5 min., and then washed in 200 µl of Advanced DMEM F12.

Following these treatments, Paneth and *Lgr5*$^{+}$ stem cells were centrifuged at 300g for 5 minutes and subsequently reconstituted by resuspension in 30 µl Matrigel (BD Bioscience), and culture in 96 Well Flat

Bottom dishes (Corning). Alternatively, they were plated singularly where indicated. The composition of the culture medium was as previously described for whole crypts after supplementation with 10 µM Y-27632 (Sigma) and 1 mM Jagged-1 (AnaSpec). Brightfield pictures of organoids were taken using the Zeiss Primovert inverted microscope.

***Ex vivo* lineage tracing**

Lys^{CreERT2}/*R26*$^{LSL-YFP}$ were treated with Tamoxifen as described above to induce Cre recombination. Mice were then either left untreated or treated with 3% DSS in drinking water for 7days. 3 days after removal of DSS, intestinal crypts were isolated, single cell digested and YFP^{+} cells within the Paneth cell gates (CD24^{hi}SSC^{hi}) were sorted by FACS. YFP^{+} Paneth cells (n=4000) were then plated in 30 µl Matrigel in a single well of a glass bottom 96 well plate and maintained at 37˚C and 5% CO2. Culture medium (as described for the reconstitution assay) was changed every other day. For SCF treatments, YFP^{+} cells from control mice were either left untreated or treated with 150 ng/ml SCF for 30 min. before plating. Also in this case, culture medium (including 150 ng/ml SCF, for the SCF treated conditions) was replenished on a daily basis. At day 7, organoids were counterstained with 2µg/ml (Hoechst 34580) and imaged using a Zeiss CLSM510 Meta confocal microscope.

IF analysis of whole-mount intestinal crypts

Whole crypts were extracted from the small intestine by incubating the minced tissues with 2 mM EDTA for 30 min. at 4°C. Crypts were then pelleted and passed through a 70 µm strainer. Pelleted crypts were resuspended either in Advanced DMEM F12 or Advanced DMEM containing 50 ng/ml recombinant murine SCF ((#250-03, Peprotech), transferred to Eppendorf LoBind microcentrifuge tubes (#Z666505-100EA, Sigma) and incubated for 10 min. at 37°C. Subsequently, crypts were pelleted (300 g, 5 min. at 4°C) and fixed with 4% buffered formaldehyde solution (Klinipath) for 20 min. at 25°C. Crypts were washed twice with cold PBS and resuspended in block (5% milk powder in PBS-T) and incubated for 30 min. at 25°C. Afterwards, the crypts were stained with primary antibodies against the following proteins: phospho-GSK3β (Ser9) (1:100; #9323, CST), Gsk3β (D5C5Z) (1:100; #12456, CST), phospho-Akt (Ser473)(1:100; #9271, CST), panAkt (40d4) (1:100; #2920, CST), lysozyme (C19) (1:100; sc-27958, Santa Cruz), in blocking buffer overnight at 4°C. After washing in PBS-T, slides were incubated for 2 hours with the following secondary antibodies: goat anti-rabbit IgG (H+L) secondary antibody, Alexa Fluor® 568 conjugate (1:250, # A-11011, Life Technologies), donkey anti-rabbit IgG (H+L)

secondary antibody, Alexa Fluor® 568 conjugate (1:250, # A-21202, Life technologies) or donkey anti-goat secondary antibody, Alexa Fluor® 633 conjugate (1:250; #A-21082, Life technologies). Tissues were counterstained with Alexa Fluor® 568 Phalloidin (1:100; #A12380, Invitrogen) or Alexa Fluor® 633 Phalloidin (1:100; #A22284, Invitrogen) and DAPI (#D8417, Sigma) for 30 min. at 25°C and washed in PBS-T. Crypts were then resuspended in VECTASHIELD HardSet Antifade Mounting Medium (#H-1400, Vector Labs), transferred to glass slides and covered with a coverslip. Images were taken with a Zeiss LSM700 confocal microscope and processed with ImageJ (U.S. National Institutes of Health, Bethesda, MD, USA). The relative phospho-GSK3β intensity of Paneth cells was quantified by setting Paneth cells as region of interest (ROI) and measuring the average intensity of the phospho-GSK3β signal within the ROI. Paneth cells of at least 10 crypts per mouse per condition were analyzed.

Western blot analysis

Paneth and Lgr5-EGFP cells from C57BL/6J mice were extracted and FACS sorted as described for the organoid reconstitution assay. Sorted cells were incubated either in Advanced DMEM F12 medium or medium containing 50 ng/ml recombinant murine SCF (#250-03, Peprotech) for 30 min. at 25°C. Subsequently, cells were lysed in RIPA lysis buffer (50 mM TrisHCl pH 7.5, 150 mM NaCl, 0.5% TritonX, 10% Glycerol, 10% DTT, and 1x NuPAGE LDS Sample Buffer (Life Technologies, #NP0008)). Lysates were subjected to standard SDS-PAGE and western blotting procedures using primary antibodies directed against c-Kit (D13A2)(1:1000; #3074, CST), phospho-Akt (Ser473) (1:1000; #9271, CST), panAkt (40d4) (1:2000; #2920, CST), phospho-GSK3β (Ser9) (1:1000; #9323, CST), Gsk3β (D5C5Z) (1:1000; #12456, CST), GFP (1:500; #GTX26658, Genetex) and β-actin (D6A8) (1:1000; #8457, CST) and anti-Rabbit-HRP (1:1000, #A16066), anti-Mouse-HRP (1:1000,#A16096) secondary antibodies (Life Technologies) as well as HRP-Streptavidin Conjugate (1:1000; #43-4323, Invitrogen). Signal detection was performed by using the enhanced chemiluminescence system (ECL; Thermo Fisher Scientific, Schwerte, Germany) and the Molecular Imager® Gel Doc™ XR System (Bio-Rad). Protein bands were quantified using ImageJ (U.S. National Institutes of Health, Bethesda, MD, USA). Phospho-Akt and phospho-Gsk3β bands were normalized to the total Akt or Gsk3β bands, respectively, as well as to β-actin bands and fold values were calculated upon comparison with the negative background of the C57BL/6J lysates. As no significant differences between the fold inductions of both ways of normalization was detected we used the normalization of phospho vs total protein bands as result in our manuscript.

FACS quantification and analysis of *Lgr5*$^{+}$-, Paneth-, and YFP^{+} cells by

Intestinal crypts from untreated or DS- treated *Lgr5*$^{EGFP\text{-}IRES\text{-}creERT2}$ or tamoxifen-injected *Lys*^{CreERT2}/*R26*$^{LSL\text{-}YFP}$ mice were isolated, single cell digested, and subjected to FACS analysis. *Lgr5*$^{+}$ and Paneth (CD24^{hi}SSC^{hi}) cells were identified and quantified by using previously established gates (Roth et al., 2012). For control or DSS treated *Lys*^{CreERT2}/*R26*$^{LSL\text{-}YFP}$ mice, YFP^{+} and YFP^{-} cells were identified as in Fig. 4B, and the percentage of YFP^{+} and YFP^{-} cells within and outside the Paneth cell gate (CD24^{hi}SSC^{hi}) was quantified.

TOP/FOP reporter assay

For the β-catenin/TCF reporter assay (TOP-Flash assay), cells were plated on 24-well plates and, when 70% confluence was reached, transfected by Fugene HD (Roche) with 250 ng of the TOP-Flash or FOPFlash reporter constructs together with 25 ng of the Renilla luciferase vector for normalization purposes. SCF was added were indicated at 150ng/ml. Luciferase activity was measured by Dual–Luciferase Reporter Assay System (Promega) 48h post-transfection. Luminescence was measured using a Glomax Luminometer.

RNA isolation, RNA sequencing and quantitative real-time PCR

Paneth cells [CD24hiSSChi] and *Lgr5*+ stem/progenitor cells derived from *Lgr5*-EGFP mice were sorted as described for the organoid reconstitution assay from crypt preparations of the small intestine and RNA was isolated from cells using TRIzol^{TM} Reagent (15596018, ThermoFisher Scientific) according to the manufacturer's instructions. RNA quality and quantity was evaluated on a 2100 Bio-analyzer (Agilent) using the Agilent RNA 6000 Pico Kit (5067-1513, Agilent Technologies). For RNA sequencing analysis, RNA samples were further processed by GATC-Biotech (Konstanz, Germany) according to the INVIEW^{TM} Transcriptome Explore library preparation protocol (Illumina based).

RNA-seq data of Paneth cell samples (n = 7) was performed using UCSC mouse genome build mm10 (reference strain C57BL/6J) and GENCODE annotation release M15 (GRCm38.p5). FASTQC (v0.11.5)(Schmieder and Edwards, 2011) was applied on the single-end FASTQ files for quality control, both before and after running trimmomatic (v0.36) (Bolger et al., 2014), which removed TrueSeq adapter sequences. STAR (v2.5.3a)(Dobin et al., 2013) was used as aligner, with 2-pass mapping for each sample separately. Mapping quality plot was generated and checked based on sambamba Flagstat statistics(Tarasov et al., 2015). Count files, with the

number of reads for each gene were created with subread FeatureCounts (1.5.2)(Liao et al., 2014). R (version 3.4.3) was used for further calculating statistics and data visualizations. Differential expression analysis were performed with condition 'DSS treatment' (n = 4) versus 'Control' (n = 3) using the DESeq2 package (v1.18.1)(Love et al., 2014) and the Wald-test. P-values were adjusted using the Benjamini-Hochberg procedure. Heatmap visualization (Z-Scores averages per condition) was performed with the ggplot2 package (v2.1.0) on Regularized Log (from the DESeq2 package) transformed data and Z-Score were calculated with the base R 'scale' function (column scaling, followed by column centering). For quantitative RT-PCR purposes, RNA was converted into cDNA using the High Capacity RNA-to-cDNA kit (Applied Biosystems) and employed in a pre-amplification step using the Taqman®PreAmp Master Mix (Applied Biosystems) according to manufacturer's instructions. The linearity of the pre-amplification reaction was controlled for all primers. Assays were carried out as duplicate reactions using the 7500 Real Time system (Applied Biosystems). Finally, quantitative PCR was performed using inventoried TaqMan assays (Applied Biosystems) according to manufacturer's instructions. The *Actb* gene was employed as housekeeping gene. The assay number of the Taqman probes employed in this study for qRT-PCR purposes: Axin2 Mm00443610_m1, Actb Mm02619580_g1, Jun Mm00495062_s1, Ccnd1 Mm00432359_m1

The RNAseq data from this study have been submitted to the Gene Expression Omnibus (GEO) (Edgar et al., 2002) database under the accession number GSExxx.

References

Adolph, T.E., Tomczak, M.F., Niederreiter, L., Ko, H.J., Bock, J., Martinez-Naves, E., Glickman, J.N., Tschurtschenthaler, M., Hartwig, J., Hosomi, S*., et al.* (2013). Paneth cells as a site of origin for intestinal inflammation. Nature *503*, 272-276.

Andersson, E., Bergemalm, D., Kruse, R., Neumann, G., D'Amato, M., Repsilber, D., and Halfvarson, J. (2017). Subphenotypes of inflammatory bowel disease are characterized by specific serum protein profiles. PLoS One *12*, e0186142.

Barker, N., van Es, J.H., Kuipers, J., Kujala, P., van den Born, M., Cozijnsen, M., Haegebarth, A., Korving, J., Begthel, H., Peters, P.J*., et al.* (2007). Identification of stem cells in small intestine and colon by marker gene Lgr5. Nature *449*, 1003-1007.

Barnett, S.F., Defeo-Jones, D., Fu, S., Hancock, P.J., Haskell, K.M., Jones, R.E., Kahana, J.A., Kral, A.M., Leander, K., Lee, L.L*., et al.* (2005). Identification and characterization of pleckstrin-homology-domain-dependent and isoenzyme-specific Akt inhibitors. Biochem J *385*, 399-408.

Bolger, A.M., Lohse, M., and Usadel, B. (2014). Trimmomatic: a flexible trimmer for Illumina sequence data. Bioinformatics *30*, 2114-2120.

Broudy, V.C. (1997). Stem cell factor and hematopoiesis. Blood *90*, 1345-1364.

Buczacki, S.J., Zecchini, H.I., Nicholson, A.M., Russell, R., Vermeulen, L., Kemp, R., and Winton, D.J. (2013). Intestinal label-retaining cells are secretory precursors expressing Lgr5. Nature *495*, 65-69.

Clevers, H. (2016). Modeling Development and Disease with Organoids. Cell *165*, 1586-1597.

Clevers, H.C., and Bevins, C.L. (2013). Paneth cells: maestros of the small intestinal crypts. Annu Rev Physiol *75*, 289-311.

Comar, M., Secchiero, P., De Lorenzo, E., Martelossi, S., Tommasini, A., and Zauli, G. (2012). JCV+ Patients with Inflammatory bowel disease show elevated plasma levels of MIG and SCF. Inflamm Bowel Dis *18*, 1194-1196.

Cooper, H.S., Murthy, S.N., Shah, R.S., and Sedergran, D.J. (1993). Clinicopathologic study of dextran sulfate sodium experimental murine colitis. Lab Invest *69*, 238-249.

Dahlen, D.D., Lin, N.L., Liu, Y.C., and Broudy, V.C. (2001). Soluble Kit receptor blocks stem cell factor bioactivity in vitro. Leukemia research *25*, 413-421.

Davidson, L.A., Goldsby, J.S., Callaway, E.S., Shah, M.S., Barker, N., and Chapkin, R.S. (2012). Alteration of colonic stem cell gene signatures during the regenerative response to injury. Biochim Biophys Acta *1822*, 1600-1607.

Dobin, A., Davis, C.A., Schlesinger, F., Drenkow, J., Zaleski, C., Jha, S., Batut, P., Chaisson, M., and Gingeras, T.R. (2013). STAR: ultrafast universal RNA-seq aligner. Bioinformatics *29*, 15-21.

Doble, B.W., and Woodgett, J.R. (2003). GSK-3: tricks of the trade for a multi-tasking kinase. Journal of cell science *116*, 1175-1186.

Dubreuil, P., Letard, S., Ciufolini, M., Gros, L., Humbert, M., Casteran, N., Borge, L., Hajem, B., Lermet, A., Sippl, W*., et al.* (2009). Masitinib (AB1010), a potent and selective tyrosine kinase inhibitor targeting KIT. PLoS One *4*, e7258.

Durand, A., Donahue, B., Peignon, G., Letourneur, F., Cagnard, N., Slomianny, C., Perret, C., Shroyer, N.F., and Romagnolo, B. (2012). Functional intestinal stem cells after Paneth cell ablation induced by the loss of transcription factor Math1 (Atoh1). Proc Natl Acad Sci U S A *109*, 8965-8970.

Edgar, R., Domrachev, M., and Lash, A.E. (2002). Gene Expression Omnibus: NCBI gene expression and hybridization array data repository. Nucleic acids research *30*, 207-210.

Elsheikh, W., Flannigan, K.L., McKnight, W., Ferraz, J.G., and Wallace, J.L. (2012). Dextran sulfate sodium induces pan-gastroenteritis in rodents: implications for studies of colitis. J Physiol Pharmacol *63*, 463-469.

Fatrai, S., van Schelven, S.J., Ubink, I., Govaert, K.M., Raats, D., Koster, J., Verheem, A., Borel Rinkes, I.H., and Kranenburg, O. (2015). Maintenance of Clonogenic KIT(+) Human Colon Tumor Cells Requires Secretion of Stem Cell Factor by Differentiated Tumor Cells. Gastroenterology *149*, 692-704.

Fordham, R.P., Yui, S., Hannan, N.R., Soendergaard, C., Madgwick, A., Schweiger, P.J., Nielsen, O.H., Vallier, L., Pedersen, R.A., Nakamura, T.*, et al.* (2013). Transplantation of expanded fetal intestinal progenitors contributes to colon regeneration after injury. Cell Stem Cell *13*, 734-744.

Fuchs, E. (2009). The tortoise and the hair: slow-cycling cells in the stem cell race. Cell *137*, 811-819.

Garabedian, E.M., Roberts, L.J., McNevin, M.S., and Gordon, J.I. (1997). Examining the role of Paneth cells in the small intestine by lineage ablation in transgenic mice. J Biol Chem *272*, 23729-23740.

Gaspar, C., and Fodde, R. (2004). APC dosage effects in tumorigenesis and stem cell differentiation. Int J Dev Biol *48*, 377-386.

Geiser, J., Venken, K.J., De Lisle, R.C., and Andrews, G.K. (2012). A mouse model of acrodermatitis enteropathica: loss of intestine zinc transporter ZIP4 (Slc39a4) disrupts the stem cell niche and intestine integrity. PLoS Genet *8*, e1002766.

Grun, D., Muraro, M.J., Boisset, J.C., Wiebrands, K., Lyubimova, A., Dharmadhikari, G., van den Born, M., van Es, J., Jansen, E., Clevers, H.*, et al.* (2016). De Novo Prediction of Stem Cell Identity using Single-Cell Transcriptome Data. Cell Stem Cell *19*, 266-277.

Itzkowitz, S.H., and Yio, X. (2004). Inflammation and cancer IV. Colorectal cancer in inflammatory bowel disease: the role of inflammation. Am J Physiol Gastrointest Liver Physiol *287*, G7-17.

Jeon, S., Kim, N.H., Kim, J.Y., and Lee, A.Y. (2009). Stem cell factor induces ERM proteins phosphorylation through PI3K activation to mediate melanocyte proliferation and migration. Pigment Cell Melanoma Res *22*, 77-85.

Jia, Q., Lupton, J.R., Smith, R., Weeks, B.R., Callaway, E., Davidson, L.A., Kim, W., Fan, Y.Y., Yang, P., Newman, R.A.*, et al.* (2008). Reduced colitis-associated colon cancer in Fat-1 (n-3 fatty acid desaturase) transgenic mice. Cancer Res *68*, 3985-3991.

Kielman, M.F., Rindapaa, M., Gaspar, C., van Poppel, N., Breukel, C., van Leeuwen, S., Taketo, M.M., Roberts, S., Smits, R., and Fodde, R. (2002). Apc modulates embryonic stem-cell differentiation by controlling the dosage of beta-catenin signaling. Nature genetics *32*, 594-605.

Klimpel, G.R., Chopra, A.K., Langley, K.E., Wypych, J., Annable, C.A., Kaiserlian, D., Ernst, P.B., and Peterson, J.W. (1995). A role for stem cell factor and c-kit in the murine intestinal tract secretory response to cholera toxin. J Exp Med *182*, 1931-1942.

Klimpel, G.R., Langley, K.E., Wypych, J., Abrams, J.S., Chopra, A.K., and Niesel, D.W. (1996). A role for stem cell factor (SCF): c-kit interaction(s) in the intestinal tract response to Salmonella typhimurium infection. J Exp Med *184*, 271-276.

Lennartsson, J., and Ronnstrand, L. (2012). Stem cell factor receptor/c-Kit: from basic science to clinical implications. Physiol Rev *92*, 1619-1649.

Lewin, K. (1968). Neoplastic Paneth cells. J Clin Pathol *21*, 476-479.

Li, N., Yousefi, M., Nakauka-Ddamba, A., Jain, R., Tobias, J., Epstein, J.A., Jensen, S.T., and Lengner, C.J. (2014). Single-cell analysis of proxy reporter allele-marked epithelial cells establishes intestinal stem cell hierarchy. Stem Cell Reports *3*, 876-891.

Liao, Y., Smyth, G.K., and Shi, W. (2014). featureCounts: an efficient general purpose program for assigning sequence reads to genomic features. Bioinformatics *30*, 923-930.

Love, M.I., Huber, W., and Anders, S. (2014). Moderated estimation of fold change and dispersion for RNA-seq data with DESeq2. Genome Biol *15*, 550.

M'Koma, A.E. (2013). Inflammatory bowel disease: an expanding global health problem. Clin Med Insights Gastroenterol *6*, 33-47.

Metcalfe, D.D., Baram, D., and Mekori, Y.A. (1997). Mast cells. Physiol Rev *77*, 1033-1079.

Miettinen, M., and Lasota, J. (2005). KIT (CD117): a review on expression in normal and neoplastic tissues, and mutations and their clinicopathologic correlation. Appl Immunohistochem Mol Morphol *13*, 205-220.

Montgomery, R.K., Carlone, D.L., Richmond, C.A., Farilla, L., Kranendonk, M.E., Henderson, D.E., Baffour-Awuah, N.Y., Ambruzs, D.M., Fogli, L.K., Algra, S.*, et al.* (2011). Mouse telomerase reverse transcriptase (mTert) expression marks slowly cycling intestinal stem cells. Proc Natl Acad Sci U S A *108*, 179-184.

Munoz, J., Stange, D.E., Schepers, A.G., van de Wetering, M., Koo, B.K., Itzkovitz, S., Volckmann, R., Kung, K.S., Koster, J., Radulescu, S.*, et al.* (2012). The Lgr5 intestinal stem cell signature: robust expression of proposed quiescent '+4' cell markers. Embo J *31*, 3079-3091.

Mustata, R.C., Vasile, G., Fernandez-Vallone, V., Strollo, S., Lefort, A., Libert, F., Monteyne, D., Perez-Morga, D., Vassart, G., and Garcia, M.I. (2013). Identification of Lgr5-independent spheroid-generating progenitors of the mouse fetal intestinal epithelium. Cell reports *5*, 421-432.

Na, Y.J., Baek, H.S., Ahn, S.M., Shin, H.J., Chang, I.S., and Hwang, J.S. (2007). [4-t-butylphenyl]-N-(4-imidazol-1-yl phenyl)sulfonamide (ISCK03) inhibits SCF/c-kit signaling in 501mel human melanoma cells and abolishes melanin production in mice and brownish guinea pigs. Biochemical pharmacology *74*, 780-786.

Orford, K.W., and Scadden, D.T. (2008). Deconstructing stem cell self-renewal: genetic insights into cell-cycle regulation. Nat Rev Genet *9*, 115-128.

Parry, L., Young, M., El Marjou, F., and Clarke, A.R. (2013). Evidence for a crucial role of paneth cells in mediating the intestinal response to injury. Stem Cells *31*, 776-785.

Paterson, J.C., and Watson, S.H. (1961). Paneth cell metaplasia in ulcerative colitis. Am J Pathol *38*, 243-249.

Potten, C.S. (1998). Stem cells in gastrointestinal epithelium: numbers, characteristics and death. Philos Trans R Soc Lond B Biol Sci *353*, 821-830.

Ray, P., Krishnamoorthy, N., Oriss, T.B., and Ray, A. (2010). Signaling of c-kit in dendritic cells influences adaptive immunity. Ann N Y Acad Sci *1183*, 104-122.

Rosen, J.M., and Jordan, C.T. (2009). The increasing complexity of the cancer stem cell paradigm. Science *324*, 1670-1673.

Roth, S., and Fodde, R. (2011). Quiescent stem cells in intestinal homeostasis and cancer. Cell Commun Adhes *18*, 33-44.

Roth, S., Franken, P., Sacchetti, A., Kremer, A., Anderson, K., Sansom, O., and Fodde, R. (2012). Paneth cells in intestinal homeostasis and tissue injury. PLoS One *7*, e38965.

Rothenberg, M.E., Nusse, Y., Kalisky, T., Lee, J.J., Dalerba, P., Scheeren, F., Lobo, N., Kulkarni, S., Sim, S., Qian, D.*, et al.* (2012). Identification of a cKit(+) colonic crypt base secretory cell that supports Lgr5(+) stem cells in mice. Gastroenterology *142*, 1195-1205 e1196.

Sangiorgi, E., and Capecchi, M.R. (2008). Bmi1 is expressed in vivo in intestinal stem cells. Nat Genet *40*, 915-920.

Sasaki, N., Sachs, N., Wiebrands, K., Ellenbroek, S.I., Fumagalli, A., Lyubimova, A., Begthel, H., van den Born, M., van Es, J.H., Karthaus, W.R.*, et al.* (2016). Reg4+ deep crypt secretory cells function as epithelial niche for Lgr5+ stem cells in colon. Proc Natl Acad Sci U S A *113*, E5399-5407.

Sato, T., van Es, J.H., Snippert, H.J., Stange, D.E., Vries, R.G., van den Born, M., Barker, N., Shroyer, N.F., van de Wetering, M., and Clevers, H. (2011). Paneth cells constitute the niche for Lgr5 stem cells in intestinal crypts. Nature *469*, 415-418.

Sato, T., Vries, R.G., Snippert, H.J., van de Wetering, M., Barker, N., Stange, D.E., van Es, J.H., Abo, A., Kujala, P., Peters, P.J.*, et al.* (2009). Single Lgr5 stem cells build crypt-villus structures in vitro without a mesenchymal niche. Nature *459*, 262-265.

Schewe, M., and Fodde, R. (2018). Multitasking Paneth cells in the intestinal stem cell niche. In Advances in Stem Cells and their Niches, D. Bonnet, ed. (Elsevier), pp. 41-75.

Schewe, M., Franken, P.F., Sacchetti, A., Schmitt, M., Joosten, R., Bottcher, R., van Royen, M.E., Jeammet, L., Payre, C., Scott, P.M.*, et al.* (2016). Secreted Phospholipases A2 Are Intestinal Stem Cell Niche Factors with Distinct Roles in Homeostasis, Inflammation, and Cancer. Cell Stem Cell *19*, 38-51.

Schewe, M., Sacchetti, A., Schmitt, M., and Fodde, R. (2017). The Organoid Reconstitution Assay (ORA) for the Functional Analysis of Intestinal Stem and Niche Cells. J Vis Exp.

Schmieder, R., and Edwards, R. (2011). Quality control and preprocessing of metagenomic datasets. Bioinformatics *27*, 863-864.

Stelzner, M., Helmrath, M., Dunn, J.C., Henning, S.J., Houchen, C.W., Kuo, C., Lynch, J., Li, L., Magness, S.T., Martin, M.G.*, et al.* (2012). A nomenclature for intestinal in vitro cultures. Am J Physiol Gastrointest Liver Physiol *302*, G1359-1363.

Tarasov, A., Vilella, A.J., Cuppen, E., Nijman, I.J., and Prins, P. (2015). Sambamba: fast processing of NGS alignment formats. Bioinformatics *31*, 2032-2034.

Tetteh, P.W., Basak, O., Farin, H.F., Wiebrands, K., Kretzschmar, K., Begthel, H., van den Born, M., Korving, J., de Sauvage, F., van Es, J.H.*, et al.* (2016). Replacement of Lost Lgr5-Positive Stem Cells through Plasticity of Their Enterocyte-Lineage Daughters. Cell Stem Cell *18*, 203-213.

Tian, H., Biehs, B., Warming, S., Leong, K.G., Rangell, L., Klein, O.D., and de Sauvage, F.J. (2011). A reserve stem cell population in small intestine renders Lgr5-positive cells dispensable. Nature *478*, 255-259.

Vajravelu, B.N., Hong, K.U., Al-Maqtari, T., Cao, P., Keith, M.C., Wysoczynski, M., Zhao, J., Moore, J.B.t., and Bolli, R. (2015). C-Kit Promotes Growth and Migration of Human Cardiac Progenitor Cells via the PI3K-AKT and MEK-ERK Pathways. PLoS One *10*, e0140798.

van der Flier, L.G., Haegebarth, A., Stange, D.E., van de Wetering, M., and Clevers, H. (2009a). OLFM4 is a robust marker for stem cells in human intestine and marks a subset of colorectal cancer cells. Gastroenterology *137*, 15-17.

van der Flier, L.G., van Gijn, M.E., Hatzis, P., Kujala, P., Haegebarth, A., Stange, D.E., Begthel, H., van den Born, M., Guryev, V., Oving, I.*, et al.* (2009b). Transcription factor achaete scute-like 2 controls intestinal stem cell fate. Cell *136*, 903-912.

van Es, J.H., Jay, P., Gregorieff, A., van Gijn, M.E., Jonkheer, S., Hatzis, P., Thiele, A., van den Born, M., Begthel, H., Brabletz, T.*, et al.* (2005). Wnt signalling induces maturation of Paneth cells in intestinal crypts. Nat Cell Biol *7*, 381-386.

van Es, J.H., Sato, T., van de Wetering, M., Lyubimova, A., Yee Nee, A.N., Gregorieff, A., Sasaki, N., Zeinstra, L., van den Born, M., Korving, J.*, et al.* (2012). Dll1+ secretory progenitor cells revert to stem cells upon crypt damage. Nat Cell Biol *14*, 1099-1104.

Vowinkel, T., Kalogeris, T.J., Mori, M., Krieglstein, C.F., and Granger, D.N. (2004). Impact of dextran sulfate sodium load on the severity of inflammation in experimental colitis. Dig Dis Sci *49*, 556-564.

Wada, R. (2009). Proposal of a new hypothesis on the development of colorectal epithelial neoplasia: nonspecific inflammation--colorectal Paneth cell metaplasia--colorectal epithelial neoplasia. Digestion *79 Suppl 1*, 9-12.

Wada, R., Miwa, H., Abe, H., Santo, R.M., Kitamura, S., Kuwabara, N., Suda, K., Kondo, K., Yamada, S., Hamada, T.*, et al.* (1992). Incidence of Paneth cells in minute tubular adenomas and adenocarcinomas of the large bowel. Acta Pathol Jpn *42*, 579-584.

Wada, R., Yamaguchi, T., and Tadokoro, K. (2005). Colonic Paneth cell metaplasia is pre-neoplastic condition of colonic cancer or not? J Carcinog *4*, 5.

Wen, P.Y., Lee, E.Q., Reardon, D.A., Ligon, K.L., and Alfred Yung, W.K. (2012). Current clinical development of PI3K pathway inhibitors in glioblastoma. Neuro Oncol *14*, 819-829.

Yan, K.S., Chia, L.A., Li, X., Ootani, A., Su, J., Lee, J.Y., Su, N., Luo, Y., Heilshorn, S.C., Amieva, M.R.*, et al.* (2012). The intestinal stem cell markers Bmi1 and Lgr5 identify two functionally distinct populations. Proc Natl Acad Sci U S A *109*, 466-471.

Yasuda, A., Sawai, H., Takahashi, H., Ochi, N., Matsuo, Y., Funahashi, H., Sato, M., Okada, Y., Takeyama, H., and Manabe, T. (2007). Stem cell factor/c-kit receptor signaling enhances the proliferation and invasion of colorectal cancer cells through the PI3K/Akt pathway. Dig Dis Sci *52*, 2292-2300.

Yousefi, M., Li, L., and Lengner, C.J. (2017). Hierarchy and Plasticity in the Intestinal Stem Cell Compartment. Trends Cell Biol *27*, 753-764.

Figure Legends

Figure 1. SCF expression is increased upon intestinal inflammation and positively affects organoid growth.

A) Comparison by IHC analysis of SCF expression in healthy (left) and CD-derived small intestinal tissues (right). The arrowheads indicate SCF expressing cells close to the intestinal crypts. The images are representative of 2 healthy and 4 CD patients; scale bars = 100 μm.

B) SCF ISH analysis of small intestinal tissues derived from control (upper panel) and DSS-treated (lower panel) mice 1 day after DSS removal. Increased SCF RNA levels can be observed in the intestinal epithelium and submucosa of inflamed mice. Pictures show representative examples of n= 3 mice; (scale bar: upper panel = 200 μm, lower panel = 50 μm, grid lines indicate intestinal crypts).

C) Weight loss graphs relative to mice treated with 3% DSS alone, ISCK03 alone (0.1 mg/ml in the drinking water), and 3% DSS + ISCK03 for 7 days (n=6 for DSS and DSS + ISCK03 treated mice; n=3 for ISCK03 treated mice).

D) DAI score relative to the mice described in B (*p< 0.05). Details of scoring are shown in Figure S1D and in the Materials and Methods section.

E) Organoid multiplicities from whole crypts of control and 3% DSS-treated mice (7 days). Crypts were isolated and plated 3 days after DSS withdrawal. Pictures show representative organoids of each condition at day 5 of culture (scale bar = 50 μm; $**p < 0.01$, n=4).

F) Organoid multiplicities from whole crypts of control and 3% DSS-treated mice (7 days). Crypts were plated 3 days after DSS withdrawal in the presence or absence of the soluble c-Kit receptor (500 ng/ml) or masitinib (200 nM)($**p < 0.01$, n=3).

G) Organoid multiplicities from whole crypts grown in control medium with or without murine SCF (50 ng/ml). Pictures show representative organoids of each condition at day 5 of culture (scale bar = 50 μm; $**p < 0.01$, n=3).

Figure 2. DSS-induced intestinal inflammation causes loss of intestinal stem cells.

A) FACS analysis of *Lgr5*$^{+}$ cells from control or DSS-treated mice 3 days after DSS withdrawal (FACS plot are representatives of 5 independent experiments; *Lgr5*-EGFP^{high} cells are labelled in green).

B) Average percentage of *Lgr5*$^{+}$ and Paneth cells in control and DSS-treated mice, as quantified by FACS ($**p$ <0.01, n.s.= not significant; n=5).

C) Confocal microscopy images of small intestinal tissues from Tamoxifen-treated *Lgr5*$^{EGFP\text{-}IRES\text{-}creERT2}$/*R26*$^{LSL\text{-}RFP}$ mice kept on normal or 3% DSS-supplemented drinking water for 7 days. Tissues were harvested 3 days after withdrawal of DSS.

D) Quantification of lineage tracings events in control and DSS-treated *Lgr5*$^{EGFP\text{-}IRES\text{-}creERT2}$/*R26*$^{LSL\text{-}RFP}$ mice (n=3,*p <0.05).

E) Olfm4 IHC analysis of intestinal tissues from control and DSS-treated mice 1 day after removal of DSS.

F) Quantification of Olfm4^{+} cells/crypt from control and DSS-treated mice (n=4, *p <0.05).

Figure 3. Inflammation induces proliferation and *de novo* organoid formation from Paneth cells via activation of the SCF/c-Kit signaling axis.

A) Ki67 IHC analysis of mouse small intestinal tissues from control and DSS-treated mice 1 day after DSS removal. Asterisks indicate Ki67-negative Paneth cells in control mice (left panels) and Ki67^{+} Paneth cells in DSS-treated mice (right panel)(scale bar upper panels = 25 µm; lower panel = zoom in).

B) Average percentage of Ki67^{+} Paneth cells in control and DSS treated mice (**p <0.01; n= 4).

C) Organoid reconstitution assay of *Lgr5*$^{+}$ and Paneth cells from control and DSS-treated mice (*p <0.05; **p<0.01; n.s.= not significant; n=3).

D) Pictures showing representative examples of organoids derived from the reconstitution assays in (C) at day 7 of culture (scale bar = 100µm).

E) Organoid reconstitution assay of untreated and SCF-treated (50 ng/ml) *Lgr5*$^{+}$ and Paneth cells (**p < 0.01; ***p <0.005; n.s.= not significant; n=3).

F) Left panel: organoids derived from Paneth cells of Tamoxifen-injected and DSS-treated *Lys*^{CreERT2}/*R26*$^{LSL\text{-}YFP}$ mice. Right panel: organoids derived from SCF-treated Paneth cells of Tamoxifen-injected *Lys*^{CreERT2}/*R26*$^{LSL\text{-}YFP}$ mice.

Figure 4. Paneth cells de-differentiate into stem-like cells in response to DSS induced inflammation.

A) Lineage tracing analysis of Tamoxifen-injected *Lys*^{CreERT2}/*R26*$^{LSL\text{-}YFP}$ mice at several time points after DSS treatment (scale bar = 100 µm).

B) Ki67 expression analysis of *Lys*^{CreERT2}/*R26*$^{LSL\text{-}YFP}$ mice, 1 day after DSS withdrawal (scale bar = 25µm).

C) Analysis of lysozyme expression in *Lys*^{CreERT2}/*R26*$^{LSL\text{-}YFP}$ mice, 7 days after DSS withdrawal (scale bar = 25µm).

D) Analysis of Olfm4 expression $Lys^{CreERT2}/R26^{LSL\text{-}YFP}$ mice, 7 days after DSS withdrawal (scale bar = 25µm).

E) Analysis of expression of differentiation markers (Goblet cells = Muc2; entero-endocrine cells = ChrA; Tuft cells = DCLK1) in $Lys^{CreERT2}/R26^{LSL\text{-}YFP}$ mice, 7 days after DSS withdrawal (scale bar = 100µm).

Figure 5. SCF triggers Paneth cell de-differentiation via the PI3K/AKT-signaling axis.

A) IF analysis of phospho-Akt in untreated and SCF-treated (50 ng/ml) intestinal crypts from *Lgr5*-EGFP mice (arrows indicate phospho-Akt^+ Paneth cells; scale bar = 25µm). Intestinal crypts were counterstained with DAPI and phalloidin. Picture shows one representative example from at least 3 independent experiments.

B) Western blot analysis of untreated and SCF- (50 ng/ml) treated $Lgr5^+$ and Paneth cells using antibodies against c-Kit, phospho-Akt, total-Akt, GFP and actin.

C) Quantification of pAkt/Akt signal intensity from the western blot in (B)(*p<0.05; n=3).

D) Organoid reconstitution assay of $Lgr5^+$ and Paneth cells from control and DSS-treated mice. Paneth cells were either left untreated or treated with BKM120 (PI3K inhibitor; 1µM), or AKTVIII (Akt-inhibitor; 4 µM) (*p < 0.05; **p <0.01; n.s.= not significant; n=3).

E) Representative pictures of PC-derived organoids as described in (D)(scale bar = 50 µm).

F) RNAseq analysis of Paneth cells from control (=3) and DSS-treated (n=4) mice 3 days after DSS withdrawal. Heat maps show differentially expressed genes (left panel = Wnt target genes: middle panel = lysozymes and alpha-defensins; right panel = cell proliferation marker genes). Color codes indicate average Z-scores of each condition.

Figure 6. Activation of the SCF/c-Kit signaling axis inhibits Gsk3β and activates Wnt in Paneth cells.

A) IF analysis of phospho-GSK3β in untreated and SCF-treated intestinal crypts from *Lgr5*-EGFP mice. Arrows indicate phospho-GSK3β-negative Paneth cells in untreated crypts (upper panel). Among SCF treated crypts (lower panel), phospho-GSK3β Paneth cells become evident (also indicated by arrows; scale bar = 25µm). Intestinal crypts were counterstained with DAPI and phalloidin. Picture shows one representative example out of at least 3 independent experiments.

B) Relative fluorescence intensity of phospho-GSK3β in Paneth cells treated as described in (B). Paneth cells were set as ROI (region of interest) for the measurement of phospho-GSK3β intensity (*p <0.05; n=3).

C) Western blot analysis of untreated and SCF- (50 ng/ml) treated *Lgr5*$^{+}$ and Paneth cells using antibodies directed against c-Kit, phospho-GSK3β, total-GSK3β, GFP and actin.

D) Quantification of phospho-GSK3β/GSK3β signal intensity in the western blot shown in (C)(**p* <0.05; n=3).

E) TOP-Flash luciferase reporter assay of control and SCF- (50 ng/ml) treated CaCo2 cells (**p* <0.05; n=3).

F) qRT-PCR analysis of control and SCF- (50 ng/ml) treated Paneth cells using primer sets specific for the Wnt target genes Axin2, c-Jun, and Cyclin D1 (***p* <0.01; n = 3).

G) β-Catenin IHC analysis of intestinal tissues from control and 3% DSS- treated (7 days) mice 1 day after DSS withdrawal (arrows indicate Paneth cells with cytoplasmic β-Catenin; scale bar = 25 μm). Pictures show representative examples of crypts from 3 independent mouse experiments.

H) Number of organoids derived from control or Chiron- (10 μM) treated *Lgr5*$^{+}$ or Paneth cells sorted by FACS (****p* <0.005).

I) Representative pictures of organoids derived from control and Chiron- (10 μM) treated *Lgr5*$^{+}$ or Paneth cells sorted by FACS. Left panel: untreated cells did not give rise to organoids. Middle panel: Chiron-treated Lgr5^{+} and Paneth cells generate enterospheres. Right panel: upon Chiron withdrawal enterospheres give rise to differentiated enteroids.

Figure 7. SCF/c-Kit signaling inhibition counteracts DSS-induced Wnt activation and Paneth cells de-differentiation.

A) β-Catenin immunohistochemistry analysis of intestinal tissues from control and DSS, ISCK03 or DSS + ISCK03 treated mice 1 day after stop of treatment (arrows indicate Paneth cells with cytoplasmic β-Catenin; scale bar = 25 μm). Pictures show representative examples of crypts from 3 independent mice.

B) Ki67 immunohistochemistry analysis of intestinal tissues from control and DSS, ISCK03 or DSS + ISCK03 treated mice 1 day after stop of treatment (arrows indicate Ki67 expressing Paneth cells; scale bar = 25 μm). Pictures show representative examples of crypts from 3 independent mice.

C) Quantification of the percentage of crypts with Ki67^{+} Paneth cells in intestinal tissues of control, DSS and DSS + ISCK03 treated mice (**p* < 0.05; ****p* <0.005; n=3).

D) Lineage tracing analysis of Tamoxifen injected Lyz-Cre-R26-LSL-YFP mice (left= control; middle= DSS; right = DSS + ISCK03). Tissues were harvested and analyzed 7 days after removal of DSS (scale bar = 100 μm).

E) Quantification of Paneth cell lineage tracing events of mice described in D (n=4; **p* < 0.05).

Fig. 1

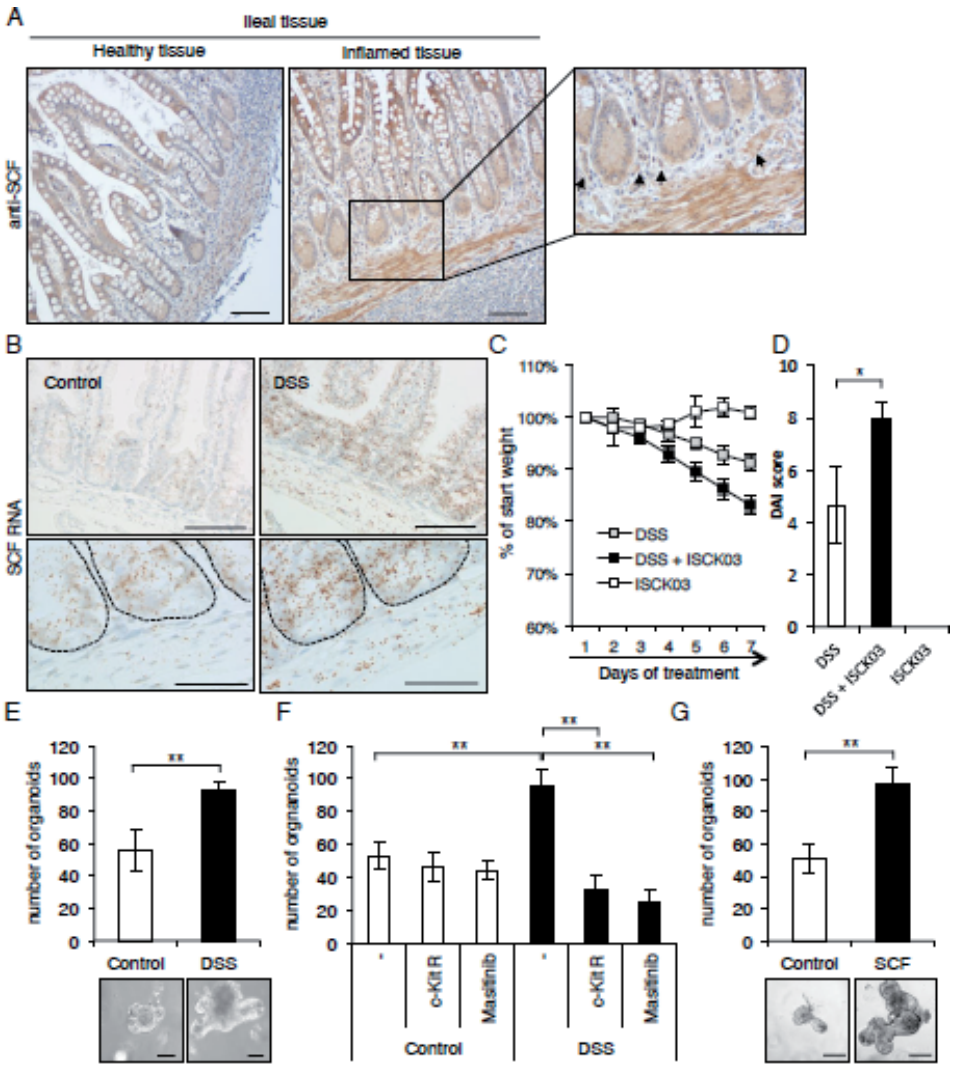
A
Ileal tissue
Healthy tissue
Inflamed tissue
anti-SCF
B
Control
DSS
SCF RNA
C
% of start weight
DSS
DSS + ISCK03
ISCK03
Days of treatment
D
DAI score
DSS
DSS + ISCK03
ISCK03
E
number of organoids
Control
DSS
F
number of organoids
-
c-Kit R
Masitinib
Control
DSS
G
number of organoids
Control
SCF

Fig. 2

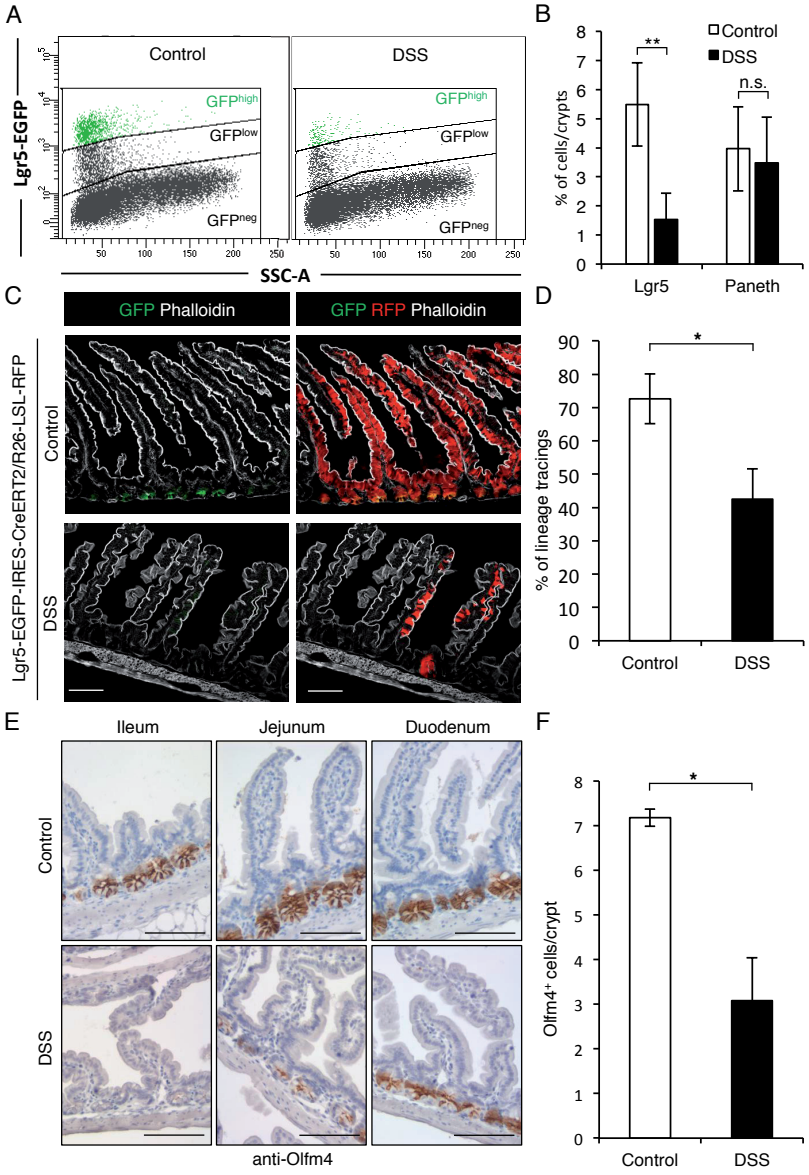
A
Control
DSS
Lgr5-EGFP
GFPhigh
GFPlow
GFPneg
SSC-A
B
Control
DSS
% of cells/crypts
**
n.s.
Lgr5
Paneth
C
GFP Phalloidin
GFP RFP Phalloidin
Lgr5-EGFP-IRES-CreERT2/R26-LSL-RFP
Control
DSS
D
% of lineage tracings
*
Control
DSS
E
Ileum
Jejunum
Duodenum
Control
DSS
anti-Olfm4
F
Olfm4+ cells/crypt
*
Control
DSS

Fig. 3

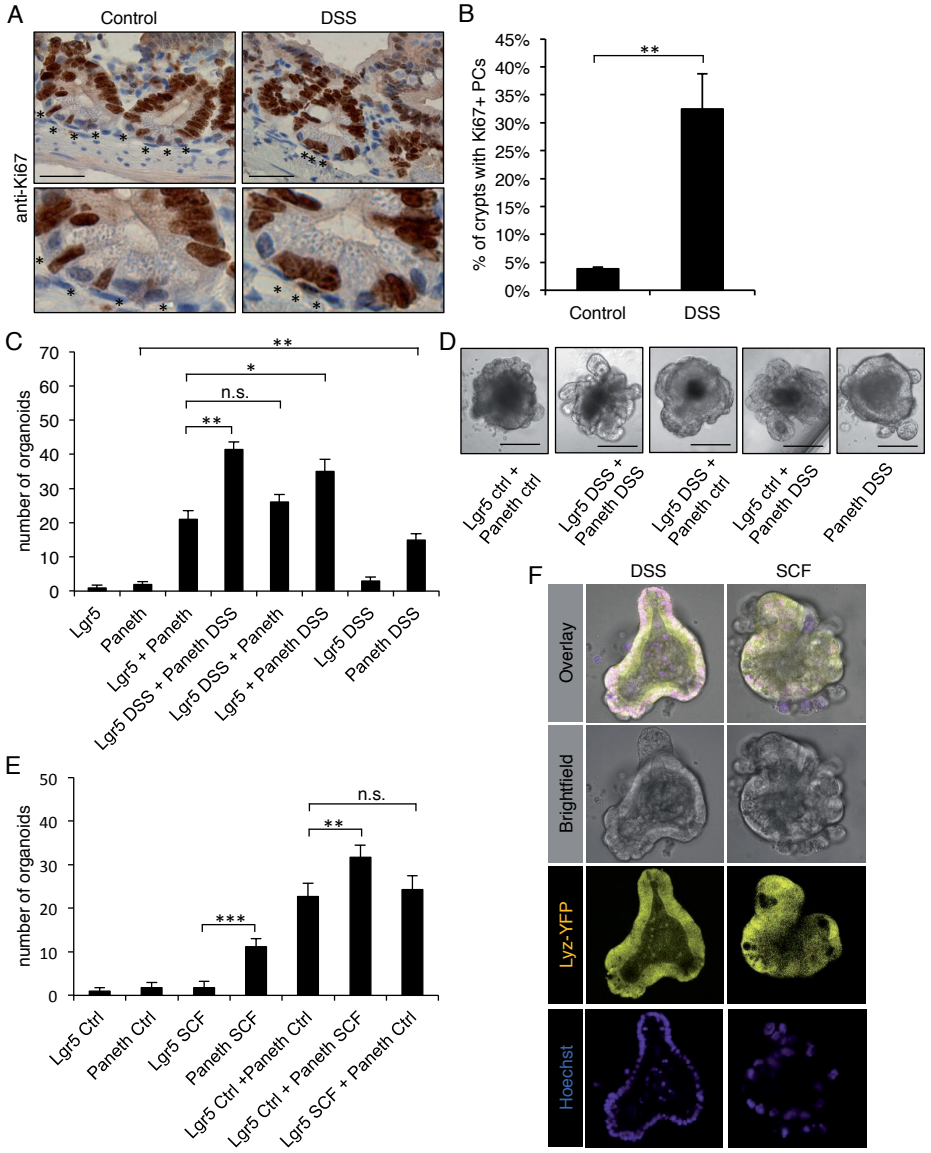
A
Control
DSS
anti-Ki67
B
% of crypts with Ki67+ PCs
45%
40%
35%
30%
25%
20%
15%
10%
5%
0%
**
Control
DSS
C
number of organoids
70
60
50
40
30
20
10
0
**
*
n.s.
**
Lgr5
Paneth
Lgr5 + Paneth
Lgr5 DSS + Paneth DSS
Lgr5 DSS + Paneth
Lgr5 + Paneth DSS
Lgr5 DSS
Paneth DSS
D
Lgr5 ctrl + Paneth ctrl
Lgr5 DSS + Paneth DSS
Lgr5 DSS + Paneth ctrl
Lgr5 ctrl + Paneth DSS
Paneth DSS
E
number of organoids
50
40
30
20
10
0
n.s.
**
***
Lgr5 Ctrl
Paneth Ctrl
Lgr5 SCF
Paneth SCF
Lgr5 Ctrl +Paneth Ctrl
Lgr5 Ctrl + Paneth SCF
Lgr5 SCF + Paneth Ctrl
F
DSS
SCF
Overlay
Brightfield
Lyz-YFP
Hoechst

Fig. 4

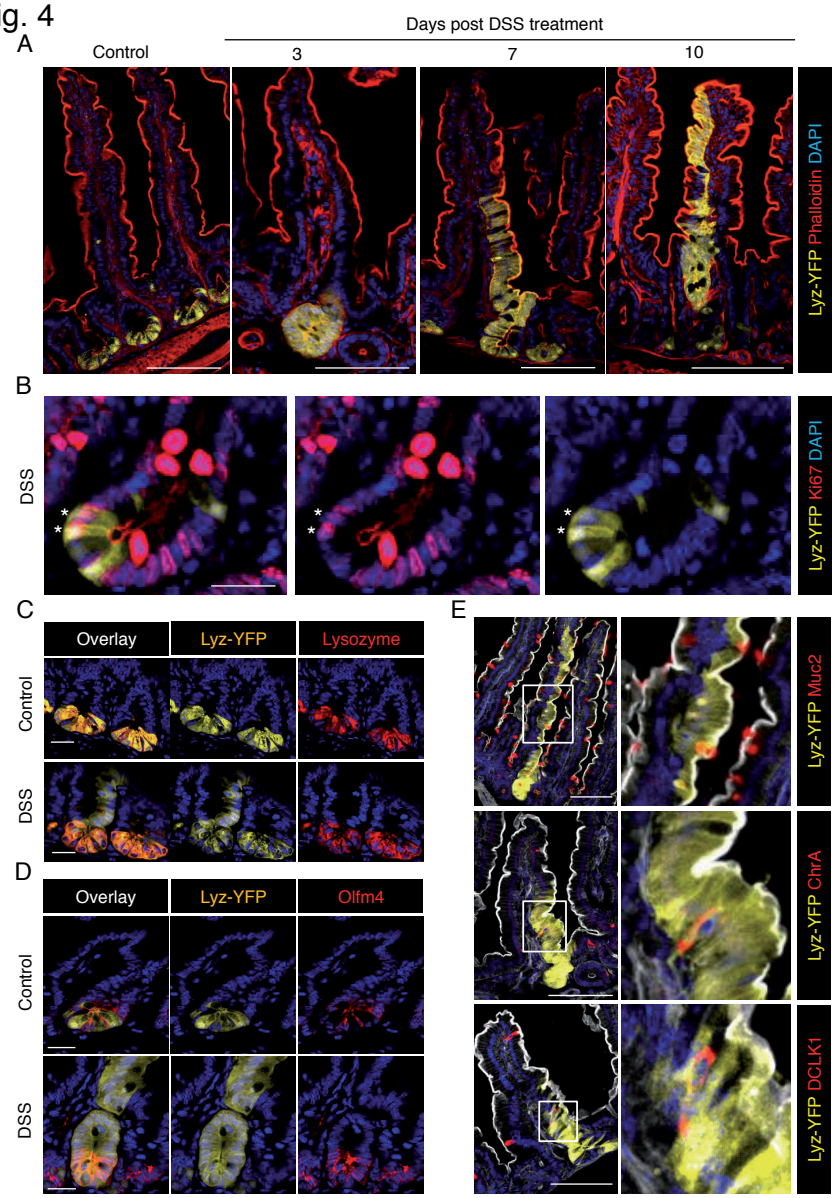
A
Days post DSS treatment
Control
3
7
10
Lyz-YFP Phalloidin DAPI
B
DSS
Lyz-YFP Ki67 DAPI
C
Overlay
Lyz-YFP
Lysozyme
Control
DSS
D
Overlay
Lyz-YFP
Olfm4
Control
DSS
E
Lyz-YFP Muc2
Lyz-YFP ChrA
Lyz-YFP DCLK1

Fig. 5

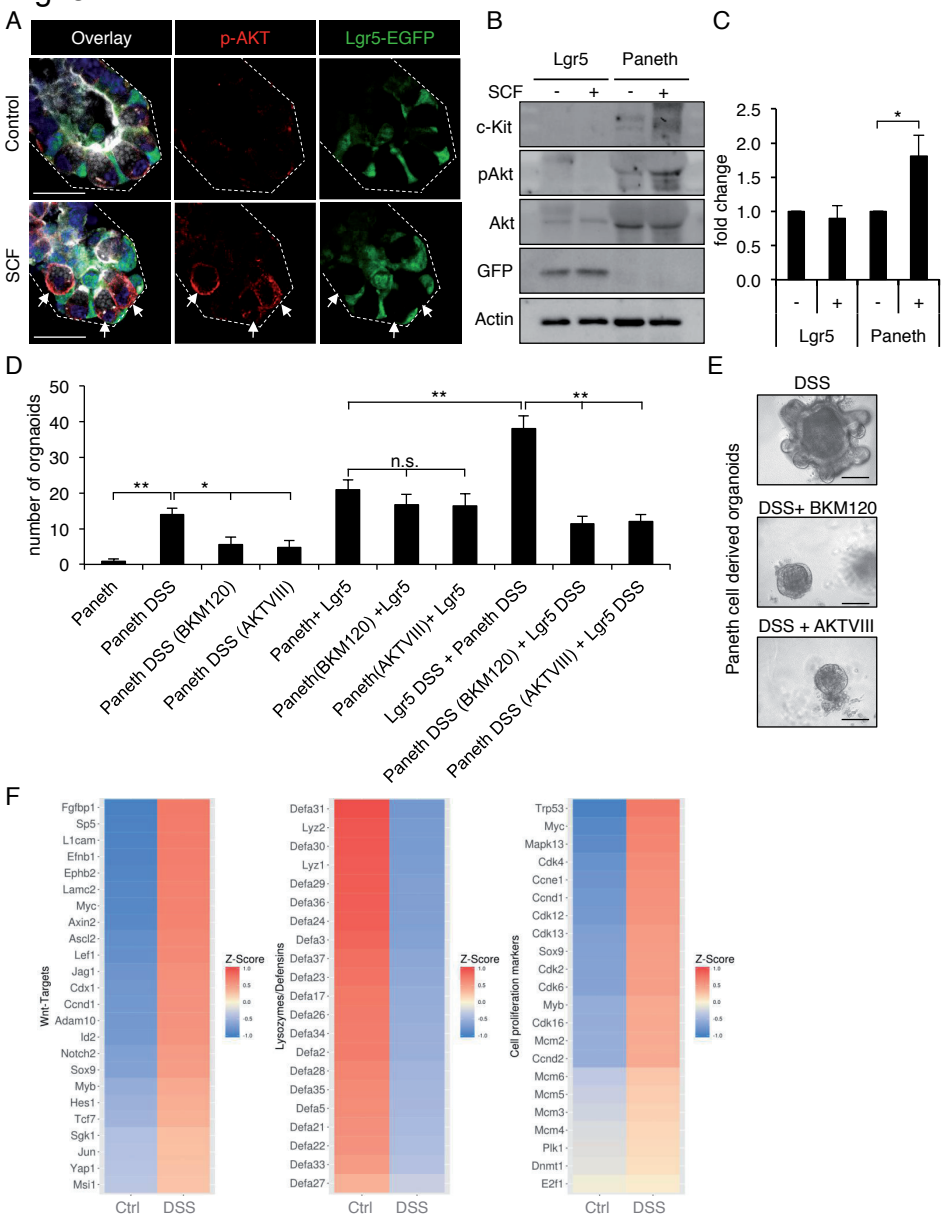
A
Overlay
p-AKT
Lgr5-EGFP
Control
SCF
B
Lgr5
Paneth
SCF
- + - +
c-Kit
pAkt
Akt
GFP
Actin
C
fold change
2.5
2.0
1.5
1.0
0.5
0.0
*
- + - +
Lgr5
Paneth
D
number of orgnaoids
50
40
30
20
10
0
**
*
n.s.
**
**
Paneth
Paneth DSS
Paneth DSS (BKM120)
Paneth DSS (AKTVIII)
Paneth+ Lgr5
Paneth(BKM120) +Lgr5
Paneth(AKTVIII)+ Lgr5
Lgr5 DSS + Paneth DSS
Paneth DSS (BKM120) + Lgr5 DSS
Paneth DSS (AKTVIII) + Lgr5 DSS
E
Paneth cell derived organoids
DSS
DSS+ BKM120
DSS + AKTVIII
F
Wnt-Targets
Fgfbp1
Sp5
L1cam
Efnb1
Ephb2
Lamc2
Myc
Axin2
Ascl2
Lef1
Jag1
Cdx1
Ccnd1
Adam10
Id2
Notch2
Sox9
Myb
Hes1
Tcf7
Sgk1
Jun
Yap1
Msi1
Ctrl
DSS
Z-Score
Lysozymes/Defensins
Defa31
Lyz2
Defa30
Lyz1
Defa29
Defa36
Defa24
Defa3
Defa37
Defa23
Defa17
Defa26
Defa34
Defa2
Defa28
Defa35
Defa5
Defa21
Defa22
Defa33
Defa27
Ctrl
DSS
Z-Score
Cell proliferation markers
Trp53
Myc
Mapk13
Cdk4
Ccne1
Ccnd1
Cdk12
Cdk13
Sox9
Cdk2
Cdk6
Myb
Cdk16
Mcm2
Ccnd2
Mcm6
Mcm5
Mcm3
Mcm4
Plk1
Dnmt1
E2f1
Ctrl
DSS
Z-Score

Fig. 6

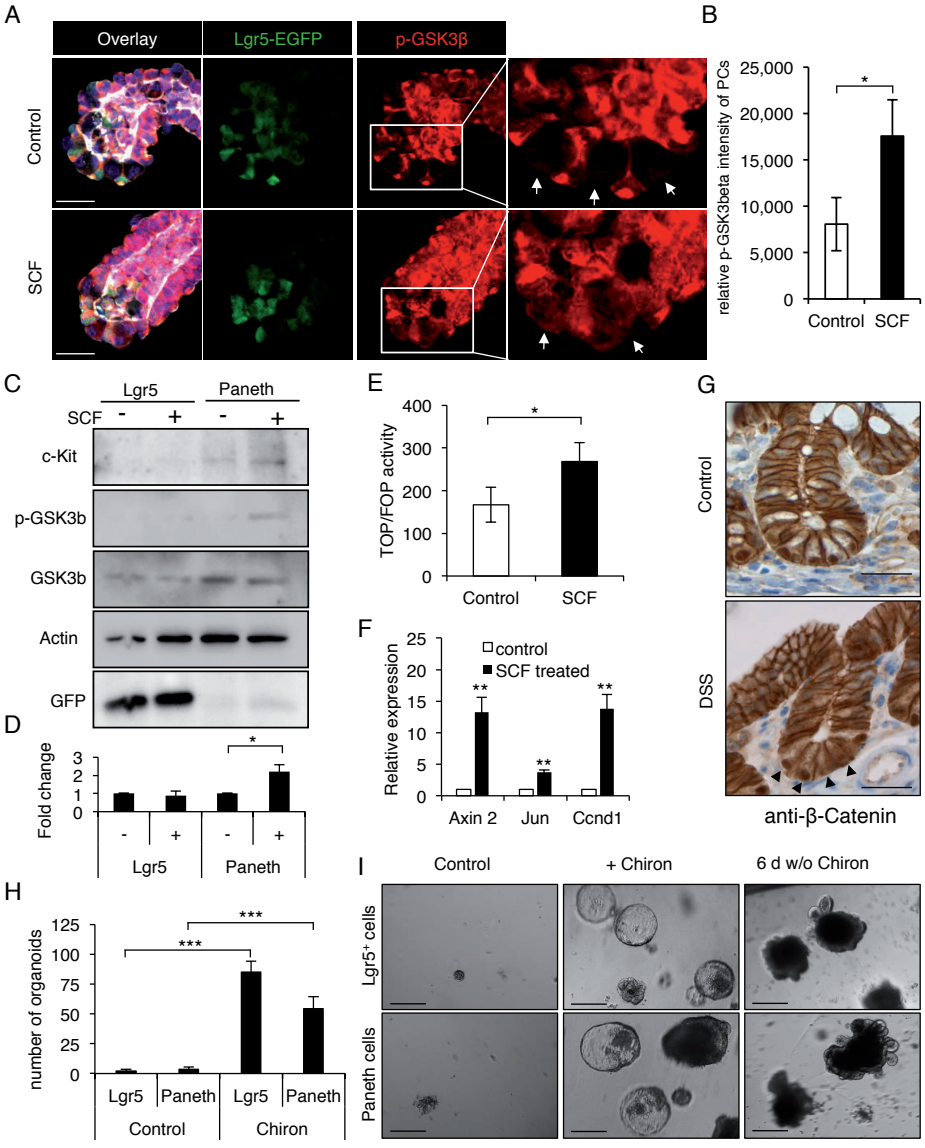
A
Overlay
Lgr5-EGFP
p-GSK3β
Control
SCF
B
relative p-GSK3beta intensity of PCs
25,000
20,000
15,000
10,000
5,000
0
*
Control
SCF
C
Lgr5
Paneth
SCF - + - +
c-Kit
p-GSK3b
GSK3b
Actin
GFP
D
Fold change
3
2
1
0
*
- + - +
Lgr5
Paneth
E
TOP/FOP activity
400
300
200
100
0
*
Control
SCF
F
Relative expression
25
20
15
10
5
0
control
SCF treated
**
**
**
Axin 2
Jun
Ccnd1
G
Control
DSS
anti-β-Catenin
H
number of organoids
125
100
75
50
25
0
***
***
Lgr5
Paneth
Lgr5
Paneth
Control
Chiron
I
Control
+ Chiron
6 d w/o Chiron
Lgr5+ cells
Paneth cells

Fig. 7

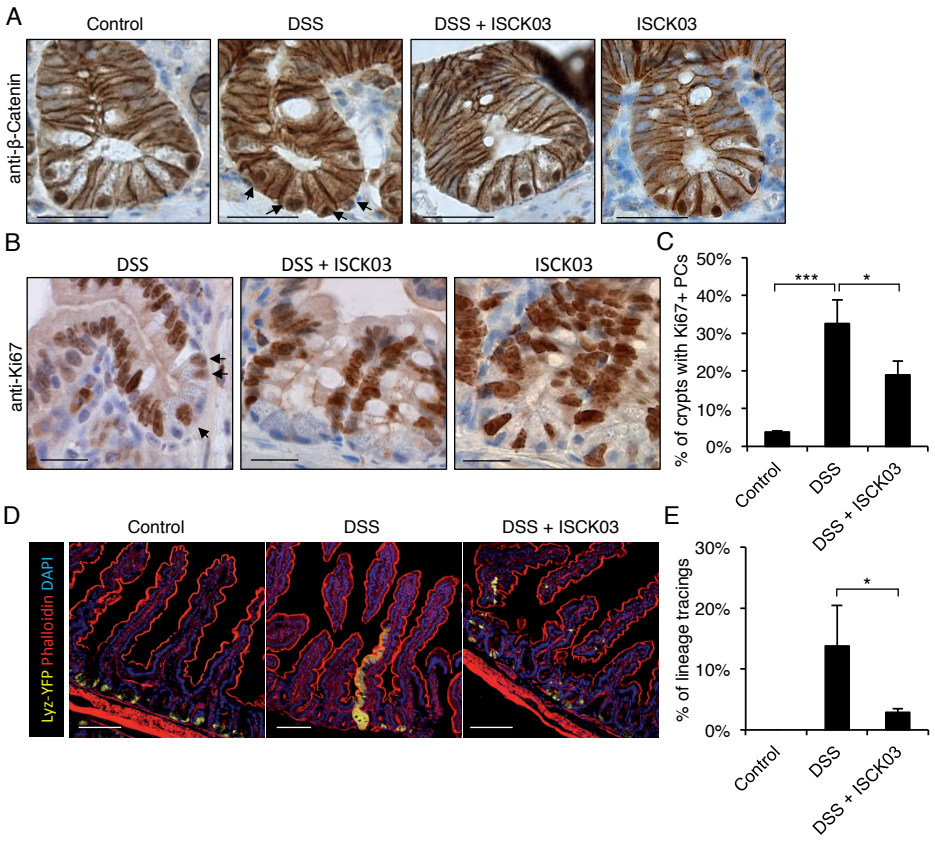
A
Control
DSS
DSS + ISCK03
ISCK03
anti-β-Catenin
B
DSS
DSS + ISCK03
ISCK03
anti-Ki67
C
% of crypts with Ki67+ PCs
50%
40%
30%
20%
10%
0%
***
*
Control
DSS
DSS + ISCK03
D
Control
DSS
DSS + ISCK03
Lyz-YFP Phalloidin DAPI
E
% of lineage tracings
30%
20%
10%
0%
*
Control
DSS
DSS + ISCK03

Supplementary Figure Legends

Supplementary Figure 1

A) SCF IHC analysis of normal and ulcerative colitis colonic tissues. Picture shows a representative example of 2 controls and 5 UC patients (scale bars = 100 µm).

B) Lysozyme IF analysis of colonic tissues from UC patients. Picture shows a representative example of metaplastic Paneth cells in the colon were found in 3 out of 5 patients (scale bar = 100µm).

C) SCF RNA ISH analysis of small intestinal tissues derived from control (left) and DSS-treated mice (right) 1 day after DSS removal. SCF expression is increased in the intestinal epithelium and submucosa of inflamed mice. PPIB RNA probes were used as positive controls. Pictures show representative examples of n= 3 mice; scale bar = 200µm).

D) Table of DAI scores and the individual parameters relative to mice treated for 7 days with DSS or DSS + ISCK. Mice were sacrificed one day after treatment withdrawal. Mice treated with ISCK03 alone (n=3) did show normal stool consistency, no blood loss, normal appearance and no weight loss and were not included in the table.

E) CD3 IHC analysis of intestinal tissues derived from control and DSS-, ISCK03-, and DSS/ISCK03-treated mice. Tissues were collected 1 day after treatment withdrawal. Asterisks indicate infiltrating $CD3^+$ T-lymphocytes (scale bar = 50 µm).

F) Quantification of infiltrating $CD3^+$ T-lymphocytes/villus in control and DSS-, ISCK03-, and DSS/ISCK03-treated mice, as described in A (*p< 0.05; n.s. = not significant; n=3).

Supplementary Figure 2

A) FACS analysis of *Lgr5*$^+$ ($EGFP^+$) and Paneth cells ($C24^{high}SSC^{high}$) in control and DSS-treated mice, 3 days after DSS withdrawal (FACS plots are representrative of 5 independent experiments; cells within the PC gate are labelled in red; *Lgr5*-$EGFP^+$ cells, as defined in Fig. 2A, are labelled in green).

B) Confocal microscopy images of small intestinal tissues from Tamoxifen-treated *Lgr5*$^{EGFP\text{-}IRES\text{-}creERT2}$/*R26*$^{LSL\text{-}RFP}$ mice on normal drinking water or 3% DSS. Tissues were harvested 3 days after DSS withdrawal. The relatively low magnification provides an overview of *Lgr5* lineage tracing events in small intestinal tissues (scale bar = 200 µm).

C) Olfm4 IHC analysis of intestinal tissues from control and DSS-treated mice, 1 day after DSS removal. Picture shows an overview of Olfm4 expression in small intestinal tissues (scale bar = 250 µm).

Supplementary Figure 3

A) Ki67/lysozyme IF analysis of small intestinal tissues from untreated (upper panel) or DSS-treated mice (lower panel). Tissues were harvested 1 day after DSS treatment (arrow indicates a Ki67/lysozyme double positive cell; scale bar = 25 µm).

B) Ki67/lysozyme IF analysis of small intestinal tissues from a CD patient (arrow indicates a Ki67/lysozyme double positive cell; scale bar = 25 µm).

Supplementary Figure 4

A) FACS analysis of Paneth cells and YFP^+ cells of Tamoxifen-injected $Lys^{CreERT2}/R26^{LSL\text{-}YFP}$ mice. Upper left plot: Paneth cells selection with the $CD24^{high}SSC^{high}$ gate on total live/Lin- cells. Red- and green-labelled cells within the highlighted $CD24^{high}SSC^{high}$ gate are Paneth (YFP^-) and YFP^+ cells, respectively. These two subgroups of $CD24^{high}SSC^{high}$ cells can be resolved by Lyz-YFP/SSC-A analysis (upper right plot). Lower left and right plots: YFP^+ cells from the live/Lin- bulk entirely fall within the Paneth cell gate ($CD24^{high}SSC^{high}$).

B) Quantification of the FACS analysis in (B). Approximately 12% of Paneth cells are labeled by YFP upon Tamoxifen administration. 97% of YFP^+ cells were detected within the Paneth cell gate (n=5).

C) IF analysis of YFP expression in $Lys^{CreERT2}/R26^{LSL\text{-}YFP}$ mice injected with 10% ethanol in sunflower oil (control, upper panel) or Tamoxifen (lower panel) (scale bar = 200µm).

D) Confocal microscopy analysis of Tamoxifen injected $Lys^{CreERT2}/R26^{LSL\text{-}YFP}$ mice using antibodies against lysozyme. The mice were treated for 7 days with 3% DSS and analyzed at day 1 after DSS withdrawal. Paneth cells are only detected at the base of the crypt. YFP expression could be only detected in $lysozyme^+$ Paneth cells (scale bar = 100µm).

Supplementary Figure 5

A) Number of organoids derived from control and SCF-treated (150 ng/ml) whole intestinal crypts. Crypts were plated in the presence or absence of inhibitors against Mapk (U-0126, 1 µM), mTor (Rapamycin 10 nM), PI3K (LY294002, 0.5 µM), and Jak1 (Ruxolitinib, 0.5µM)(**$p< 0.01$, n=3).

B) Pan-Akt IF analysis of intestinal crypts from *Lgr5*-EGFP mice (scale bar = 25µm). The images show one representative example from 3 independent experiments.

C) Phospho-Akt IF and lysozyme analysis of control and SCF-treated intestinal crypts from *Lgr5*-EGFP mice (arrows indicate phospho-Akt/lysozyme double positive cells; scale bar = 25µm). The images depict one representative example from 3 independent experiments.

D) RNAseq analysis of Paneth cells from control (n=3) and DSS-treated (n=4) mice, 3 days after DSS withdrawal. The heat map shows differentially expression of stem cell related genes. Color codes indicate average Z-scores of each condition.

Supplementary Figure 6

A) Pan-GSK3β IF analysis of intestinal crypts from *Lgr5*-EGFP mice (scale bar = 25µm). The images are relative to one representative example from 3 independent experiments.

Supplementary Figure 7

A) Ki67/lysozyme IF analysis of small intestinal tissues from control (left panel), DSS- (middle left panel), DSS/ISCK03- (middle right panel), and ISCK03-treated mice (right panel). Tissues were harvested 1 day after DSS treatment (arrows indicates a Ki67/lysozyme double positive cell; scale bar = 25 µm).

Supplementary Fig.1 (related to Fig. 1)

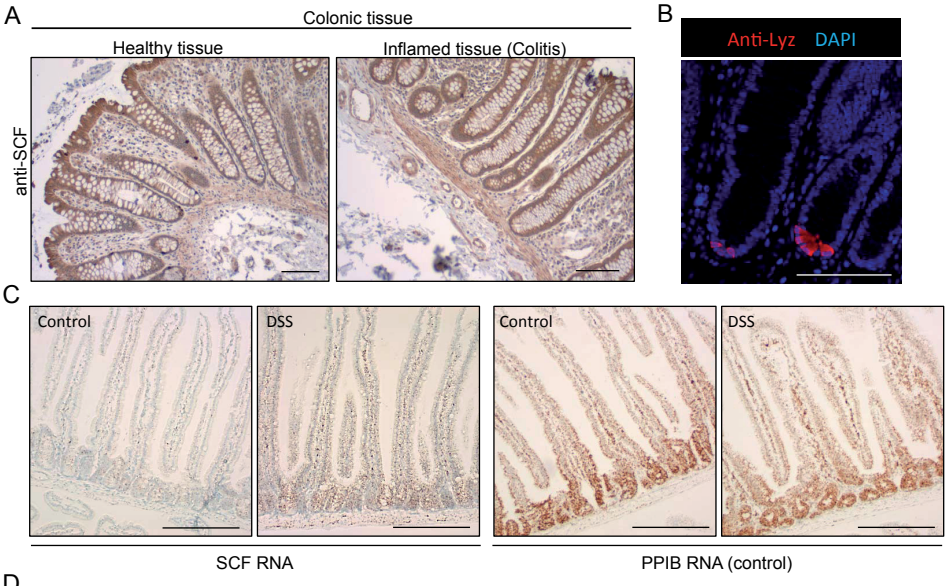

D

Mouse ID	Genotype	Treatment	Stool consistency (0-2)	Blood loss (0-1)	Appearance (0-3)	Weight loss (0-3)	DAI score
1	C57BL/6J	DSS	Diarrhea (2)	Gross bleeding (1)	Starey coat (2)	10,18% (2)	7
2	C57BL/6J	DSS	Loose (1)	No blood (0)	hunched (1)	10,75% (2)	4
3	C57BL/6J	DSS	Loose (1)	Gross bleeding (1)	hunched (1)	7,5% (1)	4
4	C57BL/6J	DSS	Loose (1)	No blood (0)	hunched (1)	9% (1)	3
5	C57BL/6J	DSS	Loose (1)	No blood (0)	Starey coat (2)	7,27% (1)	4
6	C57BL/6J	DSS	Diarrhea (2)	Gross bleeding (1)	Hunched (1)	10% (2)	6
7	C57BL/6J	DSS+ISCK03	Diarrhea (2)	Gross bleeding (1)	Lethargic (3)	20,3% (3)	9
8	C57BL/6J	DSS+ISCK03	Diarrhea (2)	Gross bleeding (1)	Starey coat (2)	22,5% (3)	8
9	C57BL/6J	DSS+ISCK03	Diarrhea (2)	Gross bleeding (1)	Lethargic (3)	16,73% (2)	8
10	C57BL/6J	DSS+ISCK03	Diarrhea (2)	Gross bleeding (1)	Starey coat (2)	16,96% (2)	7
11	C57BL/6J	DSS+ISCK03	Diarrhea (2)	Gross bleeding (1)	Lethargic (3)	19,91% (2)	8
12	C57BL/6J	DSS+ISCK03	Diarrhea (2)	Gross bleeding (1)	Lethargic (3)	19,52% (2)	8

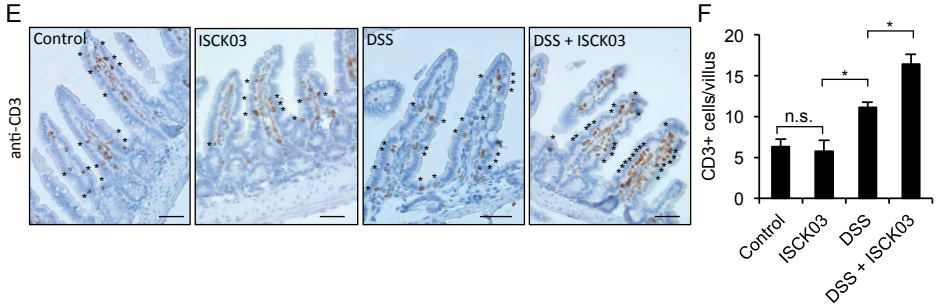

Supplementary Fig. 2 (related to Fig. 2)

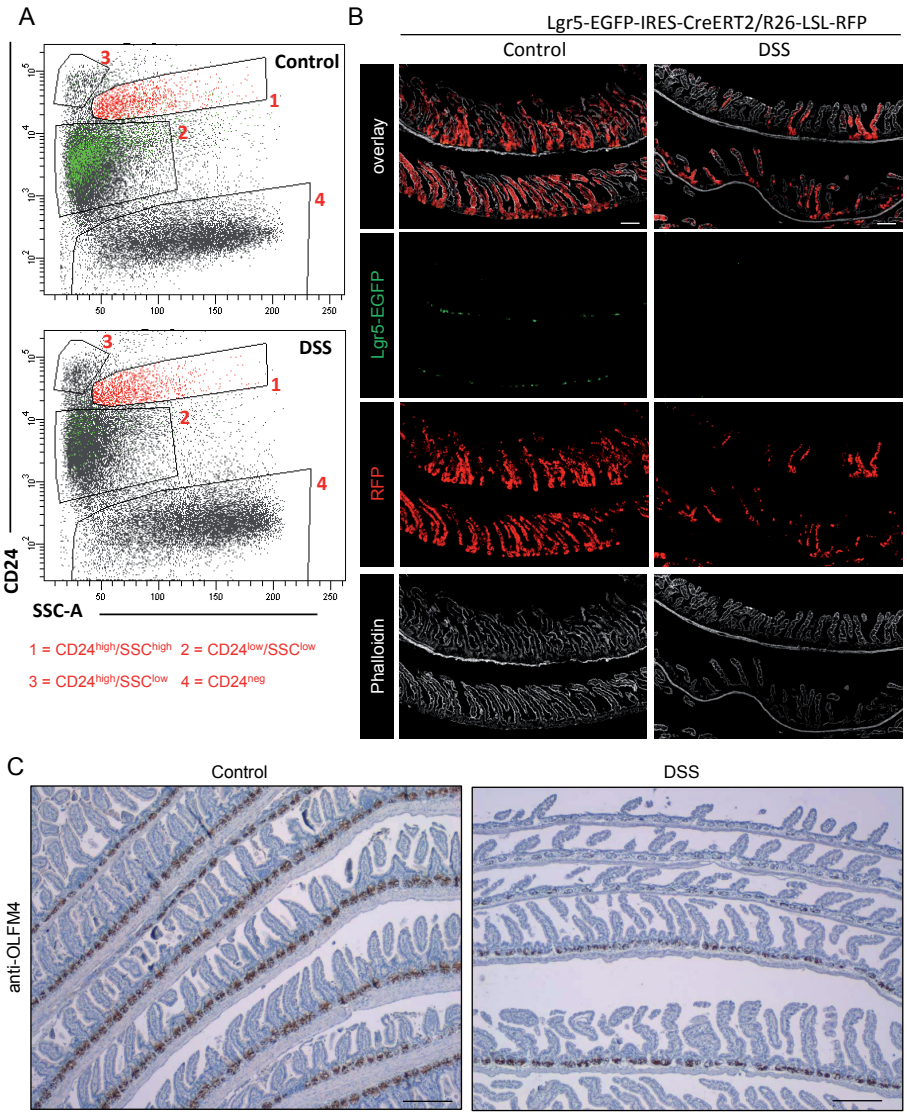

Supplementary Fig. 3 (related to Fig. 3)

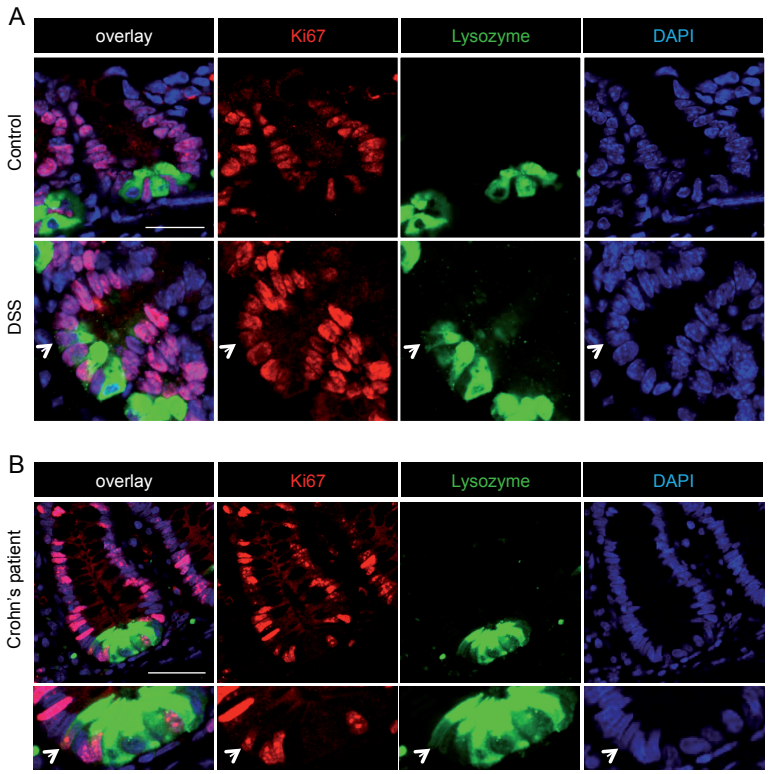

Supplementary Fig. 4 (related to Fig. 4)

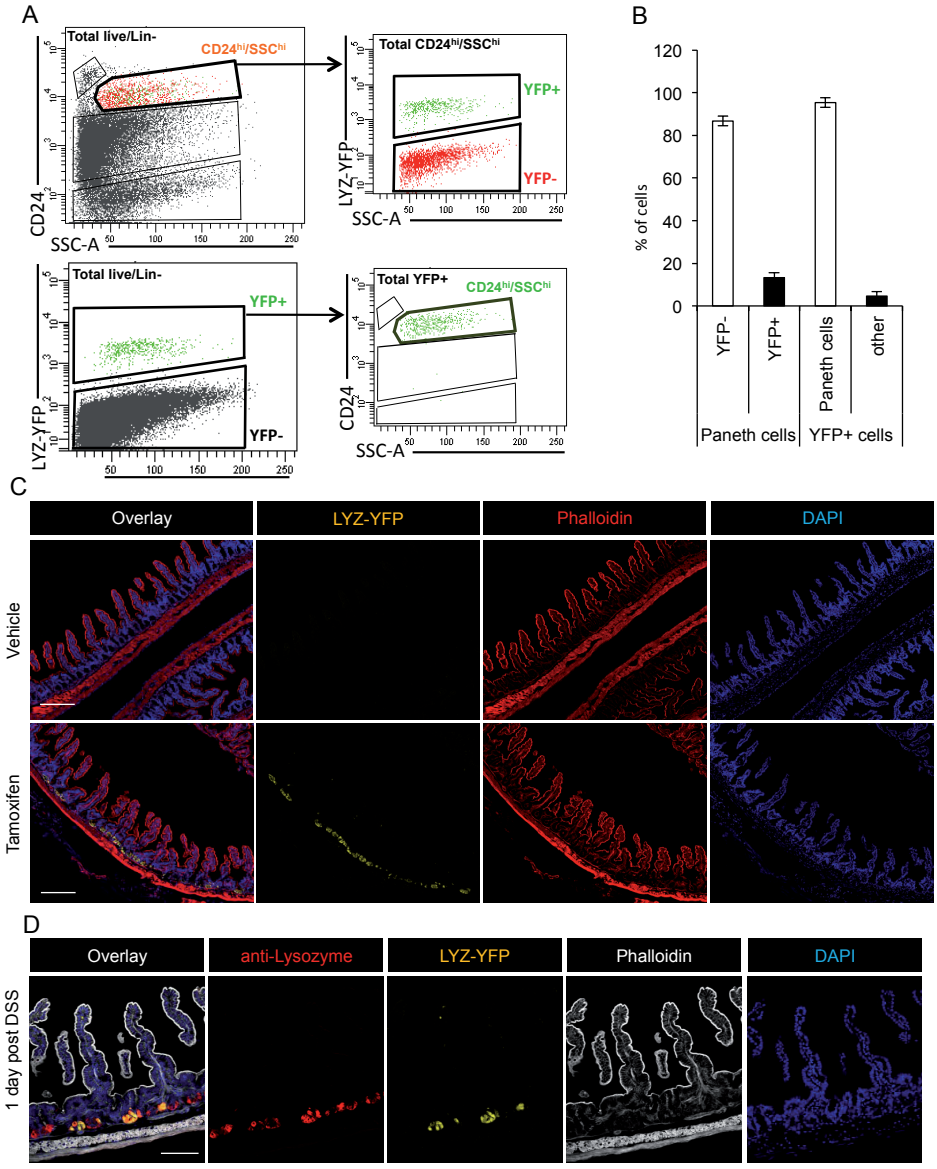

Supplementary Fig. 5 (related to Fig. 5)

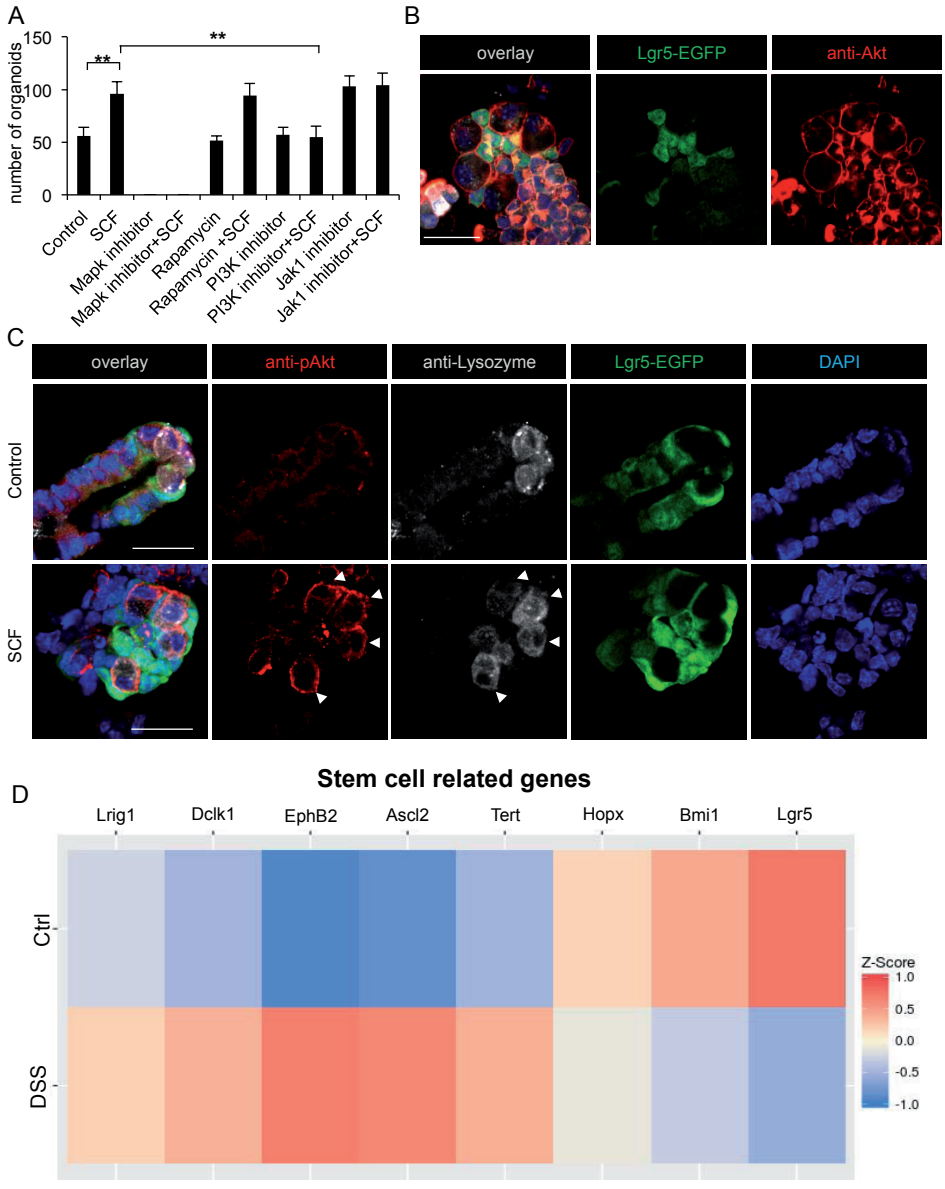

Supplementary Fig. 6 (related to Fig. 6)

A

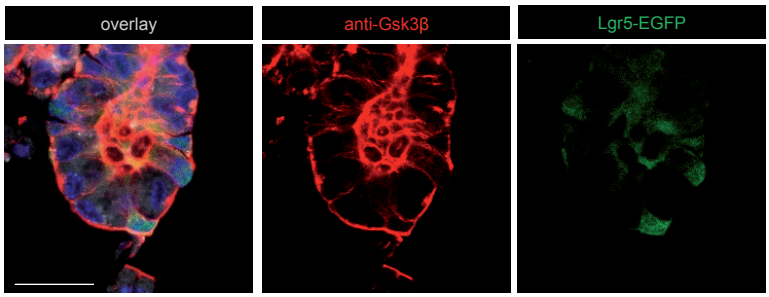

Supplementary Fig. 7 (related to Fig. 7)

A

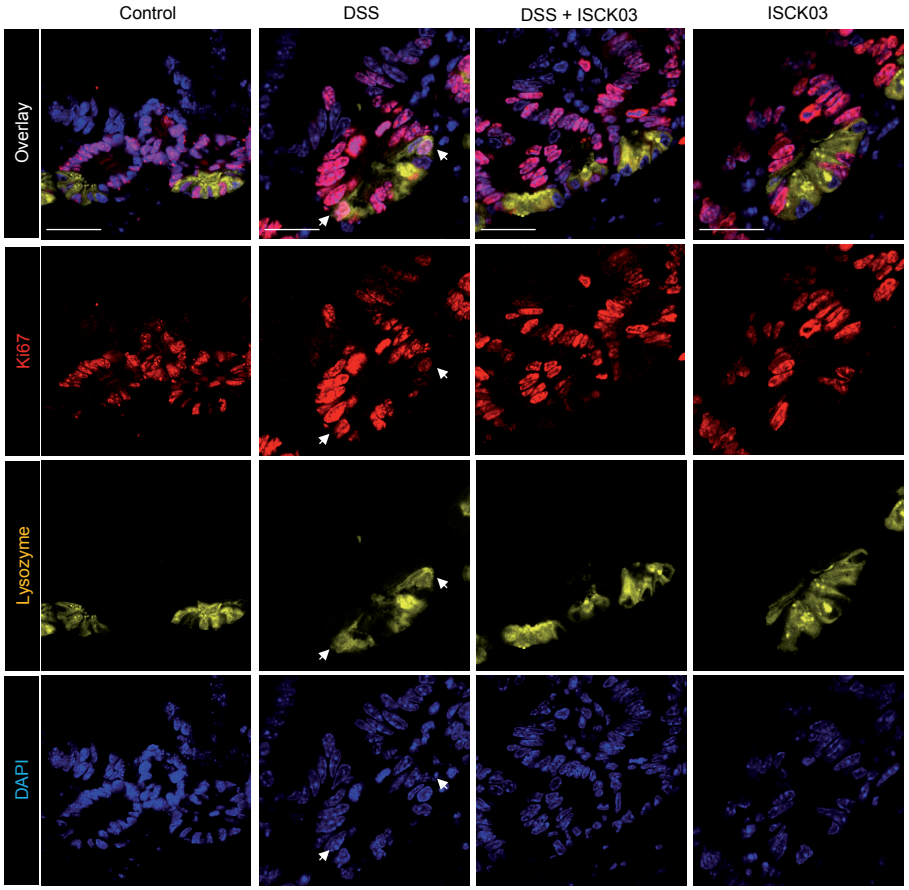

CHAPTER 6

Discussion

PANETH CELLS ARE THE METABOLIC NICHE OF LGR5$^+$ INTESTINAL CELLS

Paneth cells have been proven to provide a niche for the intestinal stem cells [1] as they positively regulate Lgr5$^+$ stem cell maintenance and self-renewal by secreting Wnt3, EGF, Dll1 as well as give structural support[1,2]. In chapter 4 of this thesis the metabolic interactions between Lgr5$^+$ intestinal stem cells and Paneth cells have been elucidated for the first time. The analysis of the metabolite profiles revealed a striking difference between cells at the bottom of the crypt. The metabolite content of Paneth cells showed a glycolytic program whereas Lgr5$^+$ stem cells have been found to have an oxidative metabolic program. Accordingly, the stem cells in the intestine were more sensitive to inhibitors of oxidative metabolism, and appear to have more mitochondria than Paneth cells.

Oxidative metabolism was found to be required for maintaining intestinal stem cell function and glycolysis in Paneth cell was found act as fuel for the Lgr5$^+$ stem cells metabolic program.

Paneth cells through their glycolytic program secrete lactate which is taken up by intestinal stem cells and converted into pyruvate to boost their oxidative phosphorylation.

This metabolic interconnection between these two cell types was already previously suggested under caloric restriction conditions where Paneth cells are sensitive to scarcity or abundance of nutrient availability[3]. This would suggest Paneth cells provide certain nutrients depending on the nutritional state of the organism[4].

In another study by Schell et al.[5], it has been found that inhibition of the mitochondrial pyruvate transporter MPC increased stem cell function, and the regenerative capacity of ex-vivo isolated crypts. Active mitochondria in Lgr5$^+$ stem cells rather than for oxidative phosphorylation are suggested to be used to oxidize lipids[5]. However, the authors of this study added Chiron and valproic acid to the culture media to grow organoids, the addition of these two drugs might switch the metabolism of the stem cells being cultured as it is the case in chapter 4 of this thesis for the WENR (Wnt, Egf, Noggin, R-spondin) cultured organoids[6]. Further studies are required to elucidate the metabolic profile of stem cells and Paneth cells in inflammation and cancer as well as under different nutritional statuses such as high fat diet.

Phospholipases determine fine-tuning of Wnt signaling in the epithelial intestinal stem cell niche

In chapter 3 of this thesis, secretory phospholipase A2 group IIA and group X (*Pla2g2a* and *Pla2g10)* have been found to down-regulate Wnt signaling in Paneth cells and Paneth-like colonic niche cells and negatively affect stemness in Lgr5$^+$ cells when localized intracellularly on their way to secretion[7]. However, when secreted under inflammatory conditions both of these proteins exhibit a positive effect on *Lgr5*$^+$ driven stemness. This study showed that phospholipases act as regulators of Wnt signaling in Paneth cells and keep the balance between cell supply and demand in homeostasis and inflammation[7].

Secretory phospholipases such as *Pla2g2a* and *Pla2g10* are lipid remodeling enzymes. The fatty acid composition of cellular membranes determines their biophysical properties and thus influence several cellular processes. The *Pla2g2a* gene was first found to be a modifier of intestinal tumorigenesis in 1993 by the group of Dove and was named main modifier of Min 1 (Mom1)[8]. Modifiers have since been defined as genes that alter multiplicity of Wnt-driven tumorigenesis in the intestine[8,9]. In chapter 3 we found that the absence of both phospholipase genes *Pla2g2a* and *Pla2g10*) confers susceptibility to colon cancer in a chemical induced inflammation model such as dextran sodium sulfate and azoxymethane (DSS and AOM) treated mice or in Apc mutated mice, suggesting these enzymes are both modifiers of colon cancer[7]. Notably, these mice were on a C57Bl6/J background, a strain resistant to colon tumorigenic protocols[10].

In our study the catalytic function of phospholipases *Pla2g2a* and *Pla2g10* on their substrate (extracellular phospholipids) did not play a role in altering Wnt signaling. However, recent studies suggest that Lpcat3, a phospholipid-remodeling enzyme and critical determinant of polyunsaturated phospholipid abundance and membrane fluidity[11-13] , affects intestinal Lgr5+ stem cell proliferation by controlling cholesterol biosynthesis[14]. In this study the increase in cellular cholesterol was sufficient to drive Lgr5$^+$ stem cell proliferation *in-vivo* as well as *ex-vivo.* The presence of *Lpcat3* suppressed Apc-min driven tumorigenesis suggesting a link between phospholipid remodeling, cholesterol biosynthesis and Lgr5+ proliferation. Lpcat 3 has been found to play an important role in Lands cycle that involve hydrolysis of sn-2 fatty acids by *Pla2g2a* and their reacylation by lysophospholipid acyltransferases. The study of Wang et al. claims that Lpcat3 suppressed Apc-min tumorigenesis in a Wnt independent fashion. However, no functional assay to determine Wnt signalling up or downregulation in the presence or absence of Lpcat3 has been performed and more experiments are required to determine whether Wnt signaling is involved in this mechanism.

As elucidated in chapter 3, we found that in Paneth cells as well as in colonic niche cells Pla2g2a and Pla2g10 are secreted in higher doses under inflammatory conditions.

Notably, *in-vitro* the catalytic activity of the Pla2g2a and Pla2g10 proteins did not display any effect on organoid growth as shown by the use of the catalytically inactive versions of these proteins mutated in the H48Q residue. The use of a mouse deficient for the Phospholipase A2 receptor 1[15], suggested that phospholipases can bind to this receptor and exert their positive function on stemness via enhancing Wnt signaling and prostaglandin E_2 (PgE_2) synthesis. The relevance of this pathway in inflammation has been confirmed by a genome wide associated study (GWAS)[16]. Further *in-vivo* studies with a genetic mouse model mutated in the catalytic site of both Pla2g10 and Pla2g2a need to be performed to understand whether both the catalytic activity and the regulation of the subcellular localization of Yap1 in colonic niche cells play a role in modulating tumor multiplicity in the mouse. One of the features transgenic Pla2g2a mice showed was a Paneth cell maturation defect[7]. The Paneth cells of these mice lacked fully mature Paneth cell markers such as Lysozyme and showed a clear-cut decrease in the expression of secreted Paneth cell specific antimicrobial peptides. In another study as well, Nakanishi et al. found that the absence of protein kinase c lambda/iota (Prkci) led to a Paneth cell maturation defect and to a striking increase in tumor size and multiplicity in both small intestine and colon in an Apc mutated background[17]. Interestingly, the positive effect brought upon tumor multiplicity by the absence of Prkci could be abrogated by treating the mice with antibiotics, suggesting that the microbiome plays a major role in this mouse model in increasing tumor multiplicity[17]. Pla2g2a and Pla2g10 are both lipid remodeling enzymes and secreted antimicrobial proteins. In these mice the change in gene expression of several Paneth cell specific antimicrobial peptides might lead to dysbiosis. Whether the microbiome also has an effect in the tumor multiplicity increase brought upon the absence of these two proteins remains to be seen. Interestingly, a recent discovery found cancer-causing bacterial biofilms in the colon of FAP patients. Individuals affected by FAP syndrome (familial adenomatous polyposis), a hereditary condition caused by germline mutation in the APC tumor suppressor gene, develop hundreds to thousands of colorectal polyps through the accumulation of somatic mutations[18]. The variation in onset and frequency of polyps within families with the same APC mutation suggests that environmental factors such as the microbiota play a role as well. Two pro-tumorigenic variants of E. Coli and Bacteroides fragilis secreting mainly two oncotoxins, colybactin and Bacteroides fragilis toxin, have been found to be specifically associated with an earlier onset of colorectal polyps and a more severe disease progression[18]. Colonization of Apc/min deficient mouse strains with these two bacterial strains confirmed this hypothesis as it led to a more severe phenotype and earlier disease onset in these mice[18]. Further studies are required to understand the role of microbiota in colorectal cancer initiation and progression and whether Apc mutation in Paneth cells and colonic Paneth-like cells lead to a change in the antimicrobial peptide secretion and initiation and progression of colorectal cancer.

Fully mature Paneth cells acquire stem cell characteristics under inflammatory conditions

As previously described in the introduction, mammalian tissues have evolved to harbour both rapid and slow cycling stem cells[19]. The adaptation of fast renewing mammalian tissues to have both quiescent and rapid cycling stem cells is linked to longevity of the organism and functions as a mechanism to avoid adult stem cell exhaustion[20]. In the small intestine, stem cells have been found to be earmarked by the expression of the Lgr5 gene and they are rapid cycling dividing every 24 hours (Figure 1)[21]. Several studies have proposed an alternative quiescent stem cell pool in the intestine which resides at the +4 position in the crypt and is able to retain DNA label, indicating that these cells have stem cell properties. Many markers have been proposed for this alternative stem cell pool such as Bmi1, mTert, Hopx and Lrig1[22-25]. However, none of these markers are uniquely expressed at the +4 position and as a matter of fact their highest expression has been found in Lgr5$^+$ cells. RNA-sequencing analysis indicates that quiescent stem cells have a mixed gene signature between Lgr5$^+$ stem cells and cells committed towards the secretory lineage, suggesting that a population of daughter cells arising from Lgr5$^+$ stem cells and retaining Lgr5 mRNA represents this quiescent stem cell population[26]. Recently another marker for quiescent intestinal stem cells has been identified namely the RNA binding protein Mex3A. Mex3A expressing cells as predicted also express Lgr5 and are found at the +4 position (Figure 1)[27]. The current model of cell hierarchy in the intestine presupposes that rapid cycling stem cells are at the top of the hierarchy giving rise to both differentiated and quiescent Lgr5$^+$ Mex3aA$^+$ stem cells.

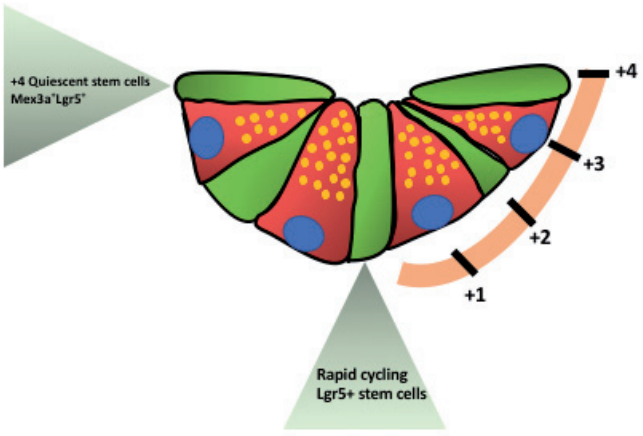

Figure 1. Stem cells under homeostatic conditions. Under homeostatic conditions Lgr5$^+$ rapidly dividing stem cells regenerate the tissue, slow dividing Lgr5$^+$Mex3A$^+$ positive stem cells reside at +4.

All tissues occasionally face traumatic injuries. As the current model suggests, rapid cycling stem cells are exquisitely sensitive to injury stimuli, such as inflammation and radiation, and when exposed to these stimuli rapid cycling stem cells undergo apoptosis. On the contrary, slowly dividing stem cells are thought to exit their quiescent status upon injury, become actively proliferating and repair the tissue[19]. Lgr5$^+$ intestinal stem cells as predicted have been proved to be sensitive to radiation injury and chemically induced inflammation[28], (Schmitt et al. submitted). Furthermore, genetic ablation of Lgr5$^+$ stem cells showed that other cell types can contribute to tissue regeneration in their absence[29]. Nonetheless, Lgr5$^+$ cells have been proved to be indispensable for tissue repair[28]. This postulates that different cell types contributing to regeneration will either start expressing Lgr5 or divide and give rise to a Lgr5$^+$ stem cell. Depending on the gravity of the stress and injury, terminally differentiated cells have also been described to acquire stem cell capabilities and be able to regenerate the tissue as resident adult stem cells would do[30]. The phenomenon of dedifferentiation is described in chapter 5 of this thesis. The intestine is thus a prime example of cellular plasticity, where not only the two-stem cell model rapid and slow cycling stem cells, but also many other cell types can contribute to tissue repair under the right environmental cues or severe damage. Secretory precursors that reside right above the stem cell zone express the Notch ligand Delta like 1 (Dll1)[31]. Under homeostatic conditions these cells give rise to short lived clones of Paneth, goblet and enteroendocrine cells[31]. However, when Lgr5$^+$ stem cells are genetically ablated, these cells can give rise to Lgr5$^+$ stem cells and contribute to intestinal regeneration (Figure 2). Another cell type able to de-differentiate and repopulate the crypt are enterocyte precursors expressing Alpi as a marker[30]. These cells residing at position +6 in the crypt and on their way to become fully mature absorptive enterocytes, are able to repopulate the crypt and give rise to Lgr5$^+$ stem cells under radiation injury (Figure 2)[30]. In chapter 5 of this thesis we investigated the role of Paneth cells in severe injury conditions such as high dose radiation injury (10 Gy), acute inflammation (3%DSS) and chronic inflammation (3 cycles of 1,5% DSS). Surprisingly, the terminally differentiated post-mitotic Paneth cells were able to dedifferentiate and give rise to all intestinal lineages (Figure 2)(Schmitt et al. submitted). In the model presented in Chapter 5, dedifferentiation of Paneth cells occurs through and increase in Wnt via the SCF/c-kit signalling axis. Interestingly, Paneth cells already exhibit hallmarks of activated Wnt signalling (nuclear Beta catenin accumulation) and this pathway is required for their maturation[32]. We suggested that increased Wnt dosage, namely “super-activation”, might guide these cells to dedifferentiate and lead to intestinal regeneration (Schmitt et al. in press). In a recent study by Yu et al. Notch signalling and its reactivation have been found to be the main driver for dedifferentiation of Paneth cells in mice treated with 10 Gy irradiation[33]. In this study the authors found that dedifferentiation of Paneth

cells occurred in a Wnt independent manner. By using a mouse model where exon 3 of beta catenin was deleted and plating ex-vivo isolated Paneth cells the authors showed that super activation of Wnt signalling is not sufficient for these cells to form organoids[33]. However the authors of this study used a company based patented medium called Intesticult which already shows signs of Wnt "super-activation" when added to organoid cultures. This renders the study of the Notch pathway unreliable as it does not consider whether "superactivation" of Wnt signalling is required or not for Paneth cells to dedifferentiate. Furthermore, the use of 10 Gy radiation as a mean to mimic chronic inflammatory stimuli and inflammatory bowel disease raises questions about the relevance of the model. Dextran sulfate sodium salt has been proven to cause inflammation throughout the gastrointestinal tract, a condition called pan-gastroenteritis and as such it would be more relevant as a model in this scenario[7,34]. In chapter 5 of this thesis, by using a chronic colitis model (3 cycles of 1,5% DSS) in the mouse increased frequency of Paneth cell lineage tracing was demonstrated (Schmitt et al. submitted). The increased frequency of lineage tracing in this model suggested a major role for Paneth cells in regeneration in patients affected by Chron's disease and ulcerative colitis. However, the percentage of lineage tracing, and as such tissue regeneration, from Paneth cells does not account for all the regeneration occurring under inflammatory conditions. This thus suggests a communal effort from different types of cells able to de-differentiate and to contribute together to the common goal of tissue repair. As also Paneth cells are able to de-differentiate and contribute to tissue regeneration, all cell types in positions 0 to +6 of the crypt have been shown to be able to behave as facultative stem cells under the right environmental cues. It is possible that intestinal cells behave as a community to achieve homeostasis and balance between cell division and apoptosis. To achieve this common goal, redundancy between several cell types and constant replenishment of the rapid dividing $Lgr5^{+}$ stem cell pool under tissue injury in the crypt is a key feature. Redundancy is commonly found in nature when the goal to be achieved is critical and necessary for the functioning of the system or community. The more a system is redundant, the more it is resilient to disturbance or conditions that in this case alter homeostasis. In the case of the intestine, the critical goal is to still remain within a stable state able to absorb nutrients, while maintaining a rapid cell turnover. Understanding the cellular plasticity of the intestine and how cells work in a community to regulate each other's fate through metabolic, stromal or immune cell mediated signals in response to environmental stimuli, will be of critical importance for prevention and treatment of cancer as well as for auto-immune and chronic inflammatory diseases.

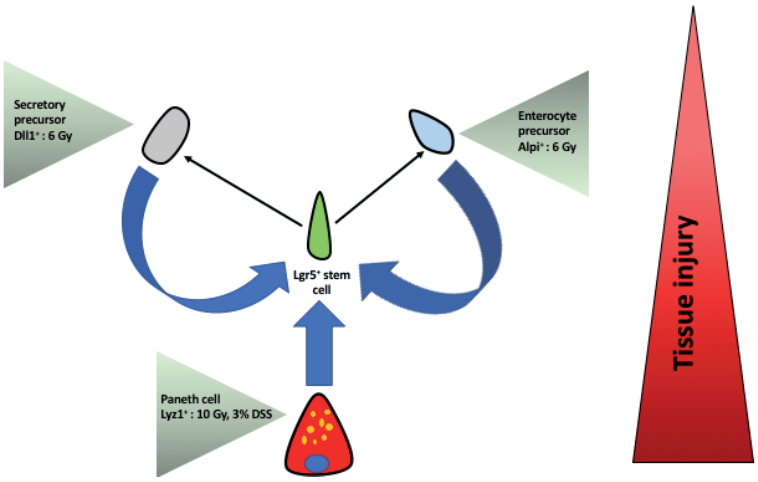

Figure 2. Paneth cells dedifferentiate under inflammatory conditions. As shown in this figure, Paneth cells a terminally differentiated post-mitotic cell type acquire stem cell features and contribute to tissue regeneration. Enterocyte precursors as well as secretory precursors contribute to tissue regeneration under these circumstances as well.

Plasticity and the environment: a stem cell is defined by its niche

Cell plasticity under severe damage is essential for restoring homeostasis. Cell types endowed with plasticity and the molecular mechanisms governing such plasticity are still being elucidated. A central role in cell plasticity is played by the local tissue environment, which under damage undergoes drastic changes in the quantity and quality of stimuli such as molecules secreted by neighbouring stromal and epithelial cells, alterations in extracellular matrix (ECM) composition and tissue architecture[35]. As such, the capacity of cells to differentiate or dedifferentiate is highly dependent on the niche or microenvironment in which they are located[35]. This is the case for the fate of hair follicles stem cells which is niche dependent and differentiated cell compartments can rapidly compensate for stem cell loss[36]. However, in the absence of the perineural niche the plasticity of upper bulge hair follicle stem cells is inhibited[37].

In this thesis, as elucidated in Chapter 5, the ligand of the c-kit receptor or stem cell factor (SCF) secreted from neighbouring epithelial and stromal cells in acute and chronically inflamed mice induces de-differentiation of Paneth cells. Notably SCF expression is significantly increased in IBD patients as well, suggesting that this environmentally regulated plasticity plays a major role in this category of patients. Plasticity is not only regulated via secreted factors from the stem cell niche but also via direct cell-cell contact. In the trachea, the dedifferentiation of secretory Clara cells is

inhibited by direct cell-cell contact with basal stem cells[38]. Nutrients as well are able to modify and influence stem cell activity. Calorie restriction affects intestinal Lgr5^{+} stem cell behaviour by modulating cyclic-ADP production in Paneth cells[3]. ECM factors are a key component of the stem cell niche and necessary for maintaining stem cell function and differentiation[39]. The stiffness of the ECM affects stem cells and their differentiation[40,41]. Also transient expression of Yap1, a transcription factor relevant in mechanosensing and the translation of ECM stiffness into gene expression patterns[42,43], is able to reprogram mammary, neural and pancreatic cells into stem or progenitor cells[44]. Plasticity is likely governed by epigenetic modifications that act in concert with cell type specific transcription factors. However, as it is the case for the intestine, active chromatin marks at tissue specific enhancers and promoter methylation patterns showed surprisingly little dynamics during intestinal stem cell differentiation, hinting that changes in transcription factors in response to external stimuli are sufficient for differentiated cells to switch to a different state[45,46]. This suggested that cells can switch fate by expressing or repressing specific transcription factors in response to various stimuli, as it is the case in the ablation of the transcription factor Cdx2 that converts intestinal stem cells into gastric stem cells[47], or the ablation of the Atoh transcription factor which leads to the loss of the secretory lineage in the intestine[48].

In conclusion more studies are required to further understand how transcription factors and epigenetic mechanisms might control cell plasticity in order to be a useful tool that can be used in tissue regeneration or as a therapeutic target in cancer.

REFERENCES

1 Sato, T. *et al.* Paneth cells constitute the niche for Lgr5 stem cells in intestinal crypts. *Nature* 469, 415-418 (2011).

2 Gracz, A. D. *et al.* A high-throughput platform for stem cell niche co-cultures and downstream gene expression analysis. *Nat Cell Biol* 17, 340-349, doi:10.1038/ncb3104 (2015).

3 Yilmaz, O. H. *et al.* mTORC1 in the Paneth cell niche couples intestinal stem-cell function to calorie intake. *Nature* 486, 490-495, doi:nature11163 [pii] 10.1038/nature11163 (2012).

4 Dayton, T. L. & Clevers, H. Beyond growth signaling: Paneth cells metabolically support ISCs. *Cell Res* 27, 851-852, doi:10.1038/cr.2017.59 (2017).

5 Schell, J. C. *et al.* Control of intestinal stem cell function and proliferation by mitochondrial pyruvate metabolism. *Nat Cell Biol* 19, 1027-1036, doi:10.1038/ncb3593 (2017).

6 Rodriguez-Colman, M. J. *et al.* Interplay between metabolic identities in the intestinal crypt supports stem cell function. *Nature* 543, 424-427, doi:10.1038/nature21673 (2017).

7 Schewe, M. *et al.* Secreted Phospholipases A2 Are Intestinal Stem Cell Niche Factors with Distinct Roles in Homeostasis, Inflammation, and Cancer. *Cell Stem Cell* 19, 38-51 (2016).

8 Dietrich, W. F. *et al.* Genetic identification of Mom-1, a major modifier locus affecting Min-induced intestinal neoplasia in the mouse. *Cell* 75, 631-639 (1993).

9 Cormier, R. T. *et al.* Secretory phospholipase Pla2g2a confers resistance to intestinal tumorigenesis. *Nat Genet* 17, 88-91, doi:10.1038/ng0997-88 (1997).

10 Rosenberg, D. W., Giardina, C. & Tanaka, T. Mouse models for the study of colon carcinogenesis. *Carcinogenesis* 30, 183-196, doi:10.1093/carcin/bgn267 (2009).

11 Wang, B. *et al.* Intestinal Phospholipid Remodeling Is Required for Dietary-Lipid Uptake and Survival on a High-Fat Diet. *Cell Metab* 23, 492-504, doi:10.1016/j.cmet.2016.01.001 (2016).

12 Rong, X. *et al.* LXRs regulate ER stress and inflammation through dynamic modulation of membrane phospholipid composition. *Cell Metab* 18, 685-697, doi:10.1016/j.cmet.2013.10.002 (2013).

13 Rong, X. *et al.* Lpcat3-dependent production of arachidonoyl phospholipids is a key determinant of triglyceride secretion. *Elife* 4, doi:10.7554/eLife.06557 (2015).

14 Wang, B. *et al.* Phospholipid Remodeling and Cholesterol Availability Regulate Intestinal Stemness and Tumorigenesis. *Cell Stem Cell* 22, 206-220 e204, doi:10.1016/j.stem.2017.12.017 (2018).

15 Hanasaki, K., Yokota, Y., Ishizaki, J., Itoh, T. & Arita, H. Resistance to endotoxic shock in phospholipase A2 receptor-deficient mice. *J Biol Chem* 272, 32792-32797 (1997).

16 Liu, J. Z. *et al.* Association analyses identify 38 susceptibility loci for inflammatory bowel disease and highlight shared genetic risk across populations. *Nat Genet* 47, 979-986, doi:10.1038/ng.3359 (2015).

17 Nakanishi, Y. *et al.* Control of Paneth Cell Fate, Intestinal Inflammation, and Tumorigenesis by PKClambda/iota. *Cell Rep* 16, 3297-3310, doi:10.1016/j.celrep.2016.08.054 (2016).

18 Dejea, C. M. *et al.* Patients with familial adenomatous polyposis harbor colonic biofilms containing tumorigenic bacteria. *Science* 359, 592-597, doi:10.1126/science.aah3648 (2018).

19 Fuchs, E. The tortoise and the hair: slow-cycling cells in the stem cell race. *Cell* 137, 811-819, doi:10.1016/j.cell.2009.05.002 (2009).

20 Visvader, J. E. & Clevers, H. Tissue-specific designs of stem cell hierarchies. *Nat Cell Biol* 18, 349-355, doi:10.1038/ncb3332 (2016).

21 Barker, N. *et al.* Identification of stem cells in small intestine and colon by marker gene Lgr5. *Nature* 449, 1003-1007 (2007).

22 Sangiorgi, E. & Capecchi, M. R. Bmi1 is expressed in vivo in intestinal stem cells. *Nat Genet* 40, 915-920, doi:10.1038/ng.165 (2008).

23 Montgomery, R. K. *et al.* Mouse telomerase reverse transcriptase (mTert) expression marks slowly cycling intestinal stem cells. *Proc Natl Acad Sci U S A* 108, 179-184, doi:10.1073/pnas.1013004108 (2011).

24 Takeda, N. *et al.* Interconversion between intestinal stem cell populations in distinct niches. *Science* 334, 1420-1424, doi:10.1126/science.1213214 (2011).

25 Powell, A. E. *et al.* The pan-ErbB negative regulator Lrig1 is an intestinal stem cell marker that functions

as a tumor suppressor. *Cell* 149, 146-158, doi:10.1016/j.cell.2012.02.042 (2012).

26 Munoz, J. *et al.* The Lgr5 intestinal stem cell signature: robust expression of proposed quiescent '+4' cell markers. *EMBO J* 31, 3079-3091, doi:10.1038/emboj.2012.166 (2012).

27 Barriga, F. M. *et al.* Mex3a Marks a Slowly Dividing Subpopulation of Lgr5+ Intestinal Stem Cells. *Cell Stem Cell*, doi:10.1016/j.stem.2017.02.007 (2017).

28 Metcalfe, C., Kljavin, N. M., Ybarra, R. & de Sauvage, F. J. Lgr5+ stem cells are indispensable for radiation-induced intestinal regeneration. *Cell Stem Cell* 14, 149-159, doi:10.1016/j.stem.2013.11.008 (2014).

29 Tian, H. *et al.* A reserve stem cell population in small intestine renders Lgr5-positive cells dispensable. *Nature* 478, 255-259, doi:10.1038/nature10408 (2011).

30 Tetteh, P. W. *et al.* Replacement of Lost Lgr5-Positive Stem Cells through Plasticity of Their Enterocyte-Lineage Daughters. *Cell Stem Cell* 18, 203-213, doi:10.1016/j.stem.2016.01.001 (2016).

31 van Es, J. H. *et al.* Dll1+ secretory progenitor cells revert to stem cells upon crypt damage. *Nat Cell Biol* 14, 1099-1104, doi:10.1038/ncb2581 (2012).

32 van Es, J. H. *et al.* Wnt signalling induces maturation of Paneth cells in intestinal crypts. *Nat Cell Biol* 7, 381-386, doi:10.1038/ncb1240 (2005).

33 Yu, S. *et al.* Paneth Cell Multipotency Induced by Notch Activation following Injury. *Cell Stem Cell*, doi:10.1016/j.stem.2018.05.002 (2018).

34 Elsheikh, W., Flannigan, K. L., McKnight, W., Ferraz, J. G. & Wallace, J. L. Dextran sulfate sodium induces pan-gastroenteritis in rodents: implications for studies of colitis. *J Physiol Pharmacol* 63, 463-469 (2012).

35 Varga, J. & Greten, F. R. Cell plasticity in epithelial homeostasis and tumorigenesis. *Nat Cell Biol* 19, 1133-1141, doi:10.1038/ncb3611 (2017).

36 Rompolas, P., Mesa, K. R. & Greco, V. Spatial organization within a niche as a determinant of stem-cell fate. *Nature* 502, 513-518, doi:10.1038/nature12602 (2013).

37 Brownell, I., Guevara, E., Bai, C. B., Loomis, C. A. & Joyner, A. L. Nerve-derived sonic hedgehog defines a niche for hair follicle stem cells capable of becoming epidermal stem cells. *Cell Stem Cell* 8, 552-565, doi:10.1016/j.stem.2011.02.021 (2011).

38 Tata, P. R. *et al.* Dedifferentiation of committed epithelial cells into stem cells in vivo. *Nature* 503, 218-223, doi:10.1038/nature12777 (2013).

39 Lu, P., Weaver, V. M. & Werb, Z. The extracellular matrix: a dynamic niche in cancer progression. *J Cell Biol* 196, 395-406, doi:10.1083/jcb.201102147 (2012).

40 Watt, F. M. & Huck, W. T. Role of the extracellular matrix in regulating stem cell fate. *Nat Rev Mol Cell Biol* 14, 467-473, doi:10.1038/nrm3620 (2013).

41 Swift, J. *et al.* Nuclear lamin-A scales with tissue stiffness and enhances matrix-directed differentiation. *Science* 341, 1240104, doi:10.1126/science.1240104 (2013).

42 Dupont, S. *et al.* Role of YAP/TAZ in mechanotransduction. *Nature* 474, 179-183, doi:10.1038/nature10137 (2011).

43 Aragona, M. *et al.* A mechanical checkpoint controls multicellular growth through YAP/TAZ regulation by actin-processing factors. *Cell* 154, 1047-1059, doi:10.1016/j.cell.2013.07.042 (2013).

44 Panciera, T. *et al.* Induction of Expandable Tissue-Specific Stem/Progenitor Cells through Transient Expression of YAP/TAZ. *Cell Stem Cell* 19, 725-737, doi:10.1016/j.stem.2016.08.009 (2016).

45 Kim, T. H. *et al.* Broadly permissive intestinal chromatin underlies lateral inhibition and cell plasticity. *Nature* 506, 511-515, doi:10.1038/nature12903 (2014).

46 Kaaij, L. T. *et al.* DNA methylation dynamics during intestinal stem cell differentiation reveals enhancers driving gene expression in the villus. *Genome Biol* 14, R50, doi:10.1186/gb-2013-14-5-r50 (2013).

47 Simmini, S. *et al.* Transformation of intestinal stem cells into gastric stem cells on loss of transcription factor Cdx2. *Nat Commun* 5, 5728, doi:10.1038/ncomms6728 (2014).

48 Yang, Q., Bermingham, N. A., Finegold, M. J. & Zoghbi, H. Y. Requirement of Math1 for secretory cell lineage commitment in the mouse intestine. *Science* 294, 2155-2158, doi:10.1126/science.1065718 (2001).

CHAPTER 7

Summary/Samenvatting

SUMMARY

The focus of this thesis is the study of Paneth cells and their role in the intestinal stem cell niche in homeostasis, injury and tissue repair and cancer. Paneth cells are niche cells for the rapidly dividing Lgr5^{+} intestinal stem cells. In chapter 2 we describe a method designed to elucidate and dissect genetic and/or biochemical modifications in Lgr5^{+} intestinal stem cells or Paneth cells. We used the striking ability of these cells to attach to each other and form organoids or 3D "mini-guts" *ex-vivo.* The developing of this method was essential for the rest of the discoveries elucidated in this thesis. In chapter 3 the role of the secretory phospholipase A2 group IIa (*Pla2g2a*) or *Mom1* in Paneth cells is studied. The study elucidated the role of phospholipases in homeostasis to downregulate canonical Wnt signalling in Paneth cells by upregulating yes associated protein 1 (*Yap*). Under tissue injury conditions *Pla2g2a* was highly secreted and acted in opposite fashion thus by upregulating canonical Wnt signaling. In Chapter 4, the metabolism of the intestinal niche and stem cells is elucidated. Strikingly Paneth cells were found to be highly glycolytic whereas Lgr5+ stem cells used oxidative phosphorylation for their metabolic needs. The work done elucidated that lactate, the end product of glycolysis, secreted by Paneth cells was taken up by Lgr5+ stem cells and used by stem cells to fuel their metabolism. In other terms Paneth cells provide a metabolic niche for intestinal stem cells. In chapter 5 of this thesis another important role of Paneth cells is described. Under severe tissue injury conditions these cells can de-differentiate and regenerate the small intestine, giving rise to all intestinal cell lineages.

In Chapter 4, the metabolism of the intestinal niche and stem cells is elucidated. Strikingly Paneth cells were found to be highly glycolytic whereas Lgr5^{+} stem cells used oxidative phosphorylation for their metabolic needs. The work done elucidated that lactate, the end product of glycolysis, secreted by Paneth cells was taken up by Lgr5+ stem cells and used by stem cells to fuel their metabolism. In other terms Paneth cells provide a metabolic niche for intestinal stem cells. In chapter 5 of this thesis another important role of Paneth cells is described. Under severe tissue injury conditions these cells can de-differentiate and regenerate the small intestine, giving rise to all intestinal cell lineages.

SAMENVATTING

De focus van dit proefschrift ligt op de studie van Paneth-cellen en hun rol in de intestinale stamcellen niche in homeostase, letsel en weefselherstel en kanker. Paneth-cellen zijn nichecellen voor de zich snel delende Lgr5^{+} intestinale stamcellen. In hoofdstuk 2 beschrijven we een methode om genetische en/of biochemische modificaties in Lgr5^{+} intestinale stamcellen of Paneth-cellen te bestuderen. We gebruikten het opvallende vermogen van deze cellen om zich aan elkaar te hechten en organoïden of 3D “mini-darmen” ex-vivo te vormen.

Het ontwikkelen van deze methode was essentieel voor de rest van de ontdekkingen die in dit proefschrift worden toegelicht. In hoofdstuk 3 wordt de rol van de secretoire fosfolipase A2 groep IIa (Pla2g2a) of Mom1 in Paneth cellen bestudeerd.

De studie ontdekte de rol van fosfolipasen in de homeostase om canonieke Wnt-signalering in Paneth-cellen te downreguleren door Yap-associated protein 1 (Yap) te reguleren. Onder omstandigheden van weefselbeschadiging werd Pla2g2a sterk uitgescheiden en werkte het op tegenovergestelde wijze, dus door de canonieke Wnt-signalering op te waarderen.

In hoofdstuk 4 wordt het metabolisme van de “niche” en stamcellen in de darm toegelicht. Opvallend was dat Paneth-cellen zeer glycolytisch bleken te zijn, terwijl Lgr5 + -stamcellen oxidatieve fosforylering gebruikten voor hun metabole behoeften. Het werk verduidelijkte dat lactaat, het eindproduct van glycolyse, uitgescheiden door Paneth-cellen, werd opgenomen door stamcellen van Lgr5 + en werd gebruikt door stamcellen om hun metabolisme te voeden. Met andere woorden: Paneth-cellen vormen een metabolische nis voor intestinale stamcellen. In hoofdstuk 5 van dit proefschrift wordt een andere belangrijke rol van Paneth-cellen beschreven. Onder omstandigheden van ernstig weefselbeschadiging kunnen deze cellen differentiëren en de dunne darm regenereren, waardoor alle intestinale cellijnen ontstaan.

APPENDICES

List of Publications
PhD Portfolio
Acknowledgements
Curriculum Vitae

List of Publications

Schewe M, Franken PF, Sacchetti A, Schmitt M, Joosten R, Böttcher R, van Royen ME, Jeammet L, Payré C, Scott PM, Webb NR, Gelb M, Cormier RT, Lambeau G, Fodde R. 2016 Secreted Phospholipases A2 Are Intestinal Stem Cell Niche Factors with Distinct Roles in Homeostasis, Inflammation, and Cancer. Cell stem Cell Jul 7;19(1):38-51

Hilkens J, Timmer NC, Boer M, Ikink GJ, **Schewe M** , Sacchetti A, Koppens MAJ, Song JY, Bakker ERM. 2016 RSPO3 expands intestinal stem cell and niche compartments and drives tumorigenesis. Gut Jun;66(6):1095-1105.

Rodríguez-Colman MJ, **Schewe M**, Meerlo M, Stigter E, Gerrits J, Pras-Raves M, Sacchetti A, Hornsveld M, Oost KC, Snippert HJ, Verhoeven-Duif N, Fodde R, Burgering BM. 2017 Interplay between metabolic identities in the intestinal crypt supports stem cell function. Nature Mar 16;543(7645):424-427

Schewe, M., Sacchetti, A., Schmitt, M., Fodde, R. The Organoid Reconstitution Assay (ORA) for the Functional Analysis of Intestinal Stem and Niche Cells. J. Vis. Exp. (129), e56329, doi:10.3791/56329 (2017).

Schewe M., Fodde R., Multitasking Paneth cells in the intestinal stem cell niche. Advances in Stem Cells and their Niches # 2018 Elsevier Inc. ISSN 2468-5097

PhD portfolio

Name PhD student	Matthias Schewe
Erasmus MC Department	Pathology
Research School	Molecular Medicine
Supervisor	Prof. Riccardo Fodde

PhD training

Courses	**Year**
Workshop on excel advanced	2016
Workshop on excel (basic)	2016
Workshop on Photoshop and Illustrator	2016
8th workshop on innovative mouse models	2015
Research management for PhD students	2015
Basic and translational oncology	2012
Workshop on presenting skills for junior researchers	2012
Laboratory animal course (Artikel 9)	2012
Epigenetic regulation in health and disease, Leiden, LUMC	2012

Seminars	**Year**
Monthly JNI Oncology Lectures	2012-2017
JNI Scientific Meetings	2012-2017
Annual Molecular Medicine Day	2012-2017
Pathology lab meeting (PALM)	2014-2017
Hubrecht 100 Congress	2016
Daniel den Hoed Day	2016
DSSCR	2012, 2013, 2014, 2015, 2016

Teaching activities	**Year**
12-months supervision (Master student Tania Garcia, Erasmus MC, Molecular Medicine)	2014-2015

Presentations	**Year**
Molecular Medicine Day (Oral, best publication award)	2012-2015
JNI Scientific Meetings (Oral)	2013, 2014, 2015, 2016, 2017
KWF Tumor cell biology Annual Meeting (Oral)	2013
EMBO CSC conference (Poster)	2015
Cell symposium: Stem cell metabolism (Poster)	2016

International Conferences	**Year**
EMBO CSC meeting	2014
Cell symposium: Stem cell Metabolism	2014
ISSCR	2016

Acknowledgements

First of all, the very first thank you goes to my supervisor Riccardo, the greatest gift a man can do to another is to believe in him. Since I was a goofy 16 year old teenager you have been to put it in Dante's words "mio duca e maestro", a teacher, a mentor, a second father, a friend, a source of inspiration. I simply would not be who I am today without you.

For all the people in the lab Cate, Martino, Rosalie, Joel, Andrea, Fanny, Alem, Yaser hope i am not forgetting anybody you have been my family the last 6 six years thank you for that.

To Pat and Mark that need to be singled out since they have been working with me (not an easy task) day after day, thank you. My successes would never have been possible without you.

To Tommaso and Ning Qing you are two great scientists and friends and I will never forget the barbecues, the drunken science talks or anything else we have come up with.

To Rene' and David who have been extraordinary friends, two of the most open minded people I had the pleasure to meet in these years, I learned so much from both of you.

To all the people in the pathology department thank you for everything-in these years.

To Maria, from San Francisco to Nature, it was and will be great to keep working with you.

To Danny, you are a great student and I expect great things from you in science, but most of all you are a great friend.

To Bob and Gerard, thank you for hosting me in your labs it has been a wonderful experience.

To John and Jenny for still being willing to spend time and go out with PhD students I wish more people were like you.

To Pekka, thank you for the next chapter of my scientific life and for all the great scientific discussions, the future holds a lot of good things.

To Simon, after Pat and Mark you got the hard task to work with me, jokes aside, thanks for being there everyday in this new scientific journey.

To Emilia for being a great scientific coordinator and for always being there professionally and as a friend, thank you.

To all the UH and KI peeps thank you, we are a great team.

To my aunt Alessandra, you have been an influence for me all my life. All my literature knowledge and many visions on society I have thanks to talking with you as a teenager. Thank you for being always there.

To my parents, there are no words to describe the wonderful journey the three of us are in and no words to describe how thankful and humbled I am when I see you. I cannot imagine a better model to follow and I cannot stress how much I owe you for who I am today.

Last but not least to my wonderful girlfriend we share everything together, all the good and bad things in life, you are the best companion I wished for and I am so lucky to have you in my life.

Curriculum Vitae

Matthias Schewe was born in Cagliari, Sardinia. After graduating at “Liceo Scientifico Pitagora” in Selargius, moved to study in Pavia, north Italy. In Pavia he obtained a Bachelor Degree in Biology and a Master of Science in Molecular biology and Genetics. During his Master thesis he worked in the laboratory of Professor Antonio Peverali at IGM-CNR. Professor’s Peverali’s lab studies origins of replication. After graduating with 110 cum laude, Matthias joined Prof. Dr. Riccardo Fodde’s lab to pursue his PhD degree. During his PhD his work focused mainly on the study of Paneth cells in homeostasis, inflammation and cancer. After the end of his contract in August 2017 Matthias joined the kab of DR. Pekka Katajisto to pursue a post-doctoral project on circadian rhythm, metabolism and IBD.